EINDHOVEN UNIVERSITY OF TECHNOLOGY

The structure and catalytic properties of supported platinum catalysts

Citation for published version (APA):
Vaarkamp, M. (1993). *The structure and catalytic properties of supported platinum catalysts*. [Phd Thesis 1 (Research TU/e / Graduation TU/e), Chemical Engineering and Chemistry]. Technische Universiteit Eindhoven. https://doi.org/10.6100/IR392485

DOI:
10.6100/IR392485

Document status and date:
Published: 01/01/1993

Document Version:
Publisher's PDF, also known as Version of Record (includes final page, issue and volume numbers)

Please check the document version of this publication:

• A submitted manuscript is the version of the article upon submission and before peer-review. There can be important differences between the submitted version and the official published version of record. People interested in the research are advised to contact the author for the final version of the publication, or visit the DOI to the publisher's website.
• The final author version and the galley proof are versions of the publication after peer review.
• The final published version features the final layout of the paper including the volume, issue and page numbers.

Link to publication

General rights
Copyright and moral rights for the publications made accessible in the public portal are retained by the authors and/or other copyright owners and it is a condition of accessing publications that users recognise and abide by the legal requirements associated with these rights.

• Users may download and print one copy of any publication from the public portal for the purpose of private study or research.
• You may not further distribute the material or use it for any profit-making activity or commercial gain
• You may freely distribute the URL identifying the publication in the public portal.

If the publication is distributed under the terms of Article 25fa of the Dutch Copyright Act, indicated by the "Taverne" license above, please follow below link for the End User Agreement:

www.tue.nl/taverne

Take down policy
If you believe that this document breaches copyright please contact us at:

openaccess@tue.nl

providing details and we will investigate your claim.

Download date: 04. Oct. 2023

The Structure and Catalytic Properties of Supported Platinum Catalysts

M. Vaarkamp

The Structure and Catalytic Properties of Supported Platinum Catalysts

The Structure and Catalytic Properties of Supported Platinum Catalysts

De structuur en katalytische eigenschappen van gedragen platina katalysatoren

PROEFSCHRIFT

ter verkrijging van de graad van doctor aan de Technische Universiteit Eindhoven, op gezag van de Rector Magnificus, prof. dr. J.H. van Lint, voor een commissie aangewezen door het College van Dekanen in het openbaar te verdedigen op donderdag 4 maart 1993 om 16.00 uur

door

Marinus Vaarkamp

geboren te Woudenberg

Dit proefschrift is goedgekeurd door de promotoren

prof. dr. ir. D.C. Koningsberger[¥]
en
prof. dr. R.A. van Santen.

Part of the research described in this thesis was financially supported by Amoco Oil Research, Naperville, IL, USA. The Dutch Organization for Scientific Research (NWO) supplied the beam time at the Synchrotron Radiation Source in Daresbury, UK.

[¥] sinds 1 januari 1992 verbonden aan de Rijksuniversiteit Utrecht

Contents

1. Introduction 1

2. EXAFS data analysis 7

3. A comparison of theoretical methods for Extended X–ray Absorption Fine Structure calculations 21

4. Structure activity relation of a Pt/BaK–LTL catalyst.
   Part 1. Pt clusters in BaKL zeolite: Characterization by transmission electron microscopy, hydrogen chemisorption, and X–ray absorption spectroscopy. 41
   Part 2. Sulfur Poisoning of a Pt/BaK–LTL catalyst: a catalytic and structural study using hydrogen chemisorption and X–ray absorption spectroscopy. 51

5. The Structure of the Metal–Support Interface of Platinum catalysts.
   Part 1. Hydrogen Temperature Programmed Desorption (H_2 TPD) of supported platinum catalysts. 65
   Part 2. Influence of hydrogen pretreatment on the structure of the metal-support interface in Pt/zeolite catalysts. 83

6. A study of the structural changes in a Pt/γ–Al_2O_3 catalyst incduced by hydrogen treatment. 101

7. On the relation between electronic structure and catalytic properties of supported platinum catalysts. 123

8. Methylcyclopentane ringopening over supported platinum catalysts. 139

9. Summary and concluding remarks. 155

Samenvatting 159

Epiloog 163

Curriculum Vitae 165

Abbreviations

EXAFS	Extended X–ray Absorption Fine Structure	
LDOS	Local Density of States	
MCP	MethylCycloPentane	
TOF	TurnOverFrequency	[molecules site^{-1} s^{-1}]
TOS	Time On Stream	
TPD	Temperature Programmed Desorption	
UHV	UltraHigh Vacuum	
WHSV	Weight Hour Space Velocity	[h^{-1}]
XAFS	X–ray Absorption Fine Structure	
XAS	X–ray Absorption Spectroscopy	

Chapter 1

Introduction

The study of the structure and reactivity of small metal clusters has been a prospering branch of both physics and chemistry in the last decades. The fundamental interest of these studies is to understand the physics involved in the transition from the continuous energy band in metals to the discrete energy levels of the isolated atom. In heterogeneous catalysis, maximization of the active surface area of a catalyst is important to reduce the size of the reactor and in the case of noble metals, to reduce the cost of the catalyst. Hence, the knowledge of the structure of small metal particles and their reactivity are of tremendous importance in the development of catalysts.

The change in catalytic properties of metal-catalysts with a change in particle size can be partially attributed to the geometric requirements of the reaction(s) under investigation[1]. However, beam experiments with small metal clusters indicate the importance of differences in the electron-energy distribution of surface atoms compared to bulk atoms[2]. In homogeneous catalysis the knowledge about the influence of ligands on the electron-energy distribution is applied to change the properties of catalytic centres[3].

Already in 1950, both Beeck[4] and Boudart[5] noted a correlation between catalytic activity and the d-band character of catalysts. Sinfelt[6] presented a correlation between the catalytic activity of supported metal catalysts and the d-band character of the corresponding bulk metal. In addition the number of unfilled d-states has been shown to depend on the particle size[7, 8] and the presence of cations[8, 9]. However, contradicting results have also been reported[10].

Saillard and Hoffmann[11] showed with extended Hückel calculations of a 36 atom nickel slab that the d-band of surface atoms is narrowed compared to the d-band of bulk atoms. Ravenek et al.[12] calculated that in neutral clusters the number of unfilled d-states decreased with the coordination number (cluster size). The decrease is counteracted by cluster polarization when a core electron is removed. The influence of polarization effects due to neighbouring cations (typical in zeolites) on

the adsorption of CO on Ir_4 clusters has been studied with Hartree-Fock-Slater methods by Jansen and van Santen[13]. The polarization induced by the presence of a cation increases the metal–CO distance and shifts the CO stretch vibration upwards, indicating an increase in CO bond strength. These changes are found to depend on the relative orientation of adsorbed CO and cation.

The study of the structure and catalytic properties of small metal particles is hampered by a number of experimental problems and the interference of several factors which affect the catalytic performance. Experimental problems are the preparation of metal particles with a narrow particle size distribution and the characterization of these particles under reaction conditions. Electron microscopy can only be applied in UHV conditions, X–ray Diffraction is not applicable to particles of less than 20 Å diameter due to the needed long range order.

X–ray Absorption Spectroscopy can be applied *in-situ* on both small and large particles and is thus particularly suited to characterize supported metal catalysts. Furthermore, information about the structure of the metal-support interface can be obtained when the particles are sufficiently small.

A number of studies have appeared in the literature using EXAFS to investigate the structure of supported metal catalysts. In the early studies, only the structural properties of the metal particle were characterized[14-16]. Because the metal particles were relatively large, the fraction of metal atoms at the metal-support interface was small, and accurate information about the interface could not be obtained. Later studies indicated that the metal particle is supported directly on the oxide surface with reported metal-oxygen distances between 1.92 and 2.07 Å for platinum on alumina[17], platinum on silica[18], and rhodium on magnesia[19]. These distances approximate the known metal-oxygen bond lengths in metal oxide compounds, and are about equal to the sum of the covalent radii of the metal and oxygen atoms. However, even in these later studies, the metal particles were still larger than about 15 atoms ($N \geq 6$), limiting the accuracy with which the metal-support distance could be determined. With very small Ir particles on alumina, an iridium-oxygen distance of 2.19 Å was observed after evacuation[20].

By contrast, longer metal-oxygen distances (ca. 2.7 Å) have been reported for rhodium[21-23], iridium[24], and platinum[25] on alumina, iridium on magnesia[26], palladium[27] and platinum[28] in zeolites, and rhodium on titania[29]. For Rh/alumina[22] the Rh–O contribution was found to increase as the metal particle size decreased, indicating that this Rh-O distance arises from the metal-support interface. The longer metal-oxygen distance has been suggested to be due to the presence of hydrogen or OH groups in the metal-support interface[20]. The presence of the longer metal-oxygen distance is restricted to samples that were neither evacuated, nor treated with helium at high temperature after reduction. This suggests that hydrogen is an important factor in the formation of the longer metal-oxygen distance. However, a clear understanding of the nature of the longer metal-oxygen distance is still lacking[30].

The adsorption and desorption of hydrogen on platinum has been studied for single crystals and catalysts. Temperature programmed desorption of hydrogen from supported and unsupported platinum typically shows multiple peaks above 100°C[31-33]: one at low temperature (ca. 150°C) assigned to hydrogen chemisorbed to the metal surface[33], and one or more higher-temperature peaks (ca. 300–500°C). These high–temperature peaks have been assigned by various authors to spillover hydrogen[37, 35, 39], to strongly chemisorbed hydrogen[31, 32, 38], to hydrogen in sub–surface layers of the platinum[36], or to oxidation of the reduced metal by support protons[40, 41].

Scope of this thesis

The catalytic properties of small metal particles have been reported to depend on the type of metal, the support used, the pretreatment, the particle size and the interaction between the support and the metal particles. The aim of this thesis is to study the relation between the structure of the metal particles and the metal-support interface, the electronic structure, and the catalytic properties of supported metal catalysts. We have limited ourselves to platinum supported on two amorphous supports (silica and alumina) and zeolite L. To maximize the effect of the support on the structure of the metal particles, the structure of the metal-support interface, the electronic structure, and the catalytic properties we prepared catalysts with very small particles.

The main characterization method applied in this thesis is X–ray Absorption Spectroscopy (XAS). In chapter 2 improvements to the generally used methods of analysis of the Extended X–ray Absorption Fine Structure (EXAFS) are discussed. It is shown by model calculations that the relatively weak signal from the support is easily overlooked. The statistical errors arising from the noise in the data and the correlations between the refined structural parameters are used to calculate errors in the structural parameters. Systematic errors arising from the used phase and backscattering amplitude are studied in chapter 3. In addition theoretical methods to calculate the phase and backscattering amplitude are evaluated.

The sulphur sensitivity of the highly active and selective dehydrocyclization catalyst Pt/BaK–LTL has been studied in chapter 4. Sulfur induces a growth of the platinum crystallites and when the size of the crystallites approaches the size of the pores a relative large part of the active surface is lost because the hydrocarbon molecules are unable to penetrate into the small space between the crystallites and the pore wall.

The structure and morphology of the platinum clusters and the structure of the metal-support interface of Pt/zeolite and Pt/γ–Al_2O_3 catalysts is studied in chapter 5 and 6 respectively. Hydrogen TPD measurements show that besides chemisorbed and spill-over hydrogen an additional type of hydrogen is present. The desorption of

this hydrogen is accompanied by a shortening of the distance between platinum clusters and support.

In chapter 7 the number of unfilled d-states of the Pt/zeolite and Pt/γ-Al_2O_3 catalysts is determined from the intensity of the platinum L_{III} and L_{II} X–ray Absorption edges. The influence of adsorbates, metal-support interaction, and particle size on the LDOS are evaluated. Efforts have been made to relate the changes in the LDOS to changes in propane hydrogenolysis activity.

The influence of support and reduction temperature on the activity and selectivity of supported platinum catalysts in methylcyclopentane ring opening is reported in chapter 8.

References

1. M. Che and C. O. Bennett, Adv. Catal., **36** (1989) 55.
2. R. L. Whetten, D. M. Cox, D. F. Trevor, and A. Kaldor, Phys. Rev. Lett., **54** (1985) 1494.
3. P. W. N. M. van Leeuwen and C. F. Roobeek, J. Organometalic Chem., **258** (1983) 343.
4. O. Beeck, Discuss. Faraday Soc., **8** (1950) 118.
5. M. Boudart, J. Am. Chem. Soc., **72** (1950) 1040.
6. J. Sinfelt, AIChE J., **19** (1973) 673.
7. D. R. Short, A. N. Mansour, J. W. Cook Jr., D. E. Sayers, and J. R. Katzer, J. Catal., **82** (1983) 299.
8. H. Yoshitake, and Y. Iwasawa, J. Phys. Chem., **95** (1991) 7368.
9. P. Gallezot, R. Weber, R. A. Dalla Betta, and M. Boudart, Z. Naturforsch. A, **34** (1979) 40.
10. M. G. Samant and M. Boudart, J. Phys. Chem., **95** (1991) 4070.
11. J. Y. Saillard and R. Hoffmann, J. Am. Chem. Soc., **106** (1984) 2006.
12. W. Ravenek, A. P. J. Jansen, and R. A. van Santen, J. Phys. Chem., **93** (1989) 6445.
13. A. P. J. Jansen and R. A. van Santen, J. Phys. Chem., **94** (1990) 6764.
14. J. H. Sinfelt, G. H. Via, and F. W. Lytle, J. Chem. Phys., **68** (1978) 2009.
15. F. W. Lytle, P. S. P. Wei, R. B. Greegor, G. H. Via, and J. H. Sinfelt, J. Chem. Phys., **70** (1979) 4849.
16. G. H. Via, J. H. Sinfelt, and F. W. Lytle, J. Chem. Phys., **71** (1979) 690.
17. P. Lagarde, T. Muraka, G. Vlaic, E. Freund, H. Dexpert, and J. B. Bournonville, J. Catal., **84** (1983) 333.
18. F. W. Lytle, R. B. Greegor, E. C. Marques, D. R. Sandstrom, G. H. Via, and J. H. Sinfelt, J. Catal., **95** (1985) 546.
19. R. J. Emrich, A. N. Mansour, D. E. Sayers, S. T. McMillan, and J. R. Katzer, J. Phys. Chem., **89** (1985) 4261.
20. F. W. H. Kampers and D. C. Koningsberger, Faraday Discuss. Chem. Soc., **89** (1990)

137.
21. H. F. J. van't Blik, J. B. A. D. van Zon, H. F. Huizinga, J. C. Vis, D. C. Koningsberger, and R. Prins, J. Am. Chem. Soc., **107** (1985) 3139.
22. J. B. A. D. van Zon, D. C. Koningsberger, H. F. J. van't Blik, and D. E. Sayers, J. Chem. Phys., **82** (1985) 5742.
23. D. C. Koningsberger, J. B. A. D. van Zon, H. F. J. van't Blik, G. J. Visser, R. Prins, A. N. Mansour, D. E. Sayers, D. R. Short, and J. R. Katzer, J. Chem. Phys., **89** (1985) 4075.
24. F. B. M. van Zon, G. J. Visser, and D. C. Koningsberger, *in* "Proc. 9th Int. Cong. Catal., Calgary, (M. J. Philips and M. Ternan, Eds.), p. 1386. The Chemical Institute of Canada, Ottawa, 1988.
25. D. C. Koningsberger and D. E. Sayers, Solid State Ionics, **16** (1985) 23.
26. F. B. M. van Zon, S. D. Maloney, B. C. Gates, and D. C. Koningsberger, submitted.
27. K. Möller, D. C. Koningsberger, and T. Bein, J. Phys. Chem., **93** (1989) 6116.
28. M. S. Tzou, B. K. Teo, and W. M. H. Sachtler, J. Catal., **113** (1988) 220.
29. J. H. A. Martens, R. Prins, H. Zandbergen, and D. C. Koningsberger, J. Phys. Chem., **92** (1988) 1903.
30. D. C. Koningsberger and B. C. Gates, Catal. Lett., **14** (1992) 271.
31. P. G. Menon and G. F. Froment, J. Catal., **59** (1979) 138.
32. P. G. Menon and G. F. Froment, Appl. Catal., **1** (1981) 31.
33. K. Foger and J. R. Anderson, J. Catal., **54** (1978) 318.
34. K. Kunimori and T. Uchijima, *in* "Spillover of Adsorbed Species", (G. M. Pajonk, S. J. Teichner, and J. E. Germain, Eds.), p. 197. Elsevier, Amsterdam, 1983.
35. L.-Q. Dou, Y.-S. Tan, and D.-S. Lu, Appl. Catal., **66** (1990) 235.
36. P.-J. Levy and M. Primet, Appl. Catal., **70** (1991) 263.
37. R. Kramer and M. Fischbacher, J. Mol. Catal., **51** (1989) 247.
38. T. Szilágyi, J. Catal., **121** (1990) 223.
39. R. Kramer and M. Andre, J. Catal., **58** (1979) 287.
40. J. A. Dalmon, C. Mirodatos, P. Turlier, and G. A. Martin, *in* "Spillover of Adsorbed Species", (G. M. Pajonk, S. J. Teichner, and J. E. Germain, Eds.), p. 169. Elsevier, Amsterdam, 1983.
41. S. T. Homeyer, Z. Karpinski, and W. M. H. Sachtler, J. Catal., **123** (1990) 60.

Chapter 2

EXAFS data analysis

Abstract

The methods for the analysis of the EXAFS spectra in the subsequent chapters are described. Parameters of model EXAFS spectra are determined by non linear least squares refinement with analytical partial derivatives. The use of analytical partial derivatives decreases the CPU time needed for a refinement by over 60% for a three shell system compared to a refinement with partial derivatives calculated with the finite difference method. The standard deviation in the parameters are calculated from the statistical error in the data and the correlations between the parameters. Model calculations show that the identification of low Z scatterers should be done with a k^1 weighed spectrum. The correlation between the coordination number and the mean square relative displacement can be reduced by simultaneous optimization of k^1 and k^3 weighed phase- and amplitude-corrected Fourier transforms.

To be published: M. Vaarkamp, J. C. Linders, and D. C. Koningsberger

Introduction

Although accurate coordination distances can easily be derived from EXAFS spectra, the extraction of quantitative information about the coordination numbers from EXAFS spectra is difficult and time consuming. One can rely completely on statistical methods to determine the significant contributions to the EXAFS spectrum. This requires the (time consuming) optimization of a complete set of parameters for each combination of contributions that is possible. The choice of a set of "best fit" parameters is often very difficult due to the correlations between the parameters, especially when the number of free parameters approaches the maximum number of parameters that can be determined from the data.

Spectra with a single contribution are analyzed straightforward by the ratio method which fits the phase and amplitude separately[1]. Non linear least squares refinement in k-space of the structural parameters in a model EXAFS spectrum is widely used to analyze spectra with two or more contributions. Other methods that have been applied or proposed are i) the maximum entropy method[2], ii) non linear least squares fitting in r–space[3] and iii) a method which minimizes the area between the experimental and the model function[4]. To increase the number of parameters that can be determined Zsech and Blau have proposed to apply the Bayesian method[5], Via and coworkers[6] developed a method to fit spectra of two edges simultaneously.

Once the parameters are refined, the errors in these parameters have to be determined and several sets of parameters (models) have to be compared to check the reliability of the result. Although both error calculation and model comparison are described thoroughly in several textbooks, few scientists apply them. One of the possible causes for this is the lack of a good estimate of the errors in the datapoints in an EXAFS spectrum. These errors are essential for both error calculation and model comparison.

In this chapter a program that is able to estimate the statistical error in EXAFS spectra, perform non linear least squares fitting, estimate the errors in a set of parameters and compare EXAFS model functions is described. Furthermore, the results of model calculations that indicate a scheme to arrive in a straightforward way at the "best" model function are presented.

Refinement of Structural Parameters

Maximum number of free parameters

It is important to determine the maximum number of parameters (degrees of freedom) that can be determined from the data ranges used in the analysis, prior to any parameter refinement. The degrees of freedom is not equal to the number of

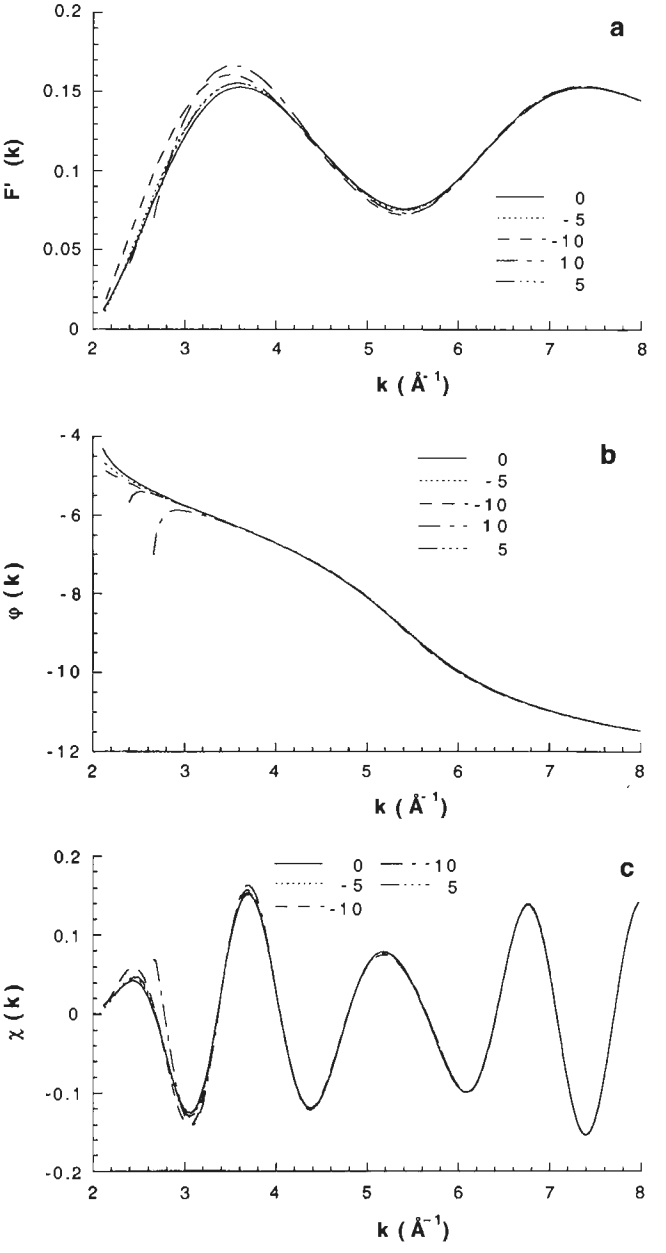

Figure 1 Calculated a) F'(k), b) φ(k), and c) χ(k) by linear extrapolation of a grid point by 10 (dash dot line), 5 (dash dot dot dot line), 0 (solid line), −5 (dotted line), and -10 (dashed line) eV.

datapoints in the spectrum, otherwise decreasing the stepsize of the monochromator during a measurement would increase the degrees of freedom available in the

analysis. An estimate of the maximum number of degrees of freedom (P) based on the available datarange in k- and r-space is given by the Nyquist theorem[7]:

$$P = \frac{2\Delta k \Delta R}{\pi} + 1 \tag{1}$$

Each contribution to the model function requires the optimization of four parameters, consequently the maximum number of contributions to a model function is P/4.

Model function

An accurate theoretical description of EXAFS spectra includes curved wave effects and an energy dependent self-energy[8, 9]. At one particular distance the curved wave EXAFS formula reduces to the plain-wave EXAFS formula (2), which is the model function in the used refinement procedure:

$$\chi(k) = \sum_{j=1}^{shells} S_0^2 \frac{N_j}{kR_j^2} e^{(-2R_j/\lambda)} e^{-2k^2\sigma_j^2} F_j(k) \sin\left(2kR_j + \varphi_j(k)\right) \tag{2}$$

Besides the coordination number N, the distance R, the mean square relative displacement (Debye-Waller factor) σ^2, the quantities S_0^2, $e^{(-2R/\lambda)}$, F(k), and $\varphi(k)$ are unknown. The backscattering amplitude F(k) and the phase $\varphi(k)$ of an absorber-backscatterer pair can be extracted by Fourier filtering from a compound in which the contributions are well separated, or calculated from first principles. To calculate F(k), S_0^2, $e^{(-2R/\lambda)}$, and σ^2 have to be known. To circumvent this requirement we assume that apart from F(k) and $\varphi(k)$, also S_0^2 and $e^{(-2R/\lambda)}$ are transferable from one compound to another. The validity of this assumption has been shown for compounds with the same absorber-backscatterer pair[10, 11], but even for absorbers or backscatterers which are neighbours in the periodic table[12, 13]. This leads to the definition of a modified backscattering amplitude (F'(k)):

$$F'(k) = S_0^2 e^{(-2R/\lambda)} e^{-2k^2\sigma^2} F(k) \tag{3}$$

This modified backscattering amplitude contains the Debye-Waller factor of the reference compound. Hence, the Debye-Waller factor obtained during non linear least squares refinement is relative to the Debye-Waller factor of the reference compound ($\Delta\sigma^2$). The function to be minimized becomes:

$$\chi_{\exp}(k) - \sum_{j=1}^{shells} \frac{N_j}{k_j' R_j^2} e^{-2k_j'^2 \Delta\sigma_j^2} F_j'(k_j') \sin\left(2k_j' R_j + \varphi_j(k_j')\right) \tag{4}$$

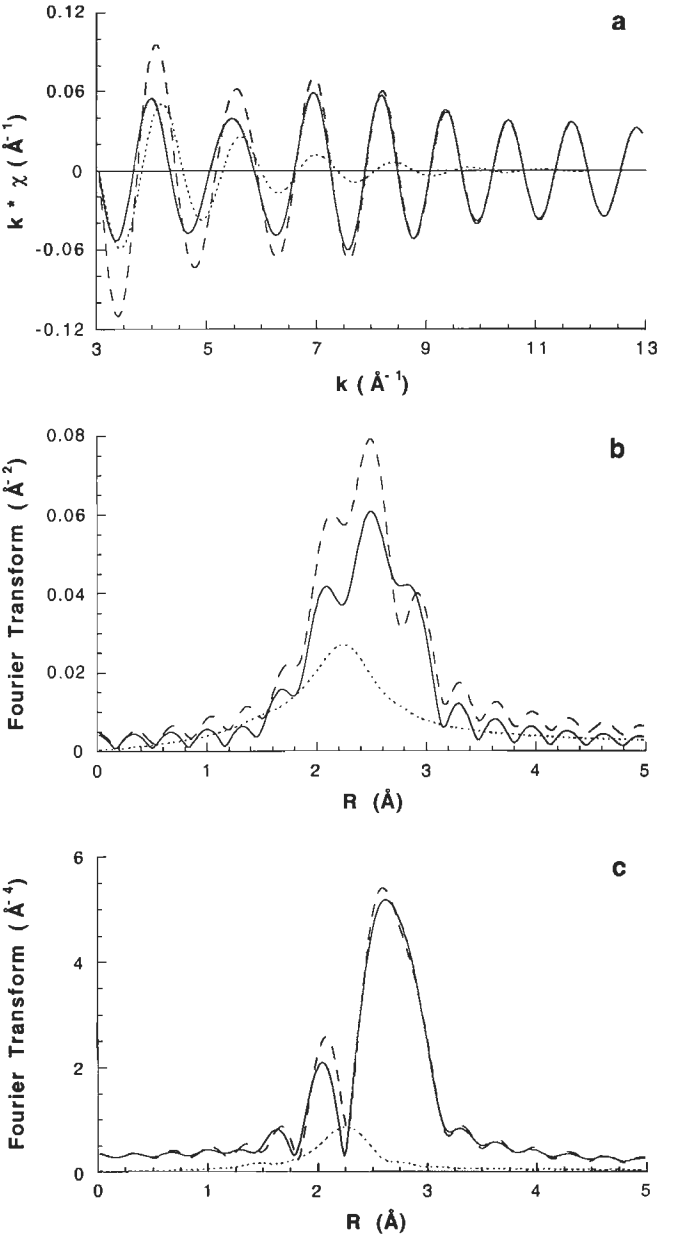

Figure 2 Simulated EXAFS spectra of Pt–Pt (solid line), Pt–O (dotted line), and Pt–Pt + Pt–O (dashed line), a) c (k), b) k^1 weighed Fourier transform |Δk: 3.5 - 13.0 $Å^{-1}$|, c) k^3 weighed Fourier transform |Δk: 3.5 - 13.0 $Å^{-1}$|.

Table 1 CPU time needed on a VAX 4200 to do a refinement.

shells	free parameters	numerical (s)	analytical (s)
1	4	6.7	6.3
2	4	10.6	8.2
2	8	19.4	11.7
3	4	8.3	13.9
3	8	61.0	22.5

Here k′ is the photo electron wave vector corrected for the difference in inner potential between the sample and the reference compound (ΔE_0):

$$k' = \sqrt{k^2 + \frac{2m_e}{\hbar}\Delta E_0} \tag{5}$$

The structural parameters N, R, and $\Delta\sigma^2$ have to be refined for every contribution (shell).

Calculation of F′(k) and φ(k)

Generally, F′(k′) and φ(k′) are not known at the values of k′ where $\chi_{exp}(k)$ has been measured due to different experimental setup or a shift of the k′ value due to a change in ΔE_0. As ΔE_0 is a fitting parameter, the values of k′, and consequently F′(k′) and φ(k′) are subject to change during a refinement. Hence, a fast and accurate method to calculate F′(k′) and φ(k′) is needed. Interpolation between the k values closest to $\chi_{exp}(k)$ is in fact an extrapolation, as the shift in k often spans several datapoints. A simple extrapolation of the phase and amplitude functions from the points on the grid of the experimental and the reference spectra is easily implemented, but can lead to significant errors for ΔE_0 values larger than ±5 eV (figure 1). Especially at k values < 6 $Å^{-1}$, the differences become comparable to the differences between experimental data and models. We have implemented an interpolation method based on the evaluation of an Akima spline[14] calculated for both the phase and the amplitude function. This method eliminates this type of errors completely as it relies on interpolation instead of extrapolation.

Computing requirements

An additional advantage of the use of cubic splines is that the derivative of the amplitude and phase functions with respect to ΔE_0 can be calculated. This opens the way towards the use of analytical partial derivatives in the refinement procedure. Table 1 gives the CPU time needed for a refinement with the use of analytical partial derivatives and the numerical estimation of the partial derivatives with the finite difference method. The speed increase is 7% for a single shell system and increases to more than 60% for a three shell system. The estimation of a partial derivative by the finite difference method calculates the complete spectrum for each partial

Table 2 Parameters used in the calculation of the EXAFS spectra of figure 2a.

Scatterer	N	R (Å)	$\Delta\sigma^2$ (Å^2)	ΔE_0 (eV)
Pt	5.0	2.77	0.0030	0.0
O	1.9	2.65	0.0060	0.0

derivative to be evaluated. In the analytical method only the contribution of the parameter of which the partial derivative is evaluated has to be calculated. The reduction in required calculations increases when the system consists of more contributions. The reduction in calculation time for a single shell system is due to the fact that all partial derivatives of a shell are calculated in a single pass, whereas with the finite difference method four EXAFS spectra with a single contribution have to be evaluated.

Model calculations

Detection of low Z scatterers

It is tempting to apply a k^2 or k^3 weighing to the EXAFS spectrum during the refinement of the structural parameters to compensate for the decay in amplitude of the spectrum with k. However, this emphasis of the high energy part of the spectrum emphasizes the high Z contributions to the spectrum (as high Z elements have more scattering power at high energy than low Z elements). Hence, the low Z contributions are diminished in a k^2 or k^3 weighed EXAFS spectrum. Figure 2a shows simulated EXAFS spectra with the parameters of table 2, these parameters are in the range of typical parameters found in the EXAFS analyses described in the next chapters. The difference between the EXAFS spectrum with only a platinum contribution and the EXAFS spectrum with a platinum and an oxygen contribution is most pronounced below 6 Å^{-1}. In the k^3 weighed Fourier transform of the spectra in figure 2a (figure 2b) the difference between the spectrum with only a platinum contribution and the EXAFS spectrum with a platinum and an oxygen contribution is small. The k^1 weighed Fourier transform (figure 2c) shows much larger differences. From this we infer that to determine properly low Z contributions to EXAFS spectra, k^1 weighed fits and/or Fourier transforms should be applied.

Correlation between N and $\Delta\sigma^2$

The determination of a unique set of parameters for a contribution to an EXAFS spectrum is often difficult due to the correlation between the value of the coordination number (N) and the Debye-Waller factor (σ^2). Kampers[15] showed that by simultaneous optimization of the parameters in the k^1 and k^3 weighed EXAFS spectrum, a unique set of parameters can be found. This can be rationalized by examining the EXAFS equation (2) and noting that the amplitude of the EXAFS

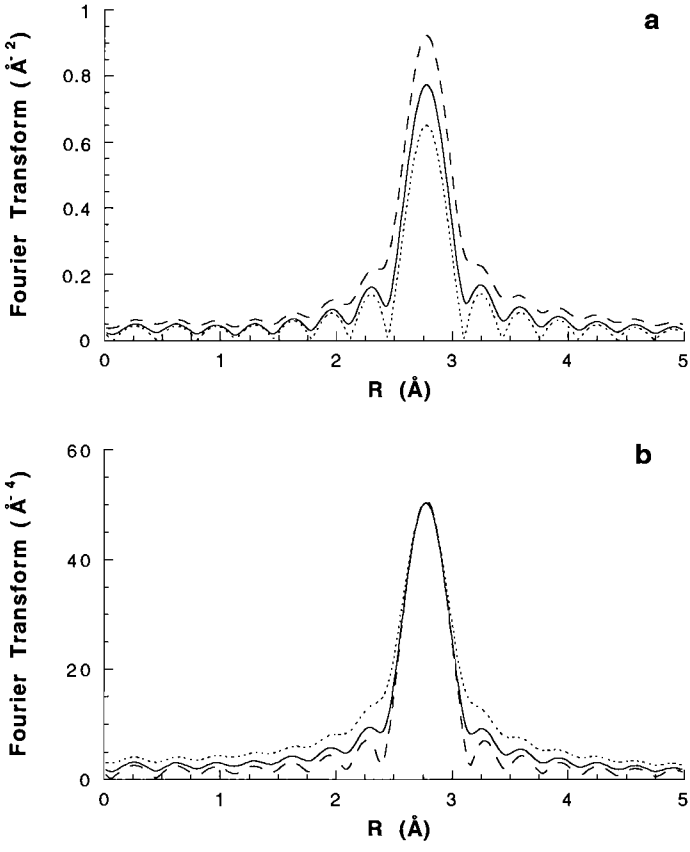

Figure 3 Fourier transforms [Pt–Pt phase- and amplitude-corrected, Δk: 3.5 - 13.0 Å^{-1}] of EXAFS spectra calculated with different combinations of coordination number (N) and Debye-Waller factor ($\Delta\sigma^2$), a) k^1 weighed, b) k^3 weighed. solid line: N=5.00, $\Delta\sigma^2$=0.003 Å^2, dotted line: N=8.55, $\Delta\sigma^2$=0.006 Å^2, and dashed line N=2.75, $\Delta\sigma^2$=0.000 Å^2.

spectrum depends on both N and σ^2. More particularly, the average amplitude of the EXAFS spectrum is proportional to the product N * exp(σ^2).

An example of this approach is given in figure 3. In figure 3b the k^3 weighed Pt–Pt phase- and amplitude-corrected Fourier transform of three EXAFS spectra with the

Table 3 Coordination number and Debye-Waller factor used in the calculation of the EXAFS spectra of figure 2. The distance was kept constant at 2.77 Å and the inner potential shift was set to 0.0 eV

Spectrum	N	$\Delta\sigma^2$ (Å^2)
1	5.0	0.0030
2	8.6	0.0060
3	2.8	0.0000

combinations of coordination number and Debye-Waller factor listed in table 3 are shown. The amplitude of the main peak in these spectra is equal, at the onset of the main peak differences are present. The k^1 weighed Pt–Pt phase- and amplitude-corrected Fourier transform of these three EXAFS spectra (figure 3a), however, shows huge differences in the main peak. Hence, if the k^1 weighed Fourier transforms agree well and the k^3 weighed Fourier transform of the model has a magnitude lower than the experimental data, then the coordination number is too high and the Debye-Waller factor is too low. If the magnitude k^3 weighed Fourier transform of the model is higher, then the coordination number is too high and the Debye-Waller factor is too low. Hence, only when the Fourier transforms with both k^1 and k^3 weighing show good agreement with the experimental data a "good" combination of coordination number and Debye-Waller factor has been selected. It is essential to use phase- or phase- and amplitude-corrected Fourier transforms when applying this method, because otherwise the asymmetry of the peaks will obscure the results.

Curved wave effects

In our analysis method we extract the phase and backscattering amplitude from reference compounds. Due to curved wave effects these phase and backscattering amplitude functions are only correct when there is no difference in distance between reference compound and unknown. Model calculations (table 4, figure 4) show that the errors introduced by the difference in distance between reference compound and unknown are less than 10% and thus are unlikely to affect the outcome of the analysis. The coordination numbers in table 4 are corrected for the distance difference between reference compound and unknown according to:

$$N_{cor} = Ne^{-2(R_{ref}-R_{fit})/\lambda} \tag{6}$$

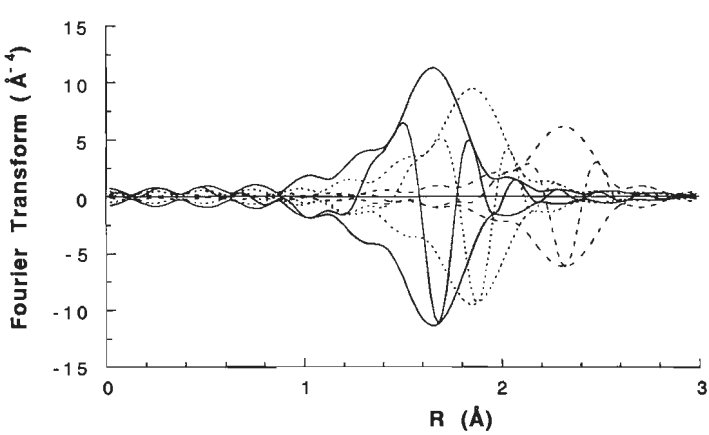

Figure 4 Fourier transform $|k^3, \Delta k: 3.5 - 13.0\ Å^{-1}|$ of simulated EXAFS spectra with a single Pt–O (N=6) contribution at 2.05 Å (solid line), 2.25 Å (dotted line), and 2.70 Å (dashed line).

Table 4 Results of fitting of Pt–O spectra calculated with FEFF 3.11 with a reference calculated with FEFF 3.11 (N=6, R=R_{calc}). Coordination numbers have been corrected for the difference in distance between reference and fit result according to (6).

R_{calc} (Å)	N_{cor}	R (Å)	$\Delta\sigma^2$ (Å^2)	ΔE_0 (eV)
2.05	6.00	2.050	0.00000	0.00
2.25	5.99	2.249	0.00007	-1.03
2.70	5.66	2.697	0.00019	-2.12

The coordination number will be systematically smaller (± 6%) than the "correct" coordination number when the radius of the unknown is much larger (≥ 25%) than the distance of the reference compound.

Fit quality and errors in parameters

To evaluate the results of a refinement it is necessary to calculate the error bars on the refined parameters. For this calculation the errors in the datapoints and the correlations between the refined parameters need to be known. The correlations and the errors in the parameters I and J are calculated from the covariance matrix:

$$Cov(I,J) = \left(\frac{1}{\sigma^2}\right)^2 \frac{\delta\chi}{\delta I}\frac{\delta\chi}{\delta J} \tag{7}$$

Here σ^2 is the error in the experimental spectrum, $\delta\chi/\delta I$ and $\delta\chi/\delta J$ are the partial derivatives of the model function with respect to parameter I and J (see Appendix). The correlations and errors in the parameters can be calculated from the covariance matrix:

$$StDev(I) = \sqrt{Cov(I,J)} \tag{8}$$

$$CrsCor(I,J) = \frac{Cov(I,J)}{\sqrt{Cov(I,I)Cov(J,J)}} \tag{9}$$

From equations (7), (8), and (9) it is evident that the errors in the parameters and the correlations between the parameters are inverse proportional to the errors in the data.

The Goodness of Fit as defined in the Proceedings of the Workshop on Standards and Criteria[16] is calculated by:

$$\varepsilon_v^2 = \frac{P}{N_{PTS}(P-p)} \sum_{i=1}^{N_{PTS}} \left(\frac{\chi_{exp}^i - \chi_{model}^i}{\sigma_{exp}^i} \right)^2 \tag{10}$$

Here N_{PTS} is the actual number of points in the k-range used for analysis, p is the number of parameters that has been refined.

Comparison of Models

When it is possible to obtain different models for the experimental data it is desirable to have a method to reject or accept a model. Furthermore, the addition of a shell to the model will always result in the decrease of the sum of the residuals, but this is no proof that the additional shell actually improves the model.

To test whether additional parameters improve the model we use a likelihood ratio test described by Draper and Smith[17] for a linear case. Letting S denote the sum of squares, p the number of parameters in the model with the additional shell, q the number of parameters in the model in the model without the additional shell, and v the degrees of freedom (P–p), we decide that the additional shell improves the model if:

$$\frac{(S_p - S_q)/(p-q)}{S_p/v} > F(p-q, v, 1-\alpha) \tag{11}$$

Although this method of testing is only approximate because the EXAFS formula is a non linear model, Bates and Watts[18] argued that the distribution of the mean square ratio (S_p/v) is only affected by intrinsic non linearity and not by parameter non linearity. They further showed that the intrinsic non linearity is generally small.

In the case of two models with the same number of free parameters, but with different scattering atoms we used the ratio of the ε_v^2 values[19]:

$$\frac{\varepsilon_v^2(1)}{\varepsilon_v^2(2)} > F(v, v, 1-\alpha) \tag{12}$$

Conclusion

Calculation of the phase and backscattering amplitude from cubic splines is more accurate than extrapolation. Analytical partial derivatives increase the speed of the refinement of structural parameters of a model EXAFS spectrum.

The analysis of EXAFS spectra of heavy atoms with contributions of light atoms is likely to result in wrong structure models when the analysis is done with k^3 weighing of the data. A unique combination of the coordination number and the mean square relative displacement can be obtained by refinement with both k^1 and k^3 weighing.

Appendix: Calculation of partial derivatives

The partial derivatives of the model functions with respect to the refined parameters can be calculated either numerically by finite difference methods or analytically. The advantage of analytical calculation is the increased accuracy and in the case of more than one shell the reduction in CPU time needed for a calculation. The partial derivative of a parameter is determined by the contribution in which this parameter resides, thus eliminating the need for calculation of the other contributions. The analytical expressions for the partial derivatives are:

$$\frac{\delta\chi(k)}{\delta N_j} = \frac{\chi_j(k)}{N_j} \tag{13}$$

$$\frac{\delta\chi(k)}{\delta\Delta\sigma_j^2} = -2k'^2\chi_j(k) \tag{14}$$

$$\frac{\delta\chi(k)}{\delta R_j} = \frac{-2}{R_j}\chi_j(k) + \frac{2N_j}{R_j^2}F_j'(k')\,e^{-2k'^2\Delta\sigma_j^2}\cos\left(\Phi_j(k')\right) \tag{15}$$

$$\frac{\delta\chi(k)}{\delta\Delta E_{0,j}} = \left\{\begin{array}{c} \left\{\dfrac{m_e}{\hbar k'}\dfrac{N_j}{k'R_j^2}e^{-2k'^2\Delta\sigma_j^2}\right\}\times \\ \sin\left(\Phi_j(k')\right)\left(\dfrac{\delta F_j'(k')}{\delta k'} - \dfrac{F_j'(k')}{k'} - 2\Delta\sigma_j^2 F_j'(k')\right) \\ +\left(2R_j + \dfrac{\delta\varphi_j(k')}{\delta k'}\right)F_j'(k')\cos\left(\Phi_j(k')\right) \end{array}\right\} \tag{16}$$

In the above formulas the following abbreviation is used:

$$\Phi_j(k') = 2k'R_j + \varphi_j(k') \tag{17}$$

References

1. G. Bunker, Nucl. Instrum. Methods, **207** (1983) 437.
2. A. K. Livesey, unpublished results.
3. T. M. Hayes and J. B. Boyce, Solid State Phys., **237** (1982) 283.
4. T. I. Guzhavina, Nucl. Instrum. Methods Phys. Res., Sect. A, **282** (1989) 664.
5. E. Zschech and W. Blau, *in* "Proc XAFS VII, Kobe, Japan, August 23 - 29, 1992", in print.
6. G. H. Via, K. F. Drake Jr., G. Meitzner, F. W. Lytle, and J. H. Sinfelt, Catal. Lett., **5** (1990) 25.
7. E. O. Brigham, *The Fast Fourier Transform* (Prentice Hall, Inc., Englewood Cliffs, New Jersey, 1974).
8. A. G. McKale, B. W. Veal, A. P. Paulikas, S. -K. Chan, and G. S. Knapp, J. Am. Chem. Soc., **110** (1988) 3763.
9. M. Vaarkamp, I. Dring, R. J. Oldman, E. A. Stern, and D. C. Koningsberger, submitted (1992). (chapter 3)
10. P. H. Citrin, P. Eisenberger, and B. M. Kincaid, Phys. Rev. Lett., **22** (1976) 3551.
11. B. A. Bunker and E. A. Stern, Phys. Rev. B, **27** (1983) 1017.
12. B. Lengeler, J. Phys. (Paris), **47** (1986) 75.
13. B. K. Teo and P. A. Lee, J. Am. Chem. Soc., **101** (1979) 2815.
14. H. Akima, J. ACM, **17** (1970) 589.
15. F. W. H. Kampers, PhD Thesis, Eindhoven University of Technology, 1989,
16. F. W. Lytle, D. E. Sayers, and E. A. Stern, Physica B, **158** (1988) 701.
17. N. R. Draper and H. Smith *Applied Regression Analysis* (John Wiley & Sons, Inc., New York, 1966)
18. D. M. Bates and D. G. Watts, *Nonlinear Regression Analysis and its Applications* (John Wiley & Sons, New York, 1988).
19. A. J. Dobson, *An introduction to generalized linear models* (Chapman and Hall, 1990).

Chapter 3

A Comparison of Theoretical Methods for Extended X–ray Absorption Fine Structure Calculations

Abstract

Single scattering calculations of the Extended X–ray Absorption Fine Structure amplitude and phase were compared with the experimental first shell of copper, rhodium, and platinum metal. Theoretical standards used were the tables of Teo and Lee, the tables of McKale et al. and the codes EXCURV90, MUFPOT, and FEFF. The quality of the experimental data was shown to be very high. The experimental first shell data were obtained by Fourier filtering. The errors introduced in the separation of the first shell from the complete EXAFS spectrum by Fourier filtering were negligible as shown in a model study. The comparison of the experimental and theoretical data shows that the accuracy of a theoretical standard depends mainly on the treatment of the exchange potential and the energy dependent losses. The most accurate description of the exchange potential is the energy dependent Hedin–Lundqvist potential with an energy dependent self–energy, as used in FEFF. The use of ground state, Xα, or energy independent exchange, as in the McKale et al. tables or the codes EXCURV90 and MUFPOT is found to be inadequate and leads to large phase and amplitude errors. Addition of an energy dependent mean–free path to the tables of McKale et al. improved the accuracy with 15 – 25%.

Submitted for publication: M. Vaarkamp, I. Dring, R. J. Oldman, E. A. Stern, and D. C. Koningsberger

Introduction

Analysis of EXAFS spectra requires the knowledge of backscattering amplitudes and phase shifts. They can be extracted by Fourier filtering from the EXAFS spectrum of a compound with known structure or calculated from first principles. Both methods can introduce (systematic) errors in the analysis of unknown compounds. Extraction of backscattering amplitudes and phase shifts from reference compounds suffers from Fourier filtering truncation errors. The accuracy of calculated backscattering amplitudes and phase shifts is hampered by the approximations necessary to make calculations possible. A number of first principle methods to calculate backscattering amplitudes and phase shifts have been developed[1–5]. The most widely used programs are EXCURV and FEFF. Tables of phase shifts and backscattering amplitudes as compiled by Teo and Lee, and McKale are also widely used.

One of the goals of the International Workshop on Standards and Criteria in X-ray Absorption Spectroscopy[6] is to assess quantitatively the applicability of current theoretical models in XAFS analysis. This may be carried out by comparing the available theoretical standards with high quality experimental spectra from well characterized materials. Each of these theoretical standards is based on different prescriptions for scattering potentials and self-energies or exchange potentials. By comparing XAFS spectra calculated from these theories with experiment the relative importance of the elements of the theoretical approaches can be assessed. The most straightforward way of comparing calculated and experimental XAFS is by looking at a single absorber-backscatterer pair in a single scattering process. To isolate a single contribution in experimental data Fourier filtering is necessary.

The goal of this paper is to determine the elements of a theoretical standard that are most important for it's accuracy. The calculated phase shift and backscattering amplitude were compared with first shell experimental spectra. We used only monoatomic metals to avoid the difficulties of charged atoms in calculations. From each of the first three rows of the transition metals a readily available compound was selected (Cu, Rh, and Pt foil respectively).

Accurate experimental data are essential in a comparison of experimental data and theoretical calculations. To verify the quality of the used experimental data, data measured under different experimental conditions were compared. The separation of the single scattering first shell contribution from the complete EXAFS spectrum was carried out by Fourier filtering. The Fourier filtering suffers from truncation errors due to the limited data range used in both the forward and the inverse Fourier transform. To verify that Fourier filtering introduces errors which are negligible compared to the differences in the theoretical standards we carried out a model study to quantify the Fourier filtering errors.

From the statistical errors in the data and the differences between experimental data and fit, goodness of fit values and errors in the determined parameters are calculated. The goodness of fit values and the number of free parameters are used to

test whether the differences in fit-quality between the different theoretical references are statistically significant.

Description of Theoretical Methods

X-ray absorption fine structure (XAFS), i.e., the oscillatory structure in the x-ray absorption coefficient, contains quantitative information about the local environment of an absorbing atom. This information includes near neighbour distances R, coordination numbers N_R, and a pair distribution function about the average which, in simple cases, can be described by a mean squared deviation σ^2. These quantities appear as structural parameters in the single scattering curved-wave XAFS equation[7] together with other quantities which depend on the electronic structure of the material.

$$\chi_l = -\sum_R N_R S_0^2 \frac{|f_{eff}(\pi, k, R)|}{kR^2} \sin\left(2kR + 2\delta^c + \Phi_{eff}\right) e^{-2k^2\sigma^2} e^{-2R/\lambda(k)} \qquad (1)$$

Here, $f_{eff}(\pi,k,R) = |f_{eff}(\pi,k,R)| e^{i\Phi_{eff}}$ is the effective curved-wave backscattering amplitude[7], δ^c is the final state l–wave central atom phase shift, $\lambda(k)$ is the mean free path of the photoelectron, and S_0^2 is a many-body amplitude reduction factor. The determination of structural parameters from experimental data, which is the goal of XAFS analysis, always requires a comparison with an accurately known experimental or theoretical reference system.

The theoretical standards included in this study include tables of plain wave XAFS phases and amplitudes of Teo and Lee[1], tables of curved wave XAFS phases and amplitudes of McKale et al.[2,8], and three *ab initio* computer codes EXCURV90[3], MUFPOT[4], and FEFF[5]. Although curved wave effects are known to be important, we have included tables based on plane wave amplitudes and phases, because they are still widely used.

The tables of McKale et al.[8], MUFPOT[4], and EXCURV90[3] include curved-wave effects exactly but are based on ground-state exchange-correlation potentials and thus ignore the energy dependence of the electron. All three require the use of the energy reference or "inner potential" E_0 as a free fitting parameter. The central atom tables of Teo and Lee[1] are based on a complex Hedin-Lundqvist self-energy and atomic-potentials. The *ab initio* single-scattering code FEFF makes use of an overlapped atom scattering potential and a Hedin-Lundqvist self-energy. Implicit in the use of tables is a reliance on the hypothesis of chemical transferability in which system dependent chemical effects are neglected. Evidence exists[9] that this hypothesis is not true and some error is introduced by the use of tables. The *ab initio* computer codes do better because they account for chemical effects, though only approximately.

Experimental

Data collection

Two sets of data were collected for each foil. The samples were cooled with Liquid Nitrogen to approximately -130°C. The thickness of the foils was 7, 4, and 20 μm for copper, platinum, and rhodium, respectively ($\Delta\mu x$ was 1.7, 0.5, and 0.4). The measurements were done in the transmission mode using ion chambers filled with argon to have a μx of 20% in the first ion chamber and a μx of 80% in the second ion chamber. To reduce noise several scans were averaged for each set of data.

Copper foil data were collected at the Synchrotron Radiation Source (SRS) in Daresbury, U.K., Wiggler Station 9.2 and Station 8.1, using a flat Si (220) double crystal monochromator. Station 8.1 was equipped with a vertical and horizontal focussing mirror. The storage ring was operated with an electron energy of 2 GeV and a current between 120 and 250 mA. The estimated resolution is 2 eV at the Cu K edge. The monochromator was detuned to 50% intensity on station 9.2 and 70% intensity on station 8.1 to avoid the effects of higher harmonics present in the X–ray beam.

Platinum foil data were collected at the SRS, Wiggler Station 9.2, using a flat Si (220) double crystal monochromator. The estimated resolution was 3 eV at the Pt L_{III} edge. The monochromator was detuned to 50% intensity to avoid the effects of higher harmonics present in the X–ray beam. Additional platinum foil data were collected at the Stanford Synchrotron Radiation Laboratory (SSRL), Stanford, USA, station 1.5, using a Si (220) channel cut monochromator (3 GeV, 40 – 80 mA). To decrease detection of higher harmonics the gas filling of the second ion chamber was decreased[9].

Rhodium foil data were collected at the SSRL station 1.5, using a Si (220) channel cut monochromator. The estimated resolution was 5 eV at the Rh K edge. Additional rhodium foil data were collected at the SRS station 9.2, using a Si (220) channel cut monochromator. No precautions were taken to prevent the detection of higher harmonics.

Data reduction

To extract the EXAFS from the X-ray absorption spectrum. The pre–edge background was approximated by:

$$\text{PreEdge} = \frac{C_2}{E^2} + \frac{C_1}{E} + C_0 \qquad (2)$$

The edge energy was set to 8980 eV for copper foil at the peak of the Cu K edge feature. The platinum and rhodium edge energies were set to the maximum in the first derivative in the edge region (11564 eV and 23220 eV). The background in the

EXAFS region was approximated with a smoothing spline and optimized according to the criteria described by Cook and Sayers[10]. The spectra were normalized by the edge step at 50 eV behind the edge.

Calculations

Parameters used to calculate the first shell EXAFS spectra are listed in table 1. Distances are taken from X-Ray Diffraction (XRD) measurements[11]. All compounds have a FCC structure, thus the first shell coordination number for all compounds is 12. The Debye-Waller factors for copper and platinum foil were taken from Stern et al.[12]. The Debye-Waller factor for rhodium foil has been calculated from the value determined by XRD[13] and the displacement correlation function[14]. The imaginary potentials V_0 used to describe inelastic losses in EXCURV90 and MUFPOT were selected by optimizing fits on foils measured separately at room temperature. Phase

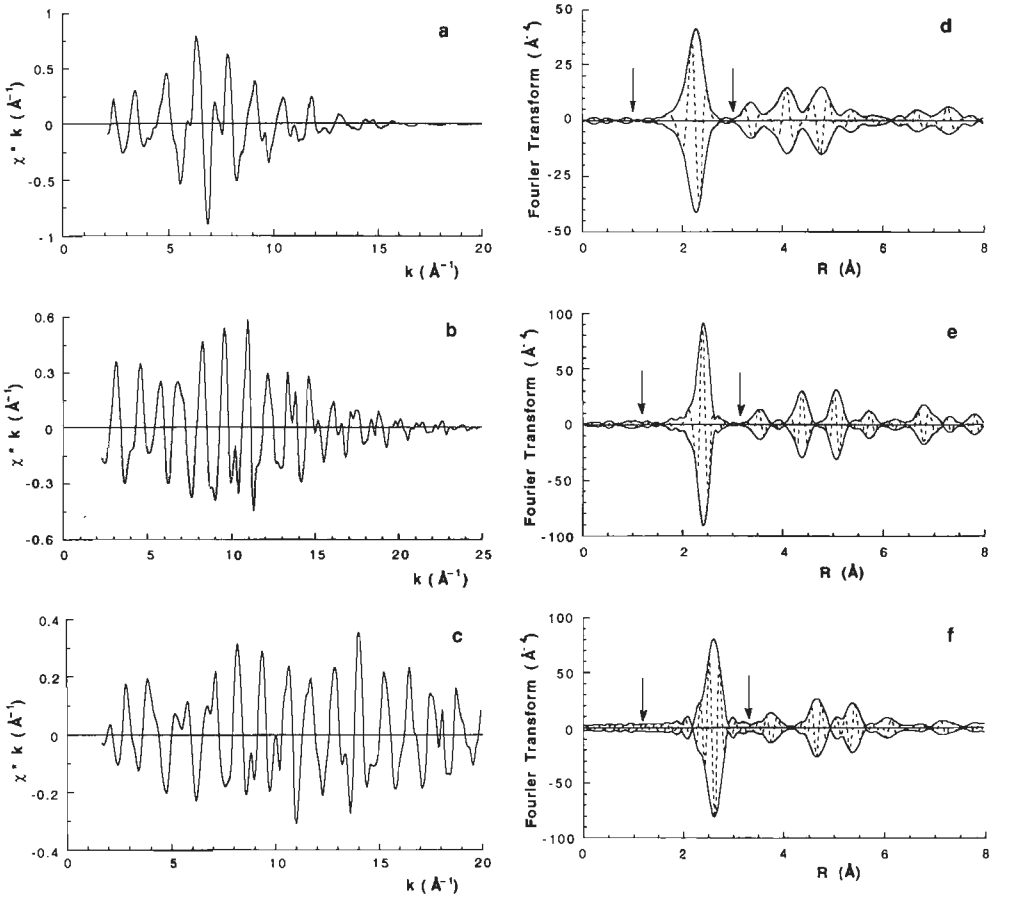

Figure 1 k^1 weighed EXAFS spectra of a) copper foil (SRS 8.1), b) rhodium foil (SSRL 1.5), c) platinum foil (SRS 9.2) and their k^3 weighed Fourier transforms (d, e, and f respectively). Fourier transform ranges are listed in table 2.

Table 1 Input parameters for theoretical calculations.

Absorber	Backscatterer	R (Å)	N	σ^2 (Å^2)	V_0 (eV)
Pt^0	Pt^0	2.774	12	.00261	−8.5
Rh^0	Rh^0	2.687	12	.00140	−8.5
Cu^0	Cu^0	2.560	12	.00328	−5

shifts and backscattering amplitudes from the tables of Teo and Lee were taken from calculations with Clementi-Roetti wavefunctions for copper and from the calculations with Herman–Skillmann wavefunctions for rhodium and platinum. The average of the ruthenium and palladium results was used for rhodium. Data from the tables of McKale et al. were interpolated on a 1/R grid.

The many body reduction factor S_0^2 is used as a scaling factor by all theoretical standards. However, the values used differ and are mostly obtained from fitting a compound with known structure with calculated phase shift and backscattering amplitude. We have chosen to set S_0^2 to 1 in all calculations to be able to directly relate the coordination numbers obtained in the analysis to the magnitude of the calculated backscattering amplitudes.

Errors in data

Averaging χ functions and Fourier filtered χ functions gives the opportunity to average out statistical errors in background subtraction and Fourier filtering procedures. The errors in both background subtracted χ functions and Fourier filtered χ functions were calculated from averages of 5, 3 and 4 datasets of copper, rhodium, and platinum foil, respectively.

Results and Discussion

To compare theoretical and experimental EXAFS spectra, very accurate experimental data are necessary. We identified three possible sources of errors: i) statistical

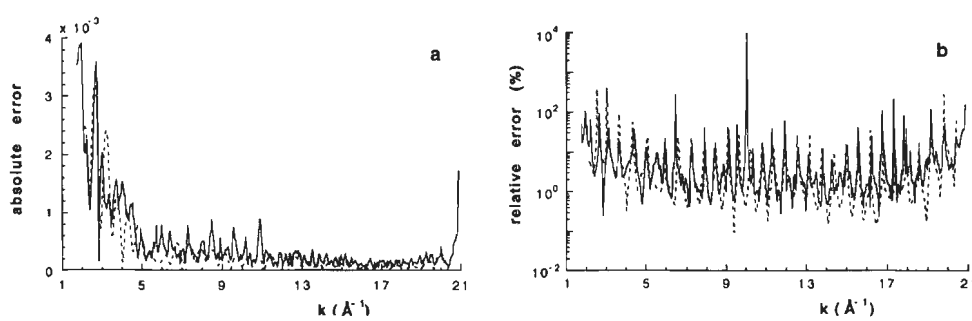

Figure 2 Errors in the raw (solid line) and Fourier filtered (dashed line) EXAFS spectrum of Pt foil measured at SRS 9.2, a) absolute errors, b) relative errors.

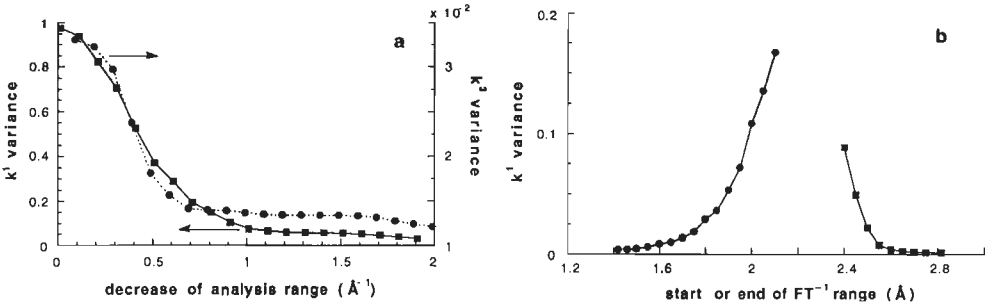

Figure 3 Variance of the analysis of a Fourier filtered EXAFS spectrum with its original phase shift and backscattering amplitude. a) Dependence of variance on analysis range in k-space. Solid line (squares) increasing the start of the analysis range while keeping the end fixed at 18.5 Å^{-1}. Dashed line (circles) decreasing the end of the analysis range while keeping the start fixed at 3.3 Å^{-1}. b) Dependence of variance for k^1 weighed analysis from 3.5 – 18.0 Å^{-1} on the inverse FT range. Solid line (squares) increasing the start inverse transform range. Dashed line (circles) decreasing the end of the inverse transform range.

uncertainty, ii) Fourier filtering errors, and iii) errors due to specific experimental conditions used. The statistical uncertainty (error) in the experimental data used in this study is calculated for the average of a number of datasets. The Fourier filtering errors are estimated by a model study. The errors due to changes in experimental conditions are estimated by comparison of EXAFS spectra measured under different experimental conditions.

Raw data and statistical errors

The k^1 weighed EXAFS spectra of copper, rhodium and platinum foil are presented in figure 1 together with their k^3 weighed Fourier transforms. Up to six shells can be distinguished in the Fourier transform implying these are very high quality EXAFS spectra.

Four scans of platinum foil taken at SRS 9.2 were background subtracted and normalized. Their χ functions were averaged and the standard deviation (σ, error) in the average χ function was calculated. Subsequently all four χ functions were Fourier filtered to separate the first shell EXAFS from the other contributions. The thus obtained Fourier filtered χ functions were averaged and the standard deviation (σ, error) in the average Fourier filtered χ function was calculated. The absolute errors in the unfiltered and filtered platinum foil χ functions are shown in figure 2a, the peaks correspond to nodes in χ. There is a clear decrease in the magnitude of the errors of both raw and Fourier filtered data with increasing k value. The magnitude of the noise in the Fourier filtered data is slightly less than the magnitude of the noise in the raw data. The fact that the noise is so strongly varying with k indicates that it is not purely statistical but has added a large amount of systematic noise. It is likely that the increased magnitude of the statistical errors at low k is caused by the uncertainties in the background subtraction procedure. The relative errors are

Table 2 Dataranges for Fourier Filtering

dataset	forward FT range ($Å^{-1}$)	inverse FT range (Å)
copper foil	2.2 – 19.4	1.0 – 3.0
rhodium foil	2.9 – 24.4	1.2 – 3.0
platinum foil	2.2 – 20.3	1.1 – 3.1

shown in figure 2b. It is striking that the relative errors in the raw and the Fourier filtered EXAFS spectrum are of the same magnitude over the complete k–range examined. The bigger errors in the raw data are compensated by the larger amplitude of the raw EXAFS. The absence of any k–dependence in the relative errors has also to be attributed to the decrease in absolute errors value accompanied by a comparable decrease in amplitude of the EXAFS. The average relative error between 2.3 and 19.1 $Å^{-1}$ is 6 %.

Fourier filtering truncation errors

The aim of Fourier filtering is to separate the contribution of a single absorber-backscatterer pair from the contributions of other absorber-backscatterer pairs. This is either to facilitate analysis or to extract experimental phase shifts and backscattering amplitudes from the EXAFS spectrum of a compound with known structure.

To quantify the errors made in this procedure a test first shell copper foil EXAFS spectrum was calculated with the phase shift and backscattering amplitude obtained with FEFF. This test EXAFS spectrum was Fourier filtered over a number of forward and inverse ranges. By analyzing the Fourier filtered EXAFS spectrum with the phase shift and backscattering amplitude used to calculate the test first shell EXAFS spectrum, filtering errors were quantified. The agreement between calculated (test) and Fourier filtered spectrum is expressed as the k^n variance:

$$k^n \text{ variance} = 100 \frac{\int \left\{k^n\left(\chi_{model}(k) - \chi_{exp}(k)\right)\right\}^2}{\int \left\{k^n \chi_{exp}(k)\right\}^2} \qquad (3)$$

As Fourier truncation errors are largest at the start and end of the Fourier transform interval the range and weighing of analysis were varied. To see the effect of window functions, forward transforms ending and starting at nodes or maxima and minima were compared.

Analysis of a Fourier filtered χ function obtained with a forward range of 2.3 – 19.4 $Å^{-1}$ and an inverse range of 0 – 8 Å resulted in a variance of zero, inferring that in this case there are no Fourier filtering errors. Analysis of a Fourier filtered χ function obtained with a forward range of 2.3 – 19.4 $Å^{-1}$ and an inverse range of 1.3 – 3.1 Å resulted in a non–zero variance. Figure 3a shows the decrease of the variance

upon shrinking the interval for analysis. The maximum variance has been calculated over the k–space interval 2.4 – 19.3 $Å^{-1}$. The start and end of the interval were varied separately. To emphasize the low or high k region in the analysis the k weighing in the analysis was varied. Comparisons with varying beginning of the analysis interval were done with k^1 weighing, comparisons with varying end of the analysis interval were done with k^3 weighing. The agreement between Fourier filtered and unfiltered spectrum increases when the range of comparison is shortened. The decrease in variance is bigger at the start than at the end of the analysis range; truncation errors are larger at low than at high k. Shrinking 1.0 $Å^{-1}$ at the start and 0.8 $Å^{-1}$ at the end gives excellent agreement between original and Fourier filtered data (k^1 variance 0.07). Using this range for fitting the Fourier filtered data leads to coordinations parameters which are nearly identical to the original values. Maximum deviations are: the coordination number ±2%, the Debye–Waller factor ±0.0002 $Å^2$, the distance ±0.003 Å, and E_0 ±0.5 eV.

While keeping the forward Fourier transform range at 2.3 - 19.4 $Å^{-1}$, the end and start of the inverse Fourier transform range were varied separately. Either the end of the inverse Fourier transform range was fixed at 3.1 Å or the start was fixed at 1.3 Å. The Fourier filtered spectra were analyzed over the interval 2.8 - 18.5 $Å^{-1}$ with the phase shift and backscattering amplitude used to calculate the test first shell EXAFS spectrum. Shrinking of the range of the inverse Fourier transform results in an increase of the k^1 variance from 0.07 to 20 (figure 3b). As long as the complete main peak is included in the inverse Fourier transform excellent agreement over the complete analysis range can be obtained. Omitting only a small part of the main peak results in relatively large errors over the complete Fourier transform range.

Changing the start and/or end of the forward Fourier transform range from nodes to maxima and minima does not result in a significant increase of the variance.

Errors induced by changes in experimental conditions

Changes in experimental conditions (temperature, higher harmonic rejection etc.) affect the measured EXAFS spectrum. To estimate the magnitude of these changes we compared spectra measured under different experimental conditions. The comparison was quantified by analyzing the first shell of an EXAFS spectrum

Table 3 Numerical results of the k^1 weighed analysis of experimental data with a reference measured under different experimental conditions over a k–range of 3.5 – 18.0 $Å^{-1}$. The listed coordination numbers (N_{cor}) have been corrected for the difference in distance between reference and analysis result. Data: synchrotron where the data were measured. Ref: synchrotron where the reference was measured.

foil	data	ref	N_{cor}	R (Å)	$\Delta\sigma^2$ ($Å^2$)	ΔE_0 (eV)	k^1 variance
Cu	SRS 8.1	SRS 9.2	12.37	2.565	0.00091	–0.86	0.6
Rh	SSRL 1.5	SRS 9.2	13.59	2.684	–0.00069	0.65	0.8
Pt	SRS 9.2	SSRL 1.5	11.89	2.769	0.00016	0.74	0.1

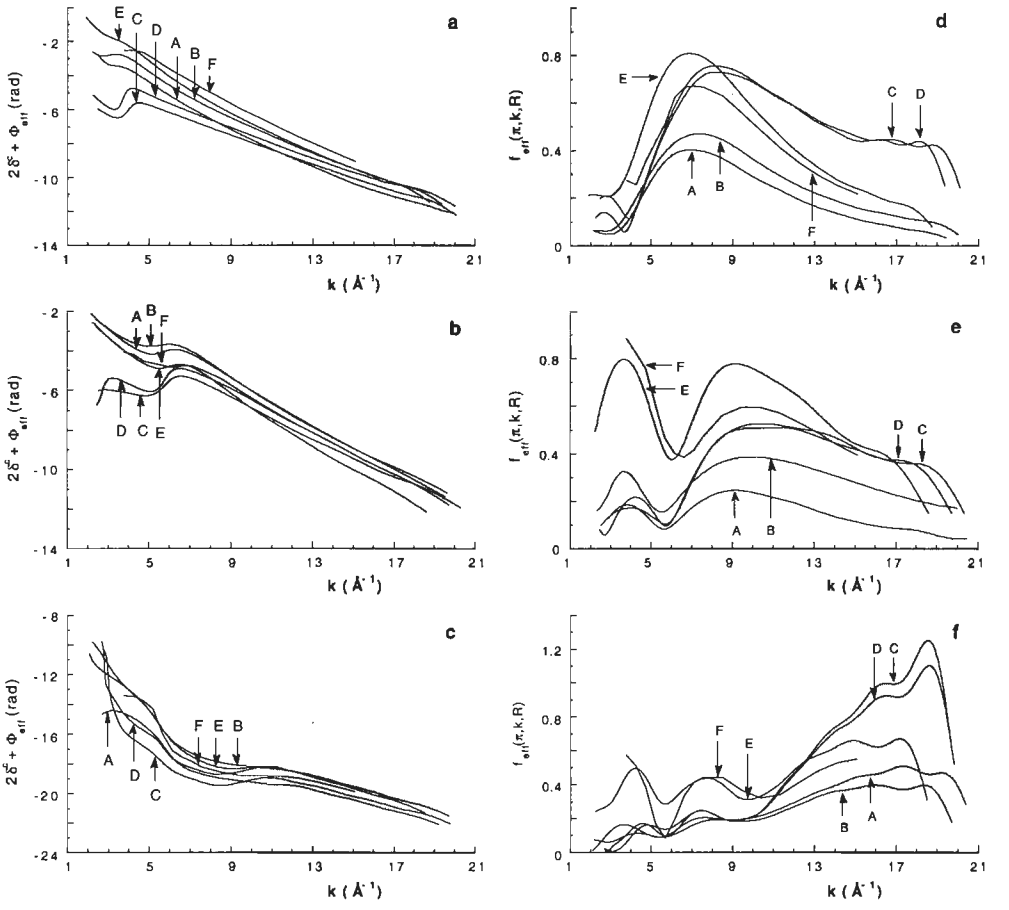

Figure 4 Phases and Backscattering Amplitudes. A) experiment measured at SRS 9.2, B) FEFF, C) EXCURV90, D) MUFPOT, E) McKale et al. F) Teo and Lee. a) phase of copper, b) phase of rhodium, c) phase of platinum, d) backscattering amplitude of copper, e) backscattering amplitude of rhodium, f) backscattering amplitude of platinum.

measured at one synchrotron with phase shift and backscattering amplitude functions extracted from the EXAFS spectrum of the same foil measured under different experimental conditions. The results of these analysis are listed in table 3. There is excellent agreement between the experimental spectra as shown by the very low variance values. The distances are within 0.005 Å of the expected values, whereas both the Debye–Waller factor and the inner–potential shift are very close the expected value of 0.

The coordination numbers of copper and platinum foil deviate less than 0.4 (4 %) from the expected value of 12. The coordination number of 13.6 found in analyzing rhodium foil data measured at SSRL with a reference measured at SRS deviates 30 % from the expected value of 12. This indicates the systematic error that can be

Table 4 Numerical results of the k^1 weighed analysis of copper foil over a k–range of 3.5 – 18.0 $Å^{-1}$. The listed coordination numbers (N_{cor}) have been corrected for the difference in distance between reference and analysis result.

standard	N_{cor}	R (Å)	$\Delta\sigma^2$ ($\times 10^{-5}$ $Å^2$)	ΔE_0 (eV)	k^1 variance
FEFF	11.01	2.542	166	−3.63	1.2
EXCURV90	10.27	2.534	395	13.90	2.3
MUFPOT	10.00	2.527	416	9.27	2.6
McKale et al.	5.57	2.547	68	−9.38	6.2
Teo and Lee	7.73	2.499	220	−7.37	40.7

introduced by higher harmonics. The channel-cut monochromators used in these measurements do not allow any higher harmonics rejection. The critical energy of the SSRL is lower than the critical energy of the Wiggler beamline at SRS, therefore the data measured at SRS contain more higher harmonics. This will result in a too low backscattering amplitude in the reference and consequently a too high coordination number for unknowns analyzed with this backscattering amplitude. The platinum foil data are not affected because detection of higher harmonics was decreased by adjusting the gas-fillings of the ion-chambers.

Phase shifts and backscattering amplitudes

Phase shifts and backscattering amplitudes were extracted from experimental data, FEFF, EXCURV90, and MUFPOT by Fourier filtering, ranges are listed in table 2. The experimental phase shifts and backscattering amplitudes were extracted from the spectra measured at SRS 9.2 for copper and platinum and from the spectrum measure at SSRL 1.5 for rhodium. All theoretical phase shifts and backscattering amplitudes were calculated using the parameters listed in table 1. Phase shifts and backscattering amplitudes as tabulated by Teo and Lee and McKale et al. were generated directly from the tables to maximize the range usable for data-analysis.

Backscattering amplitudes and phase shifts of the experimental data are shown in figure 4 together with their calculated values. The phase shifts of the experimental data are parallel to the phase shifts calculated with the Hedin–Lundqvist exchange

Table 5 Numerical results of the k^1 weighed analysis of rhodium foil over a k–range of 3.5 – 18.0 $Å^{-1}$. The listed coordination numbers (N_{cor}) have been corrected for the difference in distance between reference and analysis result.

standard	N_{cor}	R (Å)	$\Delta\sigma^2$ ($\times 10^{-5}$ $Å^2$)	ΔE_0 (eV)	k^1 variance
FEFF	9.19	2.689	17	−1.88	2.1
EXCURV90	11.15	2.682	186	14.36	2.5
MUFPOT	10.57	2.671	184	12.36	3.2
McKale et al.	3.87	2.721	−84	1.71	3.5
Teo and Lee	3.59	2.691	−183	3.73	9.2

Table 6 Numerical results of the k^1 weighed analysis of platinum foil over a k–range of 3.5 – 18.0 $Å^{-1}$. The listed coordination numbers (N_{cor}) have been corrected for the difference in distance between reference and analysis result.

standard	N_{cor}	R (Å)	$\Delta\sigma^2$ ($\times 10^{-5}$ $Å^2$)	ΔE_0 (eV)	k^1 variance
FEFF	9.37	2.764	–72	–8.09	1.2
EXCURV90	9.88	2.749	106	13.23	6.3
MUFPOT	10.17	2.739	130	6.00	6.1
McKale et al.	3.49	2.769	–176	–8.19	5.4
Teo and Lee	3.07	2.772	–290	–4.80	9.2

potential or the phase shifts derived from the tables of Teo and Lee or the tables of McKale et al. The shift has a maximum value of 2 radians. The phase shifts calculated with the Xα exchange potential have a deviation from the experimental that varies with electron energy. At high energy the agreement is pretty good, but at for k values smaller than 5 $Å^{-1}$ deviations become as large as π. The backscattering amplitudes have the same shape, showing one maximum for copper, two for rhodium and three for platinum. However, the relative amplitude of the maxima is not the same for the experimental data and the theoretical standards. Too high amplitudes at high k values will result in too high Debye–Waller factors. If the relative amplitude of the maxima agrees with the experimental data only a scaling factor is needed.

Comparison of theoretical methods

The comparisons were carried out with k^1 weighed EXAFS spectra to emphasize the differences at low k. Our choice for k^1 weighed comparisons was based on the importance of the low k–region in EXAFS data analysis. Virtually all applications of EXAFS consist of measuring the XAFS of relatively heavy atoms in a matrix of low Z atoms. To determine the contribution of these low Z scatterers analysis of the heavy scatterers in the low k–part of the spectrum has to be accurate. Errors in phase or backscattering amplitude of heavy scatterers at low k will perturb the EXAFS signal at low k and thus results in unreliable results for low Z scatterers. We also carried out k^3 weighed comparisons, differences in such comparisons are much smaller and the obtained parameters more accurate.

To obtain the experimental first shell χ functions that have been analyzed, the spectra plotted in figure 1 were Fourier filtered, table 2 gives the dataranges for the forward and the inverse Fourier transforms. To minimize the influence of Fourier filtering truncation errors on the results of the data-analysis the interval of data-analysis was set to 3.50 – 18.00 $Å^{-1}$, which is the forward Fourier transform range plus at least 0.6 $Å^{-1}$ at the start and minus at least 0.8 $Å^{-1}$ at the end. The phase shifts and backscattering amplitudes plotted in figure 4 were used in the analysis. The structural parameters N, R, $\Delta\sigma^2$ and ΔE_0 were optimized by non-linear least-squares

fitting in k-space.

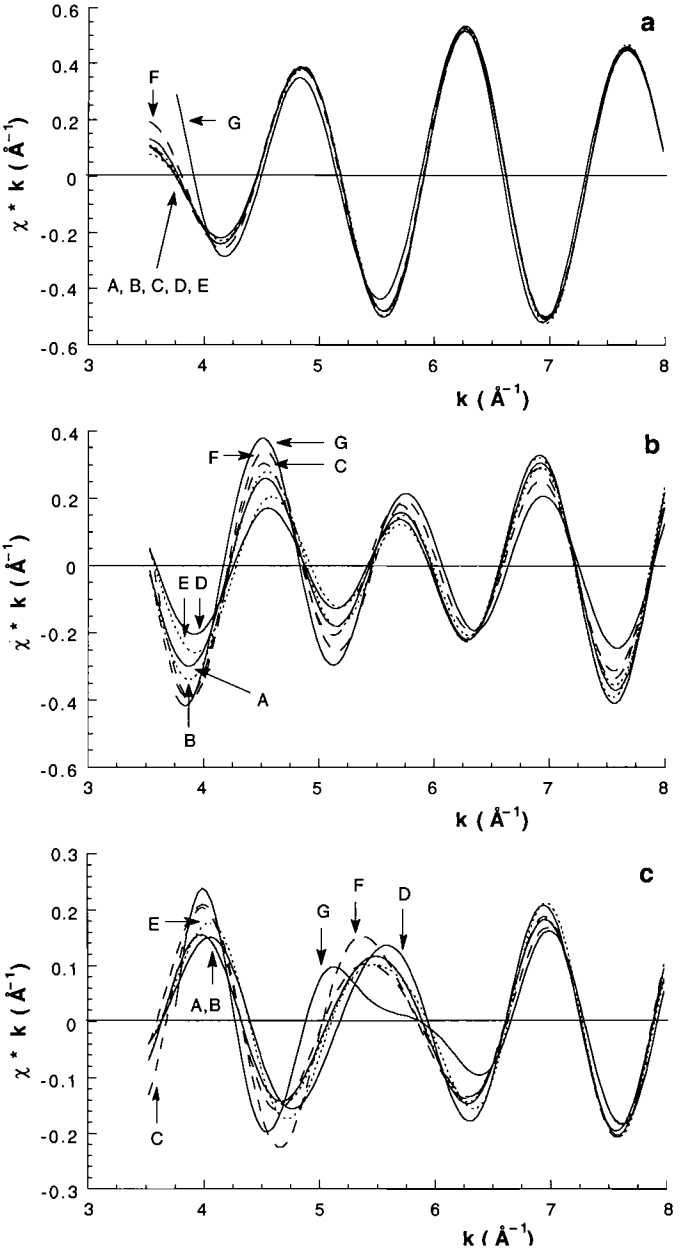

Figure 5 Analysis results (χ functions). A) experimental data, B) experimental reference, C) FEFF, D) EXCURV90, E) MUFPOT, F) McKale et al. G) Teo and Lee, a) copper data measured at SRS 8.1, copper reference measured at SRS 9.2, b) rhodium data measured at SSRL 1.5, rhodium reference measured at SRS 9.2, c) platinum data measured at SRS 9.2, platinum reference measured at SSRL 1.5.

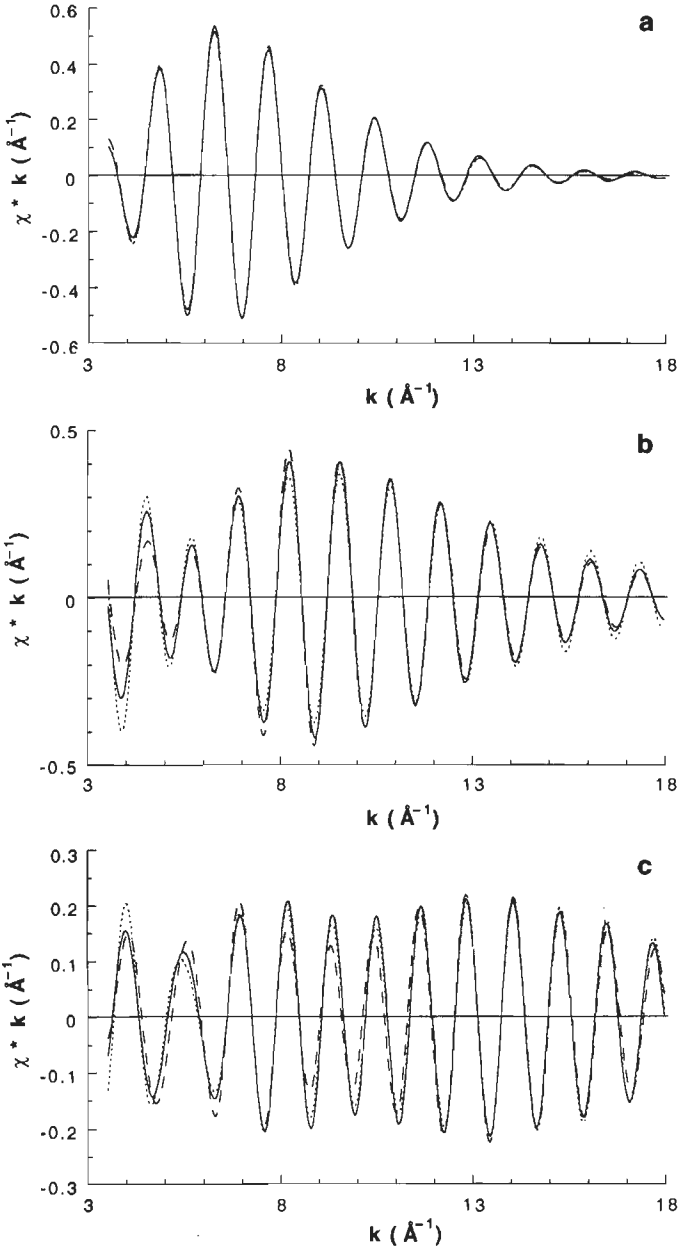

Figure 6 Fit of experimental data (solid line) and a model function calculated with phase shift and backscattering amplitude from FEFF (dotted line) or EXCURV90 (dashed line) a) copper, b) rhodium, c) platinum.

In figure 5 the experimental data are compared to the EXAFS spectra calculated with the Xα or the Hedin–Lundqvist exchange correlation potential over the complete datarange of comparison. Spectra calculated with other theoretical standards have been omitted for clarity. Figure 6 shows the differences between the experimental data and the fits obtained for the different theoretical standards over a shorter data range. Numerical results are listed in tables 4 – 6 for copper, rhodium, and platinum foil respectively.

The copper foil spectra of figure 5a and 6a show that above 4.5 $Å^{-1}$ hardly any differences between the spectra are detectable. Below 4.5 $Å^{-1}$ differences in amplitude of maximum 15 % are evident. The parameters listed in table 17 show that theoretical references refine to a distance of .02 - .04 Å too short. The tables of Teo and Lee refine to a distance 0.06 Å too short. Coordination numbers are as expected from the plots of the backscattering amplitudes with the highest backscattering amplitude giving the lowest coordination number. Variance values in table 4 show that a reference calculated with a Hedin–Lundqvist exchange potential (FEFF) yields the best fit. EXCURV90 and MUFPOT are nearly identical in fit quality. Fit quality achieved with the tables of Teo and Lee is poor.

Results for rhodium foil are plotted in figure 5b and 6b and listed in table 5. By comparing figure 5a and 5b it is evident that the degree of agreement between the different spectra is less for rhodium than for copper. Only above 10 $Å^{-1}$ the differences are very small. Below 10 $Å^{-1}$ the differences in amplitude increase with decreasing k value. Furthermore, below 7 $Å^{-1}$ differences in phase as reflected in the shifted nodes are evident. The determined distances listed in table 5 deviate less than .02 Å of the expected value with exception of the value determined from the McKale et al. tables that deviates almost .04 Å. The obtained coordination numbers are again as expected from the backscattering amplitude plots, but differences are larger than for copper foil. Variance values show that references calculated with a Hedin–Lundqvist or Xα exchange potential (FEFF or EXCURV) yield the best fit. Fit quality of MUFPOT and the tables of McKale et al. is nearly identical. Fit quality achieved with the tables of Teo and Lee falls behind.

Platinum foil results are shown in figure 5c and 6c and table 6. Comparing figure 5c with figure 5b and 5a leads to the conclusion that the differences between the various references are bigger for platinum than for copper or rhodium. Differences in both phase and amplitude are evident below 12 $Å^{-1}$. Only references obtained from calculations with a Hedin–Lundqvist exchange potential give acceptable fits. The determined distances are however within .04 Å of the expected value of 2.774 Å. Coordination numbers reflect the differences in backscattering amplitudes shown in figure 4f. The tables of McKale, EXCURV90 and MUFPOT are nearly identical in fit quality. Fit quality achieved with the tables of Teo and Lee falls behind.

Debye–Waller factors are heavily dependent on the type of phase shift and backscattering amplitude used. Calculations with Xα exchange potentials always yield positive values. Calculations with a Hedin–Lundqvist exchange potential

(FEFF), the tables of McKale et al. and the tables of Teo and Lee result in either positive or negative values with both tabulations giving large deviations in either positive or negative direction.

It has been suggested that the quality of the backscattering amplitude in the tables of McKale et al. and Teo and Lee can be improved by multiplying the backscattering amplitude with an energy dependent mean free path term (4), which at high energies is equal to the constant complex self energy used in EXCURV90 and MUFPOT. The energy (E) is in eV.

$$\exp\left(\frac{2RV_0}{3.9\sqrt{E}}\right) \tag{4}$$

We tested this for the tables of McKale et al. with the same values of V_0 as used in the calculation with the $X\alpha$ exchange potential (table 1). Analysis of the experimental data with these modified backscattering amplitude and the original phase shift resulted in an increase in coordination number (14%) and $\Delta\sigma^2$ and a decrease in variance of 24, 20 and 16% for copper, rhodium and platinum foil respectively.

The normalization procedure in the background subtraction influences the envelope of the obtained χ function. Thus values of the Debye–Waller factor and the coordination number are subject to change. However it has been shown[5] that changing the normalization procedure from step to the "correct" McMaster normalization only affects the values of Debye–Waller factors.

The values for ΔE_0 are also very dependent on the method of calculation. References calculated with a Hedin–Lundqvist exchange potential yields negative values, the $X\alpha$ exchange potential gives rather large positive values, the tables of McKale et al. and the tables of Teo and Lee show inconsistent behaviour. The differences between the various codes are ascribed to the different definition of the energy zero among the theoretical standards. However, changes with element as in the tables of McKale et al. and the tables of Teo and Lee indicate an improper definition of the energy zero.

Errors in obtained parameters due to noise in the experimental data

Due to the low noise level in the experimental data and the large interval used in the data analysis errors in the obtained parameters are very small. Maximum errors calculated from the errors in the data and the correlations between the parameters using standard procedures[15] are as follows: coordination numbers 0.07, distance 0.001 Å, $\Delta\sigma^2$ 4×10^{-5} Å^2, and ΔE_0 0.6 eV.

Statistical significance of differences in fit quality

Although the variance values give an absolute indication of the agreement between experiment and theory, they are not a good criterium to evaluate whether these differences are real or can originate from the statistical errors in the experimental

Table 7 Ratios (column / row) of ε_v^2 values (F values) of models calculated for first shell Cu foil EXAFS. All models, except Teo and Lee, are calculated over a k-range of 3.5 – 18.0 $Å^{-1}$ and a R–range of 1.0 – 3.0 Å. The model based on the tables of Teo and Lee is calculated over a k–range of 3.8 – 15.1 $Å^{-1}$. The 0.95 confidence limit of the F distribution ($F(v_{column}, v_{row}, 0.95)$) is 2.4.

	FEFF	MUFPOT	EXCURV90	McKale et al.	Teo and Lee
experiment	2.1	3.8	4.4	7.7	82.8
FEFF		1.8	2.1	3.6	38.6
MUFPOT			1.2	2.0	21.8
EXCURV90				1.7	18.7
McKale et al.					10.8

data. However, by applying a F–test[16] to the ε_v^2 [6] values of the fits of the EXAFS spectra calculated with different theoretical standards conclusions about the significance of the differences between theoretical methods can be drawn. Tables 7, 8 and 9 show ratios of the calculated ε_v^2 for all fits, the ratios between experimental and theoretical references are included for clarity. Comparison of these ratios with tabulated values of the F distribution indicate that the difference in fit quality is statistically significant in a number of cases. From table 7 (copper foil) it is inferred that phase shift and backscattering amplitude functions calculated with a Hedin–Lundqvist exchange potential are in better agreement with experiment than functions calculated from the tables of McKale et al. or the tables of Teo and Lee. Although theoretical spectra calculated with the Xα exchange potential yield higher variance values in the comparison with experiment than theoretical spectra calculated with a Hedin–Lundqvist exchange potential, they are not large enough to infer that the spectra calculated with a Hedin–Lundqvist exchange potential are in etter agreement with experiment than the spectra calculated with a Xα exchange potential. The ε_v^2 ratios for rhodium foil (table 8) lead to the same conclusion: spectra calculated with either the Xα or the Hedin–Lundqvist exchange potential are in better agreement with experiment than the spectra calculated with either the tables of McKale et al. or the tables of Teo and Lee. There is no statistical significant difference between the spectra calculated with either the Xα or the Hedin–Lundqvist

Table 8 Ratios (column / row) of ε_v^2 values (F values) of models calculated for first shell Rh foil EXAFS. All models, except Teo and Lee, are calculated over a k-range of 3.5 – 18.0 $Å^{-1}$ and a R–range of 1.2 – 3.0 Å. The model based on the tables of Teo and Lee is calculated over a k–range of 3.8 – 15.1 $Å^{-1}$. The 0.95 confidence limit of the F distribution ($F(v_{column}, v_{row}, 0.95)$) is 2.5.

	EXCURV90	FEFF	MUFPOT	McKale et al.	Teo and Lee
experiment	2.3	2.6	3.2	5.4	13.2
EXCURV90		1.2	1.4	2.4	5.8
FEFF			1.2	2.0	5.0
MUFPOT				1.7	4.1
McKale et al.					2.4

Table 9 Ratios (column / row) of ε_v^2 values (F values) of models calculated for first shell Pt foil EXAFS. All models, except Teo and Lee, are calculated over a k-range of 3.5 – 18.0 $Å^{-1}$ and a R–range of 1.0 – 3.0 Å. The model based on the tables of Teo and Lee is calculated over a k–range of 3.8 – 15.1 $Å^{-1}$. Values in parenthesis are the 0.95 confidence limit values of the F distribution ($F(v_{column}, v_{row}, 0.95)$).

	FEFF	McKale et al.	Teo and Lee	MUFPOT	EXCURV90
experiment	20.1 (2.4)	103.4 (2.4)	111.6 (2.7)	112.0 (2.4)	129.1 (2.4)
FEFF		5.1 (2.4)	5.5 (2.7)	5.5 (2.4)	6.4 (2.4)
McKale et al.			1.1 (2.7)	1.1 (2.4)	1.2 (2.4)
Teo and Lee				1.0 (2.5)	1.2 (2.5)
MUFPOT					1.2 (2.4)

exchange potential. For platinum foil (table 9) the spectrum calculated with the Hedin–Lundqvist exchange potential is in better agreement with experiment than any of the other theoretical standards. There is no statistical significant difference between the spectra calculated with either the Xα exchange potential or the tables of McKale et al. or the tables of Teo and Lee. The higher variance values for heavier elements indicate that theoretical calculation of EXAFS spectra of heavy elements is not as accurate as for light elements.

The ratios of the ε_v^2 values of theoretical and experimental references indicate that the ideal experimental references are better than theoretical references. However, the limited availability of such ideal experimental references, means that in practice experimental standards may not be more accurate than theory. Furthermore, for complicated (biological) structures experimental references might not be available at all and therefore theoretical references have to be used.

Conclusion

The variance values found in the quantification of Fourier filtering errors (figure 3) is about an order of magnitude less than the errors found in the comparison of the theoretical standards. Coordination parameters are virtually unaffected by Fourier filtering. Fourier filtering errors can be minimized by using a smaller part of the filtered EXAFS spectrum than the original. Typically the first 1.0 $Å^{-1}$ and the last 0.8 $Å^{-1}$ of the filtered EXAFS spectrum should not be used. From this we infer that Fourier filtering errors have negligible influence on the results of the comparison of theoretical standards as carried out in this paper. Furthermore, Fourier filtering errors will have a very small influence on the structural parameters found in EXAFS data analysis.

Analysis of EXAFS spectra with theoretically obtained phase shifts and backscattering amplitudes will result in accurate distance determinations (±0.03 Å). Other parameters vary with the type of calculation used. To obtain accurate coordination numbers a scaling factor, whose value will depend on the description

of the exchange potential and the treatment of the inelastic losses, is needed. The value of this scaling factor is not transferable from one element to another. Theoretically it is expected that a scaling factor S_0^2 is required to correct the calculations for the decrease in the overlap of the passive electrons between the initial and final states of the absorbing atom. The required scaling factors to correct the coordination numbers are within the expected spread for the *ab initio* calculations.

It appears that the choice of an energy dependent self-energy, as used in FEFF[¥], is the most important consideration, and that the method of potential construction is secondary, at least in monoatomic metals. The use of ground state, Xα, or energy independent exchange, as in the McKale et al. tables or the codes EXCURV90 and MUFPOT is found to be inadequate and leads to large phase and amplitude errors.

References

1. B. K. Teo and P. A. Lee, J. Am. Chem. Soc. **101** (1979) 2815.
2. A. G. McKale, G. S. Knapp and S. -K. Chan, Phys. Rev. B **33** (1986) 841.
3. N. Binsted, S. L. Cook, J. Evans, G. N. Greaves and R. J. Price, J. Am. Chem. Soc. **109** (1987) 3669.
4. SERC Daresbury Laboratory MUFPOT program based on the work described in: J. B. Pendry, *Low energy electron diffraction* (Academic Press, London, 1974).
5. J. Mustre de Leon, J. J. Rehr, S. I. Zabinsky and R. C. Albers, Phys. Rev. B. **44** (1991) 4146.
6. F. W. Lytle, D. E. Sayers and E. A. Stern, Physica B **158** (1988) 701.
7. J. J. Rehr, R. C. Albers, C. R. Natoli and E. A. Stern, Phys. Rev. B **34** (1986) 4350.
8. A. G. McKale, B. W. Veal, A. P. Paulikas, S. -K. Chan and G. S. Knapp, J. Am. Chem. Soc. **110** (1988) 3763.
9. D. C. Koningsberger and D. E. Sayers, Solid State Ionics **16** (1985) 23.
10. J. W. Cook Jr and D. E. Sayers, J. Appl. Phys. **52** (1981) 5024.
11. W. G. Wyckoff, *Crystal Structures* (Interscience, New York, 1974).
12. E. A. Stern, B. A. Bunker and S. M. Heald, Phys. Rev. B **21** (1980) 5521.
13. L. J. Clarke, *Surface crystallography: an introduction to low energy diffraction* (Wiley-Interscience, Chichester, 1985).
14. G. Beni and P. M. Platzman, Phys. Rev. B **14** (1976) 1514.
15. W. H. Press, B. P. Flannery, S. A. Teukolsky and W. T. Vetterling, *Numerical Recipes. The art of scientific computing* (Cambridge University Press, Cambridge, 1989).
16. A. J. Dobson, *An Introduction to generalized linear models.* (Chapman and Hall, 1990)

[¥] EXCURV92 has an option to use an energy dependent self-energy.

Chapter 4
part 1

Pt Clusters in BaKL Zeolite: Characterization by Transmission Electron Microscopy, Hydrogen Chemisorption, and X–ray Absorption Spectroscopy

Abstract

Platinum supported on BaKL zeolite was characterized by transmission electron microscopy (TEM), hydrogen chemisorption, and Extended X–ray Absorption Fine Structure (EXAFS) spectroscopy. The results of all three techniques indicate the presence of highly dispersed platinum in the zeolite pores. There is no evidence of platinum outside the zeolite pores. The EXAFS data determine a Pt–Pt coordination number of 3.7, suggesting that the average platinum cluster in the zeolite consists of 5 or 6 atoms, consistent with the TEM and chemisorption data. The EXAFS data also provide evidence of the platinum–zeolite interface, indicated by Pt–O contributions at 2.14 and 2.70 Å, and a Pt–Ba contribution at 3.8 Å. The Pt/BaKL zeolite is one of the most highly dispersed supported platinum samples and one of the most structurally uniform supported metal catalysts.

Published: M. Vaarkamp, J. van Grondelle, J. T. Miller, D. J. Sajkowki, F. S. Modica, G. S. Lane, B. C. Gates, and D. C. Koningsberger, Catal. Lett., **6** (1990) 369.

Introduction

Platinum supported on L zeolite has been found to be a highly active and selective catalyst for dehydrocyclization of straight–chain paraffins, giving high yields of benzene from n–hexane[1,2,3]. Characterization of these catalysts by techniques including infrared spectroscopy with adsorbed CO[4] and transmission electron microscopy[3] gives evidence that small platinum clusters are incorporated within the intracrystalline pores of the zeolite. Varying fractions of the platinum have also been found outside of these pores in most of the reported catalysts; an exception is that of Rice et al.[5], who used dark-field microscopy to image the clusters in the pores. The reported work raises fundamental questions about the size and electronic structure of the metal clusters, the nature of the metal–zeolite interactions, and the origin of the catalytic selectivity. Some authors[6,7] have attributed the remarkable selectivity to a property of the narrow zeolite pores, but electronic effects may play a role[8], and particle size effects should not be ruled out.

The goal of this research was to characterize the structure of a Pt/L zeolite having virtually all the metal confined to the intracrystalline space. The characterization techniques are extended X–ray absorption fine structure (EXAFS) spectroscopy, transmission electron microscopy (TEM), and hydrogen chemisorption.

Experimental and analytical methods

Preparation of catalyst

The KL zeolite was obtained from Linde and found by analysis to contain 6.4 wt% Al, 11.3 wt% K, and 0.04 wt% Na. The zeolite was ion exchanged with excess aqueous barium nitrate, washed, and dried at 400 K. The resulting Ba–exchanged zeolite was analyzed and found to contain 7.4 wt% Ba. The BaKL zeolite was impregnated with tetraamine platinum (II) nitrate to give a sample containing 1.2 wt% Pt. Prior to any further experiments the sample was reduced at 773 K for 1 h.

Transmission electron microscopy

The electron microscope was a Philips 400T TEM operated at 120 kV with magnifications from 28,000 to 175,000. Further magnification was obtained by enlargement of the negatives. The energy dispersive X–ray (EDX) spectra were obtained with a Tracor Northern 5500 energy dispersive X–ray spectrometer. The prereduced samples were ground to a fine powder, embedded in LR white resin, and sectioned with an ultramicrotome. The thin sections were mounted on copper grids and lightly coated with carbon.

Hydrogen chemisorption

Volumetric hydrogen chemisorption measurements were performed with a

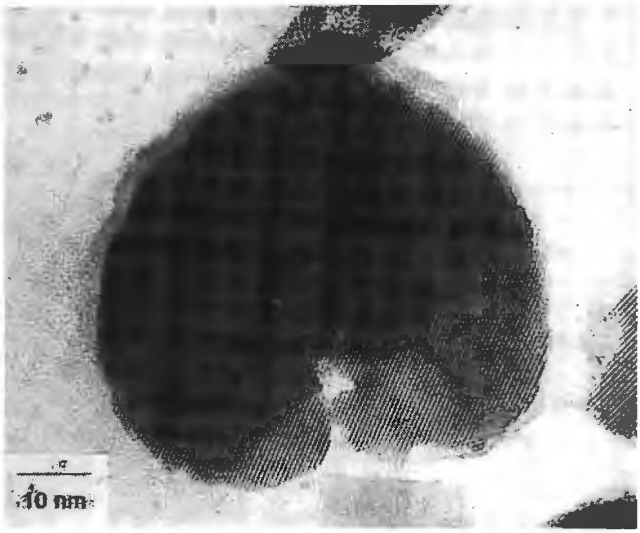

Figure 1 Representative transmission electron micrograph of a 1.2 wt% Pt/BaKL after a reducing pretreatment of the platinum salt. This micrograph shows very small Pt clusters. The lattice images of the zeolite are also evident.

conventional glass system at 298 K. Hydrogen was dried by passage over silica. Before measurement of a chemisorption isotherm, the catalyst sample was treated in flowing hydrogen, it was heated at a rate of 5 K/min to 773 K and held at that temperature for 1h. The sample was then evacuated (10^{-2} Pa) for 1 h at 773 K. After hydrogen admission at 473 K (hydrogen partial pressure = 93 kPa), desorption isotherms were measured at room temperature. The total number of chemisorbed H atoms was obtained by extrapolating the linear high–pressure part of the isotherm to zero pressure. Details are as given elsewhere[9].

EXAFS data collection

The sample was characterized by EXAFS spectroscopy at the Synchrotron Radiation Source in Daresbury, U.K., Wiggler Station 9.2, using a Si (220) double crystal monochromator. The storage ring was operated with an electron energy of 2 GeV and a current between 120 and 250 mA. At the Pt L_{III} edge (11564 eV), the estimated resolution was 3 eV. The monochromator was detuned to 50% intensity to avoid the effects of higher harmonics present in the X–ray beam. The measurements were done in the transmission mode. To decrease low- and high- frequency noise as much as possible, each data point was counted for 1 s and 6 scans were averaged.

The sample was pressed into a self–supporting wafer (calculated to have an absorbance of 2.5) and placed in a controlled–atmosphere cell[10], with the sample handled in the absence of air. The sample was heated at a rate of 5 K/min to 723 K in flowing, purified, and dried hydrogen at atmospheric pressure. The sample was held at this temperature for one additional hour, then cooled to room temperature as

hydrogen flow was continued. The measurements were done with the sample at liquid–nitrogen temperature in the presence of hydrogen at atmospheric pressure.

EXAFS data analysis

Standard procedures were used to extract the EXAFS functions from the absorption spectra[11, 12]. Experimentally determined reference data for the phase shifts and backscattering amplitudes were obtained from EXAFS measurements of platinum foil and $Na_2Pt(OH)_6$[13]. The computer software provided by Mustre de Leon and Rehr[14] was used to calculate the phase shift and backscattering amplitude of the Pt–Ba absorber–backscatterer pair. To determine reliably the parameters characterizing the high–Z (Pt and Ba) and low–Z (O) contributions, multiple–shell fitting in k space and in r space was done, with application of k^1 and k^3 weighing[13]. Further optimization of the fit was done by applying the difference file technique and phase- and amplitude–corrected Fourier transforms[12, 13].

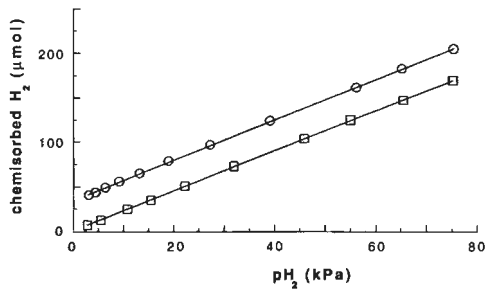

Figure 2 Desorption isotherms of hydrogen for 1.2 wt% Pt/BaKL zeolite (0.867 g, circles) and KL zeolite (0.50 g, squares) at room temperature. Extrapolation by linear least squares fitting of the data of Pt/BaKL gives an H/Pt = 1.3.

Results and discussion

A representative electron micrograph of the L zeolite–supported platinum catalyst is shown in figure 1. The micrographs show zeolite particles with rounded or rectangular cross sections. No large Pt particles were present. In the particles with rectangular cross sections lattice images are evident with spacings of 1.6 nm parallel to the unidirectional channels. At this magnification small platinum particles are evident between the lattice spacings. Only very few platinum particles larger than 2 nm are visible.

EDX spectroscopy was used to analyze several areas of this catalyst. The spectra indicate Si, Al, K, Ba, and Pt, providing evidence that the platinum is present within the interior of the imaged crystallites. Since the platinum particles were not imaged by the electron microscope, we infer that the platinum particles are very small and likely well dispersed in the zeolite crystallites.

The hydrogen adsorption data are plotted in figure 2. There was substantial fysisorption on the zeolite support (with and without Pt). Extrapolation to zero pressure shows that adsorption on the support itself was negligible in this limit; the data of the platinum catalyst yield a value of H/Pt equal to 1.3. This result, consistent with the microscopy data, is indicative of highly dispersed platinum.

The raw EXAFS data for the catalyst following treatment in hydrogen at 723 K are shown in figure 3a. The signal to noise ratio is estimated to be 15 at 4 $Å^{-1}$. A Fourier transform of the data (k^2 weighed, Δk: 2.6 – 12.4 $Å^{-1}$) is shown in figure 3b. The Pt–Pt absorber–backscatterer pair has a nonlinear phase shift and a k–dependent backscattering amplitude. Consequently, it is inferred that there are several peaks in the Fourier transform of a single Pt–Pt contribution[12, 13, 15].

A k^1 weighed Fourier transform was calculated for the EXAFS data characterizing Pt foil (fig. 3c dashed line) and the catalyst (figure 3c solid line). The magnitude of the Pt foil EXAFS function was adjusted until the first–shell Pt–Pt peak in the Fourier transform scaled with the corresponding peak derived from the Pt/BaKL EXAFS data. A comparison of the curves in figure 3c clearly shows the absence of higher Pt–Pt coordination shells in the Pt/BaKL zeolite. This result provides yet another indication of highly dispersed platinum. Moreover, the differences in the Fourier transform (1 < R < 4 Å, both the magnitude and the imaginary part) point to the presence of additional scatterers besides platinum. This can be seen more clearly in a Pt–Pt phase- and amplitude- corrected Fourier transform. The first Pt–Pt peak of the data characterizing Pt foil (figure 3d dashed line) appears as a single symmetrical peak. The peak located at 2.75 Å in the Fourier transform of the EXAFS data

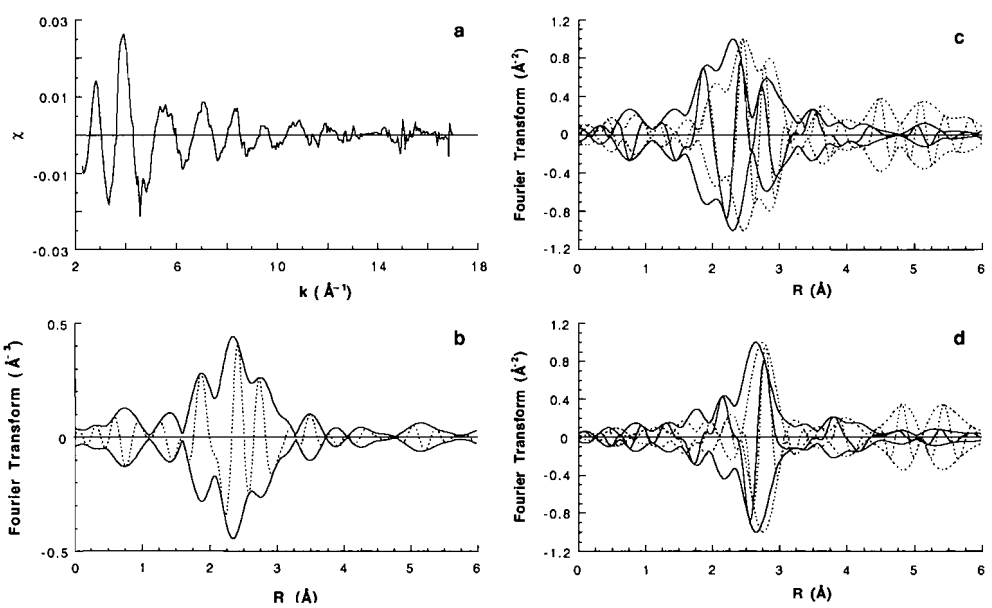

Figure 3 a) EXAFS data for Pt/BaKL zeolite in the presence of hydrogen at liquid nitrogen temperature; b) k^2 -weighed Fourier transform of spectrum a |Δk: 2.6 - 12.4 $Å^{-1}$|; c) k^1-weighed Fourier transform of spectrum a |Δk: 2.6 - 12.4 $Å^{-1}$| (solid line) and k^1-weighed Fourier transform of EXAFS spectrum of Pt foil |Δk: 2.7 - 12.6 $Å^{-1}$| (dashed line) (the latter is scaled to match the amplitude of the former); d) k^1-weighed Pt-Pt phase- and amplitude-corrected Fourier transform of spectrum a |Δk: 3.0 - 12.4 $Å^{-1}$| (solid line) and k^1-weighed Fourier transform of EXAFS spectrum of Pt foil |Δk: 3.1 - 12.6 $Å^{-1}$| (dashed line) (the latter is scaled to match the amplitude of the former).

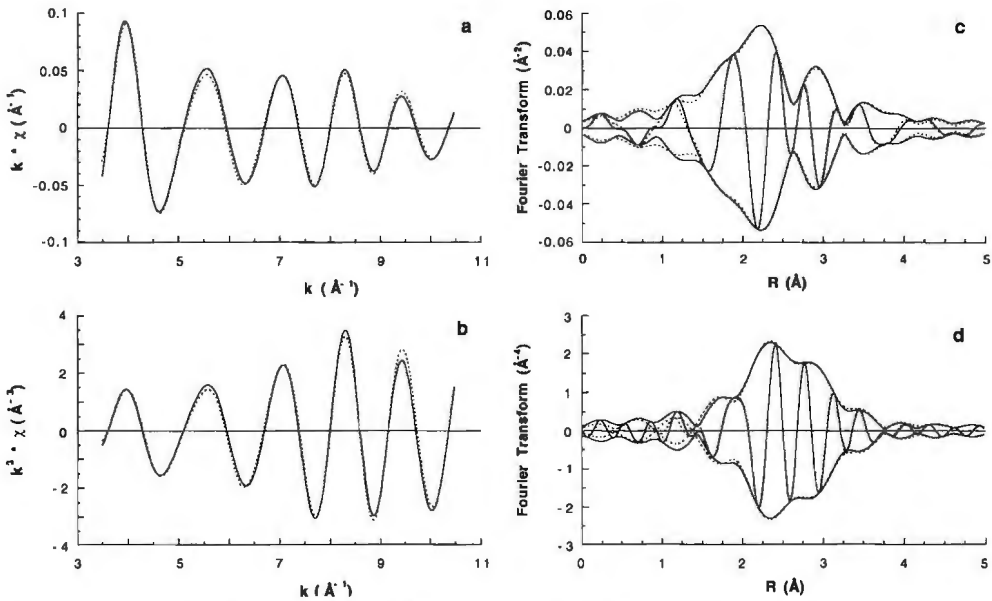

Figure 4 a) k^1-weighed Fourier filtered EXAFS spectrum of Pt/BaKL zeolite (fig. 3a) (solid line) and spectrum calculated with parameters of table 1 (dashed line); b) as in a, but with k^3-weighing; c) k^1-weighed Fourier transform of spectra in fig. 4a |Δk: 3.5 - 10.5 $Å^{-1}$|; d) as in c, but with k^3-weighing.

characterizing the Pt/BaKL catalyst has an asymmetrical magnitude and imaginary part (figure 3d solid line). This is an indication that further confirms the presence of additional scatterers, most probably from the Pt–zeolite interface.

The isolation of the EXAFS contributions giving rise to peaks in the normal Fourier transform between 1 and 5 Å was carried out by applying an inverse Fourier transform (ΔR: 1.1 – 3.8 Å) to the data shown in fig. 3b. First–guess Pt–Pt parameters were obtained by applying a k^3–weighed fit in the range from 6 to 12 $Å^{-1}$ to emphasize the high–Z (viz. Pt-Pt and Pt–Ba) contributions and deemphasize the low–Z contributions (viz. the Pt–zeolite interface). Subtraction of the metal–metal contribution resulted in an EXAFS function which was fitted with contributions characterizing the metal–zeolite interface. An iterative fitting procedure was used to optimize the fits over the whole range of k (3.5 – 10.5 $Å^{-1}$), both in k space and in r space. A comparison of the fit with the raw data in k space and in r space (with both k^1 and k^3 weighing) is shown in figure 4. The agreement is very good.

The result of this fitting is the identification of four significant contributions (table 1), a Pt–Pt contribution at 2.75 Å, a Pt–O contribution at 2.14 Å, a second Pt–O contribution at 2.7 Å, and a Pt–Ba contribution at 3.8 Å. The separate contributions to the EXAFS spectrum are shown in figure 5, both in k space and in r space. The Pt–O phase–corrected Fourier transform of the difference file obtained by subtracting the Pt–Pt and the Pt–Ba contributions from the primary EXAFS (i.e., the inverse Fourier transform of the raw data) is shown in figure 5b. The presence of two Pt–O

Table 1 Structural parameters from EXAFS for 1.2wt% Pt/BaK–LTL reduced at 450°C

Backscatterer	N	R (Å)	$\Delta\sigma^2$ (x 10^{-5} Å^2)	ΔE_0 (eV)
Pt	3.7 ± 0.3	2.75 ± 0.02	32 ± 5	1.4 ± 0.5
O	0.6 ± 0.1	2.14 ± 0.03	67 ± 10	1.8 ± 0.5
O	1.1 ± 0.2	2.71 ± 0.03	95 ± 20	2.1 ± 1
Ba	1.4 ± 0.2	3.76 ± 0.05	90 ± 20	6.6 ± 1

contributions is indicated by beating oscillations in k space (figure 5a). The Pt–Ba contribution is shown in figure 5c, and the Pt–Ba phase–corrected Fourier transform is shown in figure 5d. The results of figure 5c (solid line) show typical high–Z backscattering behaviour.

The number of adjustable parameters used in the fit was 16. The number of statistically allowable adjustable parameters calculated from the forward and the inverse Fourier transform range according to the Nyquist theorem (given in the proceedings of a workshop on standards and criteria in X–ray absorption spectroscopy[16]) is 14. Therefore the appropriateness of the parameters requires

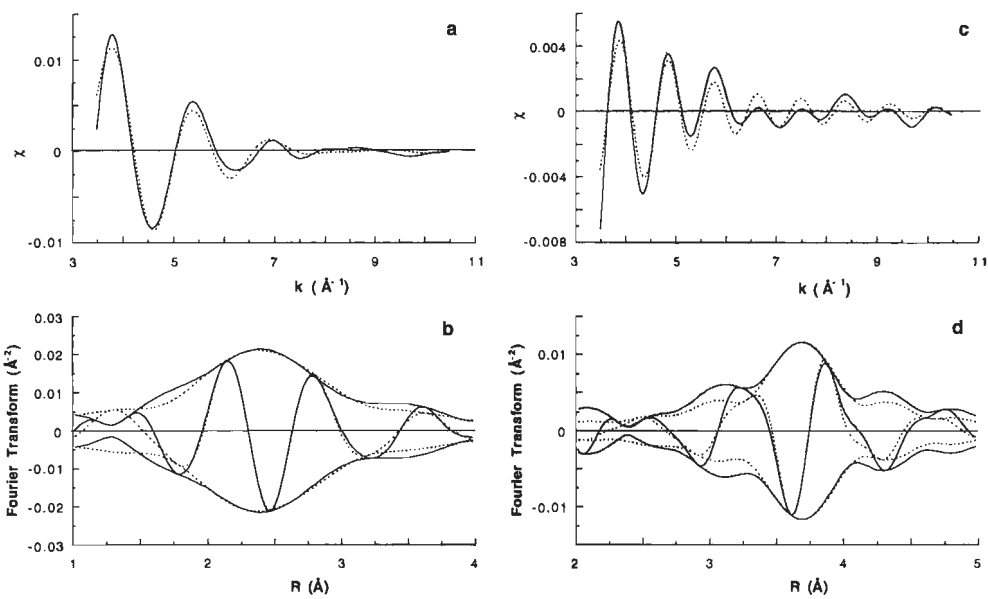

Figure 5 a) Experimental Pt-O contribution, calculated by subtraction of the calculated Pt-Pt and Pt-Ba contributions from the Fourier-filtered EXAFS data (fig. 4a, solid line) (solid line) and calculated Pt-O contributions (dashed line); b) Pt-O phase-corrected k^1-weighed Fourier transform of experimental spectrum a |Δk: 3.5 - 9.0 Å^{-1}| and Pt-O phase-corrected k^1-weighed Fourier transform of calculated Pt-O contributions of spectrum a (dashed line); c) Experimental Pt-Ba contribution, calculated by subtraction of the calculated Pt-Pt and Pt-O contributions from the Fourier-filtered EXAFS data (fig. 4a, solid line) (solid line) and calculated Pt-Ba contributions (dashed line); d) Pt-Ba phase-corrected k^1-weighed Fourier transform of experimental spectrum c |Δk: 3.5 - 10.5 Å^{-1}| and Pt-Ba phase-corrected k^1-weighed Fourier transform of calculated Pt-Ba contribution of spectrum c (dashed line).

further justification. The statistical significance of the Pt–O and Pt–Ba contributions can be assessed by comparison of the amplitude of these EXAFS contributions with the noise present in the raw data. The noise amplitude in the raw data is estimated to be 3×10^{-3} at $k = 12$ Å^{-1}. The amplitude of the calculated Pt–O and Pt–Ba contributions is determined to be 10×10^{-3} and 8×10^{-3} at $k = 4.5$ Å^{-1} (figure 5a and 5c). Since the ratios of the amplitudes of each contribution to the noise is approximately 3, it is inferred that these contributions are statistically significant.

The Pt–Pt coordination number of 3.7 points to extremely small Pt clusters. If there were a bulk–like fcc packing of the Pt atoms in a cluster the results would imply a cluster of 5 or 6 atoms. The absence of higher Pt–Pt coordination shells, combined with the microscopic evidence of the lack of platinum outside the zeolite and the uniqueness of the structure of the intracrystalline zeolite pores, points to a nearly unique cluster size.

Extremely small metal particles covered with chemisorbed hydrogen show metal–metal distances equal to bulk values[12, 15]. This type of behaviour is also observed in this Pt/BaKL sample.

The hydrogen chemisorption data confirm the high dispersion of the platinum. Extrapolation of the correlation between H/Pt and the coordination number determined by EXAFS spectroscopy for Pt supported on γ–Al_2O_3, determined by Kip et al.[9] for a series of samples characterized by different Pt contents and temperatures of treatment in hydrogen, leads to an estimate for the coordination number of 4 for the Pt in zeolite L. This estimate is in agreement with EXAFS results; it has been used to extend the correlation of Kip et al. (figure 6).

The results of the EXAFS analysis (table 1) give evidence of two distinct Pt–O distances. The longer of these (2.7 Å) is virtually the same as that determined earlier by EXAFS spectroscopy for highly dispersed Pt/γ–Al_2O_3[15]. Similar distances have been found by EXAFS spectroscopy for other highly dispersed metals[17 - 20].

In summary, we conclude that the Pt/BaKL zeolite reported here is one of the most highly dispersed platinum samples and one of the most structurally uniform supported metals. The sample consequently offers a unique set of opportunities for resolving some fundamental issues in catalysis by supported metals. Specifically, further data for this catalyst are expected to provide an elucidation of the role of the narrow zeolite pores, in contrast to the size and electronic structure of the small platinum clusters (which are too small to fill the zeolite cage) in accounting for the selectivity of this catalyst[6, 7]. Further, on the basis of the precise

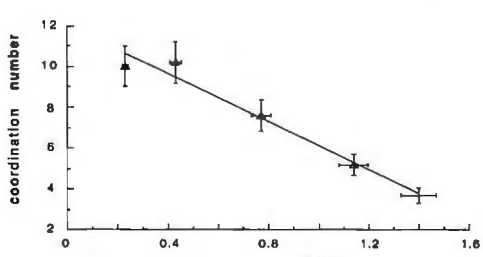

Figure 6 Correlation of hydrogen chemisorption and first-shell Pt-Pt EXAFS coordination number data. Data represented by triangles from Kip et al.[9].

structural characterization of the sample the platinum d–band density of states can now be determined from the white line intensities from the platinum L_{II} and L_{III} X–ray absorption edges. This information is expected to allow progress towards resolution of the fundamental issue of particle size vs. electronic effects in catalysis. In addition, the EXAFS data provide evidence for a Pt–Ba interaction. This interaction might provide experimental opportunities for assessment of the importance of polarization effects, which, on the basis of theoretical results, have recently been suggested to explain the influence of promoter ions on catalytic properties of small metal particles[21, 22]. The smallness of the Pt clusters, combined with the uniformity of the zeolite pores, also indicates an excellent opportunity for precise characterization of the metal–support interface, which may lead to further elucidation of the nature of the interactions between metals and supports.

References

1. J. R. Bernard, *in* "Proc. 5th Int. Zeolite Conf., Napels, Italy, 2-6 June 1980", (L. V. C. Rees, p. 686. Heyden, London, 1980.
2. P. W. Tamm, D. H. Mohr, and C. R. Wilson, *in* "Catalysis 1987", (J. W. Ward, Ed.), p. 335. Elsevier, Amsterdam, 1988.
3. T. R. Hughes, W. C. Buss, P. W. Tamm, and R. L. Jacobson, *in* "New developments in zeolite science and technology. Proc. 7th Int. Zeolite Conf., Tokyo, August 17-22, 1986", (Y. Murakami, A. Iijima, and J. W. Ward, Eds.) p. 725. Elsevier, Amsterdam, 1986.
4. C. Besoukhanova, J. Guidot, D. Barthomeuf, M. Breysse, and J. R. Bernard, J. Chem. Soc, Far. Trans. I, **77** (1981) 1595.
5. S. B. Rice, J. Y. Koo, M. M. Disko, and M. M. J. Treacy, Ultramicroscopy, **34** (1990) 108.
6. E. G. Derouane and D. J. Vanderveken, Appl. Catal., **45** (1988) L15.
7. S. J. Tauster and J. J. Steger, Mat. Res. Soc. Symp. Proc., **111** (1988) 419.
8. G. Larsen and G. L. Haller, Catal. Lett., **3** (1989) 103.
9. B. J. Kip, F. B. M. Duivenvoorden, D. C. Koningsberger, and R. Prins, J. Catal., **105** (1987) 26.
10. F. W. H. Kampers, T. M. J. Maas, J. van Grondelle, P. Brinkgreve, and D. C. Koningsberger, Rev. Sci. Instr., **60** (1989) 2635.
11. J. W. Cook Jr. and D. E. Sayers, J. Appl. Phys., **52** (1981) 5024.
12. J. B. A. D. van Zon, D. C. Koningsberger, H. F. J. van't Blik, and D. E. Sayers, J. Chem. Phys., **82** (1985) 5742.
13. F. W. H. Kampers, PhD. Thesis, Eindhoven University of Technology, Eindhoven, 1989.
14. J. Mustre de Leon, J. J. Rehr, S. I. Zabinsky, and R. C. Albers, Phys. Rev. B., **44** (1991) 4146 - 4156.

15. D. C. Koningsberger and D. E. Sayers, Solid State Ionics, **16** (1985) 23.
16. F. W. Lytle, D. E. Sayers, and E. A. Stern, Physica B, **158** (1988) 701.
17. M. S. Tzou, B. K. Teo, and W. M. H. Sachtler, J. Catal., **113** (1988) 220.
18. K. Möller, D. C. Koningsberger, and T. Bein, J. Phys. Chem., **93** (1989) 6116.
19. F. B. M. van Zon, G. J. Visser, and D. C. Koningsberger, *in* "Proc. 9th Int. Cong. Catal.", (M. J. Philips and M. Ternan, Eds.), The Chemical Institute of Canada, Ottawa, (1988) vol. 3, p. 1386.
20. J. H. A. Martens, R. Prins, and D. C. Koningsberger, J. Phys. Chem. **93** (1989) 3179.
21. W. Ravenek, A. P. J. Jansen, and R. A. van Santen, J. Phys. Chem., **93** (1989) 6445.
22. A. P. J. Jansen and R. A. van Santen, J. Phys. Chem., **94** (1990) 6764.

Chapter 4
part 2

Sulphur poisoning of a Pt/BaK–LTL Catalyst: A Catalytic and Structural Study Using Hydrogen Chemisorption and EXAFS

Abstract

The sulphur poisoning of a Pt/BaK-LTL catalyst has been studied with X-ray Absorption Spectroscopy and hydrogen chemisorption. The fresh catalyst contained highly dispersed platinum inside the zeolite pores. EXAFS analysis determined a Pt-Pt coordination number of 3.7, suggesting an average platinum cluster size of 5 or 6 atoms, consistent with the TEM and chemisorption data (H/Pt=1.4).

The catalyst was poisoned with H_2S until the dehydrocyclization activity of n-hexane decreased to 30% of fresh activity. The first shell Pt-Pt coordination number increased to 5.5, indicating a growth of the average platinum cluster size to 13 atoms. Hydrogen chemisorption measurements of the poisoned catalyst show a decrease in the H/Pt value to 1.0. The EXAFS data also provide evidence for the presence of sulphur adsorbed on the surface of the platinum particles with a Pt-S bond distance of 2.27 Å.

The high sensitivity of the Pt/LTL catalyst to poisoning by very low levels of sulphur is attributed to the loss of active platinum surface by adsorption of sulphur and the growth of the platinum clusters. Much of the available platinum surface was found to be capable of chemisorbing hydrogen, but with no activity for dehydrocyclization. Growth of the platinum particle was sufficient to block the pore. In the sulphur-poisoned catalyst, only the sulphur-free platinum atoms exposed through the pore windows remain active. The evidence suggests the location of the sulphur was at or near the metal-zeolite interface. Since both high activity and selectivity require extremely small platinum particles, regeneration of sulphur-poisoned catalysts will require removal of the adsorbed sulphur and restoration of the original particle size.

Published: M. Vaarkamp, J. T. Miller, F. S. Modica, G. S. Lane, and D. C. Koningsberger, J. Catal., **138** (1992) 675.

Introduction

Platinum supported on LTL zeolite has been found to be a highly active and selective catalyst for dehydrocyclization of straight-chain paraffins, giving high yields of benzene from n-hexane[1,2]. Despite its excellent catalytic properties, this catalyst suffers from a high sensitivity to sulphur poisoning[2]. Therefore, feedstocks with a sulphur content lower than 1 ppm must be used[3]. Several authors have characterized the Pt/LTL catalyst with techniques including IR[4] and TEM[4-6], demonstrating the presence of small platinum clusters incorporated within the pores of the zeolite.

In a recent publication[6] we described a detailed EXAFS study of a Pt/BaK-LTL catalyst. EXAFS analysis determined a Pt-Pt coordination number of 3.7, suggesting that the average platinum cluster in the zeolite consists of 5 or 6 atoms, consistent with TEM and chemisorption data. EXAFS also detects the platinum-zeolite interface, indicated by Pt-O contributions at 2.14 Å and 2.71 Å, and a Pt-Ba contribution at 3.8 Å.

Here we report the results from sulphur poisoning of the same Pt/BaK-LTL catalyst. The objective of this study was to determine the effect of sulphur on the catalyst structure and relate those changes to the catalytic performance. The catalyst was uniformly poisoned with H_2S to a level of 30% of the original activity. The results of our hydrogen chemisorption and EXAFS experiments show that after poisoning, the average platinum particle size increases and that sulphur is bonded to the surface of a metallic platinum particle. In addition to changes in the catalytic activity, sulphur also affects the hydrogenolysis selectivity.

Experimental

Preparation of catalyst

The K-LTL zeolite was obtained from Linde and found by analysis to contain 6.4 wt% Al, 11.3 wt% K, and 0.04 wt% Na. The zeolite was ion-exchanged with 0.6 M barium nitrate for 3 hr at 363 K, washed, and dried at 400 K. The resulting Ba-exchanged zeolite contained 7.4 wt% Ba. The BaK-LTL zeolite was impregnated with tetraamine platinum (II) nitrate to give a sample containing 1.2 wt% Pt. Prior to any further experiments, the sample was reduced at 773 K for 1 hr.

Sulphur poisoning

After reduction, the sample was cooled to room temperature and transferred to a round bottom flask. Small quantities of H_2S in H_2 were added to the gas above the catalyst, and the catalyst was rapidly shaken. Following H_2S addition, the catalyst was rereduced at 773 K. The activity of the poisoned catalyst (n-hexane conversion, described below) was about 30% of fresh activity. Sulphur levels were too low to be

reliably determined by elemental analysis.

Table 1 Dehydrocyclization of n-hexane

	relative activity	benzene selectivity
fresh	1.0	0.90
sulphur-poisoned	0.3	0.85

Hydrogen chemisorption

Volumetric hydrogen chemisorption measurements were performed in a conventional glass system at 298 K. Hydrogen was dried by passage over silica. Before measurement of the chemisorption isotherm, the catalyst samples were rereduced for 1 hr (heating rate, 5 K/min) at 773 K and evacuated (10^{-2} Pa) for 1 hr at 773 K. After hydrogen admission at 473 K (hydrogen partial pressure = 93 kPa), desorption isotherms were measured at room temperature. The amount of chemisorbed H_2 was obtained by linear extrapolation of the high-pressure part of the isotherm to zero pressure. Details are given elsewhere[7].

Catalyst testing

The fresh and sulphur-poisoned catalysts were rereduced at 773 K for 1 hr before testing. Catalytic activity and selectivity for n-hexane conversion were evaluated at 673 K using 2.0 g of catalyst in a fixed-bed, continuous-flow, bench-scale reactor. The reactor was operated at atmospheric pressure under flowing hydrogen at 150 ml/min (measured at room temperature and atmospheric pressure). A syringe pump was used to deliver the n-hexane (99+% purity) at flow rates of 1.5 and 3.4 g/hr, equivalent to 0.75 and 1.7 WHSV, respectively. Catalytic activity and selectivity were measured 30 minutes after reactor temperature and reactant flow rates had stabilized. Product analyses were conducted by off-line gas chromatography using a 1/8" x 6' n-octane on Porasil C column.

EXAFS data collection

The sample was characterized by EXAFS spectroscopy at the Synchrotron Radiation Source in Daresbury, U.K., Wiggler Station 9.2, using a Si (220) double crystal monochromator. The storage ring was operated with an electron energy of 2 GeV and a current between 120 and 250 mA. At the Pt L_{III} edge (11564 eV), the estimated resolution was 3 eV. The monochromator was detuned to 50% intensity to avoid the effects of higher harmonics present in the X-ray beam. The measurements were done in the transmission mode. To decrease low- and high-frequency noise as much as possible, each data point was counted for 1 second and 6 scans were averaged.

The sample was pressed into a self-supporting wafer (calculated to have an absorbance of 2.5) and placed in a controlled-atmosphere cell[8], with the sample handled in the absence of air. The sample was heated at a rate of 5 K/min to 723 K in flowing hydrogen (purified and dried) at atmospheric pressure. The sample was held at this temperature for one additional hour, then cooled to room temperature as hydrogen flow was continued. The measurements were done with the sample at liquid nitrogen temperature in the presence of hydrogen at atmospheric pressure.

EXAFS data analysis

Data reduction. Standard procedures were used to extract the EXAFS data from the measured absorption spectra[9,10]. Normalization was done by dividing the absorption intensities by the height of the absorption edge, the background was approximated by a cubic spline. The final EXAFS function was obtained by averaging the individual background-subtracted and normalized EXAFS functions (6 scans). The standard deviations were calculated for the individual EXAFS data points as a measure of the random error in the final EXAFS function. The EXAFS data analysis is usually performed on an isolated part of the data obtained by an inverse Fourier transformation over a selected range in r-space. The final isolated EXAFS function was obtained by averaging the inverse Fourier transformations of the EXAFS functions. The standard deviation calculated from the individual data points of the isolated EXAFS functions provided a measure of the random error in the average (final) isolated EXAFS function.

Reference Data. Data for the phase shifts and backscattering amplitudes were obtained from EXAFS measurements of reference compounds. Pt foil was used as a reference for the Pt-Pt contributions, $Na_2Pt(OH)_6$ for the Pt-O contributions, and H_2PtCl_6 for the Pt-S contributions. The justification for the use of the latter reference is provided by both theoretical[11] and experimental[12] results. The procedures used to obtain the reference data for Pt foil and $Na_2Pt(OH)_6$ are described elsewhere[13]. The determination of the EXAFS reference data for Pt-S was also straight-forward, as the first-shell peak in the Fourier transform of H_2PtCl_6 shows no overlap with higher shells.

Data Analysis. To reliably determine the parameters characterizing the high-Z (Pt) and low-Z (O, S) contributions, multiple-shell fitting in k-space and in r-space was done, with application of k^1 and k^3 weighing. Further optimization of the fit was done by applying the difference file technique and phase- and amplitude-corrected Fourier transforms[6,10,13].

Results

Catalytic experiments

The reaction network for conversion of n-hexane over Pt/LTL zeolite catalyst is well established[2,14,15]. The formation of benzene from n-hexane is irreversible and occurs via direct 1-6 ring closure. In addition, n-hexane reversibly reacts via 1-5 ring closure to form methylcyclopentane, which can ring-open to form methylpentanes. Hydrogenolysis to light gases (C_1-C_5) also occurs. Methylcyclopentane and the methylpentanes were not considered converted products since they can eventually react back to n-hexane and subsequently to benzene and light gases. Conversion as we have defined it here, therefore, includes only the irreversible reactions, and

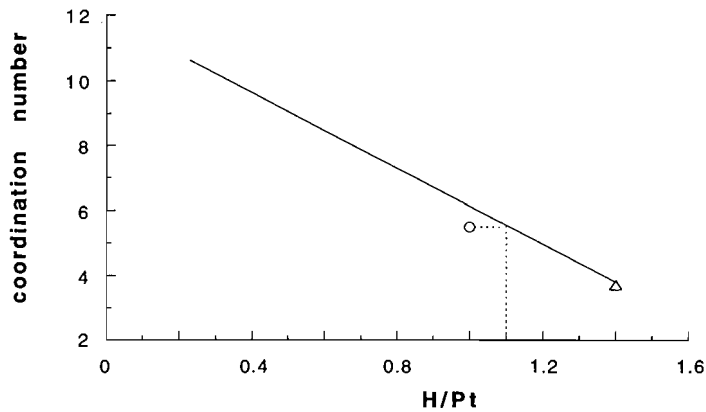

Figure 1 Comparison of hydrogen chemisorption and first-shell Pt-Pt EXAFS coordination number for fresh (triangle) and sulphur-poisoned (circle) Pt/BaK-LTL catalysts. Correlation from Kip et al[7] as extended by Vaarkamp et al[6].

represents the sum of hydrogenolysis products (C_1-C_5) plus 1-6 ring closure (benzene). Selectivity to benzene was defined as the yield of benzene divided by the conversion. Hydrogenolysis selectivity was defined as the yield of C_1-C_5 product divided by the conversion.

The results of the catalyst testing are given in table 1. Relative activity of the fresh catalyst is defined as 1.0. The relative activity of the sulphur-poisoned catalyst has decreased to 0.3. The benzene selectivity decreased from 0.90 to 0.85. The limit of accuracy for the determination of the selectivity is 0.02, indicating a small, but real, effect of sulphur on benzene selectivity.

Hydrogen chemisorption

Extrapolation to zero pressure yields a value of H/Pt of 1.0 (± 0.1) for the sulphur-poisoned catalyst. While the chemisorption method we used systematically gives higher H/Pt values (by about 20%) compared to the conventional procedure[16,17], this method was used in order to enable direct comparison with the correlation of Kip et al.[7]. The hydrogen chemisorption data of the fresh and the sulphur poisoned catalysts are plotted in figure 1 together with a correlation derived from Kip et al. for several Pt/alumina catalysts.

EXAFS data analysis

The raw EXAFS data for the fresh and sulphur-poisoned catalyst are shown in figure 2a. The signal to noise ratio is calculated to be 20 at k=4 $Å^{-1}$ and 2 at k=12 $Å^{-1}$. The larger EXAFS amplitude of the sulphur-poisoned catalyst points to a larger Pt-Pt contribution. The growth of the Pt-Pt contribution of the sulphur-poisoned catalyst is more clearly seen in the Fourier transform (k^1 weighed, Δk: 2.6-12 $Å^{-1}$) of the data (see figure 2b).

The Pt-Pt absorber-backscatterer pair has a non linear phase shift and a

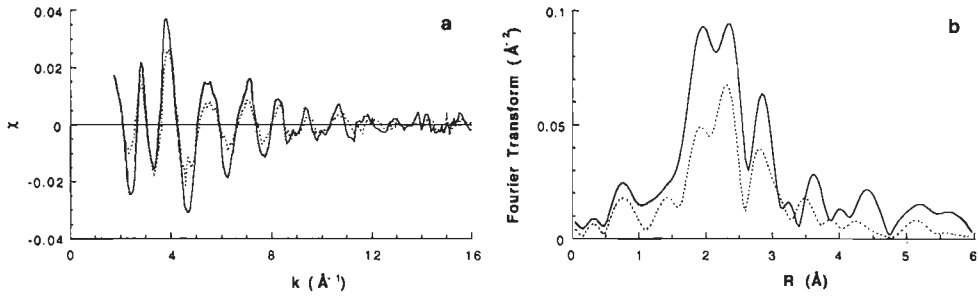

Figure 2 EXAFS spectrum and Fourier transform of the fresh (dashed line) and sulphur-poisoned (solid line) Pt/BaK-LTL catalyst. a) raw EXAFS spectrum; b) Fourier transform (magnitude) $|k^1$, Δk=2.6-12 $Å^{-1}|$

backscattering amplitude which is strongly dependent on k. This leads to the presence of multiple peaks in a normal, uncorrected Fourier transform of a single Pt-Pt contribution, most clearly seen when a normal uncorrected Fourier transform is weighed with k^2 or k^1. Applying a Pt-Pt phase- and amplitude-correction leads to a single symmetrical Pt-Pt peak in the Fourier transform of a single Pt-Pt EXAFS contribution (figure 3).

A Fourier transform with the same weighing and over the same k range was also calculated for the EXAFS data characterizing Pt foil (figure 4, dotted line). The magnitude of the Pt foil EXAFS function was adjusted until the first-shell Pt-Pt peak in the Fourier transform scaled with the corresponding peak derived from the sulphur-poisoned catalyst. A comparison of the Fourier transforms (both Magnitude and Imaginary Parts) in figure 4 clearly shows the presence of higher Pt-Pt coordination shells in the sulphur-poisoned Pt/BaK-LTL zeolite. As expected, the first Pt-Pt peak in a Pt-Pt phase- and amplitude-corrected Fourier transform of the Pt

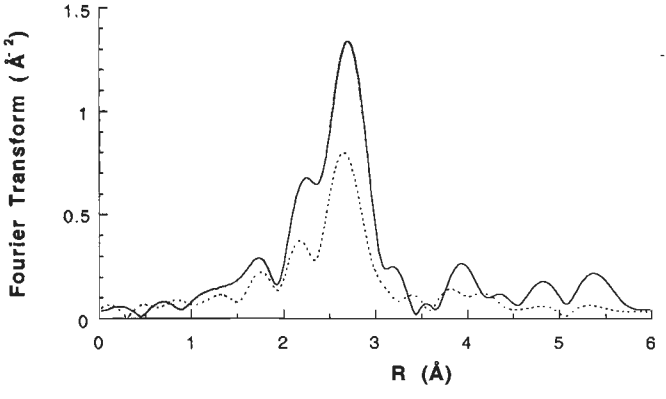

Figure 3 Fourier transform (magnitude) $|k^1$, Δk=3-12 $Å^{-1}$, Pt-Pt phase- and amplitude-corrected] of EXAFS data for fresh (dashed line) and sulphur-poisoned (solid line) Pt/BaK-LTL catalyst.

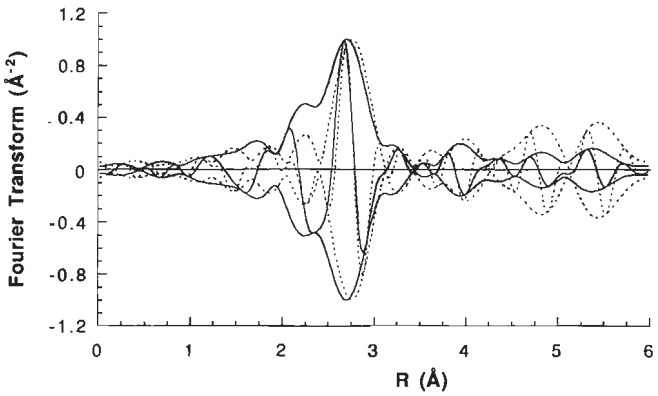

Figure 4 Fourier transform (magnitude and imaginary part) [k^1, Δk=3-12 $Å^{-1}$, Pt-Pt phase- and amplitude-corrected] of EXAFS data for the poisoned Pt/BaK-LTL catalyst (solid line) and Pt foil (dashed line). Both Fourier transforms have been normalized.

foil data (figure 4, dotted line) appears as a single symmetrical peak. The peaks located at 2.75 Å in the Pt-Pt phase- and amplitude-corrected Fourier transforms of the sulphur poisoned sample have asymmetrical magnitudes and imaginary parts. This indicates the presence of additional scatterers besides platinum for both the fresh and sulphur-poisoned catalysts. A full analysis of the EXAFS data of the fresh catalyst showed that the observed differences were due to the presence of neighbouring atoms from the metal-zeolite interface (O and Ba)[6].The differences between the first peaks in the Fourier transforms as shown in figure 4 are caused by the presence of adsorbed sulphur atoms and neighbours from the metal-zeolite interface in the sulphur-poisoned catalyst.

The isolation of the EXAFS contributions giving rise to peaks in the normal Fourier transform between 0.65 and 3.4 Å was carried out by applying an inverse Fourier transform (ΔR: 0.65-3.4 Å) to the data shown in figure 2b. First-guess Pt-Pt parameters were obtained by applying a k^3-weighed fit in the range from 6 to 12 $Å^{-1}$ to emphasize the high-Z (viz. Pt-Pt) contributions and deemphasize the low-Z

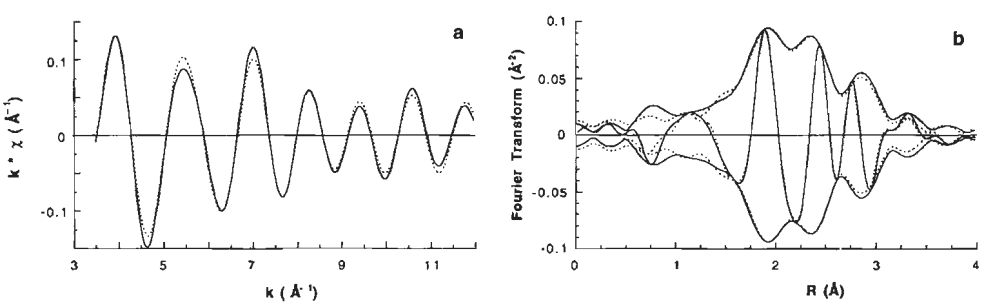

Figure 5 Isolated EXAFS (solid line) and fit (dashed line) for sulphur-poisoned Pt/BaK-LTL catalyst, a) data in k-space; b) Fourier transform [k^1, Δk: 3.5 -12 $Å^{-1}$].

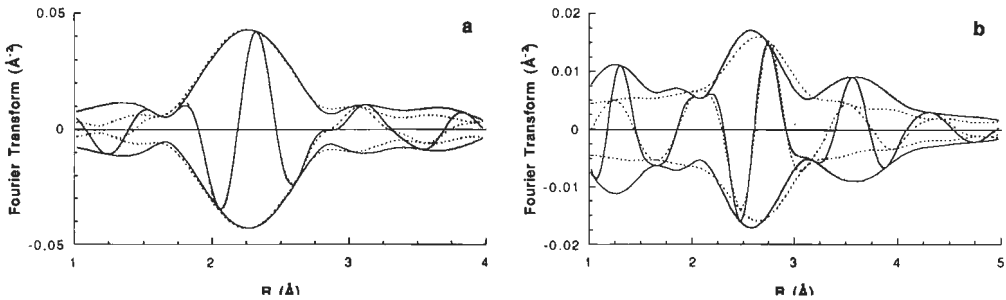

Figure 6 Fourier transform |k^1, Δk: 3.5 -9 $Å^{-1}$| of difference spectra: a) Isolated EXAFS minus the calculated Pt-Pt and Pt-O contributions (solid line) and calculated Pt-S contribution (dashed line) |Pt-S phase-corrected|. b) Isolated EXAFS minus the calculated Pt-Pt and Pt-S contributions (solid line) and calculated Pt-O contribution (dashed line) |Pt-O phase-corrected|.

contributions (viz. sulphur and the Pt-zeolite interface). Subtraction of the metal-metal contribution resulted in an EXAFS function which was fitted with contributions characterizing sulphur and the metal-zeolite interface. An iterative fitting procedure (including all contributions) was used to optimize the fits over the whole range of k (3.5-12 $Å^{-1}$), both in k-space and in r-space (using both k^1 and k^3 weighing). A comparison of the fit with the raw data in k-space and in r-space (k^1 weighing) is shown in figure 5. The result of this fitting is the identification of three significant contributions (2): a Pt-Pt contribution at 2.75 Å, a Pt-O contribution at 2.69 Å, and a Pt-S contribution at 2.27 Å. The separate contributions to the EXAFS

Table 2 Structural parameters from EXAFS with errors[a] for Fresh and sulphur-poisoned Pt/BaK-LTL.

Backscatterer	N	R (Å)	$\Delta\sigma^2$ ($Å^2 \times 10^{-5}$)	ΔE_0 (eV)
Pt				
Fresh	3.7 ± 0.3	2.75 ± 0.02	3.2 ± 0.5	1.4 ± 0.5
sulphur-poisoned	5.5 ± 0.3	2.75 ± 0.01	2.7 ± 0.4	2.4 ± 0.5
O				
Fresh	0.6 ± 0.1	2.14 ± 0.03	6.7 ± 1.0	1.8 ± 0.5
Fresh	1.1 ± 0.2	2.71 ± 0.03	9.5 ± 2.0	2.0 ± 1.0
sulphur-poisoned	1.1 ± 0.3	2.70 ± 0.03	4.0 ± 3.4	4.0 ± 2.0
Ba				
Fresh	1.4 ± 0.2	3.76 ± 0.05	9.0 ± 2.0	6.6 ± 1.0
sulphur-poisoned	—	—	—	—
S				
Fresh	—	—	—	—
sulphur-poisoned	1.2 ± 0.1	2.27 ± 0.01	3.4 ± 0.9	5.0 ± 2.0

[a] Standard deviations for sulphur-poisoned catalyst calculated from the standard deviation at each data point and the correlations between the parameters. Estimates for fresh catalyst were made from estimates of the signal/noise present in the scans.

spectrum are shown in figure 6. The Pt-S phase-corrected Fourier transform of the difference file obtained by subtracting the Pt-Pt and the Pt-O contributions from the primary EXAFS data (i.e., the inverse Fourier transform of the raw data) is shown in figure 6a. The Pt-O contribution is shown in figure 6b.

The resulting coordination parameters obtained for the poisoned catalyst together with the results of the fresh catalyst are given in table 2. The standard deviations given for the sulphur poisoned catalyst are calculated from the covariance matrix including the actual noise obtained for the Fourier filtered EXAFS function as outlined in the experimental section (EXAFS Data Analysis). The value of the goodness of fit (ε_v^2) as defined in the *Report on Standards and Criteria in XAFS Spectroscopy*[18] was 14.7 with twelve fit parameters and 3.9 degrees of freedom.

Discussion

Structural Results

The EXAFS results clearly show growth of the platinum particles after exposure to sulphur. The Pt-Pt coordination number increases from 3.7 to 5.5. A Pt-Pt coordination number of 5.5 represents, for spherical particles, an average cluster size of approximately 8 Å containing 13 platinum atoms. Consistent with the larger particles, the Debye-Waller factor decreases for the sulphur-poisoned catalyst, and higher Pt-Pt shells are observed which were not present in the fresh catalyst. The first shell Pt-Pt distance of 2.75 Å and the distances of the observed higher Pt-Pt shells are consistent with the presence of metallic platinum particles.

In addition to the particle growth, EXAFS clearly shows the presence of sulphur chemisorbed on the outer surface of the platinum particle. The observed platinum-sulphur distance of 2.27 Å is shorter than the distances for bulk PtS (2.31 Å)[19] and PtS_2 (2.40 Å), which is consistent with sulphur chemisorbed on a metallic particle. For example, LEED measurements of sulphur chemisorbed on Ni single crystals indicate that neither bulk nor surface nickel sulphides are formed, and that the Ni-S bond distance is 0.1 to 0.2 Å shorter than observed for Ni_3S_2, NiS_2 and α-NiS[20,21]. Also, a longer Pt-Pt distance at 3.54 Å, such as would be present in bulk PtS_2, is not observed. The measured coordination number of 1.2 indicates that each platinum atom sees, on average, slightly more than one sulphur atom in its first coordination shell. Since sulphur tends to adsorb on platinum faces in hollow sites, this coordination number indicates a surface S/Pt atomic ratio of about 0.4.

The presence of sulphur on the surface of the platinum particles has a pronounced effect on the structure of the platinum zeolite interface: both the Pt-O distances and coordination numbers are affected. In the fresh catalyst two Pt-O distances are observed, one at 2.14 Å and one at 2.71 Å. The distance at 2.14 Å is believed to be due to zero valent, interfacial platinum supported on an oxide

surface. The longer distance of 2.71 Å is believed to be due to the presence of hydrogen between the platinum cluster and the zeolite oxide surface[22,23]. In the sulphur-poisoned Pt/BaK–LTL catalyst, the shorter Pt-O distance of 2.14 Å is no longer observed. In addition, the total Pt-O coordination number decreases from 1.7 in the fresh catalyst to 1.0 for the sulphur-poisoned catalyst. This decrease in the contribution from the platinum-zeolite interface is consistent with an increased platinum particle size. It is also possible that the adsorbed sulphur is at or near the platinum-zeolite interface, reducing the amount of interfacial oxygen atoms in the first coordination shell.

In addition to changes in Pt-O contributions, the Pt-Ba distance observed for the fresh catalyst could not be detected in the sulphur-poisoned catalyst. This result also indicates a lower contribution from the platinum-zeolite interface.

In summary, the sulphur-poisoned catalyst has larger platinum particles than the fresh catalyst. The platinum particle, however, remains metallic in character and does not form platinum sulphide. Rather, the short Pt-S distance determined by EXAFS is consistent with sulphur chemisorbed on the surface of a metallic platinum cluster. Finally, the weakened Pt-O contribution and the absence of a Pt-Ba contribution suggests that the sulphur is located at the metal-zeolite interface.

Chemisorption and catalytic performance

As pointed out above, sulphur poisoning increased the average platinum particle size from 5-6 atoms to about 13 atoms. The fresh catalyst had an average coordination number of 3.7 and an H/Pt of 1.4, while the poisoned catalyst had an average coordination of 5.5 and an H/Pt of 1.0. Based on the previous correlation of particle size and hydrogen chemisorption[6,7], a sulphur-free platinum catalyst with a coordination number of 5.5 would be expected to have a H/Pt value of 1.1 (see dotted line in Figure 1). Thus, of the 0.4 H/Pt difference between the fresh and sulphur-poisoned catalyst, 0.3 H/Pt can be attributed to the particle growth. Only the remaining 0.1 H/Pt is due to coverage by sulphur. This difference is at or near the experimental accuracy of the technique. Assuming sulphur occupies a three-fold coordination site[24,25], the first shell Pt-S coordination number of 1.2 corresponds to about 0.4 sulphur atoms per surface platinum atom. Thus, while the EXAFS results show that the sulphur is chemisorbed on the platinum surface, nearly all of the surface platinum atoms remain capable of chemisorbing hydrogen.

With a Pt-S coordination number of 1.2, one might expect the catalyst to have little or no activity. However, since 30% of the fresh activity remained, it is clear that much of the platinum surface is not poisoned by sulphur. The unexpectedly high hydrogen chemisorption, coupled with the higher than expected activity, strongly suggests that sulphur is not evenly distributed over the platinum surface, but rather, is concentrated at or near the metal-zeolite interface, leaving most of the exposed platinum surface unpoisoned. The location of the sulphur at the metal-zeolite interface is also consistent with the observed weakening of the Pt-O and Pt-Ba

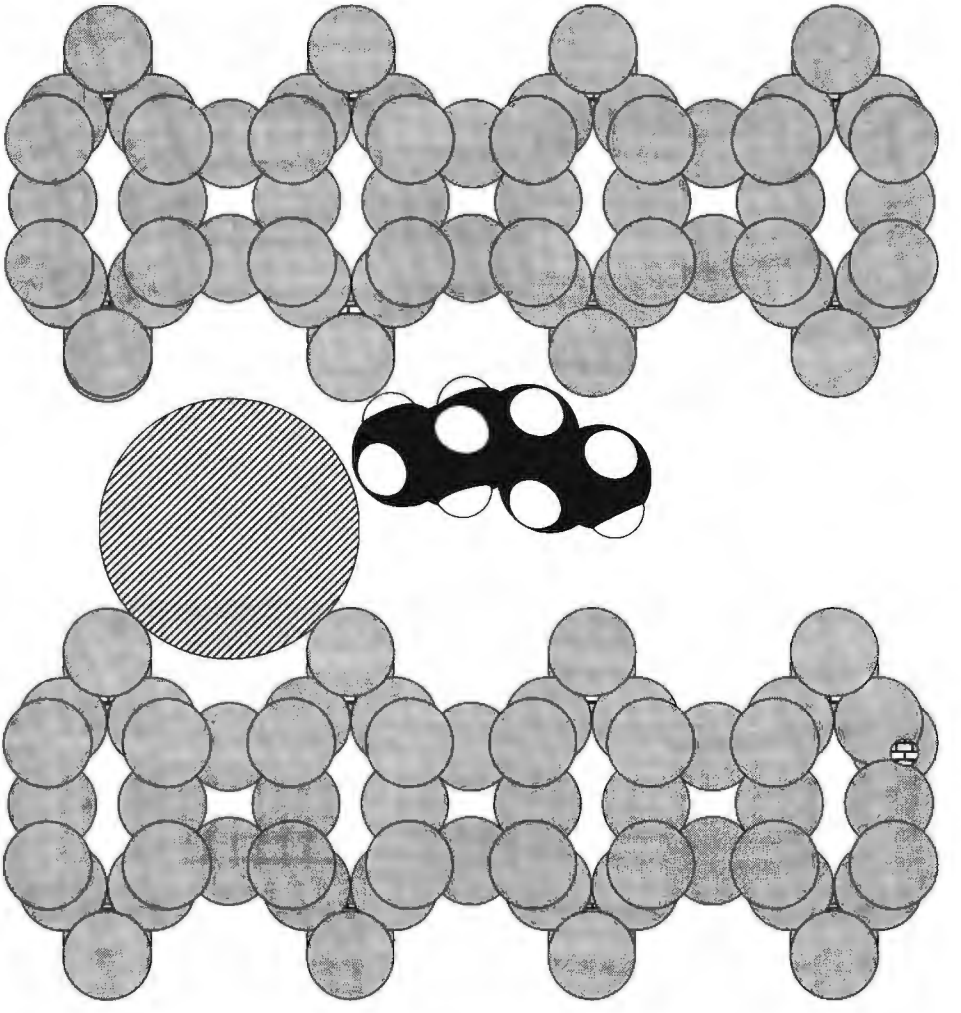

Figure 7 Molecular model of LTL zeolite channel (parallel to c-axis) containing simplified platinum cluster of 8 Å diameter. Sulphur and zeolite cations omitted for clarity. Molecule of n-hexane shown to scale.

interactions detected by EXAFS.

While the available platinum surface (as measured by hydrogen chemisorption) decreased by only 25%, the catalytic activity decreased by 70%. Therefore, a large fraction of the platinum surface remains capable of chemisorbing hydrogen, but is inactive for hexane dehydrocyclization. Although ensemble size effects cannot be ruled out, these results suggest that the larger platinum particles may partially block the zeolite channels. A 13-atom cluster is approximately 8 Å in diameter, nearly filling the zeolite channel (11 Å at its widest point) (see figure 7). It is evident from figure 7 that the space between the platinum particle and the opposite wall of the

zeolite channel is large enough to allow chemisorption of hydrogen to the platinum surface atoms but too small to admit the larger hexane molecule.

While there was a large decrease in catalytic activity, the selectivity to benzene decreased from 0.90 for the fresh catalyst to 0.85 in the sulphur-poisoned catalyst. Selectivity to light gases (C_1-C_5), i.e. hydrogenolysis selectivity, increased from 0.10 in the fresh catalyst to 0.15 in the sulphur-poisoned catalyst - a 50% increase in hydrogenolysis selectivity due to sulphur poisoning. Hydrogenolysis is well-known to be a structure sensitive reaction (the specific activity is particle size dependent)[26,27]. The observed increase in hydrogenolysis selectivity may, therefore, be attributed to the increase in the platinum particle size. This, in turn, implies a larger ensemble requirement for hydrogenolysis as compared to dehydrocyclization. Thus, as the particle size grows, larger ensembles are formed, favouring hydrogenolysis over dehydrocyclization. It is worth noting that sulphur-poisoning of large metallic particles generally results in a **decrease** in hydrogenolysis selectivity, generally attributed to the loss in the number of large, unpoisoned ensembles[28,29]. However, suppression of hydrogenolysis by sulphur passivation has been reported only for catalysts with much larger metallic particles.

Conclusions

Poisoning of Pt/BaK-LTL catalysts by sulphur results in a growth in the platinum particles. Bulk platinum sulphides are not formed - the platinum remains metallic with surface chemisorbed sulphur. Sulphur also appears to disrupt the metal-zeolite interface and the evidence suggests preferential location of sulphur at the metal-zeolite interface. Backscattering contributions from the zeolite surface oxygen are reduced and barium contributions are no longer observed. Also, the long Pt-O contribution due to interfacial hydrogen is no longer observed. The disruption of the platinum-zeolite interface by sulphur may also contribute to the observed growth in the platinum particle size.

The extreme sensitivity of Pt/LTL catalysts to poisoning by low levels of sulphur appears to be due, at least in part, to the growth of the platinum particles. Poisoning of the platinum surface by sulphur appears to be qualitatively similar to poisoning by sulphur in non-zeolitic catalysts. The promotion of particle growth by sulphur provides an additional means by which active metal surface is lost. As the platinum particle size approaches the size of the zeolite channel, much of the platinum surface is no longer accessible to reactants.

The growth of the platinum particle also effects the reaction selectivity. Hydrogenolysis selectivity increases on the larger particles, resulting in lower benzene selectivity.

The results of this study indicate that successful regeneration of sulphur-poisoned Pt/LTL catalysts requires both the removal of sulphur from the catalyst and

restoration of the original small platinum particle size. At the same time, the platinum particles must remain within the zeolite channels.

References

1. J. R. Bernard, *in* "Proc. 5th Int. Zeolite Conf., Napels, Italy, 2-6 June 1980", (L. V. C. Rees, Ed.) p. 686. Heyden, London, 1980.
2. T. R. Hughes, W. C. Buss, P. W. Tamm, and R. L. Jacobson, *in* "Proc. 7th Int. Zeolite Conf., Tokyo, August 17-22, 1986", (Y. Murakami, A. Iijima, and J. W. Ward, p. 725. Elsevier, Amsterdam, 1986.
3. W.C. Buss, L.A. Field, and L.C. Robinson, US patent 4,456,527 (1984).
4. C. Besoukhanova, J. Guidot, D. Barthomeuf, M. Breysse, and J. R. Bernard, JCS, Far. Trans. I, **77** (1981) 1595.
5. S. B. Rice, J. Y. Koo, M. M. Disko, and M. M. J. Treacy, Ultramicroscopy, **34** (1990) 108.
6. M. Vaarkamp, J. T. Miller, D. J. Sajkowski, F. S. Modica, G. S. Lane, B. C. Gates, J. van Grondelle, and D. C. Koningsberger, Catal. Lett., **6** (1990) 369.
7. B. J. Kip, F. B. M. Duivenvoorden, D. C. Koningsberger, and R. Prins, J. Catal., **105** (1987) 26.
8. F. W. H. Kampers, T. M. J. Maas, J. van Grondelle, P. Brinkgreve, and D. C. Koningsberger, Rev. Sci. Instr., **60** (1989) 2635.
9. J. W. Cook Jr. and D. E. Sayers, J. Appl. Phys., **52** (1981) 5024.
10. J. B. A. D. van Zon, D. C. Koningsberger, H. F. J. van't Blik, and D. E. Sayers, J. Chem. Phys., **82** (1985) 5742.
11. B. K. Teo and P. A. Lee, J. Am. Chem. Soc., **101** (1979) 2815.
12. B. J. Lengeler, J. Phys., Colloq, **C8(1)** (1986) 75.
13. F. W. H. Kampers, PhD Thesis, Eindhoven University of Technology, Eindhoven, 1989
14. G. S. Lane, F. S. Modica, and J. T. Miller, J. Catal., **129** (1991) 145.
15. P. W. Tamm, D. H. Mohr, and C. R. Wilson, *in* "Catalysis 1987, (J. W. Ward, Ed.) p. 335. Elsevier, Amsterdam, 1988.
16. G. Larsen and G. L. Haller, Catal. Lett., **3** (1989) 103.
17. D. J. Ostgard, L. Kustov, K. R. Poeppelmeier, and W. M. H. Sachtler, J. Catal., **133** (1992) 342.
18. F. W. Lytle, D. E. Sayers, and E. A. Stern, Physica B, **158** (1988) 701.
19. W. Heegemann, K. H. Meister, E. Bechtold, and K. Hayek, Surf. Sci. **49** (1975) 161.
20. J. E. Demuth, D. W. Jepsen, and P. M. Marcus, Phys. Rev. Let. **32** (1974) 1182.
21. P. M. Marcus, J. E. Demuth, and D. W. Jepsen, Surf. Sci. **53** (1975) 501.
22. F. W. H. Kampers and D. C. Koningsberger, Faraday Discuss. Chem. Soc., **89** (1990) 137.
23. M. Vaarkamp, J. van Grondelle, R. A. van Santen, J. T. Miller, F. S. Modica, G. S.

Lane, and D. C. Koningsberger, *in* "Proc. of the 9th Int. Zeolite Conf., Montreal, July 5-10, 1992", Butterworth-Heinemann, London, in print.
24. C. H. Bartholomew, P. K. Agrawal, and J. R. Katzer, Adv. Catal., **31** (1982) 135.
25. G. A. Martin, Catal. Rev. - Sci. Eng **30** (1988) 519.
26. M. Boudart and G. Djega-Mariadassou, "Kinetics of Heterogeneous Catalytic Reactions" (J.M. Prausnitz, L. Brewer, Eds.), Princeton University Press, 1984
27. M. Che and C. O. Bennett, Adv. Catal., **36** (1989) 55.
28. J. C. Hayes, R. T. Mitsche, E. L. Pollitzer, and E. H. Homeier, Preprints Div.Petr. Chem. ACS, Los Angeles, **19** (1974) 334.
29. V. K. Shum, J. B. Butt, and W. M. H. Sachtler, J. Catal. **96** (1985) 371.

Chapter 5
part 1

Hydrogen Temperature Programmed Desorption (H_2 TPD) of Supported Platinum Catalysts

Abstract

H_2 TPD of supported platinum catalysts, Pt/K-LTL, Pt/H-LTL, Pt/K-MAZ, Pt/H-MAZ, Pt/γ-Al_2O_3 and Pt/SiO_2, was performed after 300, 450 or 650°C reduction. For all catalysts, reversible desorption of chemisorbed hydrogen occurred at approximately 175°C. In addition to chemisorbed H_2, at least three higher temperature, irreversibly desorbed H_2 peaks were observed and assigned to spilled-over hydrogen. The quantity of spilled-over hydrogen is related to the number of support hydroxyl groups which is, in turn, determined by support acidity and the maximum reduction temperature of the catalyst. It is suggested that the irreversibility of the spilled-over hydrogen results from dehydroxylation of the support at high temperature.

The structure of Pt/K-LTL and Pt/H-LTL catalysts has been determined by EXAFS following reduction at 300, 450 and 600°C. After low temperature reduction, a layer of spilled-over hydrogen is present between the platinum particle and the support. The distance of the platinum from the support (oxide) surface is ca. 2.6-2.7 Å. During high temperature reduction, or during the TPD, this interfacial hydrogen is irreversibly lost and the platinum distance is decreased to 2.2 Å. Loss of interfacial hydrogen may correspond to one or more peaks in the TPD.

The catalysts' TOF for propane hydrogenolysis was dependent on both reduction temperature and the type of support. Platinum on acidic supports and reduced at the lowest temperature displayed the highest TOF. Qualitatively, the catalysts' hydrogenolysis activity increased with increasing amounts spilled-over hydrogen.

Submitted for publication: J. T. Miller, B. L. Meyers, F. S. Modica, G. S. Lane, M. Vaarkamp, and D. C. Koningsberger.

Introduction

The effect of reduction temperature on catalytic behaviour has been the subject of numerous investigations. Many studies have shown both reduced catalytic activity[1-5] and reduced hydrogen chemisorption capacity[1,7-10] after reduction in hydrogen at high temperatures (>500°C). However, a clear understanding of the phenomena involved is still lacking. Reduction at high temperatures may result is strongly chemisorbed hydrogen,[2] may result in the loss of spilled-over hydrogen altering the local charge transfer from the support to the metal at the particle boundary,[4] may induce changes in morphology of the metal crystallite,[6] or may affect reduction of the support resulting in the formation of an alloy with atoms from the support, for example, Al or Ti.[1,7,8]

Temperature programmed desorption of hydrogen from supported and unsupported platinum, typically, shows multiple peaks above 100°C[2,3,8-11]: one at low temperature (ca. 150°C) which is assigned to chemisorbed hydrogen on the metal surface,[11] and one or more higher-temperature peaks (ca. 300-500°C). These high temperature peaks have been assigned by various authors to spilled-over hydrogen,[4,9,13] to strongly chemisorbed hydrogen,[2,3,12] to hydrogen in subsurface layers of the platinum,[10] or to oxidation of the reduced metal by support protons.[14,15]

In this study, the H_2 TPD spectra of platinum catalysts on acidic and non-acidic supports have been determined. In addition to reversibly chemisorbed hydrogen, at least three high temperature, irreversibly desorbed hydrogen peaks were detected. Based on the EXAFS structural characterization of the Pt/K-LTL and Pt/H-LTL catalysts reduced at 300, 450 and 600°C, the assignment of the high temperature hydrogen desorption peaks is proposed. Propane hydrogenolysis TOF of the catalysts indicate that the specific activity is affected by both the support acidity and the reduction temperature.

Experimental

Catalyst preparation

The preparation of the zeolite catalysts are described elsewhere.[16,17] Briefly, the K-LTL was a commercial zeolite obtained from Union Carbide (now UOP). Excess alkali was reduced by water wash until the pH of the wash solution was 9.5 to give a K/Al molar ratio of 1.05 (elemental analysis: 11.8 wt% K and 7.7 wt% Al). Na-omega (MAZ) was synthesized following reported methods[18] and calcined at 540°C for 16 h prior to potassium exchange. The K-exchanged zeolite given a final washed with dilute KOH at a pH of 9.5. The K-MAZ had a K/Al molar ratio of 1.08 (elemental analysis: 11.0 wt% K and 7.0 wt% Al).

An H-LTL was prepared by ammonium-exchange K-LTL. The K/Al molar ratio was 0.34. The H-MAZ was prepared by ammonium-exchange of Na-MAZ (with template). Following calcination, H-MAZ contained 8.6 wt% Al and 106 ppm Na.

The SiO_2 was a commercial support (obtained from PQ Corporation) with a surface area of 215 m^2/g and a pore volume of 1.0 cc/g. K-SiO_2 was prepared by washing the silica with dilute KOH until the pH remained 9.5. The K-SiO_2 contained 0.38 wt% K.

To each zeolite (or silica), platinum was impregnated using an aqueous solution of tetraammine platinum (II) nitrate. Typically, the platinum loading was 1.5 to 2.0 wt% for catalysts analyzed by TPD while the loading was 1.2 wt% for the catalysts analyzed by EXAFS. The platinum/zeolite catalysts were dried at 120°C. The silica catalysts were calcined at 260°C.

A 1.0 wt% Pt/γ-Al_2O_3 catalyst was prepared by impregnation of γ-Al_2O_3 (200 m^2/g and 0.6 cc/g) with an aqueous solution of H_2PtCl_6. The catalyst was dried at 120°C.

H_2 Temperature Programmed Desorption (TPD)

H_2 TPD was performed on catalysts after an initial 300, 500 or 650°C reduction. Desorptions were programmed at 10°C per minute to 700°C in flowing N_2. The H_2 and N_2 were purified by passing over oxygen and hydrocarbon traps. Cryogenic traps containing 5A molecular sieve were placed directly before, and after, the furnace for water trapping. Desorbed gases were monitored by a thermal conductivity detector and periodically checked by independent gas chromatographic or mass spectroscopic analysis for H_2.

Following the first TPD, the catalyst was re-reduced in H_2 for 1h at 700°C (or cooled to 300°C and re-reduced at 300°C) and cooled to room temperature in H_2. A second H_2 TPD to 700°C was obtained as described above.

For H-LTL, after an initial TPD to 700°C the catalyst was cooled to room temperature in N_2. H_2 was then pulsed (0.066 cc H_2/pulse) over the catalyst at 40°C until no further H_2 was consumed. The carrier gas was switched to 20% H_2 (in N_2) and a temperature programmed reduction to 700°C obtained.

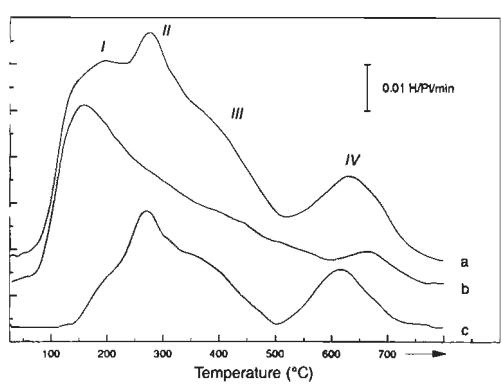

Figure 1 2.0% Pt/K-LTL a.) reduced at 300°C, cooled in H_2 and TPD to 700°C, H/Pt=1.8, b.) following the 1st TPD, the catalyst was re-reduced at 700°C, cooled in H_2 and 2nd TPD to 700°C, H/Pt=1.2, and c.) difference profile: 1a minus 1b, H/Pt=0.6.

Propane hydrogenolysis

The conversion of propane was conducted at 400°C and atmospheric pressure in a fixed-bed, bench-scale reactor using 3.78 vol.% propane in H_2. The reaction temperature of 400°C was the lowest temperature at which all catalysts gave

measurable propane conversion. The catalyst (0.01 to 0.2 g) was diluted with 2 g of α–alumina and prereduced at 450°C or 600°C. The conversion was adjusted to between 2 and 10% by changing the propane space velocity. The turnover frequencies (TOF) were determined on the basis of volumetric hydrogen chemisorption.

EXAFS

The EXAFS data were collected at the Synchrotron Radiation Source in Daresbury, U. K., Wiggler Station 9.2 using a Si (220) double crystal monochromator. The monochromator was detuned to 50% intensity to minimize the higher harmonics present in the X-ray beam. The storage ring was operated with an electron energy of 2 GeV and a current between 120 and 250 mA. The estimated resolution at the Pt L_{III} edge (11564 eV) is 3 eV. Self-supporting wafers (calculated to have an absorbance of 2.5) were reduced at 300, 450 (500) or 600°C in a controlled-atmosphere cell.[19] Samples were cooled with liquid nitrogen to -130°C, and the data were collected in the presence of H_2. Measurements were made in transmission mode, and in order to reduce the noise, six scans were averaged. Standard procedures were used to extract the EXAFS data from the measured absorption spectra.[20] The spectra were fitted with phase and amplitude functions extracted from the spectra of reference compounds.[21]

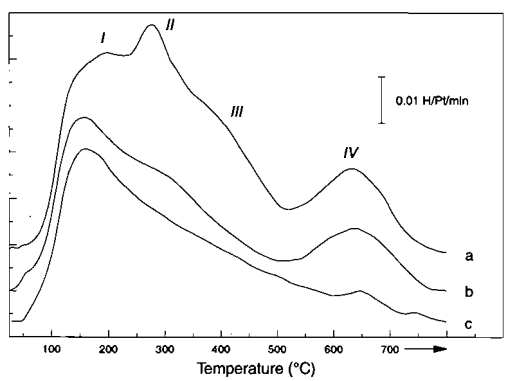

Figure 2 2.0% Pt/K-LTL reduced at a.) 300°C, H/Pt=1.8, b.) 500°C, H/Pt=1.2, and c.) 650°C, H/Pt=1.1, cooled in H_2 and TPD to 700°C.

Results

Hydrogen Temperature Programmed Desorption (H_2 TPD)

H_2 TPD profiles were obtained for six platinum catalysts, 2.0% Pt/K-LTL, 1.5% Pt/H-LTL, 2.0% Pt/K-MAZ, 1.5% Pt/H-MAZ, 1.0% Pt/γ-Al_2O_3 and 3.3% Pt/SiO_2. The characteristic features of the hydrogen desorptions were determined, primarily, by the support acidity and reduction temperature; therefore, a detailed discussion of the TPD spectra are presented only for the Pt/K-LTL and Pt/H-LTL catalysts.

A representative H_2 TPD profile for platinum supported on a non-acidic support is shown in Figure 1a for 2.0% Pt/K-LTL reduced at 300°C. Broad, overlapping desorptions of H_2 are observed at about 150 (peak I) and 275°C (peak II) with some H_2 desorbing up to 400°C (peak III). In addition, there is a distinct desorption at 610°C (peak IV). The total H_2 desorption was 1.8 hydrogen atoms/platinum atom (H/Pt).

Immediately after the first TPD, the catalyst was re-exposed to H_2 at 700°C for one hour and cooled in flowing H_2 and a second TPD obtained. The second TPD, Figure 1b, revealed only peak I with minor amounts of hydrogen desorbed at higher temperature. The total hydrogen desorption in the second TPD amounted to 1.2 H/Pt. Thus only peak I is reversible, while, the higher temperature peaks (II-IV) are irreversible. The area of peak I (1.0 H/Pt) is in reasonable agreement with the amount of hydrogen chemisorption determined volumetrically (0.97 H/Pt). Subtracting Figure 1b from Figure 1a yields Figure 1c, which represents the irreversible hydrogen desorptions. Figure 1c clearly shows the presence of peaks II and III in the 200-500°C region, in addition to peak IV at 610°C. The measured N_2 micropore volume and surface area of the K-LTL zeolite was unchanged after the TPD experiment, indicating that there was no change in the crystallinity of the zeolite. Volumetric H_2 chemisorption declined only slightly, from 0.97 H/Pt in the fresh catalyst to 0.84 H/Pt after the first TPD, indicating only a small change in the platinum dispersion during the TPD experiment.

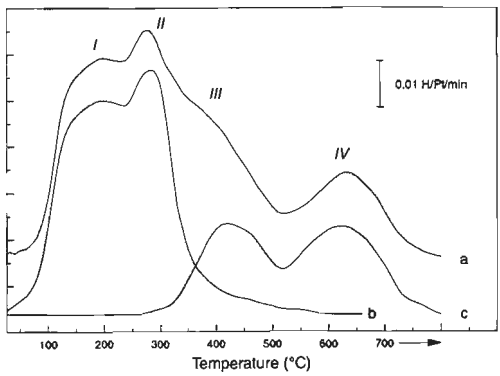

Figure 3 2.0% Pt/K-LTL reduced at a.) 300°C, cooled in H_2 and TPD to 700°C, H/Pt=1.8, b.) 300°C, cooled in H_2 and TPD to 300°C and held at 300°C for 1 hour, H/Pt=1.2, and c.) sample in Figure 3b was cooled in N_2 and TPD to 700°C, H/Pt=0.6.

The effect of increasing reduction temperature on the TPD profiles is shown in Figure 2 for Pt/K-LTL reduced at 300, 500 and 650°C. Reduction at higher temperatures progressively diminishes the total amount of hydrogen desorbed, from 1.8 H/Pt after 300°C reduction to 1.3 H/Pt after 500°C reduction and 1.1 H/Pt after 650°C reduction. After reduction at 500°C, the irreversible peaks below 500°C are absent, eg., peaks II and III, but the H_2 desorption at 610°C (peak IV) is little changed. After reduction at 650°C, only the peak I remains. The spectra in Figure 2 support the conclusion that the peak I corresponds to reversibly chemisorbed hydrogen, and the high temperature hydrogen desorptions are irreversible.

To investigate the possibility of exchange between the various forms of hydrogen identified by the TPD, a two-part TPD was performed. A fresh sample of Pt/K-LTL was reduced at 300°C, and the TPD was conducted, programming only to 300°C, and holding at this temperature for 1 h (profile in Figure 3b). The sample was cooled to room temperature under N_2 flow, and a second TPD to 700°C was done (Figure 3c). The catalyst was not exposed to hydrogen between the two TPD measurements. Total hydrogen desorption was 1.2 H/Pt in the low temperature (ambient-300°C) TPD and 0.6 H/Pt in the second TPD, for a total of 1.8 H/Pt, which is in agreement with the 1.8 H/Pt obtained in a single TPD, i.e., Figure 3a. The absence of peak I and

II in the second TPD indicates that there is no exchange of hydrogen between the low temperature (<300°C) sites and the higher temperature sites. For example, after removal of the reversibly chemisorbed hydrogen in the low temperature TPD, hydrogen does not migrate from the high temperature sites back to the platinum surface and desorb at low temperature during the second TPD.

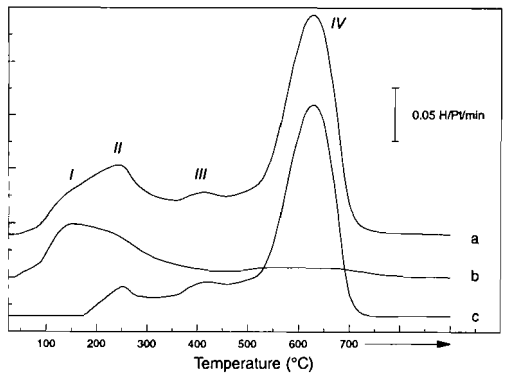

Figure 4 1.5% Pt/H-LTL reduced at a.) 300°C, cooled in H_2 and TPD to 700°C, H/Pt=4.3, b.) following the 1st TPD, the catalyst was re-reduced at 700°C, cooled in H_2 and 2nd TPD to 700°C, H/Pt=1.3, and c.) difference profile: 4a minus 4b, H/Pt=3.0.

The TPD profiles for 1.5% Pt/H-LTL (Figure 4) show desorption peaks at temperatures similar to those obtained for the Pt/K-LTL catalyst, but differing in the size of those peaks. Prominent in the spectra of Pt/H-LTL is the large desorption for peak IV at 625°C. The total hydrogen desorbed is 4.3 H/Pt. Following the first TPD, only peak I (H/Pt = 1.3) with minor amounts of higher temperature H_2 is observed in the second TPD. For comparison the volumetric hydrogen chemisorption of Pt/H-LTL reduced at 300°C was 1.10 H/Pt. As observed for Pt/K-LTL, peak I corresponds to reversibly, chemisorbed hydrogen, while higher temperature peaks represent irreversible hydrogen desorptions.

As observed for Pt/K-LTL, increasing reduction temperature results in a decrease in the size of the irreversible desorption peaks below the reduction temperature. For example, after reduction at 500°C, Figures 5b, the hydrogen desorption from peaks II and III are absent and much of the hydrogen associated with peak IV has been diminished. The total hydrogen desorption of Figure 5b is 2.6 H/Pt. After reduction at 650°C, only the peak I is present, Figure 5c, with a total desorption of 1.2 H/Pt.

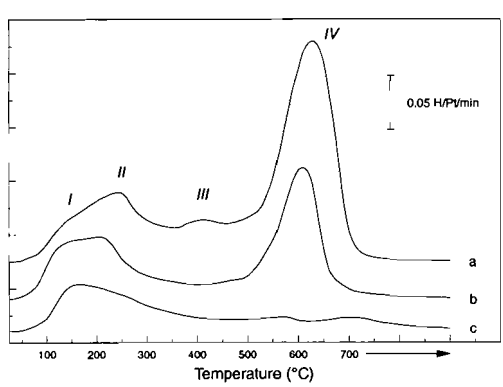

Figure 5 1.5% Pt/H-LTL reduced at a.) 300°C, H/Pt=4.3, b.) 500°C, H/Pt=2.6, and c.) 650°C, cooled in H_2 and TPD to 700°C, H/Pt=1.2.

A two-part TPD was also conducted with the Pt/H-LTL catalyst using the same procedure above as described for Pt/K-LTL (Figure 6). Total hydrogen desorption was 1.1 H/Pt in the low temperature (ambient-300°C) TPD and 3.3 H/Pt in the second TPD, for a total of 4.4 H/Pt, which is in agreement with the 4.3 H/Pt obtained in a single TPD, i.e., Figure 6a. As observed for Pt/K-LTL, the two-part TPD indicates that

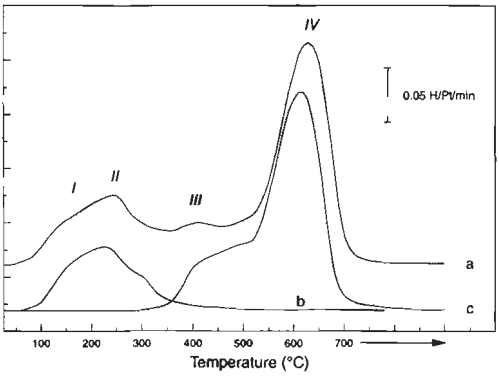

Figure 6 1.5% Pt/H-LTL reduced at a.) 300°C, cooled in H_2 and TPD to 700°C, H/Pt=4.3, b.) 300°C, cooled in H_2 and TPD to 300°C and held at 300°C for 1 hour, H/Pt=1.1, and c.) sample in Figure 6b was cooled in N_2 and TPD to 700°C, H/Pt=3.3.

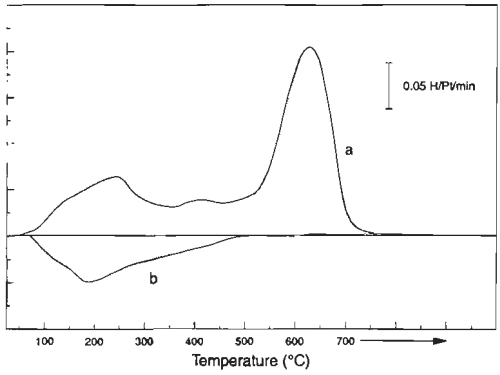

Figure 7 1.5% Pt/H-LTL reduced at a.) 300°C, cooled in H_2 and TPD to 700°C, H/Pt=4.3, b.) following the 1st TPD, the catalyst was cooled in N_2 to 40°C, H/Pt=0.88, and pulsed with hydrogen until saturation (not shown); TPR in 20% H_2/80% N_2 to 700°C; desorption=0.91 H/Pt.

there is no exchange of hydrogen between the low temperature (<300°C) sites, peaks I and II, and the higher temperature sites, peaks III and IV.

High temperature hydrogen desorptions in the TPD have been reported in the literature as being due to oxidation of the metal by support protons.[14,15] In order to evaluate this possibility, a fresh sample of Pt/H-LTL was subjected to a H_2 TPD to 700°C (Figure 7a). Following the TPD, the sample was cooled in N_2 to 40°C and pulsed with H_2. The quantity of hydrogen consumed at 40°C was 0.88 H/Pt. Subsequent temperature programmed reduction (TPR) of this sample up to 700°C (Figure 7b) resulted in the **desorption** of hydrogen equal to 0.91 H/Pt in reasonable agreement with the volumetric hydrogen chemisorption. In addition, the peak desorption temperature during the TPR (185°C) was similar to desorption temperature for chemisorbed hydrogen (175°C) in the TPD. If the high temperature desorptions in the TPD represent reversible oxidation of platinum, then the amount of hydrogen consumed in the pulsed reduction /chemisorption should have been approximately 4.3 H/Pt as observed in the TPD. The quantity of hydrogen consumed during the pulsed chemisorption, however, is only 0.9 H/Pt and is consistent

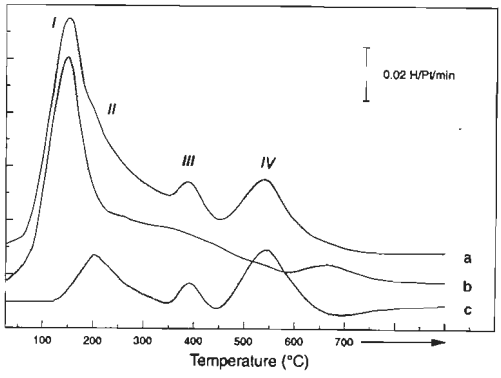

Figure 8 2.0% Pt/K-MAZ reduced at a.) 300°C, cooled in H_2 and TPD to 700°C, H/Pt=1.9, b.) following the 1st TPD, catalyst was re-reduced at 700°C, cooled in H_2 and 2nd TPD to 700°C, H/Pt=1.3, and c.) difference profile: 8a minus 8b, H/Pt=0.6.

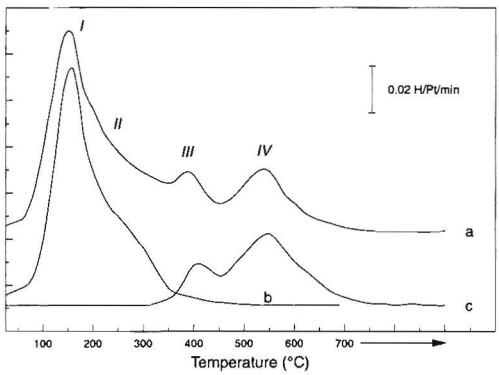

Figure 9 2.0% Pt/K-MAZ reduced at a.) 300°C, cooled in H_2 and TPD to 700°C, H/Pt=1.9, b.) 300°C, cooled in H_2 and TPD to 300°C and held at 300°C for 1 hour, H/Pt=1.3, and c.) sample in Figure 9b was cooled in N_2 and TPD to 700°C, H/Pt=0.6.

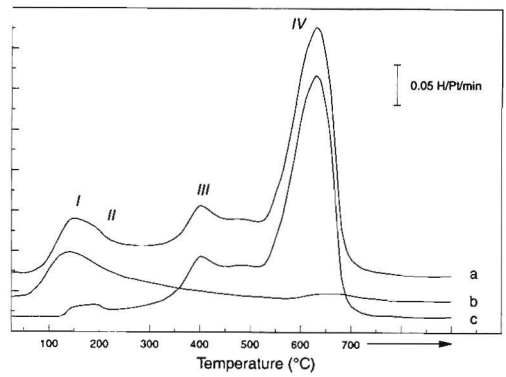

Figure 10 1.5% Pt/H-MAZ reduced at a.) 300°C, cooled in H_2 and TPD to 700°C, H/Pt=5.6, b.) following the 1st TPD, catalyst was re-reduced at 700°C, cooled in H_2 and 2nd TPD to 700°C, H/Pt=1.4, and c.) difference profile: 10a minus 10b, H/Pt=4.2.

with chemisorbed hydrogen. Thus, the high temperature hydrogen desorptions in the TPD are not a result of oxidation of platinum by support protons.

In summary, the H_2 desorptions for Pt/K-LTL and Pt/H-LTL are qualitatively similar, but the quantity of irreversible hydrogen, peaks II-IV, is significantly higher for Pt/H-LTL. In addition, for both catalysts, the hydrogen present on the low temperature (<300°C) sites and the higher temperature sites do not readily exchange, and the quantity of irreversibly desorbed H_2 decreases with increasing reduction temperature.

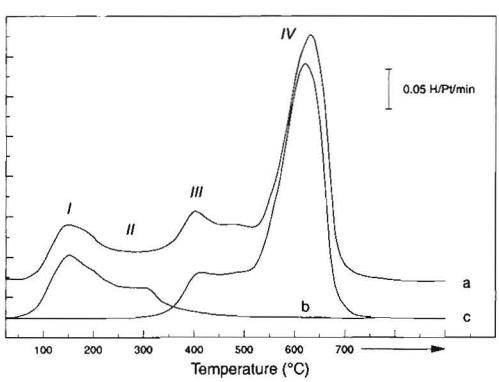

Figure 11 1.5% Pt/H-MAZ reduced at a.) 300°C, cooled in H_2 and TPD to 700°C, H/Pt=5.6, b.) 300°C, cooled in H_2 and TPD to 300°C and held at 300°C for 1 hour, H/Pt=1.4, and c.) sample in Figure 11b was cooled in N_2 and TPD to 700°C, H/Pt=4.0.

The H_2 TPD profiles of 2.0% Pt/K-MAZ and 1.5% H-MAZ are shown in Figures 8 to 11. The profiles are similar to those for Pt/K-LTL and Pt/H-LTL, although the total hydrogen desorptions were slightly higher. For Pt/K-MAZ the total hydrogen desorption was equivalent to 1.9 H/Pt, compared to 1.7 H/Pt for Pt/K-LTL. Hydrogen desorption from Pt/H-MAZ was 5.6 H/Pt, compared to 4.3 H/Pt for Pt/H-LTL. For both catalysts, peaks II-IV are absent during a second TPD (Figures 8b and 10b), and results for the two-part TPD (Figures 9b,c and 11b,c) indicate that hydrogen from the higher temperature sites does not exchange with the lower temperature sites.

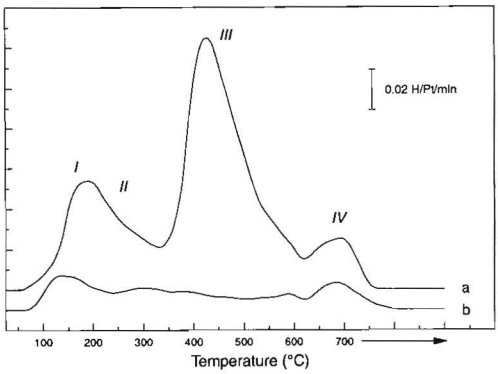

Figure 12 1.0% Pt/γ-Al_2O_3 reduced at a.) 300°C, cooled in H_2 and TPD to 700°C, H/Pt=3.6, b.) following the 1st TPD, catalyst was re-reduced at 700°C, cooled in H_2 and 2nd TPD to 700°C, H/Pt=0.6.

Hydrogen TPD for platinum on amorphous supports also shows multiple high temperature desorption peaks similar to those observed with zeolite supports. The H_2 TPD of 1.0% Pt/γ-Al_2O_3 reduced at 300°C (Figure 12a) displays three peaks centred at around 180°C (peak I), 420°C and 700°C. As with the zeolite supports, the low temperature peak corresponds to hydrogen chemisorbed on the platinum surface, and its size is consistent with the amount of chemisorbed H_2 measured volumetrically (H/Pt = 0.94). Some sintering of the platinum particles is apparent, as the size of the chemisorption peak is diminished in the repeat TPD (Figure 12b). Pt/alumina appears similar to the other acidic supports, in that the total H_2 desorption is large (3.6 H/Pt). However, unlike the zeolite supports, the largest peak (1.9 H/Pt) is observed near 400°C, while the highest temperature peak is small.

The H_2 TPD profile of 3.3% Pt/SiO_2 reduced at 300°C is given in Figure 13. The peaks in this profile are much less distinct, but a chemisorption peak at 150°C (peak I) and a higher temperature desorption at 550°C can be clearly seen.

Deuterium labelling

Hydrogen TPD profiles were obtained on Pt/K-LTL, Pt/H-LTL and Pt/γ-Al_2O_3 reduced at 300°C in D_2. In these experiments, the desorbed hydrogen was detected by mass spectrometry. The TPD profiles were identical to those presented above (Figures 1a, 4a and 12a) and all of the peaks for each catalyst were D_2. H_2 was not detected.

Additionally, Pt/H-LTL was reduced at 300°C in H_2 for one hour. At 300°C, the reducing gas was switched to D_2 for 30 minutes and cooled to ambient temperature in D_2. In the subsequent TPD, all of the desorptions were D_2 with only traces of H_2 or HD detected.

EXAFS

A full EXAFS analysis of Pt/K-LTL and Pt/H-LTL is presented elsewhere.[22] The Pt-Pt phase and amplitude corrected k^3-weighed Fourier transform of the

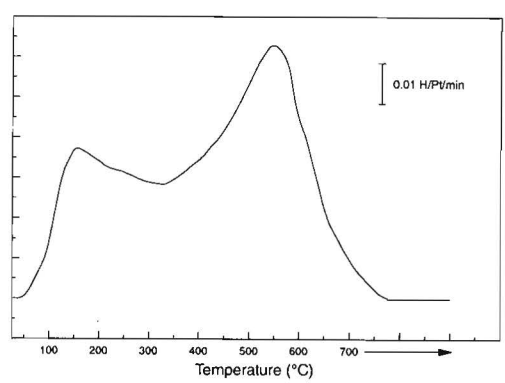

Figure 13 3.3% Pt/SiO_2 reduced at 300°C, cooled in H_2 and TPD to 700°C.

Table 1 Structural parameters from EXAFS for Pt/K-LTL.

Backscatterer	T_{red} (°C)	N	R (Å)
Pt	300	4.0	2.74
	450	4.8	2.74
	600	4.9	2.75
O	300	1.4	2.73
	450	1.3	2.77
		0.4	2.20
	600	1.3	2.24

EXAFS data of Pt/K-LTL reduced at 300, 450 and 600°C is presented in Figure 14. Qualitative inspection of Figure 14 shows that metallic Pt is present in all samples as indicated by the Pt-Pt bond distance of 2.77 Å. In addition, as the reduction temperature is increased, the amplitude of the Pt-Pt peak increases, indicating the growth of the platinum particle size, eg., increasing coordination number. For all reduction temperatures, however, the platinum particles are relatively small as denoted by the absence of higher Pt-Pt shells. The EXAFS spectra were fit in both k- and r-space, and the results of the fit are given in Table 1.

For Pt/K-LTL reduced at 300°C, the Pt-Pt coordination number corresponds to an average particle size of six atoms (N = 4.0). With increasing reduction temperature the particle size increases. At 450°C the average particle size is ca. ten atoms (N = 4.4); while, at 600°C the particle size is near twelve atoms (N = 4.9). In all of the catalysts, the particle size is sufficiently small to observe a contribution to the EXAFS from the

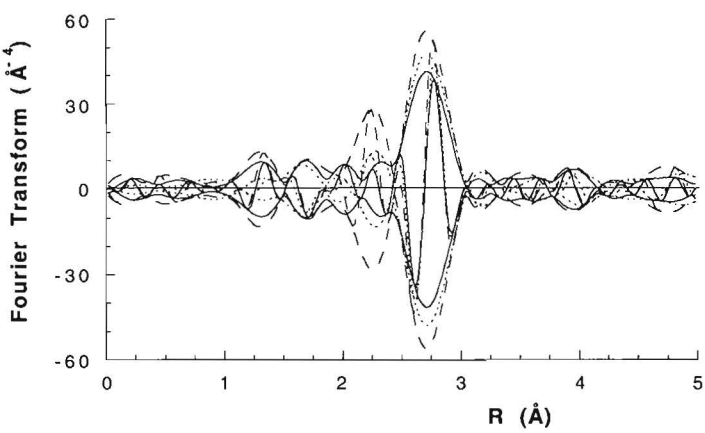

Figure 14 Fourier transform [k^3, Δk: 3.1 – 12.9 $Å^{-1}$, Pt–Pt phase- and amplitude corrected] of EXAFS spectrum of 1.2% Pt/K-LTL reduced at 300°C (solid line), 450°C (dotted line) and 600°C (dashed line).

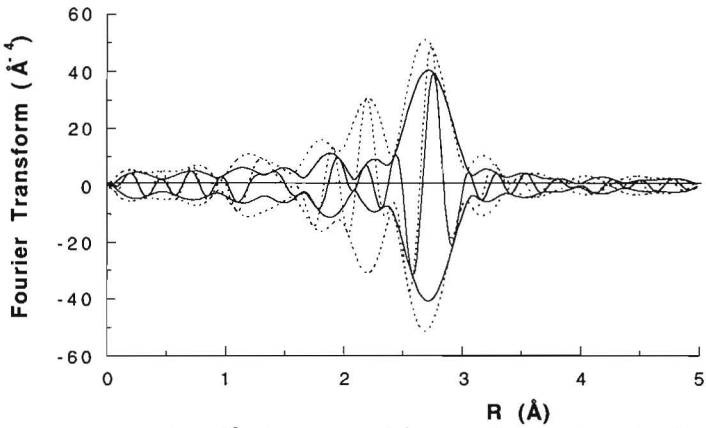

Figure 15 Fourier transform [k^3, Δk: 3.1 – 12.9 $Å^{-1}$, Pt–Pt phase- and amplitude corrected] of EXAFS spectrum of 1.2% Pt/H-LTL reduced at 300°C (solid line) and 500°C (dotted line).

oxygen atoms of the support. For Pt/K-LTL reduced at 300°C, the Pt-O coordination is 1.4 and the platinum-oxygen distance is 2.73 Å. For Pt/K-LTL reduced at 450°C, a second Pt-O distance of 2.20 Å is present with a total Pt-O coordination number is 1.7. After reduction at 600°C, only one Pt-O distance of 2.20 Å is present with a Pt-O coordination number of 1.3.

The Pt-Pt phase- and amplitude-corrected k^3-weighed Fourier transform of the EXAFS data of Pt/H-LTL reduced at 300 and 500°C is presented in Figure 15. For both catalysts, small, metallic Pt particles are present as indicated by the Pt-Pt bond distance of 2.77 Å. The EXAFS spectra were fit in both k- and r-space, the results are given in Table 2.

For Pt/H-LTL reduced at 300°C, the Pt-Pt coordination number of 4.1 corresponds to an average particle size of approximately seven atoms. In addition, a long Pt-O distance of 2.65 Å with a coordination number of 1.2 is detected. Increasing the reduction temperature to 500°C increases the Pt-Pt coordination number to 4.4, or approximately a nine atom cluster. After reduction at 500°C, the Pt-O distance is 2.24 Å and the Pt-O coordination number is 1.5.

Table 2 Structural parameters from EXAFS for Pt/H-LTL.

Backscatterer	T_{red} (°C)	N	R (Å)
Pt	300	4.0	2.73
	500	4.4	2.72
O	300	1.2	2.65
	500	1.5	2.24

Table 3 Propane hydrogenolysis activity for supported platinum catalysts at atmospheric pressure and 400°C. For stable catalysts only the initial TOF is reported.

support	T_{red} (°C)	initial TOF (molecules s^{-1} $site^{-1}$)	TOF after 10 min TOS (molecules s^{-1} $site^{-1}$)
K–LTL	450	0.064	–
	600	0.022	–
K–MAZ	450	0.032	–
K–SiO_2	450	0.0074	–
SiO_2	450	0.19	–
H–LTL	450	0.53	0.40
	600	0.14	0.10
H–MAZ	450	0.37	0.27
γ–Al_2O_3	450	0.62	–

Propane hydrogenolysis

For each catalyst, hydrogenolysis of propane yielded methane and ethane in equal molar amounts. The TOF at 400°C are given in Table 3. For Pt/K-LTL, Pt/K-MAZ, Pt/SiO_2, and Pt/γ–Al_2O_3, there was little deactivation. For Pt/H-MAZ and Pt/H-LTL, however, deactivation was more rapid. The conversion, therefore, was determined as a function of time (at one space velocity) and extrapolated to zero time, i.e., no deactivation. For these two catalysts, since the activity was changing rapidly during the first few minutes, the initial TOF and the TOF after 10 min. are reported in Table 3.

Discussion

Temperature programmed desorption of hydrogen indicates several types of hydrogen on platinum catalysts. In addition to chemisorbed hydrogen, three higher temperature hydrogen desorptions (peaks II-IV) are also observed at temperatures from about 250 to 650°C. It has been proposed that HTR can result in the formation of subsurface hydrogen,[10] i.e. hydrogen present in the platinum lattice just below the surface platinum atoms. The platinum-platinum distances measured by EXAFS are identical to those observed for bulk platinum and do not change with reduction temperature. These results rule out the presence of subsurface hydrogen or platinum hydrides. In addition, while it has been proposed that HTR can lead to the formation of platinum-aluminum alloys,[1,7,8] no backscattering by aluminum neighbours was detected in the EXAFS, and we conclude that these alloys are not responsible for any of the peaks in the TPD. HTR has also been suggested to produce

Table 4 Total hydrogen desorption (H/Pt) in the H_2 TPD. The first TPD was performed to 700°C after reduction at 300°C and cooling in H_2. Following the 1st TPD, the catalyst was re-reduced at 700°C, cooled in H_2 and the 2nd TPD to 700°C was performed.

catalyst	H/Pt 1st TPD (rev + irrev)	H/Pt 2nd TPD (rev)	difference 1st and 2nd (irrev)
K–LTL	1.8	1.2	0.6
H–LTL	4.3	1.3	3.0
K–MAZ	1.9	1.3	0.6
H–MAZ	5.6	1.4	4.2

strongly chemisorbed hydrogen,[2,3,12] leading to high temperature peaks in the TPD. In the present study, neither the size or position of the chemisorption TPD peak was affected by reduction temperature, and we conclude that the high-temperature TPD peaks are not due to strongly chemisorbed hydrogen.

Since the higher temperature desorptions do not result from hydrogen at the platinum particles, eg., strongly chemisorbed hydrogen, subsurface hydrogen, metal hydrides or platinum-aluminum alloys, we conclude that they result from desorption of hydrogen present on the support. In addition, since these hydrogen desorptions do not result from platinum oxidation by support protons, we also conclude that this hydrogen must be present as neutral species, i.e., spilled-over hydrogen.

Although the spilled-over hydrogen is initially formed at 300°C, desorption of the spilled-over hydrogen does not occur until much higher temperatures. Once the spilled-over hydrogen has been desorbed from the support, either during high temperature reduction or TPD, spilled-over hydrogen can no longer be formed by re-exposure to hydrogen. The desorption of spilled-over hydrogen, therefore, is irreversible. Since there have been only minor changes in the dispersion, chemisorption and structure of the platinum particles, the irreversibility of hydrogen desorption is likely due to a change in the structure of the support. Stabilization of spilled-over hydrogen is believed to require the presence of support hydroxyl groups[23-25] and zeolites begin to dehydroxylate above 500°C.[26,27] We propose, therefore, that the inability to spilled-over hydrogen after high temperature treatments results from irreversible dehydroxylation of the support.

Qualitatively, the number and temperature of peaks in the TPD profiles for platinum on non-acidic and acidic zeolites are similar. As discussed above, the total amount of spilled-over hydrogen is dependent on extent of support dehydroxylation. Likewise, the amount of spilled-over hydrogen is also strongly dependent on the support acidity as shown in Table IV. The effect of support acidity is most dramatically shown by the size of peak IV in the TPD profiles, and this peak is largest for platinum on acidic supports. Table 4 summarizes the total amount of hydrogen desorbed in the TPD profile for platinum supported on various acidic and

non-acidic supports. In the first TPD, both reversible (chemisorbed) and irreversible (spilled-over) hydrogen are measured, while in the second TPD, only reversible (chemisorbed) hydrogen is observed. The difference between the two TPD profiles represents the irreversible (spilled-over) hydrogen on the catalyst, i.e., peaks II-IV. The data in Table 4 clearly show that the amount of spilled-over hydrogen is much larger for platinum on acidic supports than on non-acidic supports. For example, the amount of spilled-over hydrogen is equivalent to 3.0 H/Pt for Pt/H-LTL, but only 0.7 H/Pt for Pt/K-LTL.

Even though formation of spilled-over hydrogen to the support originally occurs at 300°C, it is not desorbed at 300°C in flowing N_2, even after 1 h, nor does it migrate back to the platinum under these conditions. Once formed on the support, spilled-over hydrogen seems to be quite stable. However, under these same conditions, the spilled-over hydrogen is completely exchanged with gas-phase D_2 within 30 min. It is commonly assumed that H-D exchange of spilled-over hydrogen occurs by migration of the spilled-over hydrogen to the platinum particles and exchange with the chemisorbed deuterium on the platinum sites. However, since spilled-over hydrogen does not migrate to vacant platinum sites at 300°C, it seems unlikely that the spilled-over hydrogen would migrate to the platinum particles and exchange with chemisorbed deuterium. We, therefore, propose that the exchange takes place by direct reaction between the spilled-over hydrogen and the gas phase deuterium, without the participation of the platinum.

For all reduction temperatures, the platinum particles are small enough to reside within the zeolite pores. Because of the very small metal particle size, oxygen atoms from the support are detected by EXAFS. After high temperature reduction (HTR) (>500°C) the measured Pt-O distance is 2.2 Å, which is approximately equal to the sum of the covalent radii of the two atoms (1.37 Å for Pt and 0.74 Å for O). This is consistent with platinum atoms in direct contact with the oxide ions of the zeolite surface. Reduction at 300°C (LTR), on the other hand, results in a longer Pt-O distance of 2.77 Å. Based on the absence of additional backscatterers, it has been suggested that this long Pt-O distance results from the presence of hydrogen between the platinum atoms and the oxide support.[22,28,29] The interfacial hydrogen is may be either chemisorbed hydrogen trapped at the interface during the initial reduction or hydrogen from the support hydroxyl groups.[29] At intermediate reduction temperatures there is a mixture of both the long and short Pt-O distances. Thus, as the reduction temperature is increased from LTR to HTR there is the progressive loss of the long Pt-O distance with the simultaneous formation to the short Pt-O distance. Comparison of the H_2 TPD with the EXAFS, indicates several desorption peaks (Peaks II and III) in the same temperature range observed for the conversion of the long Pt-O distance to the short Pt-O distance, eg., from 300 to 500°C. These peaks may, therefore, correspond to the loss of interfacial hydrogen. Both the desorption temperature and the large quantity of H_2 desorbed for peak IV in acidic catalysts makes it unlikely that this peak is associated with loss of interfacial

hydrogen.

In summary, we assign the irreversible, high temperature H_2 desorptions to spilled-over hydrogen stabilized by support hydroxyl groups, both acidic and non-acidic. Peak II and/or III may be spilled-over hydrogen located at the interface between the platinum particles and the support. Peak IV also represents spilled-over hydrogen, and is much larger on acidic supports.

Effects on catalysis

Similar to other studies,[11,15,30,31] the propane hydrogenolysis activities are determined predominantly by the acidity of the support. The TOF's for platinum on acidic supports, e.g., Pt/H-LTL, Pt/H-MAZ and Pt/γ–Al_2O_3 were more than an order of magnitude higher than on the non-acidic supports, e.g., Pt/K-LTL and Pt/K-MAZ. The TOF for Pt/SiO_2, a weakly acidic support, was intermediate between the acidic and non-acidic supports. Neutralization of the silica by addition of alkali, i. e., Pt/K-SiO_2, strongly reduced the hydrogenolysis TOF.

In previous studies, the increase in hydrogenolysis activity for metals on acidic supports has been attributed to electron-deficient platinum. Results of a recent study suggest that the electron deficient nature of the platinum is an intrinsic property of the small metal particles.[32] A series of Pt/Y catalysts was investigated by several techniques, including XANES, where it was concluded that all of the observations ascribed to electron deficiency were the result of the intrinsic properties of the very small platinum particles which form on acidic supports. In our study, the platinum particle size of Pt/K-LTL, Pt/H-LTL and Pt/γ–Al_2O_3[17,23] were, within experimental error, identical. The particle size alone, therefore, cannot account for the differences in hydrogenolysis activity.

It has also been suggested that electron deficient platinum can result from donation of platinum electron density to the support,[30] or result from the formation of metal-proton adducts.[15,34] While we have previously proposed that platinum on acidic supports is electron deficient, the EXAFS white line intensity for Pt/K-LTL, Pt/H-LTL and Pt/γ–Al_2O_3 are not significantly different from one another when compared at the same reduction temperature and platinum particle size[33]. The small differences in white line intensity suggest that there is only a small change in the d-band electron density of platinum on acidic supports compared to non-acidic supports. These differences seem too small to account for the large changes in hydrogenolysis activity.

While the changes in the specific hydrogenolysis activity due not appear to result from either changes in the particle size, or changes in the Pt d-band density of states, in the present study we have found that the most active catalysts are those which have the largest amount of spilled-over hydrogen, i.e., platinum on acidic supports. As the support acidity decreases, both the propane hydrogenolysis TOF and the quantity of spilled-over hydrogen also decrease in the same order, e.g., acidic supports > silica > non-acidic supports.

In addition to the support acidity, the hydrogenolysis TOF is also affected by the reduction temperature. For Pt/K-LTL and Pt/H-LTL, as the reduction temperature increased both the specific activity and the amount of spilled-over hydrogen decreased.

While there seems to be a general correlation between the specific hydrogenolysis activity and the amount of spilled-over hydrogen, the role of spilled-over hydrogen (if any) on the rate of hydrogenolysis is uncertain and several possibilities exist. Understanding the role of spilled-over hydrogen in these catalysts, will be the subject of future investigations.

Conclusions

The H_2 TPD indicates that several types of hydrogen exist on platinum catalysts. In addition to chemisorbed hydrogen on the platinum, several types of spilled-over hydrogen are present on the support. The quantity of spilled-over hydrogen is dependent on the number of support hydroxyl groups and is greatest for platinum on acidic supports reduced at low temperature. Spilled-over hydrogen is irreversibly desorbed at high temperatures since the support is irreversibly dehydroxylated.

After low temperature reduction, a layer of spilled-over hydrogen is located between the platinum particles and the support (oxide) surface. The platinum-oxygen distance is ca. 2.7 Å. Reduction of the platinum at higher temperatures results in the progressive loss of the interfacial hydrogen. At reduction temperatures above 500°C, all of the interfacial hydrogen is lost, and the platinum is supported directly on the oxygen atoms of the zeolite support at a platinum-oxygen distance of 2.2 Å. In the TPD, two hydrogen desorption peaks observed at temperatures from 300 to 500°C may correspond to the loss of interfacial hydrogen detected by EXAFS.

The catalysts' specific activities for hydrogenolysis were affected by both the support acidity and the reduction temperature. Platinum on acidic supports and reduced at lowest temperature were most active. Qualitatively, the catalysts' hydrogenolysis activity increased with increasing amounts of spilled-over hydrogen, however, the role of spilled-over hydrogen in affecting the catalytic activity is uncertain.

References

1. G. J. den Otter and F. M. Dautzenberg, J. Catal., **53** (1978) 116.
2. P. G. Menon and G. F. Froment, J. Catal., **59** (1979) 138.
3. P. G. Menon and G. F. Froment, Appl. Catal., **1** (1981) 31.
4. R. Kramer and M. Fischbacher, J. Mol. Catal., **51** (1989) 247.

5. L. Bonneviot and G. L. Haller, J. Catal., **130** (1991) 359.
6. K. Kunimori, T. Okouchi, and T. Uchijima, Chem. Lett., (1980) 1513.
7. K. Kumimori, Y. Ikeda, M. Soma, and T. Uchijima, J. Catal., **79** (1983) 185.
8. K. Kunimori and T. Uchijima, *in* "Spillover of Adsorbed Species" (G. M. Pajonk, S. J. Teichner, and J. E. Germain, Eds.), p. 197. Elsevier, Amsterdam, 1983.
9. L. -Q. Dou, Y. -S. Tan, and D. -S. Lu, Appl. Catal., **66** (1990) 235.
10. P. -J. Levy and M. Primet, Appl. Catal., **70** (1991) 263.
11. K. Foger and J. R. Anderson, J. Catal., **54** (1978) 318.
12. T. Szilágyi, J. Catal., **121** (1990) 223.
13. R. Kramer and M. Andre, J. Catal., **58** (1979) 287.
14. J. A. Dalmon, C. Mirodatos, P. Turlier, and G. A. Martin, *in* "Spillover of Adsorbed Species, (G. M. Pajonk, S. J. Teichner, and J. E. Germain, Eds.), p. 169. Elsevier, Amsterdam, 1983.
15. G. S. Lane, J. T. Miller, F. S. Modica, N. G. Berry, and M. K. Barr, J. Catal., (1993) accepted.
16. S. T. Homeyer, Z. Karpinski, and W. M. H. Sachtler, J. Catal., **123** (1990) 60.
17. M. Vaarkamp, J. T. Miller, F. S. Modica, and D. C. Koningsberger, *in* "Proc. 7th Int. Conf. on X–ray Absorption Fine Structure, Kobe, Japan, August 23-29, 1992", in print
18. D. W. Breck, *Zeolite Molecular Sieves, Structure, Chemistry and Use* (John Wiley & Sons, New York, 1974).
19. F. W. H. Kampers, T. M. J. Maas, J. van Grondelle, P. Brinkgreve, and D. C. Koningsberger, Rev. Sci. Instr., **60** (1989) 2635.
20. J. W. Cook Jr. and D. E. Sayers, J. Appl. Phys., **52** (1981) 5024.
21. J. B. A. D. van Zon, D. C. Koningsberger, H. F. J. van't Blik, and D. E. Sayers, J. Chem. Phys., **82** (1985) 5742.
22. M. Vaarkamp, F. S. Modica, J. T. Miller, and D. C. Koningsberger, submitted (1993). (chapter 5 part 2)
23. J. A. Altham and G. Wevv, J. Catal., **18** (1970) 133.
24. R. B. Levy and M. Boudart, J. Catal., **32** (1974).
25. W. J. Ambs and M. M. Mitchell Jr., J. Catal., **82** (1983) 226.
26. T. R. Hughes and H. M. White, J. Phys. Chem., **71** (1967) 2192.
27. J. Datka, J. Chem. Soc., Faraday Trans. I, **77** (1981) 2877.
28. F. W. H. Kampers and D. C. Koningsberger, Faraday Discuss. Chem. Soc., **89** (1990) 137.
29. D. C. Koningsberger and B. C. Gates, Catal. Lett., **14** (1992) 271.
30. M. Boudart and R. A. Dalla Betta, *in* "Proc. 5th Int. Congr. Catal., Palm Beach, 1972", (J. H. Hightower, Ed.), p. 1329. North-Holland, Amsterdam, 1973.
31. C. Naccache, N. Kaufherr, M. Dufaux, J. Pandiera, and B. Imelik, *in* "Mol. Sieves-II" (J. R. Katzer, Ed.), p. 538. 1977.
32. M. G. Samant and M. Boudart, J. Phys. Chem., **95** (1991) 4070.
33. M. Vaarkamp, J. T. Miller, F. S. Modica, G. S. Lane, and D. C. Koningsberger, *in*

"Proc. 10th Int. Congr. Catal., Budapest, 19 - 24 July 1992", in print.
34. M. S. Tzou and W. M. H. Sachtler, *in* "Catalysis 1987" (J.W. Ward, Ed.), Elsevier, Amsterdam, p.233 (1988).

Chapter 5
part 2

Influence of Hydrogen Pretreatment on the Structure of the Metal-Support Interface in Pt/Zeolite Catalysts

Abstract

Platinum supported on H–LTL, K–LTL and H–MAZ were reduced at temperatures from 573 to 873 K and the structural characteristics of the metal-support interface were determined by EXAFS. In all samples, the platinum was highly dispersed, with metal particle sizes from 5-11 atoms. Reduction at 573K results in an interfacial Pt-O distance of 2.7 Å, which is significantly longer than the Pt-O distance of 2.2 Å observed after reduction at 773-873K. At intermediate reduction temperatures both the long and the short Pt-O distances were observed. The transition from the long Pt-O distance to the short Pt-O distance occurred at lower temperature for Pt/H–LTL (773 K) than for Pt/K–LTL (873 K). The shortening of the Pt-O distance is accompanied by a decrease in the Debye-Waller factor, implying a stronger interaction between the platinum atoms and the oxide support. A structural model is proposed wherein the longer Pt-O distance results from the presence of hydrogen in the interfacial layer between the metal particle and the support. During high temperature reduction, the hydrogen is released from the interface, leaving platinum in direct contact with the support. The change in the structure of the platinum–zeolite interface is related to changes in hydrogen chemisorption capacity and catalytic properties.

Submitted for publication: M. Vaarkamp, F.S. Modica, J.T. Miller, and D.C. Koningsberger.

Introduction

A number of studies have appeared in the literature using EXAFS to investigate the structure of supported metal catalysts. In the early studies, only the structural properties of the metal particle were characterized[1-3]. Because the metal particles were relatively large, the fraction of metal atoms at the metal-support interface was small, and accurate information about the interface could not be obtained. Later studies indicated that the metal particle is supported directly on the oxide surface with reported metal-oxygen distances between 1.92 and 2.07 Å for platinum on alumina[4], platinum on silica[5], and rhodium on magnesia[6]. These distances approximate the known metal-oxygen bond lengths in metal oxide compounds, and are about equal to the sum of the covalent radii of the metal and oxygen atoms. However, even in these later studies, the metal particles were still larger than about 15 atoms (N≥6), limiting the accuracy with which the metal-support distance could be determined. With very small Ir particles on alumina, a Ir-O distance of 2.19 Å was observed after evacuation[7].

By contrast, longer metal-oxygen distances (ca. 2.7 Å) have been reported for rhodium[8-10], iridium[11], and platinum[12] on alumina, iridium on magnesia[13], palladium[14] and platinum[15] in zeolites, and rhodium on titania[16]. For Rh/alumina[9] the Rh–O contribution was found to increase as the metal particle size decreased, indicating that this Rh-O distance arises from the metal-support interface. The longer metal-oxygen distance has been suggested to be due to the presence of hydrogen or OH groups in the metal-support interface[7]. However, a clear understanding of the longer metal-oxygen distance is still lacking[17].

The present study utilized X-ray absorption spectroscopy to determine the effect of reduction temperature on the structure of the metal-support interface for small platinum clusters on H–LTL, K–LTL and H–MAZ zeolites. We have also established the experimental conditions which lead to the formation of the long and short metal-oxygen distance. The structural changes in the metal-support interface are discussed in relation to changes in the measured hydrogen chemisorption capacity and catalytic properties reported in the literature.

Experimental

Preparation of catalysts

The K–LTL zeolite was obtained from Linde. The zeolite was repeatedly washed with water until the pH of the wash solution was 9.5. The resulting K–LTL zeolite was analyzed to contain 8.3 wt% Al and 13.0 wt% K. The H–LTL zeolite was prepared by ion-exchanging the as-received K–LTL with ammonium nitrate solution at 363 K, followed by a water wash. The resulting exchanged zeolite contained 5.6 wt% K. The

H–MAZ was prepared from Na-MAZ, which was synthesized following published procedures[18]. The Na-MAZ was ion-exchanged with ammonium nitrate at 363 K, followed by a water wash. The resulting exchanged zeolite contained 0.01 wt% Na. All three zeolites were dried and calcined at 700 K.

The zeolites were impregnated with tetraamine platinum (II) nitrate to yield 1.2 wt% Pt on the finished catalyst. The impregnated catalysts were dried at 400 K.

EXAFS data collection

The samples were characterized by EXAFS spectroscopy at the Synchrotron Radiation Source in Daresbury, U.K., Wiggler Station 9.2, using a Si (220) double crystal monochromator. The storage ring was operated with an electron energy of 2 GeV and a current between 120 and 250 mA. At the Pt L_{III} edge (11564 eV), the estimated resolution was 3 eV. The monochromator was detuned to 50% intensity to avoid the effects of higher harmonics present in the X-ray beam. The measurements were done in the transmission mode using ion chambers filled with argon to have a μx of 20% in the first ion chamber and a μx of 80% in the second ion chamber. To decrease low- and high-frequency noise as much as possible, each data point was counted for 1 second and 6 scans were averaged.

The samples were pressed into self-supporting wafers (calculated to have an absorbance of 2.5) and placed in a controlled-atmosphere cell[19]. The samples were reduced *in situ* in flowing hydrogen (purified and dried) at 1 atm. Samples were heated at 5 K/min to the desired reduction temperature (Pt/H–LTL: 573 K and 773 K; Pt/K–LTL: 573 K, 723 K, and 873 K; Pt/H–MAZ: 773 K) and each was reduced for 1 h. The samples were cooled to room temperature under flowing hydrogen. The measurements were done with the sample at liquid nitrogen temperature in the presence of hydrogen at atmospheric pressure.

EXAFS Data Analysis

Data reduction The PreEdge background was approximated by a modified Victoreen curve[20], the background was subtracted using cubic spline routines[21]. Spectra were normalized by dividing the absorption intensity by the height of the absorption edge at 50 eV above the edge. The final EXAFS function was obtained by averaging the

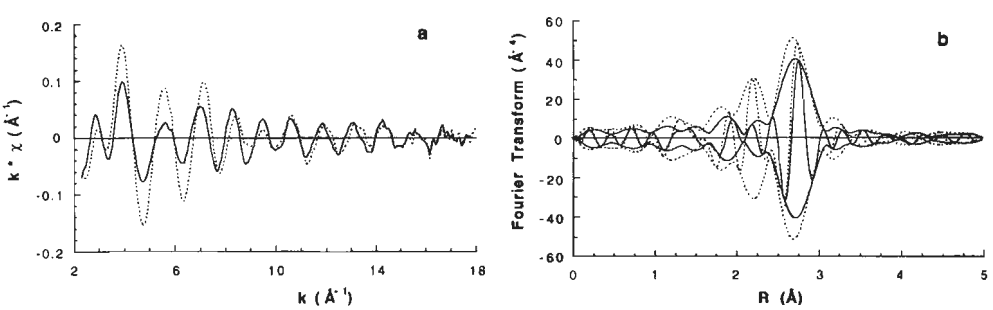

Figure 1 a) EXAFS spectra (k^1 weighed) of Pt/H–LTL reduced at 573K (solid line) and 773K (dotted line), b) Fourier transform ($|k^3$, Δk: 2.6 -13.9 $Å^{-1}$, Pt–Pt phase and amplitude corrected) of the spectra in a).

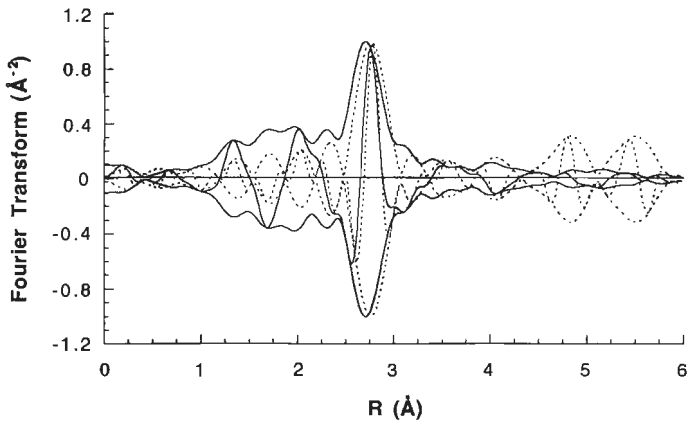

Figure 2 Normalized Fourier transform of Pt/H–LTL reduced at 573K (solid line) and Pt foil (dashed line) [k^1, Δk: 3.1 – 13.9 $Å^{-1}$, Pt–Pt phase- and amplitude-corrected].

individual background-subtracted and normalized EXAFS data (6 scans). The standard deviations were calculated for each individual EXAFS data point as an estimate of the random error in the final EXAFS function. The EXAFS data analysis is usually performed on an isolated part of the data obtained by an inverse Fourier transformation over a selected range in r-space. The isolated EXAFS functions were obtained by averaging the inverse Fourier transformations of each individual EXAFS data set (6 scans). The standard deviations calculated from the individual data points of the several isolated EXAFS functions provided an estimate of the random error in the average isolated EXAFS function.

Reference Data Data for the phase shifts and backscattering amplitudes were obtained from EXAFS data obtained from reference compounds. Pt foil was used as a reference for the Pt-Pt contributions and $Na_2Pt(OH)_6$ for the Pt-O contributions. The procedures used to obtain the reference data for Pt foil and $Na_2Pt(OH)_6$ are described elsewhere[22].

Data Analysis The parameters characterizing the high-Z (Pt) and low-Z (O) contributions were determined by multiple-shell fitting in k-space with optimization in r-space. Different backscatterers were identified by applying the difference file technique using phase- and amplitude-corrected Fourier transforms[5,9,16]. The optimal combination of the coordination number and the Debye–Waller factor was determined by optimizing the k^1 and k^3 weighed Fourier transforms[22]. The errors in the structural parameters were calculated from the covariance matrix, taking into account the statistical noise obtained for the Fourier filtered EXAFS function and the correlations between the refined parameters[23]. The values of the goodness of fit (ε_v^2) were calculated as outlined in the *Report on Standards and Criteria in XAFS Spectroscopy*[24].

Results

EXAFS analysis of Pt/H–LTL

The EXAFS data (average of 6 scans) for Pt/H–LTL reduced at 573 K (LTR) and 773 K (HTR) are shown in Figure 1a. At low k-values the amplitude of the EXAFS is higher after reduction at 773 K than after reduction at 573 K. In addition, the position of the nodes in the EXAFS are located at different k-values. The signal to noise ratio is 15 at 4 $Å^{-1}$ and 5 at 14 $Å^{-1}$ for the sample reduced at 573 K, after reduction at 773 K these values are 60 and 5, respectively. Fourier transforms (k^3 weighed, Pt–Pt phase- and amplitude-corrected) of the EXAFS data for the Pt/H–LTL catalysts are shown in Figure 1b. The Fourier transforms show an increase in the Pt–Pt contribution around 2.7 Å, indicating a growth in the Pt particle at higher reduction temperature. Furthermore, for Pt/H–LTL reduced at 773 K, an additional scatterer besides platinum is visible as a separate peak in the Fourier transform near 2.2 Å. This separate peak results from an interference which is observable in the raw EXAFS spectrum (Figure 1a) by the presence of a beating node at k=9-10 $Å^{-1}$.

The normalized k^1 weighed Fourier transforms (Pt-Pt phase- and amplitude-corrected) of the EXAFS data for Pt/H–LTL reduced at 573 K and for Pt foil are shown in Figure 2. The Fourier transforms are normalized to facilitate comparison and k^1 weighed in order to emphasize the low-Z (oxygen) contributions. Differences between the Pt/H–LTL catalyst and the Pt foil in both the magnitude and the

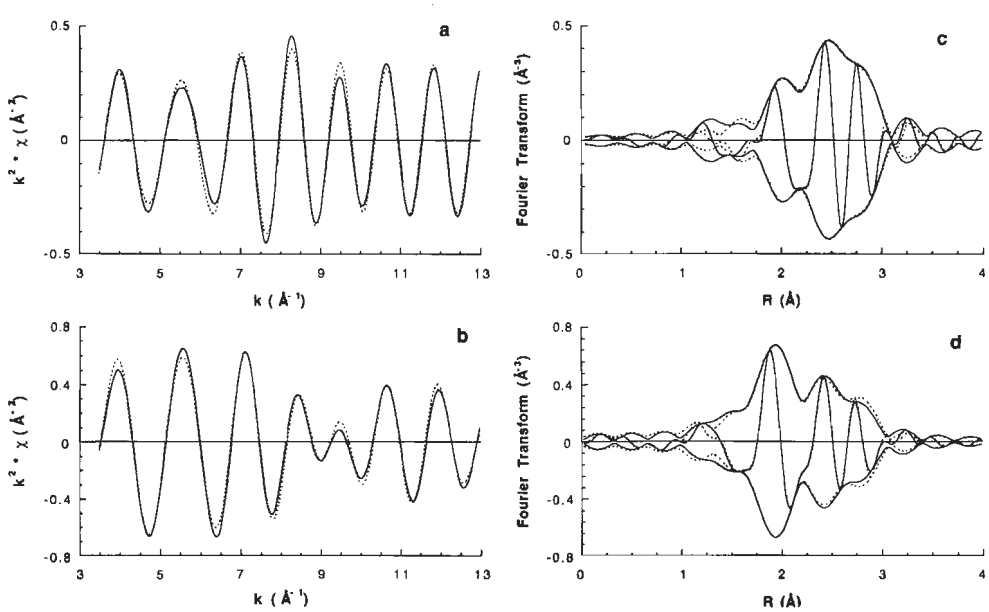

Figure 3 Results of EXAFS analysis of Pt/H–LTL reduced at a) 573K and b) 773K, solid line Fourier filtered data, dashed line model EXAFS spectrum calculated with the parameters in table 1. Fourier transforms [k^2, Δk: 3.5 – 13.0 $Å^{-1}$] of the spectra in a) and b) are shown in c) and d) respectively.

imaginary part of the Fourier transforms are observed between 2.0-3.5 Å. These differences indicate the presence of additional scatterers besides Pt in the Pt/H–LTL catalyst. Multiple-shell fitting of the Fourier filtered EXAFS spectrum (k^2, Δk: 2.6-13.9 $Å^{-1}$, ΔR: 1.2-3.3 Å) resulted in the identification of two significant contributions (Table 1): a Pt-Pt contribution at 2.73 Å and a Pt-O contribution from the zeolite framework at 2.65 Å. The goodness of fit[24] was calculated to be 21.8 with eight fit parameters and 13.7 degrees of freedom. The Pt-O contribution was statistically significant at the 88% confidence level (F=2.51). A comparison of the fitted spectrum with the Fourier filtered data in both k- and r-space is shown in Figure 3a and 3c. The Pt-O distance of 2.65 Å for this catalyst is in the same range as those previously observed for other supported metal catalysts reduced at low temperatures[8-16].

The results of the multiple-shell fitting of the Fourier filtered (k^2, Δk: 2.8-13.9 $Å^{-1}$, ΔR: 1.15-3.25 Å) EXAFS data for the Pt/H–LTL reduced at 773 K are given in Table 1. The goodness of fit[24] was calculated to be 38.7 with eight fit parameters and 13.7 degrees of freedom. Fits in k- and r-space are presented in Figure 3b and 3d. The Pt-O contribution from the zeolite framework at 2.7 Å, which was present after reduction at 573 K, is absent following reduction at 773 K, while a different Pt-O contribution from the zeolite framework appears at 2.24 Å.

Subtraction of the calculated Pt–Pt contribution from the EXAFS spectrum results in a difference spectrum with only contributions from the support. The Fourier transform (k^1 weighed, Pt–O phase corrected) of this difference spectrum and the calculated Pt–O contribution is shown for Pt/H–LTL reduced at 573 K (Figure 4a) and 773 K (Figure 4b). The effect of reduction temperature on the isolated Pt-O contributions for the Pt/H–LTL catalysts are shown in Figure 4. The different Pt-O distances in the two catalysts can be clearly seen. Reduction at 573 K results in a Pt-O distance of 2.7 Å, while reduction at 773 K results in a Pt-O distance of 2.24 Å. The peak associated with the longer Pt-O distance is significantly broader than that associated with the shorter Pt-O distance. The broader peak is an indication of a larger deviation about the mean distance, i.e., a larger Debye-Waller factor ($\Delta\sigma^2$). In

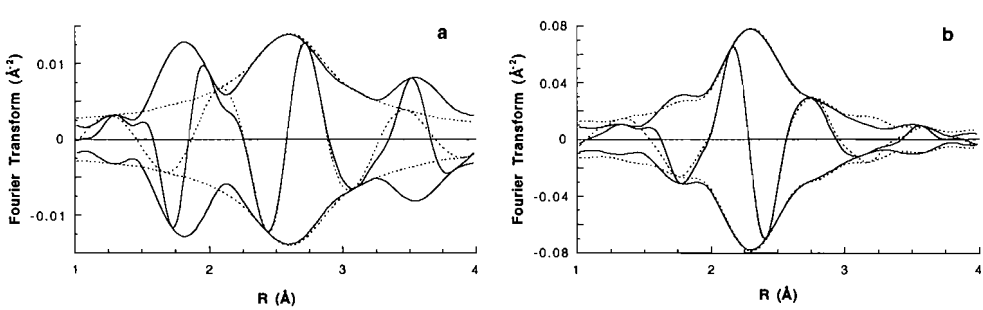

Figure 4 Fourier transform [k^1, Δk: 3.5 – 12.0 $Å^{-1}$, Pt–O phase-corrected] of the EXAFS spectrum of Pt/H–LTL minus the Pt–Pt contribution (solid line) and the Pt–O contribution calculated with the parameters in table 1 (dashed line). a) reduced at 573K, b) reduced at 773K.

Table 1 Structural parameters from EXAFS for Pt/H–LTL after reduction at 300 and 500°C.

Backscatterer	N	R (Å)	$\Delta\sigma^2$ ($Å^2 \times 10^{-3}$)	ΔE_0 (eV)
Pt				
300	4.1 ± 0.1	2.73 ± 0.01	3.4 ± 0.1	3.5 ± 0.3
500	4.4 ± 0.1	2.72 ± 0.01	4.4 ± 0.1	0.8 ± 0.2
O				
300	1.2 ± 0.1	2.65 ± 0.01	7.0 ± 1.1	5.7 ± 0.5
500	1.5 ± 0.1	2.24 ± 0.01	−2.5 ± 1.1	−13.9 ± 0.1

addition to the difference in the Debye-Waller factor, the two platinum-oxygen contributions also have different inner potential shifts (ΔE_0) (see Table 1). These differences are an indication of the different chemical nature of the interaction between the platinum clusters and the zeolite oxygens after LTR and HTR.

EXAFS analysis of Pt/K–LTL

In general, the structural features of the Pt-O interface in Pt/K–LTL and the effects of reduction temperature on these features are similar to those observed for Pt/H–LTL. The k^1 weighed EXAFS spectra are shown in Figure 5a, the amplitude of the EXAFS at low energy increases with increasing reduction temperature. In the k^3 weighed Fourier transform of these spectra (Figure 5b) around 2.2 Å a peak develops going from reduction at 573 K (LTR) to 873 K (HTR). As observed with Pt/H–LTL (Figure 1b), the Pt-O distance around 2.2 Å, is present after HTR, but not after LTR. Full fitting of the EXAFS data for the Pt/K–LTL catalysts results in the coordination parameters given in Table 2, the fits are shown in Figure 6. After reduction at 573 K, only the long (2.77 Å) Pt-O distance is present, while after 873 K reduction only the shorter (2.24 Å) Pt-O distance can be detected. At the intermediate reduction temperature of 723 K both contributions are present. Thus, there appears to be a transformation from the long Pt-O distance (ca. 2.7 Å) to a short Pt-O distance (2.2 Å) with increasing reduction temperature. Note, however, that complete elimination

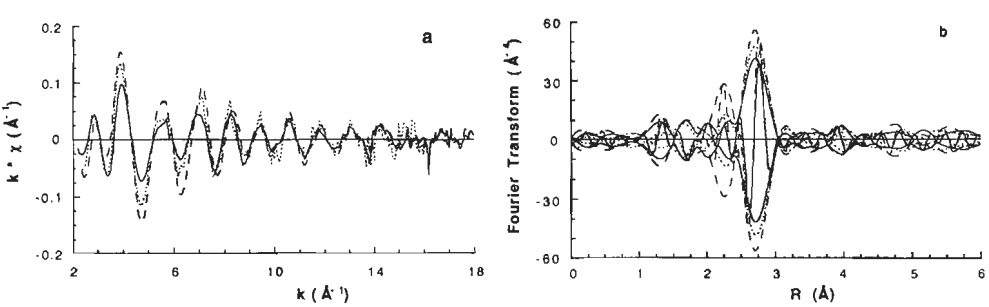

Figure 5 a) EXAFS spectra (k^1 weighed) of Pt/K–LTL reduced at 573K (solid line), 723K (dotted line), and 873K (dashed line). b) Fourier transform |k^3, Δk: 3.1 – 15.0 $Å^{-1}$, Pt–Pt phase- and amplitude-corrected| of the spectra shown in a).

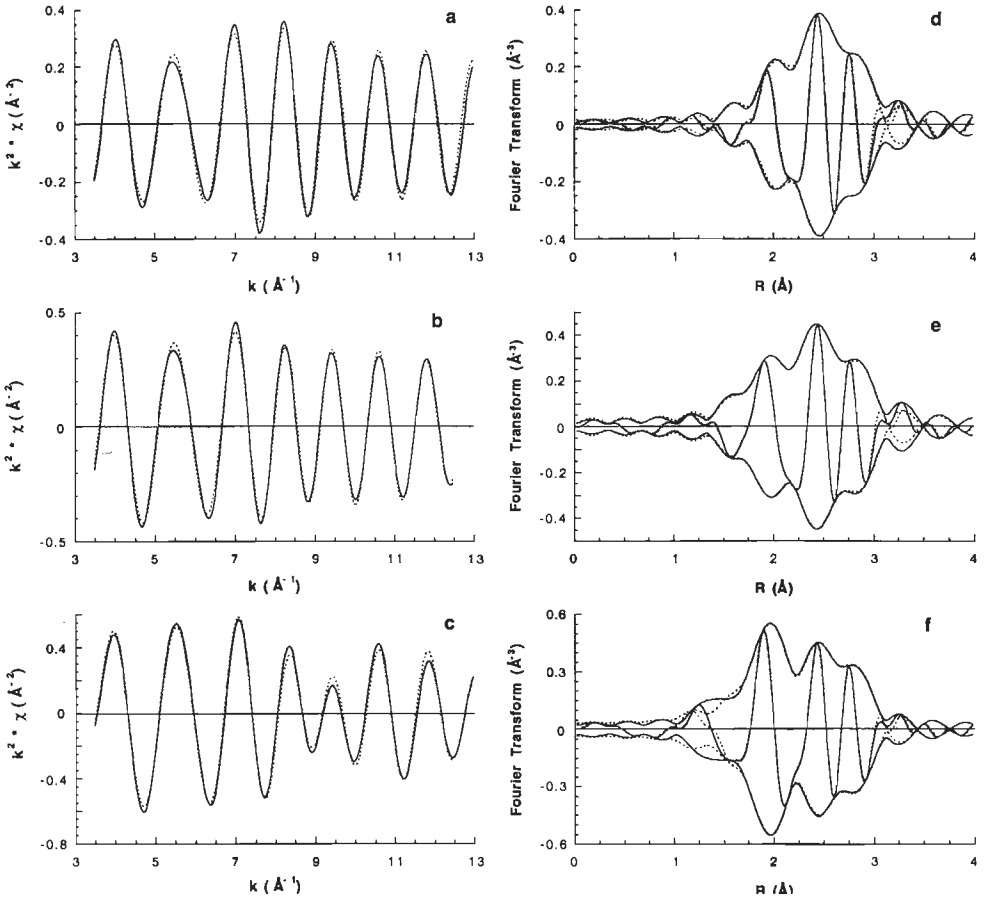

Figure 6 Results of EXAFS analysis of Pt/K–LTL reduced at a) 573K, b) 723K, and c) 873K, solid line Fourier filtered data, dashed line model EXAFS spectrum calculated with the parameters in table 2. The Fourier transform [k^2, Δk: 3.5-13.0 $Å^{-1}$] of the spectra in a), b), and c) are shown in d), e), and f), respectively.

of the longer Pt-O distance in the Pt/H–LTL catalyst is accomplished at 773 K, while the Pt/K–LTL catalyst retains much of this long Pt-O distance at 723 K. The long Pt-O coordination in Pt/K–LTL is completely removed only after reduction at 873 K. The Fourier transform (k^1 weighed, Pt–O phase corrected) of the calculated Pt-O contribution for the catalyst after reduction at 573 and 873 K are presented in Figure 7 together with the EXAFS spectra from which the calculated Pt–Pt contribution was subtracted. As was observed for Pt/H–LTL, the peak associated with the longer Pt-O distance in Pt/K–LTL is broader than that associated with the shorter Pt-O distance, i.e., it has a larger Debye-Waller factor ($\Delta\sigma^2$).

The goodness of fit values for Pt/K–LTL reduced at 573, 723, and 873 K are 27.1, 2.8, and 17.4 respectively (table 4). The low value for Pt/K–LTL reduced at 723 K

Table 2 Structural parameters from EXAFS for Pt/K–LTL after reduction at 300, 450, and 500°C. Parameters without error were fixed during the refinement.

Backscatterer	N	R (Å)	$\Delta\sigma^2$ (Å^2 x 10^{-3})	ΔE_0 (eV)
Pt				
300	4.0 ± 0.1	2.74 ± 0.01	4.4 ± 0.1	2.0 ± 0.3
450	4.8 ± 0.2	2.74 ± 0.01	4.4	2.0 ± 1.3
600	4.9 ± 0.1	2.75 ± 0.01	4.4 ± 0.1	−0.6 ± 0.2
O				
300	1.4 ± 0.1	2.73 ± 0.01	8.0 ± 1.1	0.3 ± 0.6
450	1.3 ± 0.2	2.77 ± 0.05	8.0	−2 ± 4
	0.4 ± 0.1	2.20 ± 0.02	−1.6	−9 ± 3
600	1.3 ± 0.1	2.24 ± 0.01	−1.6 ± 0.1	−13.4 ± 0.2

results from the relative high error in the data. The datarange used in the analysis of Pt/K–LTL reduced at 723 K is not large enough to justify the fitting of the twelve free parameters needed for three contributions. We choose to fix the Debye-Waller factors for the Pt-Pt and the Pt-O at 2.7 Å contribution at the values determined for Pt/K–LTL reduced at 573 K, the Debye-Waller factor for the Pt-O contribution at 2.2 Å was fixed at the value determined for Pt/K–LTL reduced at 773 K. This decreased the number of fit parameters to nine, which is now lower than the degrees of freedom (10.5) calculated from the Nyquist theorem.

EXAFS analysis of Pt/H–MAZ

The EXAFS data (average of 6 scans) for Pt/H–MAZ reduced at 723 K are shown in Figure 8a. The noise in the data is so high that analysis was only possible up to k=11.0 Å^{-1}. Analysis of the Fourier filtered data (table 3 and Figure 8b and c) shows that besides the Pt-Pt contribution a Pt-O contribution at a distance of 2.2 Å is present. The negative Debye-Waller factor and the large negative value of −10 eV for the inner potential shift of this Pt-O contribution suggests that oxygen might not be the correct backscatterer for this contribution. As there is no potassium and a very

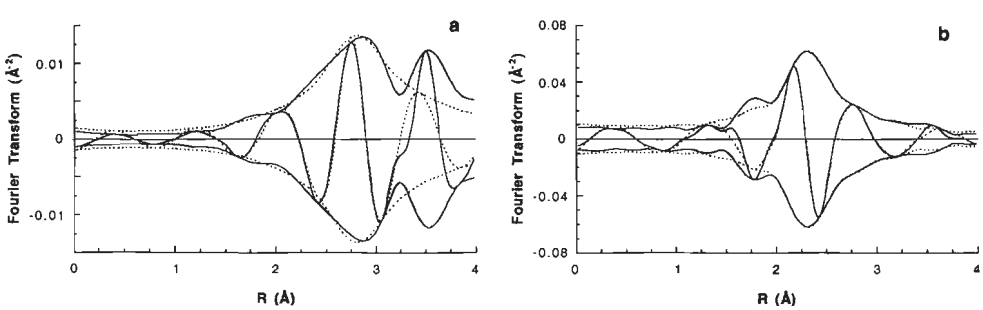

Figure 7 Fourier transform [k^1, Δk: 3.5 – 12.0 Å^{-1}, Pt–O phase-corrected] of the EXAFS spectrum of Pt/K–LTL minus the Pt–Pt contribution (solid line) and the Pt–O contribution calculated with the parameters in table 2 (dashed line). a) reduced at 573K, b) reduced at 873K.

small amount of sodium present the only other possible backscatterer is aluminum or silicon. We refined parameters for a model EXAFS function containing a platinum and an aluminum contribution, this resulted in a model function with a higher ε_v^2 than the model function with platinum and oxygen as backscatterer (17.3 vs. 11.2). This means that there is a chance of 40% that the model with oxygen as backscatterer is a better model for the data than the model with aluminum as backscatterer. A physical argument to prefer oxygen above aluminum as backscatterer is that the walls of the pores in zeolites consist of oxygen atoms.

Comparable negative Debye-Waller factors and very low values of the inner potential shift were also determined in the analysis of Pt/H–LTL and Pt/K–LTL after HTR. From the fact that we observed the same type of contribution in the EXAFS spectrum of Pt/H–MAZ were no potassium is present and the better fits obtained with oxygen it is inferred that oxygen is the correct contribution for the EXAFS spectra of samples reduced at high temperature.

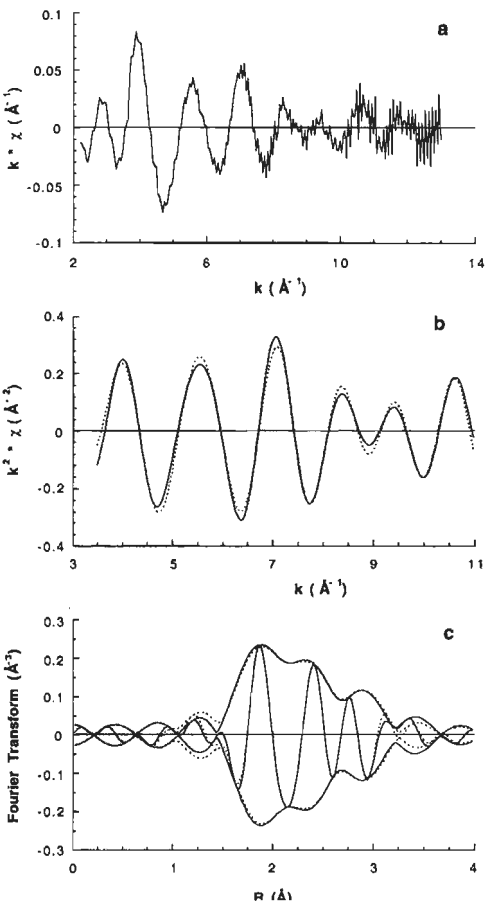

Figure 8 EXAFS results of Pt/H–MAZ reduced at 450°C, a) k^1 weighed raw data, b) k^2 weighed Fourier filtered data (solid line) with model EXAFS spectrum (dashed line) calculated with the parameters from table 3, c) Fourier transform [k^2, Δk: 3.5 - 11.0 $Å^{-1}$] of the spectra in b).

Hydrogen chemisorption

The results of the hydrogen chemisorption measurements are shown in Table 5. The H/Pt values, which are all larger than 0.8 indicate that all catalysts are highly dispersed. The H/Pt values larger than 1 indicate that a coordinatively highly unsaturated platinum atom, as present in small clusters, is capable of adsorbing more than one hydrogen atom[26]. Figure 9 is a plot of the first shell coordination number versus the H/Pt values for the samples used in this study together with the results of previous measurements[26]. Surprisingly the correlation determined by Kip at al. does not hold for the samples used in this study, in particular the decrease in hydrogen chemisorption capacity with increasing reduction temperature is not accompanied by a comparable decrease in the first shell

Table 3 Structural parameters from EXAFS for Pt/H-MAZ after reduction at 450°C.

Backscatterer	N	R (Å)	$\Delta\sigma^2$ ($Å^2 \times 10^{-3}$)	ΔE_0 (eV)
Pt	2.9± 0.2	2.75± 0.01	6.0± 0.4	−1.7± 0.5
O	0.6± 0.1	2.23± 0.01	−3.0± 0.5	−12.2± 0.6

Pt–Pt coordination number determined with EXAFS. Dividing the amount of adsorbed hydrogen by the available platinum surface area (roughly estimated by the first shell coordination number, since for these small clusters almost all atoms are available for chemisorption) and plotting H_{ads}/N_{Pt-Pt} versus the reduction temperature (Figure 10) reveals an almost linear decrease of the amount of hydrogen adsorbed per unit surface area with reduction temperature for the platinum clusters supported by zeolite LTL.

Discussion

Short Pt-O distance

The short Pt-O distance of 2.2 Å observed in this study is characteristic of oxygen atoms in contact with low- or zero-valent metal clusters. Similar metal-oxygen distances were observed by EXAFS on reduced Ir/alumina after evacuation (2.19 Å) and after oxygen adsorption at 77 K (2.21 Å)[7]. In addition, both EXAFS measurements of low-valent, supported noble metal subcarbonyls[28] and X-ray diffraction (XRD) data for lower valent noble metal compounds containing oxygen ligands[17] also indicate metal-oxygen bond lengths of 2.1-2.2 Å.

In contrast, metal-oxygen distances in higher valent metal oxides are found to be

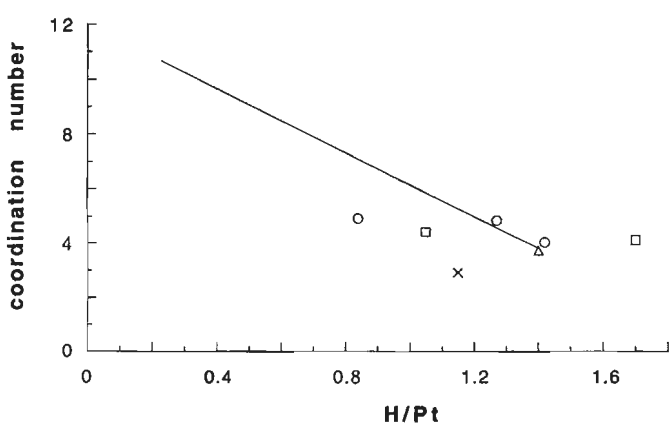

Figure 9 Hydrogen chemisorption values plotted as a function of first shell Pt–Pt coordination number. Correlation from Kip et al.[26], triangle represents extension by Vaarkamp et al.[27], square: Pt/H–LTL, circle: Pt/K–LTL, and cross: Pt/H–MAZ.

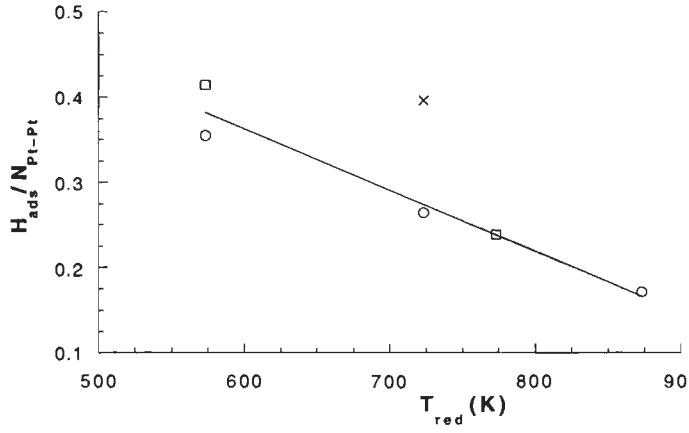

Figure 10 Amount of hydrogen chemisorbed per unit surface area of a platinum particle as a function of reduction temperature. Solid line is a linear least squares fit of the results for platinum supported by zeolite LTL, square: Pt/H–LTL, circle: Pt/K–LTL, and cross: Pt/H–MAZ.

considerably shorter than the 2.2 Å found in the present study. For example XRD data for Rh_2O_3[29] and $Na_2Pt(OH)_6$[30] indicates metal-oxygen distances of 2.05 in both cases. EXAFS studies of platinum ion-exchanged in zeolites (Pt^{+2}) also found Pt-O distances of 2.01-2.05 Å[15]. Further, oxygen chemisorption on prereduced Pt/SiO_2 at 298 K leads to a Pt-O distance of 2.03 Å[5], which is shorter than the distance observed after oxygen adsorption at 77 K (2.21 Å)[7]. The shorter (2.03 Å) distance after 298 K chemisorption is in the range expected for oxidic platinum, and may suggest oxidation of at least the surface metal atoms under these conditions.

In a few early studies of reduced supported metal catalysts, metal-oxygen distances of 1.92-2.07 Å were reported[4-6], which are shorter than the 2.2 Å found in the present study. The reasons for the difference between these values are not known. However, in the present study we used $Na_2Pt(OH)_6$ as reference for the Pt-O absorber-backscatterer pair, which is more reliable than the β-PtO_2 which was used in the earlier studies[31]. In addition, the contribution to the total EXAFS signal arising from the metal-support interface is proportionately larger in the present study due

Table 4 Fourier filtering ranges and Goodness of Fit (ε_v^2) values

Sample	T_{red} (K)	Fourier filtering Δk (Å^{-1})	ΔR (Å)	Δk_{anal} (Å^{-1})	ε_v^2
Pt/H–LTL	300	2.64 – 13.93	1.21 – 3.27	3.50 – 13.00	21.8
	500	2.79 – 13.98	1.15 – 3.25	3.50 – 13.00	38.7
Pt/K–LTL	300	2.57 – 13.90	1.60 – 3.26	3.50 – 13.00	27.3
	450	2.64 – 13.33	1.50 – 3.36	3.50 – 12.50	2.8
	600	2.72 – 13.94	1.17 – 3.27	3.50 – 13.00	17.4
Pt/H–MAZ	450	2.66 – 12.04	1.52 – 3.39	3.50 – 11.00	11.2

to the much smaller metal particle size, i.e. larger Pt-O coordination number and smaller Pt-Pt coordination number. Finally, signal-to-noise ratios in the EXAFS data are increased using current generation synchrotrons. These factors allow a much more accurate determination of the structure of the metal-support interface.

Long Pt-O distance

In the present study, we have shown that Pt-O distances of 2.6-2.7 Å are observed only after LTR (≤573 K). In addition, a number of previous studies have also reported similar long metal-oxygen distances. While some previous EXAFS studies of supported metal catalysts have reported only metal-oxygen distances shorter than 2.2 Å, in each of these cases the catalysts had been reduced at 753 K or higher. The temperature of reduction at which the long metal-oxygen distance can be detected is dependent on the metal and the support[17].

Structural model of the metal-support interface

In the conventional understanding of the structure of the interface between the metal and the support, the metal atoms are in direct contact with the oxide ions of the support. This model is consistent with the metal-oxygen distance of 2.2 Å, which is approximately equal to the sum of the covalent radii of the metal and oxygen atoms. By contrast, the results of this study indicate that a longer metal-oxygen distance is present after LTR. One possible explanation for the long platinum-oxygen distance is that an additional atom resides at the interface between the metal atoms and the support. The lack of observable backscattering from this atom in the EXAFS spectrum suggests that this interfacial atom is small, and probably hydrogen. The hydrogen may be protonic, like hydrogen from hydroxyl groups on the support, or atomic in nature, such as from chemisorbed hydrogen. Removal of chemisorbed hydrogen by evacuation from Ir/γ–Al_2O_3 after LTR resulted in a Pt–O distance of 2.19 Å[7]. Experiments with Ir/MgO on which hardly any hydroxyl groups are present provide more evidence that the hydrogen in the interface is atomic in nature[13]. During HTR, the interfacial hydrogen may be removed as H_2 or, alternatively, as H_2O during dehydration of the support at high temperatures. In either case, loss of interfacial hydrogen results in a shortening of the Pt-O distance to 2.2 Å. The fact that the interfacial hydrogen is not reintroduced during cooling in hydrogen indicates that the removal of hydrogen is irreversible, or at best, reversible only with

Table 5 Hydrogen chemisorption results

Sample	T_{red} (°C)	H/Pt
Pt/H–LTL	300	1.70
	500	1.05
Pt/K–LTL	300	1.42
	450	1.27
	600	0.84
Pt/H–MAZ	450	1.15

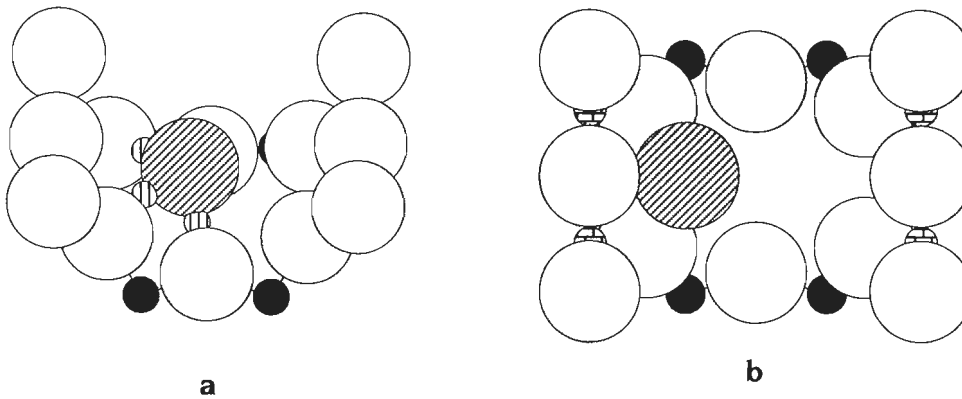

Figure 11 Part of the cavity in the wall of the LTL pore, viewed from the middle of the pore towards the cancranite cage with a platinum atom positioned in agreement with the EXAFS distances for a sample after a) LTR, b) HTR. The potassium ions have been omitted for clarity.

difficulty. The lack reversibility in hydrogen is also consistent with the strong metal-support interaction as indicated by the low Debye-Waller factor which is associated with the short Pt-O (2.2 Å) distance. The removal of hydrogen from the metal-support interface affects the nature of the interaction between the oxygen atoms of the support and the platinum clusters as is reflected in the large decrease of the inner potential shift. Analysis of the whiteline intensities of the catalysts in this study[32] showed that the loss of interfacial hydrogen results in an increased d-band density of states of the platinum clusters.

The availability of a detailed knowledge of the structure of zeolite LTL[33] and the coordination parameters determined with EXAFS challenges one to build an atomic model of the structure of the platinum particles located in the pores of the zeolite after LTR and HTR. A schematic drawing of the situation after LTR and HTR will be presented elsewhere. In Figure 11a a single platinum atom is depicted in the cavity of the pore of zeolite LTL. The location is in agreement with the EXAFS results after LTR, The hydrogen atoms are clearly visible between the platinum atom and the oxygen atoms of the framework. After HTR, when the Pt–O distance in shortened, this position is in disagreement with the EXAFS results, an alternative position is shown in Figure 11b (HTR).

Implications for catalysis

The effect of reduction temperature on the catalytic activity and selectivity has been extensively studied. High temperature reduction has been shown to suppress hydrogenolysis activity with a variety of reactants and catalysts, e.g. n-pentane over Pt on Al_2O_3, SiO_2, and TiO_2[34], ethane over Ru on SiO_2[35], propane over Pt in zeolites[36], and methylcyclopentane ring opening over Pt on SiO_2 and Al_2O_3[37]. High temperature reduction can also affect the selectivity of the reaction. For example, for MCP ring opening over Pt on SiO_2 and on Al_2O_3, high temperature reduction

Figure 12 Schematic representation of the changes in the structure of the metal-support interface as a function of the reduction temperature, a) LTR: hydrogen present in the metal-support interface, b) HTR: interfacial platinum atoms in direct contact with support.

decreased the selectivity to n-hexane[37], while for Pt on SiO_2 and Y zeolites, the ratio of isomerization to hydrogenolysis of neopentane decreased with increasing reduction temperature[38].

In addition to changes in the catalytic properties, high temperature reduction has been reported to alter the chemisorption properties of the metal. H_2 TPD indicates that chemisorbed H_2 is more strongly bound to platinum after HTR and this strongly chemisorbed H_2 was suggested to be responsible for the observed decrease in hydrogenolysis activity[39]. Also, both our results and a recent study on a Pt/SiO_2 catalyst[40] indicate that after high reduction temperature the H_2 chemisorption capacity is decreased more than is expected from the decrease in surface area.

The decrease in hydrogen chemisorption capacity of surface platinum atoms with increasing reduction temperature can be due to a decrease in hydrogen chemisorption capacity of all surface platinum atoms. Alternatively, platinum atoms in close contact with support oxygen ions can have hydrogen chemisorption properties different from platinum atoms separated from the support oxygen ions by interfacial hydrogen or platinum atoms not in contact with support oxygen ions at all (Figure 12). Hence, increasing the reduction temperature diminishes the hydrogen chemisorption capacity of a fraction of the platinum atoms changes drastically.

In the present study, we have shown that high temperature reduction leads to structural changes in the metal-support interface. At high reduction temperatures, hydrogen is lost from the metal-support interface, leaving the metal particles in closer contact with the oxide ions of the support. While the details of how these structural changes affect the catalytic properties are not yet understood, it seems likely that the structural changes of the metal-support interface alter the electronic properties of the metal, and are responsible for at least some of the changes in the catalytic properties. A first indication of the type of effects that might be expected is the decrease in hydrogen chemisorption capacity of platinum surface atoms.

Conclusions

The extremely small metal particles present in these LTL zeolite catalysts allow an accurate characterization of the structure of the metal-support interface by EXAFS. Low temperature reduction (LTR) leads to the formation of a long Pt-O distance (ca. 2.7 Å). In contrast, high temperature reduction (HTR) leads to the formation of a shorter Pt-O distance (ca. 2.2 Å). At intermediate temperatures, both Pt-O distances are observed. It is proposed that the long Pt-O distance is due to the presence of hydrogen in the interface between the platinum atoms and the oxide surface. This interfacial hydrogen is lost during high temperature reduction, leaving the platinum atoms in direct contact with the oxide surface. The stability of the interfacial hydrogen layer is dependent on both the nature of the support and the type of supported metal. The observed structural changes in the metal-support interface may be responsible for the changes in the catalytic properties associated with LTR vs. HTR, as indicated by the decrease in hydrogen chemisorption capacity of platinum surface atoms. However, a complete understanding of how the observed structural changes in the metal-support interface affect the catalytic properties of the metal is still lacking, and this will be the subject of future investigations.

References

1. Sinfelt, J. H., Via, G. H., and Lytle, F. W., *J. Chem. Phys.* **68**, 2009 (1978).
2. Lytle, F. W., Wei, P. S. P., Greegor, R. B., Via, G. H., and Sinfelt, J. H., *J. Chem. Phys.* **70**, 4849 - 4855 (1979).
3. Via, G. H., Sinfelt, J. H., and Lytle, F. W., *J. Chem. Phys.* **71**, 690 (1979).
4. Lagarde, P., Muraka, T., Vlaic, G., Freund, E., Dexpert, H., and Bournonville, J. B., *J. Catal.* **84**, 333 (1983).
5. Lytle, F. W., Greegor, R. B., Marques, E. C., Sandstrom, D. R., Via, G. H., and Sinfelt, J. H., *J. Catal.* **95**, 546 (1985).
6. Emrich, R. J., Mansour, A. N., Sayers, D. E., McMillan, S. T., and Katzer, J. R., *J. Phys. Chem.* **89**, 4261 (1985).
7. Kampers, F. W. H., and Koningsberger, D. C., *Faraday Discuss. Chem. Soc.* **89**, 137 (1990).
8. van't Blik, H. F. J., van Zon, J. B. A. D., Huizinga, H. F., Vis, J. C., Koningsberger, D. C., and Prins, R., *J. Am. Chem. Soc.* **107**, 3139 (1985).
9. van Zon, J. B. A. D., Koningsberger, D. C., van't Blik, H. F. J., and Sayers, D. E., *J. Chem. Phys.* **82**, 5742 (1985).
10. Koningsberger, D. C., van Zon, J. B. A., van't Blik, H. F. J., Visser, G. J., Prins, R., Mansour, A. N., Sayers, D. E., Short, D. R., and Katzer, J. R., *J. Chem. Phys.* **89**, 4075 (1985).

11. van Zon, F. B. M., Visser, G. J., and Koningsberger, D. C., *in* "Proc. 9th Int. Cong. Catal., Calgary, (Philips, M. J., Ternan, M., Eds.), p. 1386. The Chemical Institute of Canada, Ottawa, 1988.
12. Koningsberger, D. C., and Sayers, D. E., *Solid State Ionics* **16,** 23 (1985).
13. van Zon, F. B. M., Maloney, S. D., Gates, B. C., and Koningsberger, D. C., *submitted*
14. Möller, K., Koningsberger, D. C., and Bein, T., *J. Phys. Chem.* **93,** 6116 (1989).
15. Tzou, M. S., Teo, B. K., and Sachtler, W. M. H., *J. Catal.* **113,** 220 (1988).
16. Martens, J. H. A., Prins, R., Zandbergen, H., and Koningsberger, D. C., *J. Phys. Chem.* **92,** 1903 (1988).
17. Koningsberger, D. C., and Gates, B. C., *Catal. Lett.* **14,** 271 (1992).
18. Breck, D. W., "Zeolite Molecular Sieves, Structure, Chemistry and Use" John Wiley & Sons, New York, 1974, p. 306.
19. Kampers, F. W. H., Maas, T. M. J., van Grondelle, J., Brinkgreve, P., and Koningsberger, D. C., *Rev. Sci. Instr.* **60,** 2635 (1989).
20. Vaarkamp, M., Dring, I., Oldman, R. J., Stern, E. A., and Koningsberger, D. C., *submitted (chapter 3).*
21. Cook Jr, J. W., and Sayers, D. E., *J. Appl. Phys.* **52,** 5024 (1981).
22. Kampers, F. W. H., *PhD Thesis,* Eindhoven University of Technology, Eindhoven, 1989.
23. Vaarkamp, M., Linders, J. C., and Koningsberger, D. C., *in preparation (chapter 2).*
24. Lytle, F. W., Sayers, D. E., and Stern, E. A., *Physica B* **158,** 701 (1988).
25. Vaarkamp, M., van Grondelle, J., van Santen, R. A., Miller, J. T., Modica, F. S., Lane, G. S., and Koningsberger, D. C., *in* "Proc. 9th Int. Zeolite Conf., Montreal, July 5-10, 1992", Butterworth-Heinemann, London, in print.
26. Kip, B. J., Duivenvoorden, F. B. M., Koningsberger, D. C., and Prins, R., *J. Catal.* **105,** 26 (1987).
27. Vaarkamp, M., Miller, J. T., Sajkowski, D. J., Modica, F. S., Lane, G. S., Gates, B. C., van Grondelle, J., and Koningsberger, D. C., *Catal. Lett.* **6,** 369 (1990).
28. Chang, J. -R., Gron, L. U., Honji, A., Sanchez, K. M., and Gates, B. C., *J. Phys. Chem.* **95,** 9944 (1991).
29. Coey, J. M., *Acta Cryst.* **B 26,** 1876 (1970).
30. Trömel, M., and Lupprich, E., *Z. Anorg. Chem.* **414,** 160 (1975).
31. Mansour, A. N., Sayers, D. E., Cook Jr, J. W., Short, D. R., Shannon, R. D., and Katzer, J. R., *J. Phys. Chem.* **88,** 1778 (1984).
32. Vaarkamp, M., Miller, J. T., Modica, F. S., and Koningsberger, D. C., *in* "Proc. XAFS VII, Kobe, Japan, August 23-29, 1992", in print.
33. Barrer, R. M., and Villiger, H., *Z. Kristallogr.* **128,** 352 (1969).
34. Menon, P. G., and Froment, G. F., *Appl. Catal.* **1,** 31 - 48 (1981).
35. Guczi, L., Matusek, K., Manninger, I., Kiralay, J., and Eszterle, M., *in* "Proc. 2nd Inter. Symp. Sci. Bases for Prep. Het. Cat., Louvain–la–Neuve", Elsevier, Amsterdam.

36. Vaarkamp, M., Miller, J. T., Modica, F. S., Lane, G. S., and Koningsberger, D. C., *in* "Proc. 10th Int. Congr. Catal., Budapest, 19 - 24 July 1992", in print.
37. Kramer, R., and Fischbacher, M., *J. Mol. Catal.* **51,** 247 (1989).
38. Foger, K., and Anderson, J. R., *J. Catal.* **54,** 318 (1978).
39. Menon, P. G., and Froment, G. F., *J. Catal.* **59,** 138 (1979).
40. Lamber, R., and Jaeger, N. I., *J. Appl. Phys.* **70,** 457 (1991).

Chapter 6

A Study of the Structural Changes in a $Pt/\gamma-Al_2O_3$ Catalyst Induced by Hydrogen Treatment

Abstract

The structure and morphology of both the platinum clusters and the metal-support interface of $Pt/\gamma-Al_2O_3$ catalysts have been studied with Extended X-ray Absorption Fine Structure Spectroscopy (EXAFS), infrared spectroscopy and hydrogen temperature programmed desorption (TPD). The TPD profile after reduction at 300°C shows that three types of hydrogen are present. Reversibly adsorbed hydrogen desorbs between 80 and 200°C, spillover hydrogen desorbs above 300°C and has a maximum at 425°C. A small, but significant amount of hydrogen desorbs between 300 and 360°C. After reduction at 300°C (LTR) the metal-support interface is characterized by a Pt–O distance of 2.66 Å. Reduction at 450°C (HTR) diminishes the amount of reversibly adsorbed hydrogen and spillover hydrogen observed in the TPD, the hydrogen desorption between 300 and 360°C is absent. The metal-support interface is now characterized by a Pt–O distance of 2.24 Å. The decrease of the interfacial Pt–O distance from 2.66 Å after LTR to 2.24 Å after HTR is related to the hydrogen desorbing between 300 and 360°C. A model is presented in which hydrogen is present between the metal particles and the support after reduction at 300°C.

Introduction

During the last decade many studies on the relation between structure and catalytic properties of supported metal catalysts have been published. In particular, hydrogen pretreatment effects on the skeletal reactions of hydrocarbons over supported metal catalysts have been studied by many authors[1-6]. Metal particles supported on "reducible oxides" like titania reduced at high temperatures (500°C) show significant differences in catalytic behaviour in comparison to a reduction at low temperature. Using "nonreducible" oxides such as alumina or silica the effects of high reduction temperatures are usually smaller, but still distinct differences have been observed for the catalytic activity and selectivity in hydrocarbon reactions as hydrogenolysis, isomerization and aromatization.

Den Otter and Dautzenberg[2] and Menon and Froment[4] reported a remarkable drop in hydrogenolysis activity of a Pt/Al_2O_3 catalyst after reduction at temperatures higher than 550°C. Margitfalvi et al.[6] showed that high temperature treatment of Pt/Al_2O_3 in hydrogen resulted in a considerable change in selectivity towards aromatization. A recent study of the hydrogen pretreatment effects on the hydrogenolysis of methylcyclopentane using platinum catalysts with different dispersions prepared via HV deposition on amorphous films of silica and alumina was carried out by Kramer and Andre[3]. The TOF for MCP hydrogenolysis was highest for the most dispersed catalyst and the product distribution was dependent on the particle size according to the structure sensitivity of this reaction: selectivity towards n-hexane increased with increasing dispersion. Reduction in hydrogen at 400°C resulted in a lower activity and in a lower selectivity towards n-hexane compared to the results obtained after reduction at 275°C.

Very recently Abasov et al.[7] reported that the hydrogen chemisorption capacity of a Pt/Al_2O_3 catalyst decreases dramatically upon hydrogen treatment at temperatures above 500°C. Simultaneously the thermal stability of linear Pt–CO complexes decreased and the singleton frequency of the complex increased from 2050 to 2060 cm^{-1}, while the dipole-dipole shift decreased from 40 to 15 cm^{-1}. The observations were explained from the transition into the SMSI state of the Pt/Al_2O_3 catalyst during reduction above 500°C.

Recently, Koningsberger and Gates[8] reviewed the results of EXAFS studies on the structure of the metal-support interface in supported metal carbonyls and supported metal catalysts. Single-metal-atom carbonyls on non reducible metal oxide supports are bonded with metal-oxygen distances of approximately 2.15 Å; the bonding distance is only weakly sensitive to the oxidation state of the metal[9–14]. Nearly this same metal-oxygen distance is characteristic of the metal-support interface in metal-oxide-supported metal clusters following reduction at high temperatures (HTR: $T > 450$°C). This distance is similar to the metal-oxygen distance (determined by X-ray diffraction) in polyoxometallates[15]. When the supported metals are treated in hydrogen at low temperatures (LTR: $T < 350$°C) or prepared under He with

partially hydroxylated supports, another metal-support oxygen distance is observed, typically 2.5-2.7 Å.

The study of the metal-support interface of zeolite LTL supported platinum clusters in the preceding chapter agrees with the above described results. In addition it was concluded from hydrogen TPD measurements that the long metal-oxygen distance, present after LTR, is the result from hydrogen in the metal-support interface.

In this chapter we will extend the characterization of the metal-support interface of supported platinum catalysts to Pt/γ–Al_2O_3 catalysts. The structure of a highly dispersed 1.0wt% Pt/γ–Al_2O_3 catalyst was studied with EXAFS, temperature programmed desorption (TPD) and infrared spectroscopy after reduction at 300 or 450°C. Infrared spectroscopy is particularly suited to study the hydroxyl groups on the alumina surface, temperature programmed desorption yields information about the amount and bonding strength of hydrogen, water, and hydroxyl groups. The size and morphology of the metal clusters is studied with EXAFS. Furthermore EXAFS will yield information about the structure of the metal-support interface when the clusters are sufficiently small.

Two TPD experiments will be described, viz. TPD after reduction at 300°C (LTR) and TPD after reduction at 450°C (HTR). Infrared spectroscopy and EXAFS are applied to characterize the catalyst before the start and at different stages of the TPD experiments. The electronic structure of the Pt/γ–Al_2O_3 studied in this chapter has been studied by analysis of the intensity Pt L_{III} and L_{II} X-ray absorption edges (chapter 7). The catalytic properties of this catalyst are reported in chapter 7 (propane hydrogenolysis) and 8 (methylcyclopentane ring opening).

Experimental

Catalyst preparation

A 1.0 wt% Pt/γ–Al_2O_3 catalyst was prepared by pore volume impregnation of Ketjen CK-300 (200 m^2/g, 0.6 cm^3/g) with an aqueous solution of hydrochloric platinic acid. The catalyst was dried in air overnight at 120°C before it was reduced at 300°C (heating rate 3°/min) for 4 hours. After reduction the catalyst was passivated at room temperature. This catalyst will be referred to as sample **1**. A second 1.0 wt% Pt/γ–Al_2O_3 catalyst was prepared according to the procedure described above, but it was reduced at 450°C, this sample has been designated **2**. Prior to any experiment or treatment described in this chapter the catalyst was dried *in-situ* at 120°C for 2 hrs.

EXAFS data collection

EXAFS spectra were measured at the Synchrotron Radiation Source (SRS) in Daresbury, U.K., Wiggler Station 9.2, using a Si (220) double crystal monochromator. The storage ring was operated with an electron energy of 2 GeV and a current

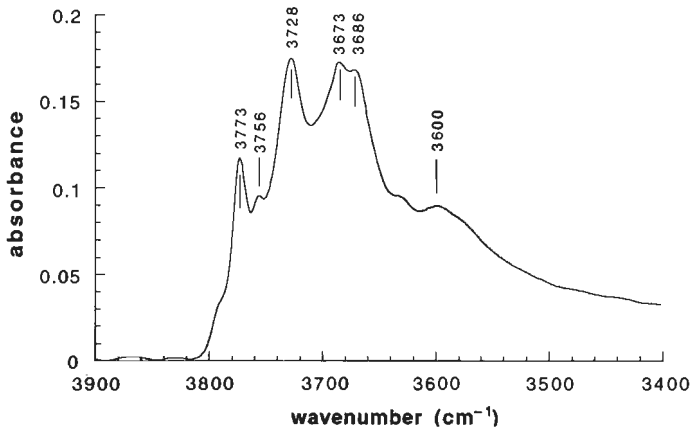

Figure 1 Hydroxyl region of the infrared spectrum of γ–Al_2O_3 after heating in vacuum to 550°C.

between 120 and 250 mA. At the Pt L_{III} edge (11564 eV), the estimated resolution was 3 eV. The monochromator was detuned to 50% intensity to avoid the effects of higher harmonics present in the X–ray beam. The measurements were done in the transmission mode. To decrease low- and high-frequency noise as much as possible, each data point was counted for 1 s and 6 scans were averaged.

The sample was pressed into a self–supporting wafer (calculated to have an absorbance of 2.5) and placed in a controlled–atmosphere cell[16], with the sample handled in the absence of air. After drying in flowing helium at 120°C for two hours the sample was heated at a rate of 5°C/min to the reduction temperature in flowing, purified, and dried hydrogen at atmospheric pressure. The sample was held at the reduction temperature for one additional hour, then cooled to room temperature (RT) as hydrogen flow was continued. After collecting the data on the reduced catalyst, the cell was evacuated to 10^{-5} Torr and heated to the evacuation temperature. Maintaining the vacuum, the cell was held at the evacuation temperature for an additional hour and cooled to RT. After collecting the data on the evacuated catalyst, hydrogen was admitted into the cell at RT. Subsequently the sample was heated to 200°C under flowing hydrogen and held there for one hour.

The measurements were done with the sample at liquid–nitrogen temperature and in the presence of hydrogen at atmospheric pressure for the reduced and readsorbed sample. The evacuated sample was measured at liquid-nitrogen temperature under a dynamic vacuum of 10^{-5} Torr.

Standard procedures were used to extract the EXAFS functions from the absorption spectra[17, 18]. Phase shifts and backscattering amplitudes were obtained from EXAFS measurements of platinum foil and $Na_2Pt(OH)_6$. The crystallinity of the $Na_2Pt(OH)_6$ was checked by XRD. The data were analyzed according to the procedures described in chapter 2.

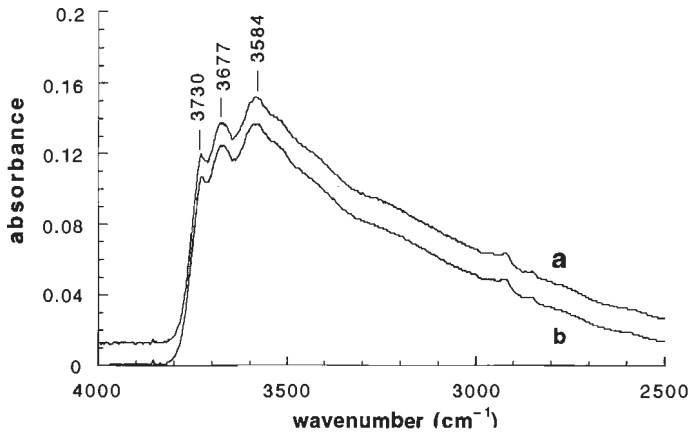

Figure 2 Infrared spectrum of Pt/γ–Al_2O_3 after a) reduction at 300°C b) a) after heating in Ar to 300°C.

Temperature Programmed Desorption

Temperature Programmed Desorptions (TPD) were programmed at 10°C/min to 550°C in flowing He. The He and H_2 gases were purified by oxygen and 5A molecular sieve traps. Desorbed gases were monitored with a Leybold quadrupole mass spectrometer.

Diffuse Reflectance Infrared Fourier Transform Spectroscopy (DRIFTS)

Samples were mounted in a DRIFTS cell connected to a gas system. After drying in flowing Ar at 120°C for two hours the sample was reduced in flowing 10% H_2/Ar at either 300 or 450°C (heating rate 5°/min) for one hour. Subsequently the sample was

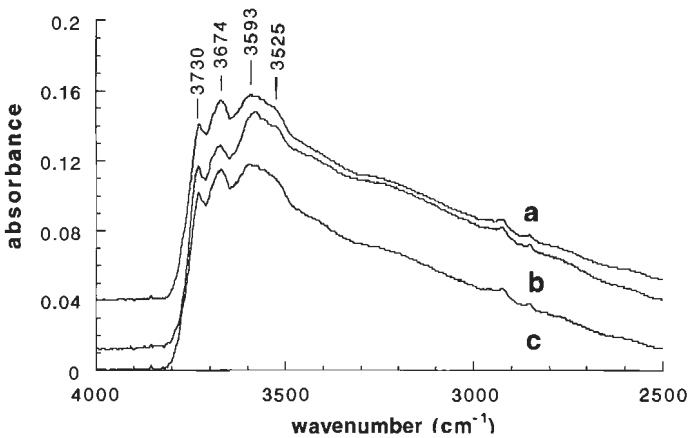

Figure 3 Infrared spectrum of Pt/γ–Al_2O_3 after a) reduction at 450°C b) a) after heating in Ar to 300°C, c) a) after heating in Ar to 450°C.

cooled in a static atmosphere of hydrogen to RT. The spectra were recorded with a Perkin-Elmer 1720X FT-IR spectrometer equipped with a DTGS detector, a diffuse reflectance accessory ('Collector', Barnes Analytic), and a standard controlled environmental chamber (Spectra-Tech, model 0030-103), 256 spectra with a resolution of 4 cm^{-1} were averaged. The reflectance from a typical catalyst sample relative to the open beam throughput, with the dome and (self-pressed) KBr windows in place was about 2% R at 2000 cm^{-1}.

The spectra are presented as diffuse absorbance ($-\log(R/R_0)$), analogous to absorbance used for transmission experiments[19]. Spectral subtraction was performed on a Perkin Elmer 3600 Data Station.

Results

Infrared spectroscopy

The hydroxyl region of the infrared spectrum of bare γ–Al_2O_3 heated in vacuum to 550°C is shown in figure 1. At least 6 peaks can be distinguished. A different type of γ–Al_2O_3 (JRC-ALO-4, a reference catalyst of the Catalysis Society of Japan[20]) evacuated at 500°C yields a spectrum[21], in which the peak at 3773 cm^{-1} is decreased in intensity, whereas the peak at 3600 cm^{-1} is increased in intensity.

The DRIFT spectrum of the Pt/γ–Al_2O_3 after reduction at 300°C is shown in figure 2a, the intensity in the hydroxyl region is increased compared to the evacuated bare γ–Al_2O_3, due to the diminished dehydroxylation during treatment at 300°C. Only three peaks can be distinguished in the hydroxyl region, two are in the region where the peaks of the bare γ–Al_2O_3 were detected, the weak peak at 3600 cm^{-1} has gained intensity and has shifted to 3586 cm^{-1}. This behaviour is consistent with behaviour

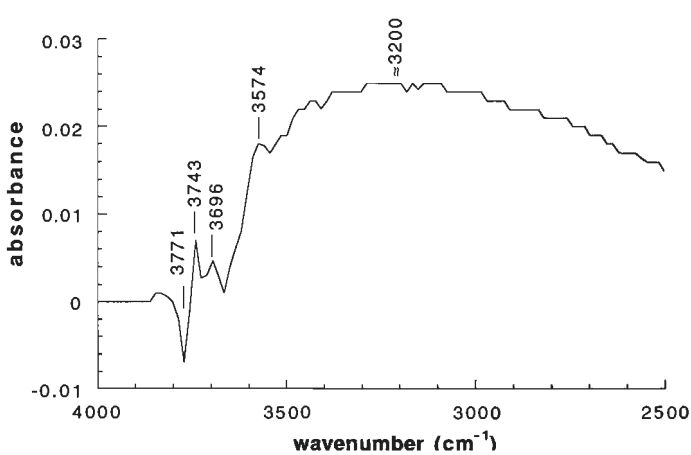

Figure 4 Difference spectrum of Pt/γ–Al_2O_3 reduced at 450°C after heating in Ar to 300°C (figure 3b) and 450°C (figure 3c).

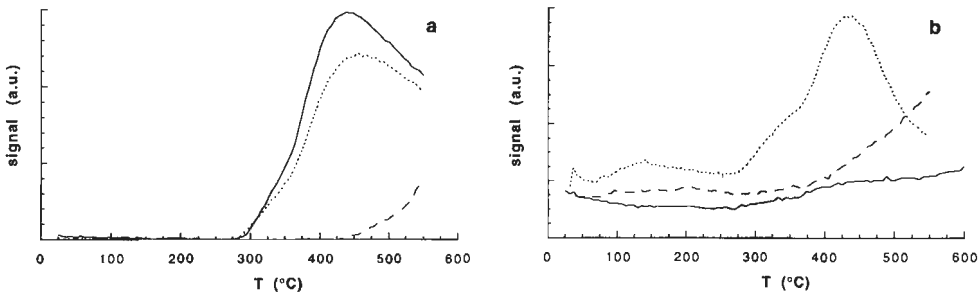

Figure 5 TPD profile of γ-Al_2O_3 (solid line) and Pt/γ-Al_2O_3 reduced at 300°C (dotted line) or 450°C (dashed line), a) water and b) hydrogen.

reported for Rh/γ-Al_2O_3[22]. Heating the sample in Ar to 300°C (figure 2b) did not affect the spectrum.

Spectra after reduction at 450°C and subsequent heating in Ar to either 300 or 450°C are presented in figure 3. The features in the spectra are similar to the features after reduction at 300°C, small differences are however present. The contamination with water is less as reflected in a decreased absorption above 2500 cm^{-1}. The peak at 3588 cm^{-1} shifts to 3580 cm^{-1} and a new peak at 3528 cm^{-1} develops. The differences between the spectra obtained after heating in Ar to 300 and 450°C are shown in figure 4. Water desorption between 300 and 450°C results in a reduction in absorption below 3600 cm^{-1}. The decreased amount of water is accompanied by a decreased intensity of the peaks at 3576, 3694, and 3740 cm^{-1}, indicating that the amount of surface hydroxyl groups decreases when the sample is treated at higher temperature[23].

Temperature Programmed Desorption (TPD)

The desorption of hydrogen and water from the catalyst was monitored by a quadrupole mass spectrometer. During all experiments chlorine and oxygen were also monitored, but no desorption was detected. The desorption of water from the catalyst and the bare support, after reduction, is shown in figure 5a. The desorption of water starts just above the reduction temperature of the sample. The amount of desorbed water is approximately equal for the support and the catalyst reduced at 300°C, after reduction at 450°C a small amount of water desorbs above 450°C.

In the hydrogen TPD of the catalyst reduced at 300°C (figure 5b), three peaks and thus three types of hydrogen can be distinguished. The first peak located between 80

Table 1 Crystallographic data and Fourier filtering ranges of reference compounds.

Compound	Abs. - Sc. pair	FT range ($Å^{-1}$)	FT^{-1} range (Å)	N	R (Å)	ref.
Pt foil	Pt–Pt	2.16 – 20.41	1.39 – 3.09	12	2.774	[24]
$Na_2Pt(OH)_6$	Pt–O	1.83 – 14.87	0.84 – 2.26	6	2.05	[25]

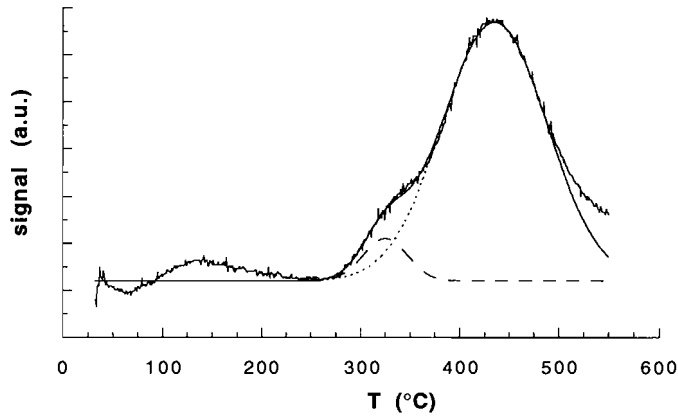

Figure 6 Deconvolution of the hydrogen TPD of Pt/γ-Al_2O_3 reduced at 300°C.

and 200°C with a maximum at 140°C is reversible and has been attributed to chemisorbed hydrogen desorbing from the platinum crystallites (see chapter 5). The broad desorption between 280 and 550°C has been deconvoluted in two gaussian peaks (figure 6): a large peak with a maximum a 435°C and a smaller with a maximum at 325°C.

After reduction at 450°C only a small amount of chemisorbed hydrogen is detected in the TPD (figure 5b), indicating that the hydrogen chemisorption capacity of the catalyst decreases by reduction at 450°C. In addition, the peak around 325°C and the large peak at 435°C are absent. Above 450°C a significant amount of hydrogen desorbs.

Additional experiments carried out with a TC detector allow quantification of the amount of desorbing hydrogen. The H/Pt stoichiometry of the total desorption above 280°C after reduction at 300°C was four. This suggests that the platinum might be oxidized by the desorbing water to give hydrogen and platinum(IV)oxide. However, a temperature programmed reduction experiment after the desorption experiment showed no hydrogen consumption. Hence, it is inferred that the platinum clusters are not oxidized.

EXAFS reference compounds

The data on the reference compounds were collected at SRS 9.2 under conditions similar to the measuring conditions of the samples. The phase and backscattering amplitude were extracted from the EXAFS spectra by k^3 weighed Fourier filtering, ranges are listed in table 1.

EXAFS data analysis

The first shell region of the EXAFS spectra was separated from the remaining background and the higher shells by k^2 weighed Fourier filtering. The Fourier filtering ranges are listed in table 2, together with the analysis range in k-space and

Table 2 Fourier filtering and analysis ranges and Goodness of Fit values (ε_v^2).

sample	treatment	FT range (Å^{-1})	FT^{-1} range (Å)	Analysis range (Å^{-1})	ε_v^2
1	H_2 300°C	2.60 – 13.89	1.57 – 3.31	3.50 – 13.00	54.1
1	H_2 450°C	2.79 – 14.03	1.14 – 3.48	3.50 – 13.00	38.9
2	H_2 300°C	2.64 – 13.88	1.25 – 3.33	3.50 – 13.00	17.2
2	H_2 300°C, vacuum 300°C	2.70 – 13.82	1.23 – 3.28	3.50 – 13.00	48.3
2	H_2 300°C, vacuum 300°C, H_2 200°C	2.65 – 13.86	1.24 – 3.33	3.50 – 13.00	15.3
2	H_2 450°C	2.66 – 12.62	1.35 – 3.32	3.50 – 12.00	6.2
2	H_2 450°C, vacuum 450°C	2.71 – 13.92	1.21 – 3.36	3.50 – 13.00	13.1

the Goodness of Fit (ε_v^2) values[26]. In the subsequent paragraphs the main features of the spectra and the analysis will be discussed, the results of the analyses are listed in tables 3–5. The errors in the refined parameters were calculated from the noise in the Fourier filtered spectrum and the correlations between the parameters. Hence, systematic errors arising from the used reference and Fourier filtering are neglected (see chapter 2 and 3).

Sample 1 reduced at 300 and 450°C

The state of the catalyst before the TPD was characterized by EXAFS. EXAFS spectra of sample **1** after reduction at 300 and 450°C are presented in figure 7. Data quality is high as indicated by the signal to noise ratio of 31 at 3.8 and 8 at 13.0 Å^{-1} for the sample reduced at 300°C. The difference in nodes and the different envelope of these

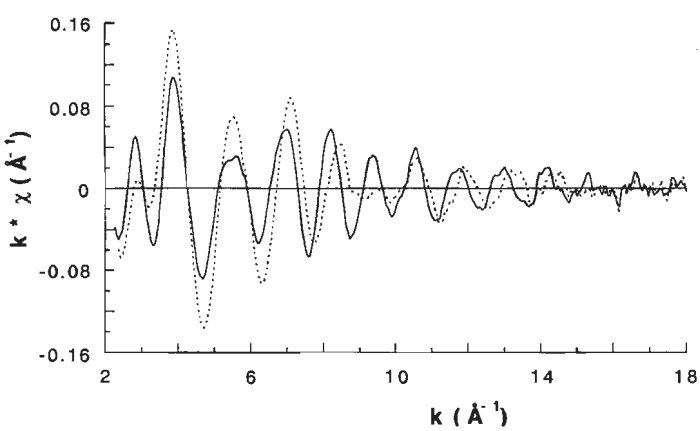

Figure 7 EXAFS spectra (k^1 weighed) of sample **1** reduced at 300°C (solid line) and 450°C (dotted line).

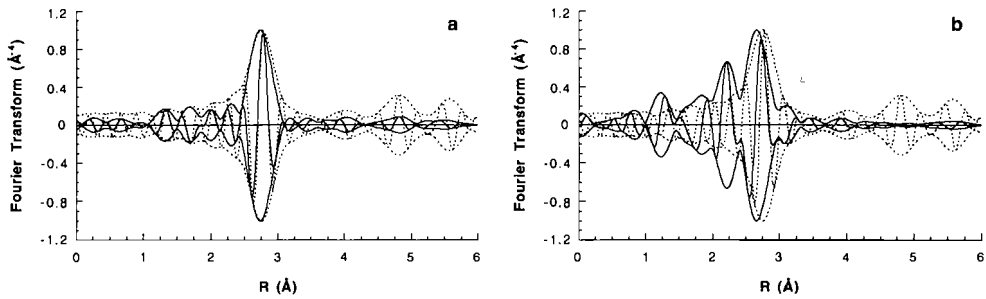

Figure 8 Fourier transform of the EXAFS spectra [k^3, Δk: 3.1 – 13.1 $Å^{-1}$, Pt–Pt phase- and amplitude-corrected] of a) sample **1** reduced at 300°C (solid line) and platinum foil (dotted line) and b) sample **1** reduced at 450°C (solid line) and platinum foil (dotted line). All transforms are normalized.

EXAFS spectra indicate that there are large changes in the structure of this catalyst upon different hydrogen treatments. The normalized k^3 weighed Pt–Pt phase and amplitude corrected Fourier transform of these spectra is shown in figure 8, together with the Fourier transform of platinum foil. These Fourier transforms were normalized to make comparison possible. The main peak of the sample reduced at 300°C is slightly shifted to a lower distance compared to the first shell Pt–Pt peak of Pt foil. The main peak of the sample reduced at 450°C exhibits a significantly larger shift to shorter distance. Furthermore, an additional peak around 2.3 Å is visible. The higher shell region (R > 3.5 Å) shows that both EXAFS spectra contain minor contributions from higher platinum or support shells. After reduction at 300°C small peaks at the location of the second and third coordination shell of platinum foil are present. Increasing the reduction temperature to 450°C results in a small shift of the peak in the second Pt–Pt shell region and the disappearance of the peak in the third shell region. This indicates a morphology change of the platinum particles from 3-dimensional to flat.

To show the presence of low Z contributions to the EXAFS spectrum the normalized k^1 weighed Pt–Pt phase and amplitude corrected Fourier transforms of

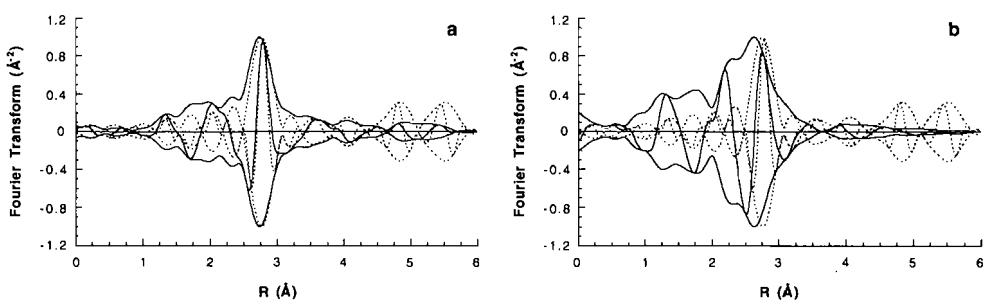

Figure 9 Fourier transform of the EXAFS spectra [k^1, Δk: 3.1 – 13.1 $Å^{-1}$, Pt–Pt phase- and amplitude-corrected] of a) sample **1** reduced at 300°C (solid line) and platinum foil (dotted line) and b) sample **1** reduced at 450°C (solid line) and platinum foil (dotted line). All transforms are normalized.

Table 3 Results of hydrogen chemisorption measurements and refinement of structural parameters for EXAFS spectra of sample **1** after reduction at 300 or 450°C.

T_{red} (°C)	H/Pt	Backscatterer	N	R (Å)	$\Delta\sigma^2$ ($\times 10^{-3}$ Å^{-2})	ΔE_0 (eV)
300	1.48	Pt	4.8 ± 0.1	2.76 ± 0.01	4.2 ± 0.1	2.1 ± 0.2
		O	1.2 ± 0.1	2.66 ± 0.01	7.0 ± 0.6	7.3 ± 0.4
450	1.16	Pt	3.8 ± 0.1	2.72 ± 0.01	5.5 ± 0.1	1.7 ± 0.2
		O	1.5 ± 0.1	2.25 ± 0.01	−2.3 ± 0.1	−13.5 ± 0.1

sample **1** after reduction at 300°C and 450°C and platinum foil are compared in figure 9. The amplitude and imaginary part of sample **1** after reduction at 300°C and platinum foil (figure 9a) are significantly different at a distance shorter than the Pt–Pt first shell distance, thus indicating the presence of an additional scatterer. After reduction at 450°C (figure 9b) the differences have increased, indicating that the magnitude of the additional contribution has increased.

The structural parameters (table 3) were obtained by non linear least squares refinement. The model EXAFS spectra calculated with these parameters are shown in figure 10a and b together with the Fourier filtered measured EXAFS spectra.

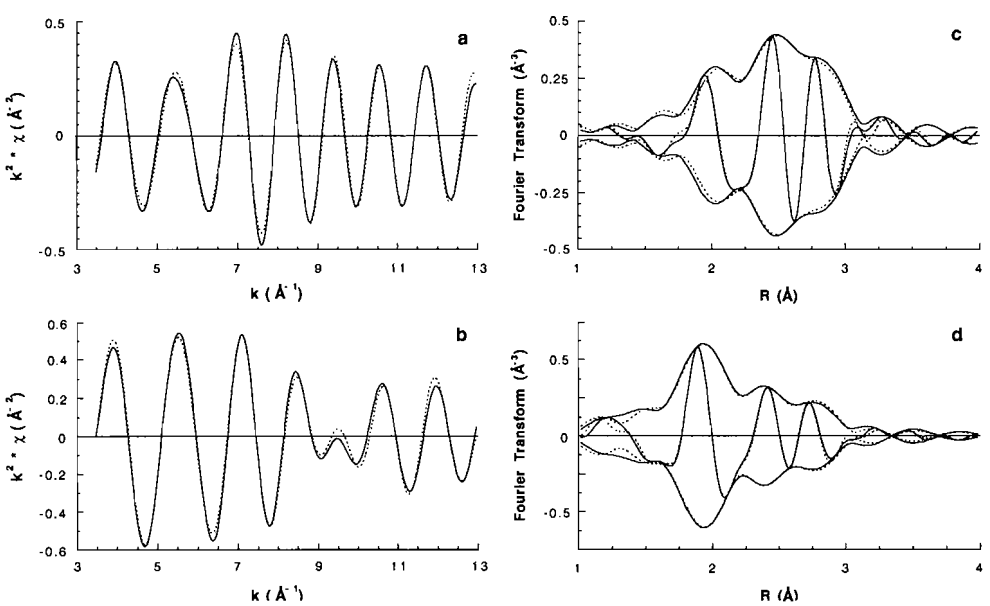

Figure 10 a) Fourier filtered EXAFS spectra (k^2 weighed) of sample **1** reduced at 300° (solid line) and a calculated EXAFS spectrum from the parameters in table 1 (dotted line), b) Fourier filtered EXAFS spectra (k^2 weighed) of sample **1** reduced at 450° (solid line) and a calculated EXAFS spectrum from the parameters in table 1 (dotted line), c) Fourier transform $|k^2, \Delta k: 3.5 - 13.0\ Å^{-1}|$ of the spectra in a), d) Fourier transform of the spectra in b).

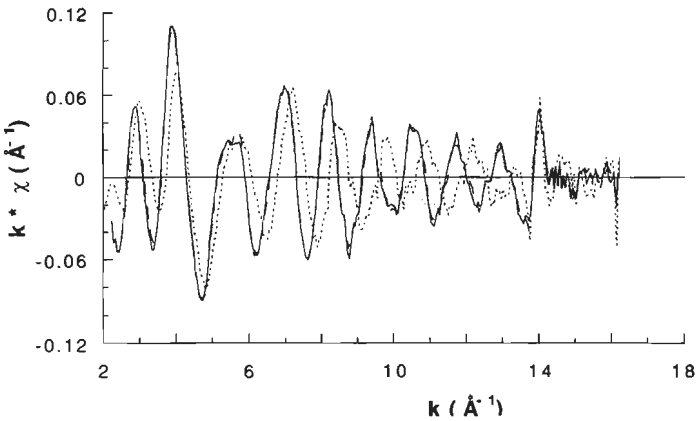

Figure 11 EXAFS spectra (k^1 weighed) of sample **2** after reduction at 300°C (solid line), reduction and evacuation at 300°C (dotted line), and reduction and evacuation at 300°C, followed by reduction at 200°C (dashed line).

Fourier transforms of these spectra are shown in figure 10c and d. In both k- and r-space the agreement between the model and the measured EXAFS spectrum is good. The difference in fit quality as reflected in the ε_v^2 values (table 2) is not due to a difference in agreement between the measured and model EXAFS spectrum, but originates from the different magnitude of the statistical errors present in the Fourier filtered spectra. The Pt–Pt distance is near the Pt–Pt bulk distance (2.774 Å) after reduction at 300°C, reduction at 450°C leads to a small but significant contraction of the first shell Pt–Pt distance. Furthermore, the Pt–Pt coordination number is decreased, while simultaneously the disorder in the first shell coordination shell has increased. After reduction at 300°C a Pt–O contribution at 2.66 Å is present in the EXAFS spectrum. This contribution is absent after reduction at 450°C, but a new contribution at 2.25 Å appears. The oxygen coordination number is slightly increased from 1.2 to 1.5, in agreement with the smaller Pt–Pt coordination number.

The low value of the Debye-Waller factor and the inner potential shift obtained after reduction at 450°C for the Pt–O contribution at 2.25 Å suggest that this oxygen contribution might not be an oxygen contribution at all. As the sample was prepared from hydrochloric platinic acid and alumina is known to retain chlorine we tried to replace the oxygen contribution with a chlorine contribution, but the fit obtained with inclusion of a chlorine contribution was inferior to the one listed in table 3. Moreover, when the sample reduced at 300°C was heated in a hydrogen flow to 450°C while monitoring the effluent gas from the reactor by mass spectrometry no chlorine was detected. Furthermore, it has recently been shown by SIMS[27] that for Rh on a model alumina support already after reduction at 200°C, no Rh–Cl interaction is present anymore, after reduction at 300°C, all the chlorine was

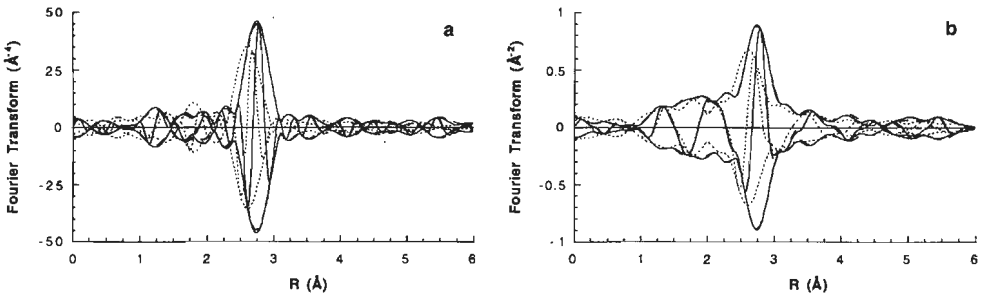

Figure 12 Fourier transform |Δk: 3.1 – 13.2 Å^{-1}, Pt–Pt phase- and amplitude-corrected| of EXAFS spectra of sample **2** reduced at 300°C (solid line), reduced and evacuated at 300°C (dotted line), and reduced and evacuated at 300°C, followed by reduction at 200°C (dashed line). a) k^3 weighed, b) k^1 weighed

removed from the alumina. The EXAFS analysis of Pt/LTL and Pt/H–MAZ reduced at 450°C revealed values of the Debye-Waller factor and the inner potential shift for a Pt–O contribution at 2.24 Å similar to the values obtained in this study[28]. In the Pt/H–MAZ no potassium or chlorine was present. We infer from all these arguments that oxygen is the correct contribution to the EXAFS spectrum.

EXAFS of Sample 2 after reduction at 300°C, evacuation at 300°C and H_2 at 200°C

Comparison of the EXAFS spectra after reduction at 300°C and evacuation at 300°C will reveal the influence of chemisorbed hydrogen on the structure of the catalyst. This treatment mimics a TPD to 300°C. Heating in H_2 to 200°C after evacuation restores the chemisorbed hydrogen on the platinum surface. The k^1 weighed EXAFS spectra of sample **2** after reduction at 300°C, evacuation at 300°C, and heating in H_2 to 200°C are shown in figure 11. The signal to noise ratio of the sample reduced at 300°C is 26 at 3.3 Å^{-1} and 5.2 at 12.8 Å^{-1}. The EXAFS spectrum obtained after evacuation at 300°C is distinctly different from the spectra after reduction at 300°C and heating in H_2 to 200°C, indicating that the changes induced by evacuation are

Table 4 Results of refinement of structural parameters for EXAFS spectra of sample **2** after reduction at 300°C, reduction and evacuation at 300°C, and reduction and evacuation at 300°C followed by reduction at 200°C.

treatment	backscatterer	N	R (Å)	$\Delta\sigma^2$ ($\times 10^{-3}$ Å^{-2})	ΔE_0 (eV)
reduction 300°C	Pt	5.0 ± 0.1	2.76 ± 0.01	4.0 ± 0.1	1.6 ± 0.2
	O	1.2 ± 0.1	2.68 ± 0.06	7.4 ± 1.2	6.6 ± 0.5
evacuation 300°C	Pt	3.8 ± 0.2	2.66 ± 0.01	4.9 ± 0.3	1.9 ± 0.5
	O	1.1 ± 0.2	2.64 ± 0.02	4.9 ± 2.1	3.7 ± 2.1
	O	0.3 ± 0.1	2.20 ± 0.01	−1.8 ± 1.2	1.5 ± 2.0
H_2 200°C	Pt	4.9 ± 0.1	2.75 ± 0.01	4.1 ± 0.1	2.0 ± 0.2
	O	1.4 ± 0.1	2.65 ± 0.01	8.0 ± 1.0	6.9 ± 0.5

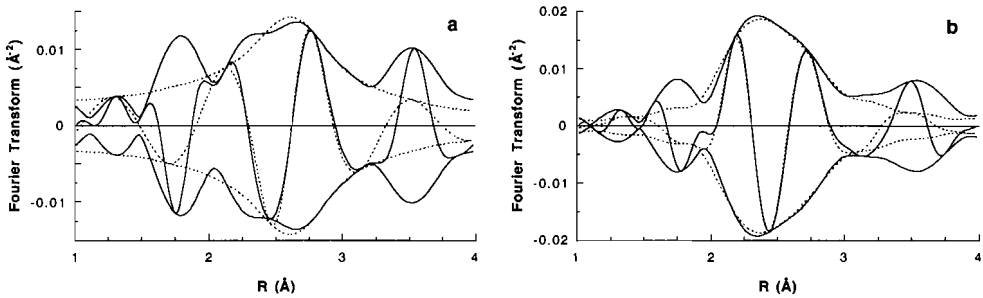

Figure 13 Fourier transform |k[1], Δk: 3.5 – 12.0 Å^{-1}, Pt–O phase corrected| of the Fourier filtered EXAFS spectrum minus the calculated Pt–Pt contribution (solid line) and the calculated Pt–O contribution(s) (dotted line) of sample **2** a) after reduction at 300°C, b) after evacuation at 300°C.

reversible. The k^3 weighed Pt–Pt phase- and amplitude corrected Fourier transform of these spectra is shown in figure 12a. After evacuation the main peak is located at a shorter distance and reduced in intensity compared to the main peak reduction at 300°C or heating in hydrogen to 200°C. This indicates a smaller distance and a reduction in coordination number of the first Pt–Pt coordination shell. The normalized k^1 weighed Pt–Pt phase- and amplitude corrected Fourier transform of these spectra (figure 12b) shows that the contribution of the low Z scatterers to the EXAFS spectrum, which dominate the Fourier transform between 1 and 2.3 Å is hardly changed, indicating that the structure of the metal-support interface is not affected by removal of chemisorbed hydrogen.

Results of the refinement of the structural parameters (table 4) shows that the structure after reduction at 300°C is nearly identical to the structure after heating in H_2 to 200°C. Evacuation at 300°C results in a contraction of the first shell Pt–Pt distance from 2.76 to 2.66 Å, in agreement with reported theoretical[29,30] and experimental[31,32] results for small metal particles. The Pt–Pt coordination number decreases upon evacuation, simultaneously a small Pt–O contribution at 2.20 Å appears. This indicates a change in the morphology of the platinum particle. Evacuation does not affect the Pt–O contribution at 2.67 Å, indicating that the structure of the metal-support interface as developed during reduction at 300°C is

Table 5 Results of refinement of structural parameters for EXAFS spectra of sample **2** after reduction at 450°C and reduction and evacuation at 450°C.

treatment	backscatterer	N	R (Å)	$\Delta\sigma^2$ ($\times 10^{-3}$ Å^{-2})	ΔE_0 (eV)
reduction	Pt	5.0 ± 0.2	2.72 ± 0.01	4.9 ± 0.3	5.0 ± 0.6
	O	0.8 ± 0.1	2.28 ± 0.01	0.3 ± 0.5	−18.2 ± 0.7
evacuation	Pt	4.1 ± 0.1	2.72 ± 0.01	4.7 ± 0.2	0.7 ± 0.3
	O	1.1 ± 0.1	2.22 ± 0.01	−2.0 ± 0.2	−12.6 ± 0.3

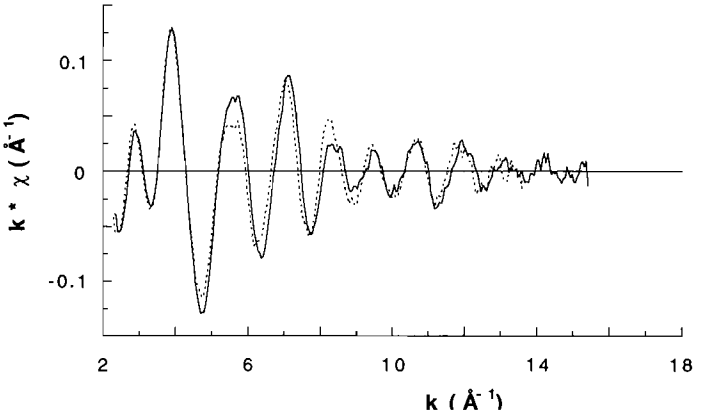

Figure 14 EXAFS spectra (k^1 weighed) of sample **2** reduced at 450°C (solid line) and reduced and evacuated at 450°C (dotted line).

not affected by evacuation. The Pt–O phase corrected Fourier transform of the calculated contribution(s) from the metal-support interface after reduction and evacuation are shown in figure 13 together with the corresponding experimental Fourier filtered EXAFS spectrum minus the calculated Pt–Pt contribution. Around 2.7 Å where the Pt–O contribution at 2.65 Å dominates the Fourier transform the differences between reduction and evacuation are negligible. Due to the presence of an additional Pt–O contribution at 2.3 Å the amplitude of the Fourier transform after evacuation is augmented at shorter distance compared to the Fourier transform after reduction.

EXAFS of sample 2 after reduction at 450°C and evacuation at 450°C

The EXAFS spectra after reduction at 450°C and evacuation at 450°C mimic a TPD to 450°C after reduction at 450°C. The EXAFS spectra (k^1 weighed) of sample **2** after reduction at 450°C and evacuation at 450°C are presented in figure 14. The changes

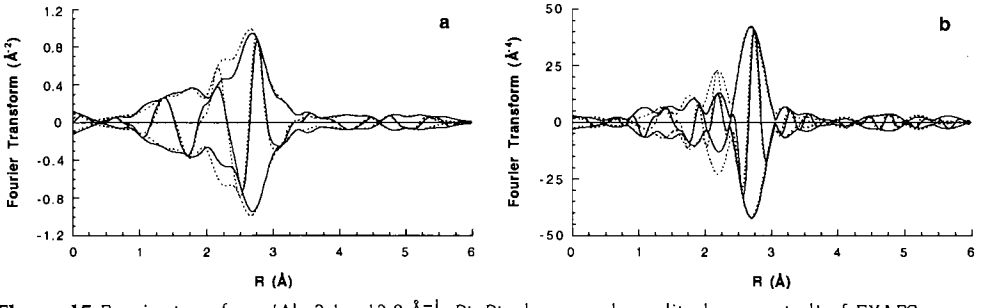

Figure 15 Fourier transform [Δk: 3.1 – 12.8 $Å^{-1}$, Pt–Pt phase- and amplitude-corrected] of EXAFS spectra of sample **2** reduced at 450°C (solid line) and reduced and evacuated at 450°C (dotted line), a) k^1 weighed, b) k^3 weighed.

in the EXAFS spectrum induced by evacuation at 450°C (after reduction at 450°C) are much smaller than the changes induced by evacuation at 300°C (after reduction at 300°C). This is also evident from the k^1 and k^3 weighed Pt–Pt phase- and amplitude corrected Fourier transforms of these spectra (figure 15). The structural parameters for these samples (table 5) show that the first shell Pt–Pt coordination number decreases upon evacuation. This decrease in first shell Pt–Pt coordination number is accompanied by an increase in the Pt–O coordination number. This behaviour is similar to the trends observed after reduction and evacuation at 300°C.

Discussion

Infrared spectroscopy

Interpretation of the spectrum obtained for the bare γ–Al_2O_3 according to the scheme proposed by Knözinger and Ratnasamy[23], would lead to the conclusion that either only (111) or a combination of (100), (110), and (111) planes of the Al_2O_3 is exposed. However, as argued by Chen and Zhang[?], Knözinger and Ratnasamy neglected the possibility of a proton residing on the lattice oxygen, which leads to additional peaks in the IR spectrum. Neutron diffraction studies of CD_4 adsorbed on γ–Al_2O_3 have indicated that the surface consists of (110) and (100) planes, no trace of the (111) plane has been found[33]. Iijima[34, 35] concluded from a HREM study γ–Al_2O_3 prepared by a dry method that the preferentially exposed plane is the (111) plane. Recently a HREM study[36] on commercial γ–Al_2O_3 provided evidence that the (110) plane is the preferentially exposed plane. As the Ketjen CK300 is similar to the Degussa studied by Heller and Cocke we assume that γ–Al_2O_3 preferentially exposes the (110) plane. Hence, we also assume that protons can reside on lattice oxygens.

The surface of γ–Al_2O_3 is covered with hydroxyl groups after reduction at 300°C, dehydroxylation has been monitored by both DRIFT and TPD experiments. The DRIFT spectra show a decrease in intensity of the hydroxyl groups, in the TPD experiments water desorbs. The water desorption is unaffected by the presence of platinum on the alumina. The explanation for the decreased desorption of water after reduction at 450°C compared to reduction at 300°C is straightforward. The alumina surface dehydroxylates (i.e. water desorbs) during reduction. As no water is readsorbed to the sample before the TPD and apparently no interconversion between types of hydroxyls takes place, water is only detected above the reduction temperature.

The conclusion from the infrared spectroscopy is that γ–Al_2O_3 preferentially exposes the (110) plane and that after reduction at either 300 or 450°C a significant amount of water (hydroxyl groups) is still present on the γ–Al_2O_3 surface.

EXAFS data analysis

To study the metal-support interface in catalysts small metal particles are required as

the EXAFS spectrum is the average over all the atoms in the metal particle. At a certain particle size the contribution(s) from the support will be so small that they can not be reliably detected anymore and only contributions from inside the metal particle will remain. In the catalysts used in this study the particle size was larger than in the studies on Pt/LTL catalysts, consequently we should pay attention to this problem. The magnitude of contributions to the EXAFS spectrum are inverse proportional to the distance of the scatterer. Therefore we choose to study the significance of the long Pt–O distance in a representative sample.

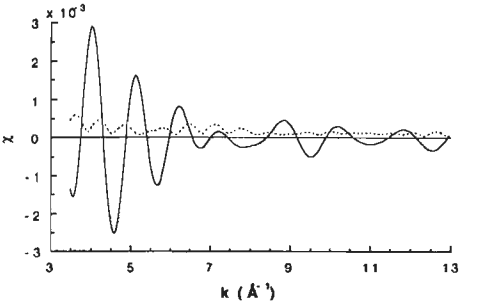

Figure 16 Difference between the Fourier filtered spectrum of sample **1** reduced at 300°C and the calculated model with a single Pt–Pt contribution (N=7.3, R=2.76 Å, $\Delta\sigma^2$=0.0060 $Å^2$, and ΔE_0=2.3 eV (solid line). The dashed line represents the statistical noise in the Fourier filtered spectrum.

After reduction of sample **1** at 300°C the best fit was obtained with a single platinum contribution with a coordination number of 7.3 and a Debye-Waller factor of 0.0060 $Å^2$. The residuals of this fit are several times the statistical noise in the Fourier filtered data (figure 16) at low k-values. The amplitude of the residuals decays with k similar to the backscattering amplitude of a low Z element[37]. The comparison of this sample and platinum foil in a k^1 weighed Fourier transform (figure 9a) also provided evidence for the presence of a low Z contribution in the EXAFS spectrum. Calculation of the average coordination numbers in the first and higher shells of metal clusters consisting of 1 - 13 atoms with varying geometries (figure 17) reveals that a first shell coordination number of 7.3 should be accompanied by significant higher shell contributions. From the k^3 weighed Pt–Pt phase and amplitude corrected Fourier transform of this spectrum (figure 8a) it is evident that higher shells are present but do not contribute significantly to the spectrum. Decreasing both the coordination number and the Debye-Waller factor,

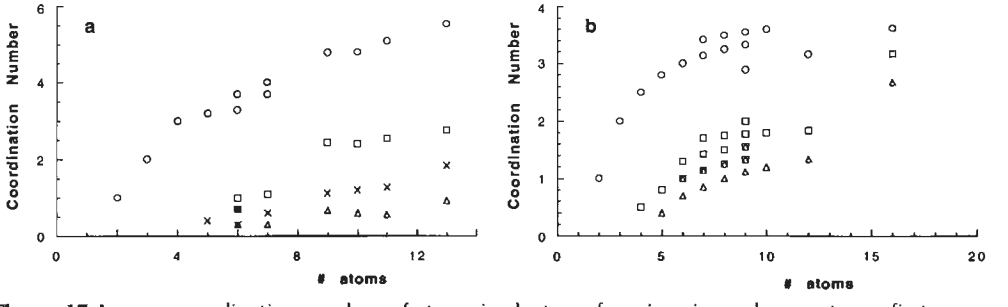

Figure 17 Average coordination number of atoms in clusters of varying size and geometry. o: first shell, x: second shell, square: third shell, Δ: fourth shell, a) 3-dimensional cluster and b) (111) raft. In a (111) raft the second shell is absent.

similar to the model studies described in chapter 2, resulted in residuals that are normally distributed. Hence, we choose to let physical considerations prevail over mathematical results in this and subsequent analyses.

Hydrogen TPD and EXAFS

The hydrogen TPD spectra of the Pt/γ–Al_2O_3 catalyst after reduction at 300°C is similar to the TPD spectra of the Pt/γ–Al_2O_3 catalyst reported in chapter 5. The temperature at which the main desorption peak appears differs slightly. Additionally, the desorption between 300 and 360°C is not resolved from the main desorption in chapter 5. We attribute these differences to the difference in heating rate (5°/min vs 10°/min). Here we will discuss the origin of the hydrogen desorption between 300 and 360°C and the additional evidence for the assignment of the TPD peaks obtained from the EXAFS spectra after evacuation.

The hydrogen TPD of Pt/γ–Al_2O_3 reduced at 300°C reveals three types of hydrogen. The first, which desorbs between 80 and 200°C is reversible and has been attributed to chemisorbed hydrogen. This assignment is supported by experiments where a TPD to 300°C is followed by a reduction at 300°C and a second TPD. The second TPD shows the same desorption of hydrogen between 80 and 200°C. EXAFS measurements on a sample reduced and evacuated at 300°C (which is equivalent to reduction at 300°C followed by a TPD to 300°C) show that the reversible desorption of hydrogen is accompanied by a contraction of the Pt–Pt distance in the small metal clusters. This contraction is reversible as shown by readsorption of hydrogen at 200°C. The contraction of the Pt–Pt distance is due to the decreased repulsion between the platinum atoms caused by the increased electron density on the platinum atoms[29,30]. The presence of the same Pt–O contribution at a distance of 2.65 Å with and without chemisorbed hydrogen present, shows that the metal-support interface formed by reduction at 300°C is not affected by the removal of chemisorbed hydrogen. The decrease in first shell Pt–Pt coordination number, the appearance of a new Pt–O contribution in the spectrum and the absence of the third Pt–Pt shell after removal of the chemisorbed hydrogen provide evidence that the morphology of the platinum particles changes from 3-dimensional to flat upon removal of chemisorbed hydrogen. The absence of the third Pt–Pt shell in the EXAFS spectrum indicates that the platinum atoms are arranged in a square geometry.

Two more types of hydrogen are desorbing above 300°C in the TPD performed after reduction at 300°C. A small peak which has a maximum at 325°C and a large peak with a maximum at 435°C. Based on the results obtained for the Pt/H–LTL catalyst (chapter 5), the peak with a maximum at 435°C has been assigned to hydrogen recombining from a spillover process that took place during reduction.

The shoulder on the main peak is similar to the desorptions observed for Pt/K–LTL in this temperature range and have been interpreted as hydrogen evolving from the metal-support interface[28]. This process was related to the

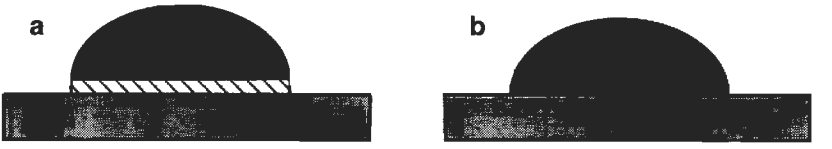

Figure 18 Schematic model of the metal-support interface after reduction at a) 300°C and b) 450°C.

decrease in Pt–O distance with increasing reduction temperature. Evacuation at 300°C does not affect the metal-support interface as inferred from the EXAFS characterization of the metal-support interface after reduction and evacuation at 300°C. Treatment of the sample at 450°C shows that the metal-support interface is dramatically changed, i.e. the distance between the platinum particle and the support oxygens decreases by 0.4 Å. In addition, Kampers and Koningsberger[38] showed that for a highly dispersed $Ir/\gamma\text{–}Al_2O_3$ catalyst evacuated at 350°C the metal-oxygen distance was 2.2 Å. These observations are fully in agreement with the reasoning presented in chapter 5 and we infer that the hydrogen desorbing around 325°C is responsible for the change in distance between metal and support atoms. It is logical to conclude that this hydrogen is located between the platinum particle and the support oxygen atoms as the desorption of this hydrogen is accompanied by a decrease in the interfacial Pt–O distance.

Removal of chemisorbed hydrogen induces a morphology change of the particle when the platinum particle is not in direct contact with the support, i.e. after reduction at 300°C the platinum particle is separated from the alumina by the interfacial hydrogen (figure 18a). When the platinum particle is already in direct contact with the support removal of chemisorbed hydrogen has a less pronounced effect on the morphology of the platinum particle due to the strong interaction between the interfacial platinum atoms and the oxygen ions of the support. These observations can be rationalized as follows: when the particle size is separated from the support oxygens by the interfacial hydrogen, the platinum particle is free to contract or to relax as evidenced by the contraction of the Pt–Pt distance by removal of the chemisorbed hydrogen and the relaxation induced by readsorption of hydrogen. When the interfacial hydrogen is not present, the platinum atoms in direct contact with the oxygen atoms from the support will try to match the distance between these oxygen atoms. Evidence for this is obtained from the decrease of the Pt–Pt distance induced by reduction at 450°C. The interaction between the interfacial platinum atoms and the support oxygens is strong as indicated by the negative Debye-Waller factor for this contribution to the EXAFS spectrum. The reduction at 450°C of sample **1** induces a morphology change even under chemisorbed hydrogen. The particles in sample **1** are apparently more influenced by the support than the slightly larger particles in sample **2**.

Hydrogen Chemisorption

A decrease in H/Pt is conventionally attributed to an increase in particle size. The decrease in H/Pt of sample **1** when the reduction temperature is increased from 300 to 450°C is not accompanied by an increase in particle size as is evident from the decrease in the Pt–Pt coordination number, but by a morphology change of the particle and the removal of chemisorbed hydrogen from the metal-support interface. Hence, a change in metal-support interaction. Therefore it is inferred that the decrease in hydrogen chemisorption capacity is due to the changing interaction of the platinum with the support.

Conclusion

The hydrogen pretreatment at 450°C causes a dramatic change in the morphology of the platinum particles and in the nature of the metal-support interaction compared to hydrogen pretreatment at 300°C. This was shown with a combination of hydrogen TPD and EXAFS. Hydrogen TPD after reduction at 300°C reveals that three types of hydrogen are present. The first type, desorbing between 80 and 200°C is chemisorbed hydrogen. The EXAFS spectrum obtained after evacuation at 300°C clearly demonstrated that removal of chemisorbed hydrogen from the surface of small metal particles decreases the first shell distance. The second type, which desorbs between 300 and 360°C was attributed to hydrogen originating from the metal-support interface. Evidence for this assignment was obtained from EXAFS measurements after evacuation at 300°C and reduction at 450°C. The third peak was attributed to spillover hydrogen, which was straightforward demonstrated by the absence of this desorption in the TPD of the bare support. The decrease in hydrogen chemisorption capacity observed after HTR is most probably caused by the change in metal-support interaction.

References

1. R. Kramer and M. Fischbacher, J. Mol. Catal., **51** (1989) 247.
2. G. J. den Otter and F. M. Dautzenberg, J. Catal., **1978** (53) 116.
3. R. Kramer and M. Andre, J. Catal., **58** (1979) 287.
4. P. G. Menon and G. F. Froment, Appl. Catal., **1** (1981) 31.
5. P. G. Menon and G. F. Froment, J. Catal., **59** (1979) 138.
6. J. Margitfalvi, P. Szedlacsek, M. Hegedüs, and F. Nagy, Appl. Catal., **15** (1985) 69.
7. S. I. Abasov, V. Y. Borovkov, and V. B. Kazansky, Catal. Lett., **15** (1992) 269.
8. D. C. Koningsberger and B. C. Gates, Catal. Lett., **14** (1992) 271.
9. J. R. Chang, L. U. Gron, A. Honji, K. M. Sanchez, and B. C. Gates, J. Phys. Chem.,

95 (1991) 9944.
10. H. F. J. van't Blik, J. B. A. van Zon, H. F. Huizinga, J. C. Vis, D. C. Koningsberger, and R. Prins, J. Am. Chem. Soc., **107** (1985) 3139.
11. F. B. M. Duivenvoorden, D. C. Koningsberger, Y. S. Uh, and B. C. Gates, J. Am. Chem. Soc., **108** (1986) 6254.
12. F. B. M. van Zon, P. S. Kirlin, B. C. Gates, and D. C. Koningsberger, J. Phys. Chem., **93** (1989) 2218.
13. Y. Asakura, M. Yamada, and Y. Iwasawa, Chem. Lett., (1985) 511.
14. N. Binsted, J. Evans, G. N. Greaves, and R. J. Price, Organometallics, **8** (1989) 613.
15. G. L. Haller and D. E. Resasco, Adv. Catal., **36** (1989) 173.
16. F. W. H. Kampers, T. M. J. Maas, J. van Grondelle, P. Brinkgreve, and D. C. Koningsberger, Rev. Sci. Instr., **60** (1989) 2635.
17. D. C. Koningsberger and D. E. Sayers, Solid State Ionics, **16** (1985) 23.
18. J. W. Cook Jr. and D. E. Sayers, J. Appl. Phys., **52** (1981) 5024.
19. N. R. Smyrl, E. L. Fuller, and G. L. Powell, Appl. Spectrosc., **37** (1983) 38.
20. Y. Murakami, *in* "Preparation of Catalysts III", (G. Poncelet, P. Grange, and P. A. Jacobs, Eds.), p. 775. Elsevier, Amsterdam, 1983.
21. Y. Okamoto and T. Imanaka, J. Phys. Chem., **92** (1988) 7102.
22. R. R. Cavanagh and J. T. Yates Jr., J. Catal., **68** (1981) 22.
23. H. Knözinger and P. Ratnasamy, Catal. Rev.-Sci. Eng., **17** (1978) 31.
24. W. G. Wyckoff, *Crystal Structures* (Interscience, New York, 1974).
25. M. Trömel and E. Lupprich, Z. Anorg. Chem., **414** (1975) 160.
26. F. W. Lytle, D. E. Sayers, and E. A. Stern, Physica B, **158** (1988) 701.
27. H. J. Borg, L. C. A. van den Oetelaar, L. J. van IJzendoorn, and J. W. Niemantsverdriet, J. Vac. Sci. Tech. A - Vac. Surf. Films, **10** (1992) 2737.
28. M. Vaarkamp, J. van Grondelle, R. A. van Santen, J. T. Miller, F. S. Modica, G. S. Lane, and D. C. Koningsberger, *in* "Proc. 9th Int. Zeolite Conf., Montreal, July 5-10, 1992", Butterworth-Heinemann, London, in print. (chapter 5)
29. B. Delley, D. E. Ellis, A. J. Freeman, E. J. Baerends, and Post D., Phys. Rev. B, **27** (1983) 2132.
30. M. B. Gordon, F. Cyrot-Lackmann, and M. C. Desjonquères, Surf. Sci., **68** (1977) 359.
31. G. Apai, J. F. Hamilton, T. Stohr, and A. Thompson, Phys. Rev. B, **43** (1979) 165.
32. B. Moraweck, G. Clugnet, and A. J. Renouprez, Surf. Sci. Lett., **81** (1979) 631.
33. J. P. Beaufils and Y. Barbaux, J. Chim. Phys., **78** (1981) 347.
34. S. Iijima, Surf. Sci., **156** (1985) 1003.
35. S. Iijima, Jpn. J. Appl. Phys., **23** (1984) L 347.
36. A. Reller and D. L. Cocke, Catal. Lett., **2** (1989) 91.
37. B. K. Teo and P. A. Lee, J. Am. Chem. Soc., **101** (1979) 2815.
38. F. W. H. Kampers and D. C. Koningsberger, Faraday Discuss. Chem. Soc., **89** (1990) 137.

Chapter 7

On the Relation between Electronic Structure and Catalytic Properties of Supported Platinum Catalysts

Abstract

The number of unfilled d-states of platinum clusters, varying in size from 6–12 atoms, supported on γ–Al_2O_3, H–LTL, and K–LTL, has been determined by X–ray Absorption Spectroscopy. The influence of chemisorbed hydrogen on the intensity of the L_{III} and L_{II} X–ray absorption edges is dramatic as was shown by removal and readsorption of hydrogen. Reduction at 300°C followed by evacuation at 300°C results in a lower number of unfilled d-states than of bulk platinum. Increasing the reduction temperature which according to previous studies is accompanied by the removal of interfacial hydrogen, a slight increase in particle size, and a reduction in hydrogen chemisorption capacity of the surface atoms also results in a decrease of the white line intensity. The influence of the support and the particle size on the number of unfilled d-states could not be established due to the masking effect of chemisorbed and interfacial hydrogen. The propane hydrogenolysis TOF for platinum supported on γ-Al_2O_3 or H-LTL is found to be more than an order of magnitude higher than for platinum supported on a K-LTL zeolite. Although the decrease in hydrogenolysis activity with increasing reduction temperature is accompanied by an increase in electron density on the platinum particles it was impossible to relate the activity differences to the electron withdrawing of donating properties of the supports due to the dominant effect of chemisorbed and interfacial hydrogen on the intensity of the X–ray absorption edges.

Parts of this chapter have been published: M. Vaarkamp, J. T. Miller, F. S. Modica, and D. C. Koningsberger, Jap. J. Appl. Phys., in print and M. Vaarkamp, J. T. Miller, F. S. Modica, G. S. Lane and D. C. Koningsberger, *in* "Proc. 10th Int. Congr. Catal., Budapest, 19 - 24 July 1992", in print.

Introduction

The electronic structure of small metal particles has been the subject of many studies during the last decades. Some of the studies were concerned with the fundamental concepts underlying these changes, others were focused on the differences in reactivity of the surface atoms compared to bulk metal. The change in catalytic properties of metal–catalysts with a change in particle size is generally attributed to the geometric requirements of the reaction(s) under investigation[1]. However, these changes might also occur due to a changing fraction of edge and corner atoms in the total amount of surface atoms, hence a change in average electron density on the surface atoms of the catalyst.

The electronic structure of metals can be measured by various methods, the most valuable being X–ray Photoelectron Spectroscopy (XPS) and X–ray Absorption Spectroscopy (XAS). XPS measures the binding energy of the ejected electron. XAS probes the number of holes in the valence band, i.e. the LDOS. In addition the equilibrium geometry and the LDOS can be calculated by various quantum chemical methods.

Both theoretical[2, 3] and experimental[4, 5] evidence exists for a decrease in interatomic distance going from bulk metal to clusters of several atoms. Local-density calculations on copper particles of different sizes[2] have clearly demonstrated that the interatomic distance in small particles is shortened compared to bulk metal. This is due to a decreased degree of delocalization (more electron density between the metal atoms) since metal atoms in small metal particles have, on average, fewer neighbouring atoms than in bulk metal.

The results of XPS studies, i.e. increasing core-level binding energy with decreasing particle size, are well established and generally accepted[6-9]. Mono-dispersed platinum clusters (1–6 atoms) on silica, produced by sputtering of a platinum surface followed by mass selection of the clusters, exhibit an increase in the Pt $4f_{7/2}$ binding energy of up to 2 eV compared to bulk Pt metal[6]. Studies on carbon supported metal clusters in which the cluster size was varied by changing the metal coverage of the carbon substrate revealed smaller shifts[7-9]. The physical origin of this shift is an area of considerable dispute. Wertheim[7] attributes the shift to the decreased screening by the conduction band electrons of the core-hole in small particles compared to the screening in the bulk metal. Mason[8, 9] states that the shift predominantly originates from a shift of the initial state. Additional evidence for the interpretation of Mason comes from ionization potential measurements on naked palladium clusters consisting of 1–120 atoms. The ionization potential decreases with cluster size for clusters of less than 20 atoms, implying a higher electron density on the atoms[10].

Information about the d-band density of states in third row transition metal clusters can be obtained from the intensity of the L_{II} (transition from $2p_{1/2}$ to $5d_{3/2}$) and the L_{III} (transition from $2p_{3/2}$ to $5d_{5/2}$ and $5d_{3/2}$) X-ray absorption edges. A basic

theory of white lines has been given by Mott[11], Brown et al.[12], and Mattheiss and Dietz[13]. The theoretical calculations of the number of unoccupied Pt d-states show that the J=5/2 final state is predominant. Brown et al.[12] showed that the J=5/2 state contributes about 14 times more to the final d-states than the J=3/2 state. Mattheiss and Dietz[13] calculated that the ratio of the unoccupied states ($h_{5/2}/h_{3/2}$) ranges from 3.5 within 0.5 eV of the Fermi level to 2.9 over the entire unoccupied conduction band. These calculations explain why the intensity of the white line of the L_{III} X-ray absorption edge is much higher than the intensity of the L_{II} edge in bulk platinum.

The interpretation of changes in the intensity of the X–ray absorption edges is complicated as they can originate from quite a few factors. The white line intensity has been reported to be affected by the metal studied, the chemical state of the atoms under study, the measuring temperature, the presence of an adsorbate on the surface of the metal particle, the size of the metal clusters, and the support.

The intensity of the L_{III} X-ray absorption edge was shown to be proportional to the number of d-electron vacancies for iridium, platinum, and gold metal[14], although no linear relationship was obtained. The effect of the chemical state was studied for a number of iridium, platinum, and gold compounds[16], a relation between the area of the L_{III} X–ray absorption edge and the coordination charge, which is related to the formal valence of the central atom and the ionicity of the bond, was derived. The intensity of X–ray absorption edges of small metal particles has been reported to decrease when the measurements are carried out at higher temperatures[15, 18]. Samant and Boudart[19] reported a decrease in the intensity of the L_{III} X–ray absorption edge of platinum upon removal of hydrogen from the surface for measurements carried out at low temperature, whereas Lytle et al.[16] reported a slight intensity increase of the L_{III} edge upon hydrogen removal. However, a decrease in intensity of the L_{II} edge upon hydrogen removal was shown. The important consequence of this observation is that both the L_{III} and the L_{II} edge have to be examined before any statement about a change in electron density can be made.

From the factors influencing the white line intensity the particle size and the support are of course of most interest in catalysis. The relation between LDOS and particle size is of interest as this might explain the particle size sensitivity of some reactions. The establishment of the effect of the support on the LDOS is expected to give a physical key to the changes in reactivity of small metal clusters on different supports or in the presence of different cations.

Measurements of the number of unfilled d-states by X–ray Absorption Spectroscopy (XAS) for platinum particles of different sizes revealed a decrease in the d-band density of states[15, 20-23] when the particle size increased. An increase in the d-band density of states of surface atoms due to the decreased degree of delocalization has been discussed by Gordon et al.[24] and Saillard et al.[25]. A recent theoretical study, using local-density methods on neutral and charged Ir_4 and Ir_{10} clusters[26] indicate a higher number of d-electrons for the Ir_4 cluster in comparison to the Ir_{10} cluster. However, introduction of a core hole, to mimic the X-ray

absorption process, into the clusters results in a lower number of d-electrons for the Ir_4^+ compared to the Ir_{10}^+ cluster. The higher electron deficiency for the smaller cluster is due to a less efficient screening of the core hole.

Changes in the intensity of the L_{III} X-ray absorption edge of a Pt/SiO_2 catalyst have been related to alterations in the d-band density of states resulting from a change in metal-support interaction after reduction at high temperatures[17]. Gallezot et al.[20, 21] reported that platinum clusters in Ce-promoted NaY zeolite have a larger number of d-holes than platinum in NaY zeolite. Recently, the number of unfilled d-states of platinum particles supported on silica were reported to become more electron deficient loading the sample with increasing amounts of Na[15].

To access the relative importance of the effects described above we have studied the influence of adsorbed hydrogen and changes in the metal-support interface on the white line intensity. In addition, propane hydrogenolysis has been used to investigate the influence of the changes in the d-band density of states due to support and/or promoter ions on the catalytic properties of the platinum particles.

Experimental

Catalyst preparation

A 1.0 wt% $Pt/\gamma\text{–}Al_2O_3$ catalyst was prepared by impregnation of Ketjen CK-300 (200 m^2/g, 0.6 cm^3/g) with an aqueous solution of hydrochloric platinic acid. The catalyst was dried in air overnight at 120°C before it was reduced at 300°C for 4 hours. After reduction the catalyst was passivated at room temperature. A second 1.0 wt% $Pt/\gamma\text{–}Al_2O_3$ catalyst was prepared according to the procedure described above, but it was reduced at 450°C. The sample reduced at 300°C will be designated Al1, the sample reduced at 450°C will be designated Al2.

K–LTL (zeolite L) was obtained from Linde. Excess alkali was reduced by water wash until the pH of the washed solution reached 9.5 to give a K/Al molar ratio of

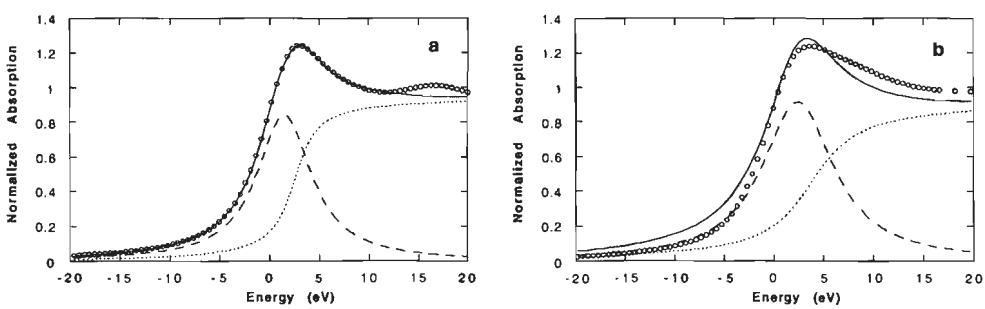

Figure 1 The Pt L_{III} edge (circles) of a) platinum foil and b) Pt/K–LTL reduced at 300°C with an arctangent (dotted line) and Lorentz (dashed line) obtained by non linear least squares fitting, solid line: sum of arctangent and Lorentz.

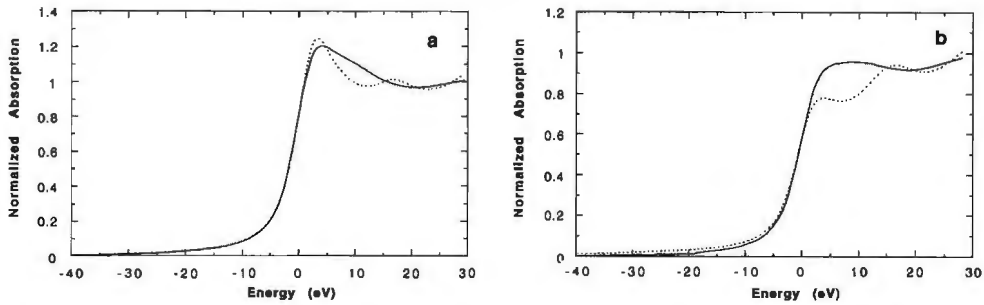

Figure 2 The a) Pt L_{III} and b) Pt L_{II} X-ray absorption edges of platinum foil (dotted line) and Pt/H–LTL (solid line) aligned with their inflection points.

1.05. H–LTL (K/Al molar ratio of 0.34) was prepared by repeated ammonium nitrate exchange of K–LTL, followed by calcination at 500°C. The zeolites were impregnated with an aqueous solution of platinum(II)tetraamine nitrate to give a 1.2 wt% Pt/K–LTL and a 1.0 wt% Pt/H–LTL catalyst. The impregnated zeolites were dried at 120°C and stored till further use.

X–ray absorption measurements

The X–ray Absorption data were obtained at the Synchrotron Radiation Source in Daresbury, U. K., Wiggler Station 9.2 in the transmission mode at liquid nitrogen temperature. The estimated resolution at the Pt L_{III} (11564 eV) and L_{II} (13273 eV) edge is 4 eV. The Si(220) monochromator was detuned to 50% intensity to avoid the effects of higher harmonics. In order to obtain an absolute energy calibration of the data a third ion chamber was used with a platinum metal foil (thickness 4 μm) placed between the second and the third ion chamber. Each spectrum was separately calibrated at the L_{III} and L_{II} edge. The spectra were normalized by the edge jump at 50 eV above the edge.

Self–supporting wafers ($\mu x = 2.5$) were reduced in flowing H_2 in an *in–situ* cell[28]. The Pt/γ–Al_2O_3 samples were rereduced at 300 and 450°C and are designated as Alx(300) and Alx(450), respectively. Similarly, Pt/K-LTL samples were reduced at 300 or 450°C and are designated as K-LTL(300) and K-LTL(450). K-LTL(600), which had been prereduced at 600°C, was rereduced in the cell at 450°C. Pt/H-LTL was reduced at 300 and 500°C, these samples are designated H-LTL(300) and H-LTL(500), respectively. After collecting the data on the reduced catalyst the cell was evacuated to 10^{-5} Torr at RT and heated to the evacuation temperature. Maintaining the vacuum, the cell was held at the evacuation temperature for an additional hour and cooled to RT. After collecting the data on the evacuated catalyst, hydrogen was admitted into the cell at RT. Subsequently the sample was heated to 200°C under flowing hydrogen and held there for one hour. Data on the reduced samples were obtained in the presence of H_2, data on the evacuated samples were obtained under dynamic vacuum.

Propane hydrogenolysis

The conversion of propane was conducted at 400°C and atmospheric pressure in a fixed-bed, bench-scale reactor using 3.78 vol% propane in H_2. The catalysts were prereduced at 450°C or 600°C, and the conversion was adjusted to between 2 to 10% by changing the propane space velocity. The turnover frequency (TOF) was determined using hydrogen chemisorption as a measure of the active platinum surface.

Results

Structural characterization

Detailed structural characterizations of the catalysts by H_2 TPD, hydrogen chemisorption, and EXAFS are reported elsewhere for Pt/γ–Al_2O_3[30], Pt/H-LTL[31] and Pt/K-LTL[31, 32]. Results are similar for all catalysts. The particle size increases with reduction temperature. After reduction at low temperature (300°C, LTR) the platinum clusters contain 5–7 atoms, after reduction at high temperature (600°C, HTR) the clusters contain ≈11 atoms. The increase in particle size is also evident from the decrease in hydrogen chemisorption capacity. Furthermore, the structure of the metal-support interface changes with reduction temperature. After LTR a Pt–O contribution at a distance of 2.7 Å is present in the EXAFS spectrum. Based on hydrogen TPD this long Pt–O distance has been attributed to a structure were atomic hydrogen is present between the platinum and the oxygen atoms of the support. Treatment in either inert or hydrogen atmosphere at high temperature removes this interfacial hydrogen. Hence, the Pt–O distance, as determined by EXAFS, is shortened to 2.2 Å. The EXAFS first-shell coordination numbers, which are important for an evaluation of the white line results are given in the table 1.

Table 1 Coordination numbers and whiteline intensities

Sample	treatment	N_{Pt-Pt}	ΔA_3	ΔA_2	Δh_T
Al1	300	4.8	0.64	1.62	5.49
	450	3.8	0.30	0.88	2.86
Pt/H–LTL	300	4.0	0.61	1.68	5.55
	500	4.4	0.13	0.90	2.53
Pt/K–LTL	300	4.0	0.71	1.74	5.95
	450	4.8	0.38	1.24	3.73
	600	4.9	0.09	0.71	1.98
Al2	300	5.0	0.57	1.58	5.23
	vac	3.8	–0.58	–0.15	–1.70
	vac, H_2	4.9	0.48	1.43	4.66
	450	5.0	0.35	1.14	3.64
	vac	4.1	–0.09	0.26	0.44

Table 2 Propane hydrogenolysis activity for supported platinum catalysts at atmospheric pressure and 400°C. For stable catalysts only the initial TOF is reported.

catalyst	T_{red} (°C)	initial TOF (molecules s^{-1} $site^{-1}$)	TOF after 10 min TOS (molecules s^{-1} $site^{-1}$)
Pt/K–LTL	450	0.064	–
	600	0.022	–
Pt/H–LTL	450	0.53	0.40
	600	0.14	0.10
Al1	450	0.62	–

Propane hydrogenolysis

For each of the catalysts, hydrogenolysis of propane yielded methane and ethane in equal molar amounts. The catalytic turnover frequencies (TOF) are given in table 2. For the Pt/K-LTL and Pt/γ-Al_2O_3 catalysts, there was little deactivation. The Pt/H-LTL catalyst, however, deactivated more rapidly, and conversion is reported at 10 minutes on stream and extrapolated to zero time on stream.

The catalytic activities fall into two groups, predominantly determined by the support. The TOF of platinum on H-LTL(450) and Al1(450), was more than an order of magnitude higher than the TOF of platinum on K-LTL(450) and K-LTL(600). Platinum on alumina was more active than platinum on H–LTL

White line intensity determination

The measured Pt L_{II} and L_{III} X–ray Absorption Edges are a combination of a smooth function representing the transition of electrons from core-levels into the continuum and a function representing the transition of core-level electrons into unfilled states in the valence band. Hence, to evaluate the number of unfilled states these two functions have to be separated. Horsley[33] showed that the Pt L_{III} edge of platinum foil can be deconvoluted in a smooth arctangent function and a Lorentz

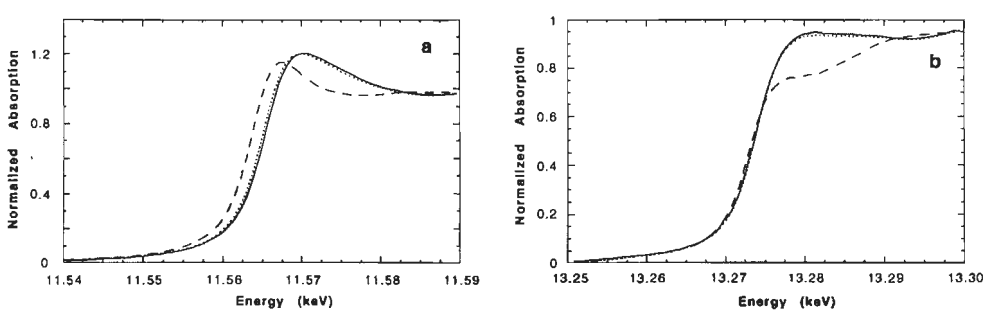

Figure 3 X–ray absorption edge of Al2 after reduction at 300°C (solid line), after reduction at 300°C and evacuation at 300°C (dotted line), and after reduction at 300°C, evacuation at 300°C, and readmission of hydrogen at 200°C (dashed line), a) L_{III} edge and b) L_{II} edge.

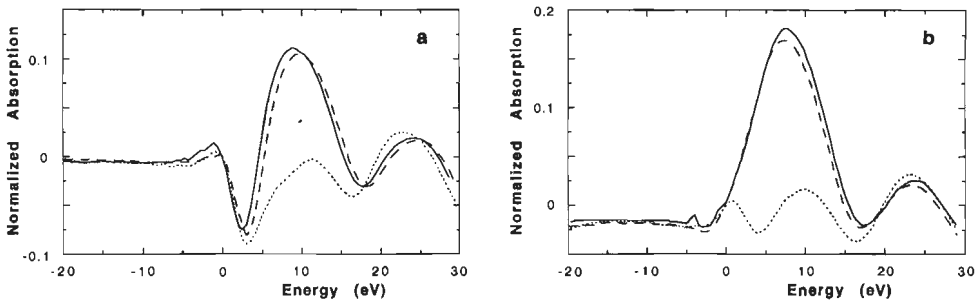

Figure 4 Difference between the X-ray absorption edges of Al2 and the corresponding edge of platinum foil after reduction at 300°C (solid line), after reduction at 300°C and evacuation at 300°C (dotted line), and after reduction at 300°C, evacuation at 300°C, and readmission of hydrogen at 200°C (dashed line), a) L_{III} edge, b) L_{II} edge.

function representing atoms transferred to the Pt 5d level (figure 1a). However, this deconvolution of the edge is unable to cope with the asymmetric form of the X-ray absorption edge of the supported platinum catalysts when hydrogen is chemisorbed on the surface. A representative example of this deconvolution (Pt/K–LTL reduced at 300°C) is shown in figure 1b. It is clear that the fitted Lorentz function is not representative of the area of the white line of Pt/K–LTL, hence an alternative approach is needed. We checked whether the white line consists of more than one Lorentz function by calculating the second derivative of the spectrum, thereby diminishing the contribution of the smooth background[34]. Only one negative peak was present indicating that the white line consists of a single transition.

To quantify the differences in white line intensity between the catalysts and platinum foil we used the approach described by Mansour et al.[23]. The normalized XAFS spectra of the Pt L_{II} and L_{III} edge of the platinum foil and the catalyst were aligned at there inflection points (figure 2). After subtraction of the platinum foil data from the data of the catalyst, the resulting curves were numerically integrated between -2 and +17 eV for both the L_{III} (ΔA_3) and the L_{II} (ΔA_2) edge. The resulting areas were combined to give the total number of unfilled states in the d-band (Δh_T)[23]:

$$\Delta h_T = 2.25\,(\Delta A_3 + 1.11\,\Delta A_2) \qquad (1)$$

A change in Δh_T of 7 (which is approximately the largest change observed in this study) corresponds to 0.08 electron per atom.

The alignment of the X-ray absorption edge of platinum foil and the catalyst has been shown to have a dramatic effect on the difference spectrum of the platinum foil and the catalyst[16]. To circumvent the problem of the changing edge position by an increase in white line intensity one should align the smooth background function in the edges of interest. The position of the smooth background function can be deduced from the position of the EXAFS wiggles. However, in the samples we

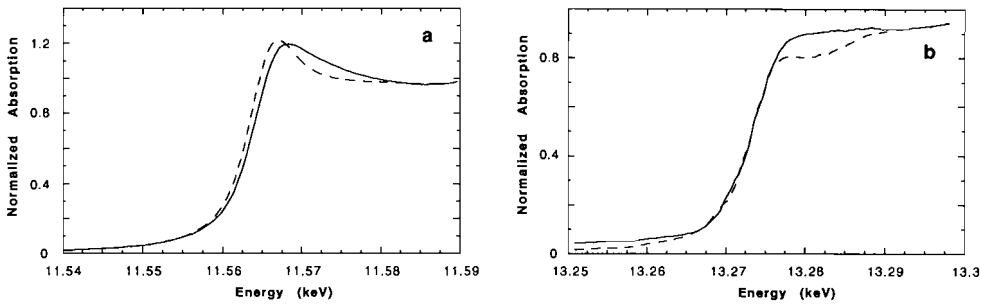

Figure 5 X–ray absorption edge of Al2 after reduction at 450°C (solid line) and after reduction at 450°C followed by evacuation at 450°C (dotted line), a) L_{III} edge and b) L_{II} edge.

studied the EXAFS wiggles are subject to change. Consequently a systematic alignment procedure based on the EXAFS wiggles is not possible. To ensure a systematic approach to the determination ΔA_3 and ΔA_2 we aligned the inflection points of the platinum foil and the sample. The aligned Pt L_{III} X–ray absorption edges of platinum foil and Pt/H–LTL have been plotted in figure 2a, figure 2b shows the alignment of the L_{II} edge.

Influence of chemisorbed hydrogen on the white line intensity

The influence of chemisorbed hydrogen on the position and intensity of the white line has been investigated for Al2 reduced at 300 and 450°C. The Pt L_{III} and L_{II} X–ray absorption edges of Al2 after reduction at 300°C, evacuation at 300°C, heating in hydrogen to 200°C are shown in figure 3. Removal of chemisorbed hydrogen causes a dramatic decrease in the intensity of both the Pt L_{III} and L_{II} X–ray absorption edge of Al2. The whiteline intensity is completely restored by readmission of hydrogen at RT and subsequent heating to 200°C. The L_{III} edge of the evacuated sample is shifted to lower energies by –1.5 eV. Readmission of hydrogen causes an upward shift of 1.4 eV, almost completely restoring the original edge position. The L_{II} edge of the evacuated sample does not show the downward shift. In addition to the position change of the L_{III} edge, also a change in shape (sharpening) is evident upon removal

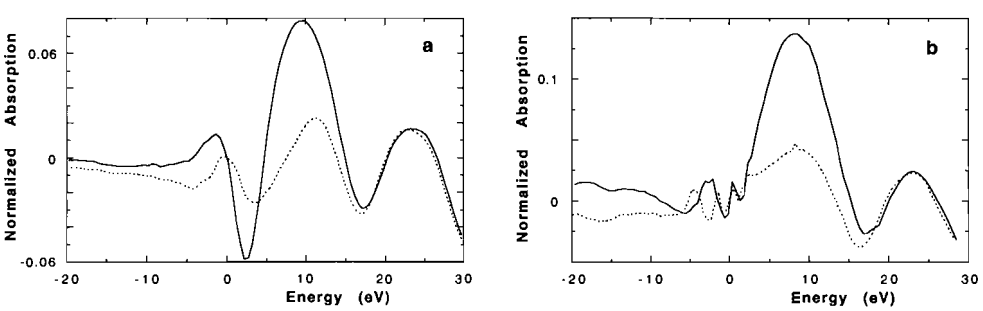

Figure 6 Difference spectrum of the a) Pt L_{III} and the b) Pt L_{II} X–ray absorption edge of Al2 reduced at 450°C (solid line) and reduced and evacuated at 450°C (dotted line).

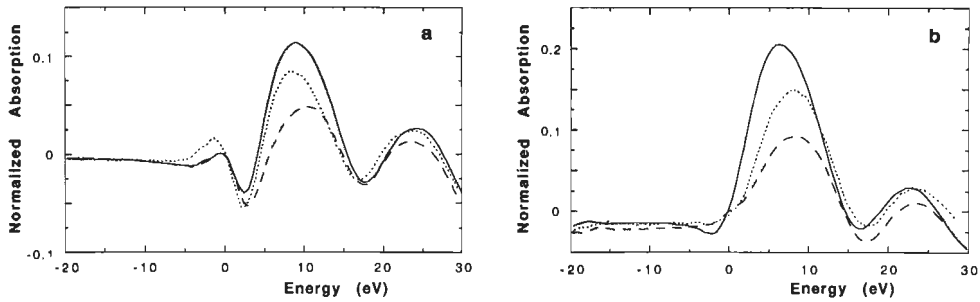

Figure 7 Difference spectrum of the a) Pt L_{III} and the b) Pt L_{II} X-ray absorption edge of Pt/K-LTL reduced at 300°C (solid line), 450°C (dotted line), and 600°C (dashed line).

of the chemisorbed hydrogen. The difference between these spectra and the corresponding X-ray absorption edge of platinum foil are plotted in figure 4, results of the numerical integration of these curves between -2 and 17 eV are listed in table 1.

The Pt L_{III} and L_{II} X-ray absorption edges of Al2 after reduction at 450°C and subsequent evacuation at 450°C are shown in figure 5. Evacuation causes a downward shift of the position of the Pt L_{III} edge of -0.7 eV, which is approximately half the shift obtained for the sample reduced at 300°C. Again no shift of the L_{II} edge was observed. The difference spectra are shown in figure 5, integration results are listed in table 1. The decrease in white line intensity by removal of chemisorbed hydrogen is not as large as after reduction and evacuation at 300°C. Furthermore, the white line intensity in the presence of chemisorbed hydrogen is lower after reduction at 450°C than after reduction at 300°C.

Changes in white line intensity with reduction temperature

The difference spectra of K-LTL(300), (450), and (600), H-LTL(300) and (500), and Al1(300) and (450) are shown in figure 7, 8, and 9 respectively. Results of numerical integration of the areas below the curves are listed in table 1. The intensity of both the L_{III} and the L_{II} X-ray absorption edge decreases with increasing reduction

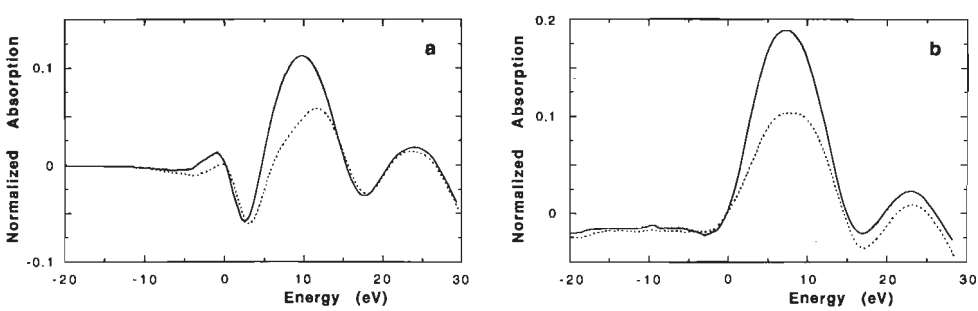

Figure 8 Difference spectrum of the a) Pt L_{III} and the b) Pt L_{II} X-ray absorption edge of Pt/H-LTL reduced at 300°C (solid line) and 500°C (dotted line).

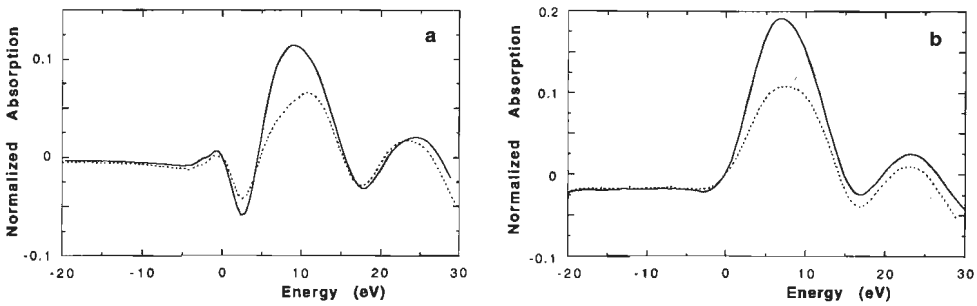

Figure 9 Difference spectrum of the a) Pt L_{III} and the b) Pt L_{II} X–ray absorption edge of Al1 reduced at 300°C (solid line) and 450°C (dotted line).

temperature, similar to the trend observed for Al2 after reduction. After reduction at 300°C the white line intensities are highest independent of the type of support or the particle size.

Discussion

The factors of interest in catalysis, reported to affect the white line intensity are the nature of the adsorbates to the surface atoms, the supporting material, and the size of the metal clusters themselves. Here we try to determine the relative importance of these factors and to relate the changes in the total number of unfilled d-states to the changes in propane hydrogenolysis activity.

Influence of chemisorbed hydrogen

The removal of chemisorbed hydrogen leads to a decrease in white line intensity (i.e. a decrease in the number of unfilled d-states). This is in agreement with literature data[18, 19, 39] where the whiteline is reported to be affected by the presence of either hydrogen or helium during the measurement. The larger decrease in white line intensity in our measurement compared to literature data originates from the smaller particles in this study. In smaller particles a larger fraction of the atoms is exposed to adsorbed gases and thus a larger effect of adsorbed gases on the white line intensity is to be expected.

After reduction and evacuation at 300°C the total number of unfilled d-states of Al2 is less than the total number of unfilled d-states in the platinum foil ($\Delta h_T = -1.7$), indicating that the platinum particles have become electron rich. In contrast, reduction and evacuation at 450°C results in a total number of unfilled d-states that is larger than the total number of unfilled d-states of platinum foil ($\Delta h_T = 0.44$), viz. the platinum particles are electron deficient. These samples differ in their particle size, morphology, and the structure of the metal-support interface[30]. Hence the difference in electron density should be attributed to one or a combination of these

factors.

The changes of the number of unfilled d-states with the first shell Pt–Pt coordination number e.g. particle size, after reduction are shown in figure 10. It is evident that the changes in the number of unfilled d-states are mainly determined by the reduction temperature. The number of unfilled d-states for a particular reduction temperature is constant in the range of extremely small particles used in this study. A particle size effect will be present when the range of particle sizes is extended to much larger particles[15].

In separate studies[30, 31] we showed that the morphology of the platinum particles of the Pt/γ–Al_2O_3 catalyst and the structure of the metal-support interface in all catalysts studied changes when the reduction temperature is increased from 300 to 450°C. After reduction at 300°C hydrogen is present in the metal-support interface. In the absence of interfacial hydrogen, e.g. after reduction at 450°C, the interfacial platinum atoms are in direct contact with the support. Intuitively, the presence of interfacial hydrogen is expected to have the same effect on the white line intensity as the presence of chemisorbed hydrogen, i.e. it is expected to increase the white line intensity. The effect of the support on the number of unfilled d-states of the platinum particles is not *a priori* known. The measurements presented here offer the opportunity the estimate the lower limit of the magnitude of the electron withdrawing or donating properties of γ–Al_2O_3. Let us assume that that the presence of interfacial hydrogen, as in Al2 after evacuation at 300°C, leads to an increase of the white line intensity. Removal of this interfacial hydrogen, as in Al2 after evacuation at 450°C, will then result in a decrease of the white line intensity. The higher white line intensity of Al2 after evacuation at 450°C compared to Al2 after evacuation at 300°C is caused by the influence of the support, which counteracts the effect of the removal of interfacial hydrogen. The magnitude of the influence is at least 2.1, which is not negligible compared to 6.9 for chemisorbed hydrogen.

The decreases of the white line intensity with increasing reduction temperature can now be explained straightforward. Increasing the reduction temperature changes the structure of the metal-support interface and decreases the hydrogen chemisorption capacity and[30-32]. The decrease in the amount of chemisorbed hydrogen decreases the white line intensity. This effect is apparently dominant over the effect of the change in the structure of the metal-support interface, e.g. increase in intensity due to the removal of interfacial hydrogen and an unknown effect of the support. Hence, to establish the effect of the support on the electronic structure of small metal particles, measurements in the absence of both chemisorbed and interfacial hydrogen should be performed. This will be the subject of future research.

The shift to lower energies of the Pt L_{III} X-ray Absorption Edge has been reported in the comparison of samples heated in hydrogen and helium[18, 39]. Surprisingly, the Pt L_{II} edge does not shift upon evacuation. The chemisorbed hydrogen apparently only interacts with the levels associated with the Pt L_{III} edge. The change in shape of the L_{III} edge is another indication of this different type of interaction.

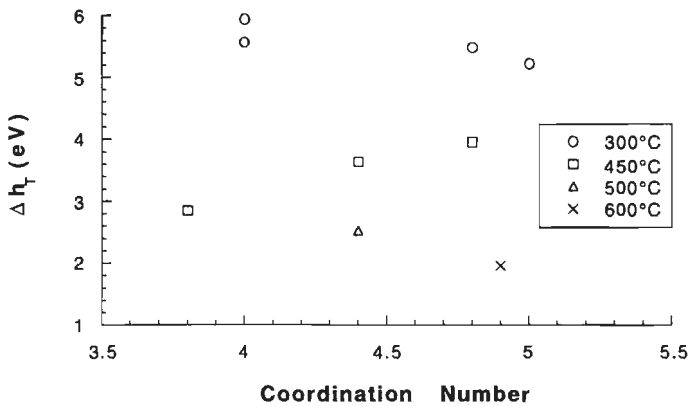

Figure 10 Correlation between first shell Pt–Pt coordination number and total number of unfilled d-states after reduction at 300 (squares), 450 (circles), 500 (triangle), and 600°C (cross).

Relation between electron density and hydrogenolysis activity

The propane hydrogenolysis TOF was determined for K-LTL(450), K-LTL(600), H-LTL(450) and Al(450) and increased in the order K-LTL < H-LTL < γ–Al_2O_3. As previously observed for hydrogenolysis of neopentane[40, 41], ethane[42, 43, 44], propane[43, 44], and butane[43, 44], the propane TOF is higher for platinum on γ–Al_2O_3 and H-LTL. In each of the previous studies, the increase in activity has been attributed to electron-deficient platinum. The electron deficient nature of the platinum was thought to be an intrinsic property of the small metal particles[42] or the result of donation of platinum electron density to the support[40, 41]. In a recent study, Samant and Boudart investigated the electron deficiency of platinum in a series of Pt/Y catalysts of similar platinum particle size by several techniques, including XANES[19]. They concluded that all of the observations previously ascribed to electron deficiency induced by the support were the result of the intrinsic properties of the very small platinum particles which form on acidic supports. If the electron deficiency is only the result of the small particle size, then the smallest platinum particles would have the highest hydrogenolysis activity. In this study, the most active catalysts for hydrogenolysis of propane, e.g., Pt/γ–Al_2O_3 and Pt/H–LTL, have the largest particles.

The propane hydrogenolysis activity decreases when the reduction temperature is increased. At the same time the white line intensity decreases. It is tempting to conclude that these observations are related. However, this study shows that the differences in white line intensities have to be corrected for the influence of chemisorbed and interfacial hydrogen before the influence of the support on the number of unfilled d-states can be determined.

Conclusion

We have shown that the white line intensity of small platinum particles is mainly determined by the adsorbates on the platinum surface and the structure of the metal-support interface. After reduction at 300°C when interfacial hydrogen is present in the metal-support interface the white line intensity is the highest. Increasing the reduction temperature which is accompanied by irreversible removal of interfacial hydrogen results in a decrease in white line intensity. The influence of the particle size on the white line intensity is shown to be negligible in the range of particle sizes studied. To determine the effect of the support on the number of unfilled d-states in platinum particles both interfacial and chemisorbed hydrogen have to be absent, i.e. the samples have to be evacuated at high temperature.

The platinum clusters on γ–Al_2O_3 and H–LTL are most active for propane hydrogenolysis. The relation between the white line intensity and the hydrogenolysis activity could not yet be established due to the lack of direct information on the influence of the support on the white line intensity.

References

1. M. Che and C. O. Bennett, Adv. Catal., **36** (1989) 55.
2. B. Delley, D. E. Ellis, A. J. Freeman, E. J. Baerends, and D. Post, Phys. Rev. B, **27** (1983) 2132.
3. M. B. Gordon, F. Cyrot-Lackmann, and M. C. Desjonquères, Surf. Sci., **80** (1979) 159.
4. G. Apai, J. F. Hamilton, T. Stohr, and A. Thompson, Phys. Rev. B, **43** (1979) 165.
5. B. Moraweck, G. Clugnet, and A. J. Renouprez, Surf. Sci. Lett., **81** (1979) 631.
6. W. Eberhardt, P. Fayet, D. M. Cox, Z. Fu, A. Kaldor, R. Sherwood, and D. Sondericker, Phys. Rev. Lett., **64** (1990) 780.
7. K. Wertheim, Z. Phys. B. Condens. Matt., **66** (1987) 53.
8. M. G. Mason, Phys. Rev. B, **27** (1983) 748.
9. M. G. Mason, *in* "NATO, Sicilië 1991",
10. P. Fayet, A. Kaldor, and D. M. Cox, J. Chem. Phys., **92** (1990) 254.
11. N. F. Mott, Proc. Phys. Soc. London, **62** (1949) 416.
12. M. Brown, R. E. Peierls, and E. A. Stern, Phys. Rev. B, **15** (1977) 738.
13. L. F. Mattheiss and R. E. Dietz, Phys. Rev. B, **22** (1980) 1663.
14. F. W. Lytle, J. Catal., **43** (1976) 376.
15. H. Yoshitake and Y. Iwasawa, J. Phys. Chem., **95** (1991) 7368.
16. F. W. Lytle, P. S. P. Wei, R. B. Greegor, G. H. Via, and J. H. Sinfelt, J. Chem. Phys., **70** (1979) 4849.
17. F. W. Lytle, R. B. Greegor, E. C. Marques, D. R. Sandstrom, G. H. Via, and J. H. Sinfelt, J. Catal., **95** (1985) 546.

18. F. W. Lytle, R. B. Greegor, E. C. Marques, V. A. Biebesheimer, D. R. Sandstrom, J. A. Horsley, G. H. Via, and J. H. Sinfelt, ACS Symp. Ser., **288** (1985) 280.
19. M. G. Samant and M. Boudart, J. Phys. Chem., **95** (1991) 4070.
20. P. Gallezot, J. Datka, J. Massardier, M. Primet, and B. Imelik, *in* "Proc. 6th Int. Congr. Catal., London, 1976", (G. C. Bond, P. B. Wells, and F. C. Tompkins, Eds.), p. 696. Chemical Society, London, 1977.
21. P. Gallezot, R. Weber, R. A. Dalla Betta, and M. Boudart, Z. Naturforsch. A, **34** (1979) 40.
22. D. R. Short, A. N. Mansour, J. W. Cook Jr., D. E. Sayers, and J. R. Katzer, J. Catal., **82** (1983) 299.
23. A. N. Mansour, J. W. Cook Jr., and D. E. Sayers, J. Phys. Chem., **88** (1984) 2330.
24. M. B. Gordon, F. Cyrot-Lackmann, and M. C. Desjonquères, Surf. Sci., **68** (1977) 359.
25. J. Y. Saillard and R. Hoffmann, J. Am. Chem. Soc., **106** (1984) 2006.
26. W. Ravenek, A. P. J. Jansen, and R. A. van Santen, J. Phys. Chem., **93** (1989) 6445.
27. A. N. Mansour, J. W. Cook Jr, D. E. Sayers, R. J. Emrich, and J. R. Katzer, J. Catal., **89** (1984) 462.
28. F. W. H. Kampers, T. M. J. Maas, J. van Grondelle, P. Brinkgreve, and D. C. Koningsberger, Rev. Sci. Instr., **60** (1989) 2635.
29. J. W. Cook Jr. and D. E. Sayers, J. Appl. Phys., **52** (1981) 5024.
30. M. Vaarkamp and D. C. Koningsberger, in preparation (chapter 6).
31. M. Vaarkamp, J. T. Miller, F. S. Modica, and D. C. Koningsberger, submitted (chapter 5 part 2).
32. M. Vaarkamp, J. van Grondelle, R. A. van Santen, J. T. Miller, F. S. Modica, G. S. Lane, and D. C. Koningsberger, *in* "Proc. 9th Int. Zeolite Conf., Montreal, July 5-10, 1992", Butterworth-Heinemann, London, in print.
33. J. A. Horsley, J. Chem. Phys., **76** (1982) 1451.
34. F. W. Lytle and R. B. Greegor, Appl. Phys. Lett., **56** (1990) 192.
35. A. P. J. Jansen and R. A. van Santen, J. Phys. Chem., **94** (1990) 6764.
36. A. N. Mansour, D. E. Sayers, J. W. Cook Jr, D. R. Short, R. D. Shannon, and J. R. Katzer, J. Phys. Chem., **88** (1984) 1778.
37. M. Vaarkamp, J. T. Miller, F. S. Modica, G. S. Lane, and D. C. Koningsberger, *in* "Proc. 10th Int. Congr. Catal., Budapest, 19 - 24 July 1992", in print.
38. J. H. Sinfelt, Catal. Rev., **3** (1969) 175.
39. B. J. McHugh, G. Larsen, and G. L. Haller, J. Phys. Chem., **94** (1990) 8621.
40. M. Boudart and R. A. Dalla Betta, *in* "Proc. 5th Int. Congr. Catal., Palm Beach, 1972", (J. H. Hightower, Ed.), p. 1329. North-Holland, Amsterdam, 1973.
41. S. T. Homeyer, Z. Karpinski, and W. M. H. Sachtler, J. Catal., **123** (1990) 60.
42. C. Naccache, N. Kaufherr, M. Dufaux, J. Pandiera, and B. Imelik, *in* "Mol. Sieves-II", ACS Symp. Ser. **40** (1977) 538.
43. G. C. Gond and M. R. Gelsthorpe, J. Chem. Soc. Faraday Trans. I, **85** (1989) 3767.
44. G. C. Bond and L. Hui, J. Catal., **132** (1992) 462.

Chapter 8

Methylcyclopentane ring opening over platinum catalysts

Abstract

The ring opening of methylcyclopentane (MCP) over well characterized Pt/SiO_2, $Pt/\gamma-Al_2O_3$, and Pt/K–LTL catalysts was studied. The Pt/K–LTL catalyst exhibited a higher selectivity towards 3-methylpentane and benzene compared to the Pt/SiO_2 and $Pt/\gamma-Al_2O_3$ catalysts. A comparative study of the ring opening activity as a function of the H_2:MCP ratio, reveals a shift of the H_2:MCP ratio at which the maximum turn-over-frequency (TOF) is reached. The competitive adsorption of MCP and hydrogen is affected by the constraints that the zeolite pore impose on the orientation of the MCP molecule. The lower TOF of MCP as well as the different optimum H_2:MCP ratio are consistent with the suppressed rate of MCP adsorption in zeolite LTL. The flattening of the platinum particle and the change in the structure of the metal-support interface of the $Pt/\gamma-Al_2O_3$ catalyst upon reduction at higher temperatures, are related to the increase of the TOF.

To be published: M. Vaarkamp, P. Dijkstra, J. van Grondelle, J. T. Miller, F. S. Modica, D. C. Koningsberger, and R. A. van Santen.

Introduction

The catalytic properties of small metal particles have been the subject of many publications (for a review see Che and Bennet[1]). Boudart[2] classified catalytic reactions as either structure sensitive or structure insensitive. An example of a structure sensitive reaction is the ring opening of methylcyclopentane (MCP). Ring opening is non selective (statistical) when catalyzed by small platinum particles, but selective (nonstatistical) over larger platinum particles[3]. In particular, the selectivity towards n-hexane increases when the particle size decreases. The hydrogen pressure at which the ring opening reaction is affected, has a paramount influence on both activity and selectivity[4].

Kazansky and Rumyantseva[5] reported the selective ring opening of MCP as early as 1947 on Pt/C catalysts. Non selective ring opening was reported in 1965 on Pt/Al_2O_3 catalysts[6]. Gault reviewed the proposed mechanisms[3]. A selective, a non selective, and a partial selective mechanism were distinguished (figure 1). The selective mechanism proceeds via a surface intermediate of two carbon atoms adsorbed to two Pt atoms ($\alpha,\alpha,\beta,\beta$ tetraadsorbed). The surface intermediate in the non selective mechanism consists of two carbon atoms adsorbed on a single Pt atom (α,β diadsorbed species). The partial selective mechanism proceeds at high temperature on catalysts with low dispersion. Experimental evidence for the existence of the partial selective mechanism originates from the non selective ring opening of MCP at high temperature over a poorly dispersed Pt/Al_2O_3 catalyst and the non selective ring opening of 1,2-dimethylcyclopentane over large particles. The partial selective mechanism is similar to the bond-shift mechanism with a metallocyclobutane intermediate. The higher temperature required for this reaction

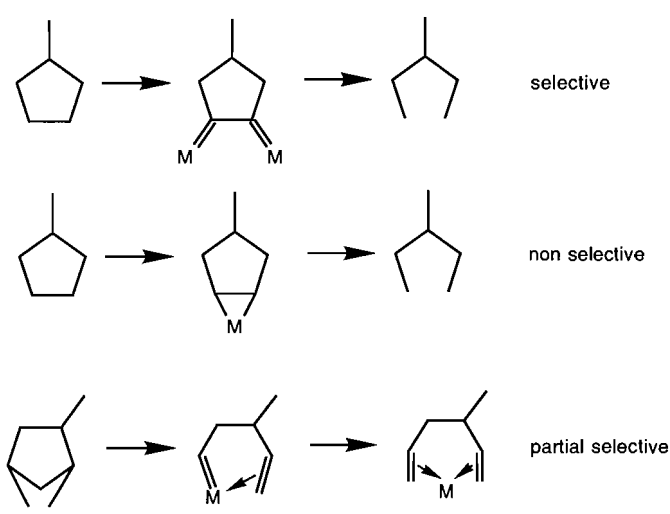

Figure 1 Mechanisms of MCP ring opening after Gault.

pathway is explained by the higher activation energy for the formation of the metallocyclobutane intermediate. Hence, according to Gault, low temperature and large particles favour the selective ring opening. The non selective ring opening is favoured by small particles and higher temperatures. It is important to note that there is no steric restriction for the occurrence of the non selective mechanism on large particles (flat surfaces).

The structure sensitivity of MCP ring opening was shown to correlate with the ensemble size by studies on bimetallic and model catalysts. Increasing the copper content in bimetallic Pt–Cu catalysts, e.g., decreasing the ensemble size, favours the non selective mechanism[7]. Platinum particles deposited on Al_2O_3, SiO_2, and MgO films[8, 9] exhibit increased non selective ring opening when they are partially covered with the support. It was proposed that the selective mechanism occurs at the surface of bulk platinum while the non selective mechanism proceeds at the metal-support phase boundary. As the support is likely to have a pronounced influence on metal atoms at the metal-support phase boundary, support effects are to be expected if the non selective mechanism occurs at the metal-support phase boundary. Kramer and Zuegg[8] observed differences between model platinum catalysts supported by SiO_2 and MgO. Anderson et al.[10] observed an increase in the selectivity towards n-hexane for a Pt/TiO_2 catalyst going from the non-SMSI to the SMSI state, and they speculated that the mechanism involves the adsorption of MCP on a Pt-Ti^{3+} site. Single crystal work[11] has shown that non selective ring opening of MCP occurs on both high and low index planes of platinum crystals. Finlayson et al.[12] proposed on the basis of work on metal films that the selective mechanism proceeds on a single Pt atom. Paál[13] provided additional evidence for this proposal from experiments with various alkylcyclopentanes.

A change in MCP ring opening activity with changing partial pressure of hydrogen has been reported for Pt/C[14], Pt black[15], Pt/SiO_2[15, 16], Pt/Al_2O_3[17], and Ir/Al_2O_3[18] catalysts. This variation in activity can be explained phenomenologically by the competition for the same surface site of the reactants. Frennet and coworkers[19, 20] proposed the "landing-site" model to account for the volcano type activity plots. This model is based on the assumption that an adsorbed hydrocarbon occupies more space than an adsorbed hydrogen. Calculation of hydrocarbon adsorption isotherms for different temperatures shows that the position of the maximum in the volcano type activity plot is not changed, but flattens at higher temperatures. MCP ring opening on a Pt/Al_2O_3 catalyst[21] at 280 and 340°C confirm the flattening.

The selectivity towards olefins and aromatics decreases with increasing hydrogen pressure for Pt on various supports[4, 15]. The ratio of selective vs. non selective ring opening, e.g., the 3MP/n-hexane ratio, increases with the hydrogen partial pressure for platinum[4, 15, 14] and iridium[18] catalysts. Paál and coworkers[15, 13] attribute the changes in selectivity to the variation in abundance of more or less saturated surface species. A surface species adsorbed via a tertiary carbon atom leads to ring opening,

whereas an unsaturated surface species leads to either ring opening or olefins.

The objective of this chapter is to extend the investigations on the ring opening of MCP to well characterized Pt/K–LTL and Pt/γ–Al_2O_3 catalysts. Earlier studies indicated significant changes in ring opening selectivity when small metal particles reside in the microcavity of a zeolite[22, 23, 24]. For platinum in the zeolite a suppression of the n-hexane/2MP ratio was reported[22]. For larger particles also a change in the 2MP/3MP ratio was found[23]. Alvarez and Resasco[24] reported similar changes for zeolite LTL. In this paper we will investigate conversion as well as selectivity of the ring opening reaction as a function of the hydrogen/hydrocarbon partial pressure ratio. The dependence of the reaction rate on the hydrogen/hydrocarbon partial pressure ratio is a measure of the competitive adsorption of hydrogen and MCP. The selectivity changes found for the zeolite systems have been ascribed to steric constraints imposed by the zeolite cavity on the orientation of the MCP molecule during the approach of the metal particle. This should affect the competitive adsorption of hydrogen and MCP, and hence, in altered dependence of the reaction rate on the hydrogen/hydrocarbon ratio. The structure of the metal-support interface and the morphology of the platinum particles is different when the Pt/γ–Al_2O_3 is reduced at 300 or 450°C[25]. The influence of these changes on the MCP ring opening activity will be reported.

Experimental

Catalyst preparation

The K–LTL zeolite was obtained from Linde. The zeolite was repeatedly washed with water until the pH of the wash solution was 9.5. The resulting K–LTL zeolite contained 8.3 wt% Al and 13.0 wt% K. Subsequently the zeolite was impregnated

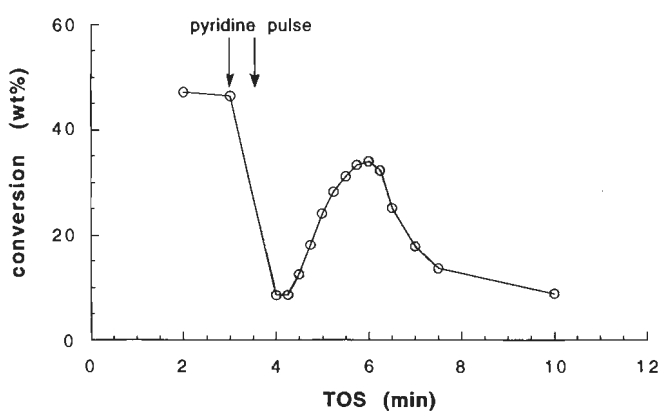

Figure 2 The effect of a pyridine pulse on the conversion of MCP of the Pt/γ–Al_2O_3 catalyst after reduction at 450°C (T = 270°C and H_2:MCP = 40).

with tetraamine platinum (II) nitrate to yield a 1.2 wt% Pt/K–LTL catalyst. The impregnated catalyst was dried at 130°C.

The 1.0 wt% Pt/γ–Al_2O_3 catalyst was prepared by pore volume impregnation of the γ-Al_2O_3 (CK300, Ketjen) with a solution of H_2PtCl_6. After overnight drying at 120°C in air, the catalyst was reduced at 300°C (heating rate 3°C/min) for 4 hrs in flowing H_2 and passivated at RT.

The 1.0 wt% Pt/SiO_2 catalyst was prepared by pore volume impregnation of the SiO_2 (Grace, 332/05) with a solution of H_2PtCl_6. After overnight drying at 120°C in air, the catalyst was calcined in flowing O_2 at 260°C for 4 hrs, followed by reduction at 300°C (heating rate 5°C/min) in flowing H_2 and passivation at RT.

Prior to the catalytic experiments the catalysts were dried *in-situ* at 120°C for at least 1 h in flowing nitrogen, followed by *in-situ* reduction in a stream of hydrogen for 1 h at the specified reduction temperature (heating rate 5°/min).

Hydrogen chemisorption

The desorption isotherms of hydrogen were measured in a conventional volumetric glass apparatus. Hydrogen was purified by passage through oxygen and 5A molecular sieve water traps. Typically 0.5 g of catalyst was dried at 120°C prior to reduction. After reduction the catalyst was cooled in H_2 to 200°C and the apparatus was evacuated to 10^{-3} Torr for 15 minutes. Subsequently a known amount of hydrogen was admitted to the sample (activated hydrogen adsorption) and the sample was cooled to room temperature. At room temperature the hydrogen desorption isotherm was measured between 10 and 80 kPa. The H/Pt value was calculated by extrapolating the hydrogen desorption isotherm to zero pressure[26].

Catalytic measurements

Methylcyclopentane (Janssen Chimica, 99+% purity) ring opening experiments were carried out at atmospheric pressure in a fixed–bed, continuous flow reactor. The internal diameter of the stainless-steel reactor was 12 mm, inside the reactor a stainless steel tube of 6 mm diameter holding a thermocouple was mounted. Typically 1 g of catalyst with particles between 125 and 450μm was used. Reaction products were analyzed on-line using a HP5995 gaschromatograph, equipped with a FID detector and a Chrompack fused silica column with an Al_2O_3/KCl coating. Initial deactivation was measured by storing samples in a 16 position loop selection valve (Valco ST16), positioned between the reactor and the gaschromatograph, for later analysis. By this method it is possible to take 15 samples within a minute.

The conversion was varied by changing the weight hour space velocity (WHSV) at a constant linear gas flow rate. Conversion is defined as the amount of MCP converted, selectivity is defined as the amount of a product divided by the amount of MCP converted. The turnover frequency (TOF) was calculated from the number of molecules of MCP converted and the H/Pt ratio, assuming that every site capable of chemisorbing hydrogen is a catalytically active site. The results reported here, except the results for the deactivation, the determination of α_{low}, and the pyridine

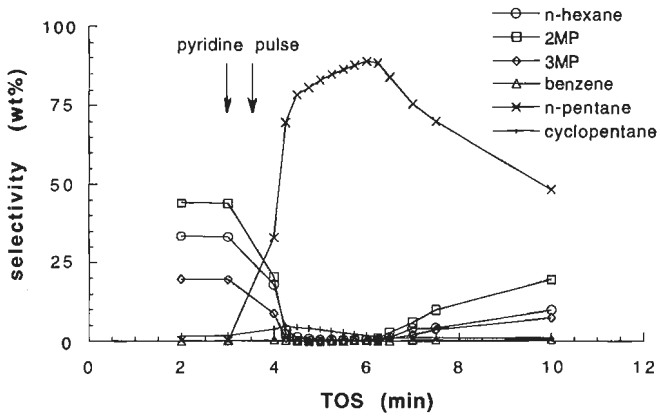

Figure 3 The effect of a pyridine pulse on the selectivity of MCP ring opening of the $Pt/\gamma-Al_2O_3$ catalyst after reduction at 450°C (T = 270°C and H_2:MCP = 40).

poisoning experiments, have been obtained under steady-state conditions. The activity of the Pt/K–LTL catalyst in aromatization of n-hexane has been reported earlier[27].

Results

Characterization

The Pt/K–LTL and $Pt/\gamma-Al_2O_3$ catalysts were extensively characterized by EXAFS and hydrogen TPD[28, 25, 29]. Results are similar for both catalysts. The particle size increases with reduction temperature. After reduction at low temperature (300°C, LTR) the platinum clusters contain 5–7 atoms, after reduction at high temperature (600°C, HTR) the clusters contain ≈11 atoms. Furthermore, the structure of the metal-support interface changes with reduction temperature. After LTR a Pt–O contribution at a distance of 2.7 Å is present in the EXAFS spectrum. Based on

Table 1 Hydrogen chemisorption and ring opening activity results. TOF (molecules of MCP converted per exposed platinum atom) determined at 270°C and H_2:MCP ratio of 40, conversion ≈10wt%.

catalyst	T_{red} (°C)	H/Pt	TOF (s^{-1})	WHSV (h^{-1})	E_{act} (kJ/mol)
Pt/K–LTL	300	1.42	0.6	0.22	158 ± 9
	450	1.27	0.8	0.22	162 ± 5
	600	0.84	0.7	0.22	159 ± 2
$Pt/\gamma-Al_2O_3$	300	1.48	1.2	0.27	138 ± 2
	450	1.16	3.1	0.27	143 ± 4
	600	1.03	2.7	0.27	129 ± 1
Pt/SiO_2	400	1.00	1.7	0.28	123 ± 4

hydrogen TPD this long Pt–O distance has been attributed to a structure were atomic hydrogen is present between the platinum and the oxygen atoms. Treatment in either inert or hydrogen atmosphere removes this interfacial hydrogen. Hence, the Pt–O distance as determined by EXAFS is shortened to 2.2 Å.

The dispersion of the catalysts was measured by hydrogen chemisorption (table 1). For both Pt/K–LTL and Pt/γ–Al_2O_3 the hydrogen chemisorption capacity decreases with the reduction temperature. The decreased hydrogen chemisorption capacity has been attributed to changes in the particle size, the particle morphology, and the structure of the metal-support interface. A detailed discussion of the relation between the hydrogen chemisorption capacity, the particle size, and the structure of the metal-support interface has been given elsewhere[29].

Acidity of Pt/γ-Al_2O_3

The presence of acidic sites will result in isomerization of the ring opening products of MCP, thereby perturbing the results of the measurements. The Pt/K–LTL catalyst is non-acidic as reported previously[27]. The Pt/γ–Al_2O_3 may contain acidic sites as the preparation was carried out with an aqueous solution of H_2PtCl_6. The isomerization of MCP to cyclohexane did not proceed on the Pt/γ–Al_2O_3 catalyst, indicating the absence of acidic sites. Poisoning of the acidic sites (if any) by a pulse of pyridine in the reactant stream decreased the conversion of MCP to virtually zero (figure 2), due to the adsorption of pyridine on the platinum surface. The maximum in the conversion at 6 min time on stream (TOS) is due to hydrogenation and

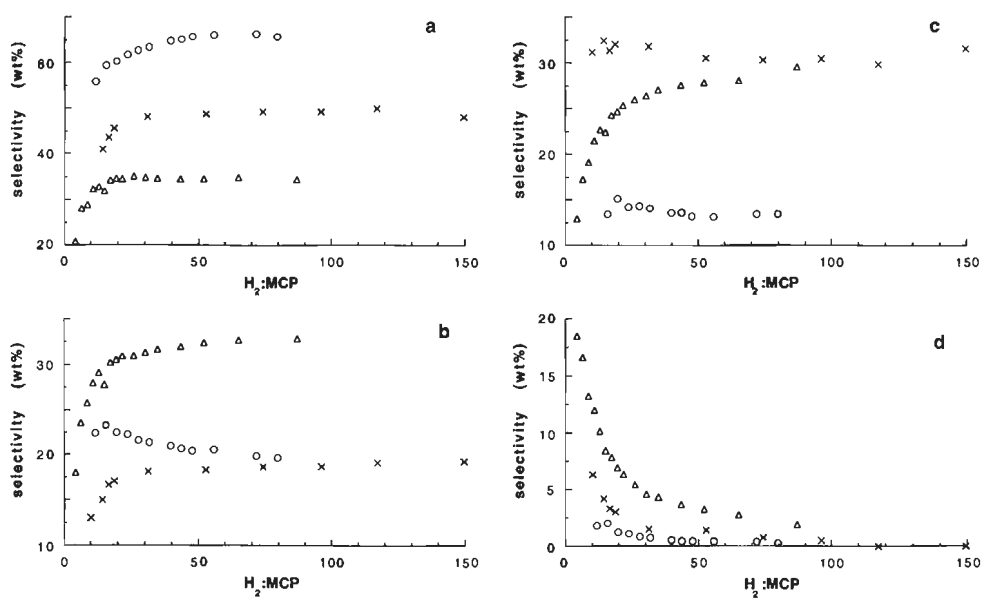

Figure 4 Selectivity of MCP ring opening as a function of H_2:MCP partial pressure ratio, x: Pt/SiO_2, Δ: Pt/K–LTL, and o: Pt/γ–Al_2O_3. All catalysts reduced at 400–450°C. a) 2-methylpentane, b) 3-methylpentane, c) n-hexane, and d) benzene

Table 2 Selectivities of MCP ring opening at 270°C and H_2:MCP ratio of 40, conversion ≈10wt%. Pt/γ–Al_2O_3 results at H_2:MCP ratio of 22.

catalyst	Pt/SiO_2	Pt/γ–Al_2O_3			Pt/K–LTL		
T_{red} (°C)	400	300	450	550	300	450	600
crack	0.5	3.8	1.7	0.5	6	1	11
2MP	51.1	62	66	68	32	39	33
3MP	19.8	21	23	23	34	30	28
n-hexane	25.8	13	9	8	24	25	24
C_6 olefins	1.1	–	–	–			
benzene	1.8	0.2	0.3	0.5	4	5	4
2MP:3MP	2.6	3.0	2.9	3.0	0.9	1.3	1.2
nC6:3MP	1.3	0.6	0.4	0.3	0.7	0.8	0.8

denitrification of the pyridine resulting in n-pentane (figure 3) and ammonia (not monitored). The disengagement of the surface for the ring opening of MCP is reflected in the increasing production of ring opening products concomitant with the decrease of n-pentane production. The selectivity ratios of the ring opening products are not affected by the poisoning of the Pt/γ–Al_2O_3 catalyst with pyridine. From the above observations we infer that the Pt/γ–Al_2O_3 catalyst contains no acidic sites that perturb the measurements.

Selectivity

The selectivities in the ring opening products varied with conversion for the amorphous catalysts. The contribution of the non selective mechanism increased with increasing conversion, above 20% conversion ring opening was non selective. The variation in selectivity with conversion is due to isomerization of ring opening products on the platinum surface or different orders in MCP of the reactants, e.g., different sites for selective and non selective ring opening. To minimize consecutive reactions and to improve the stability of the catalyst we kept the conversion at 10%, consequently the amorphous catalysts will not show the non selective ring opening that is expected for these highly dispersed catalysts. Future work will focus on the changes of selectivity with conversion.

The selectivities towards hydrogenolysis, ring opening and aromatization at 270°C are listed in table 2. The amount of hydrogenolysis products formed on the Pt/γ–Al_2O_3 catalyst decreases when the reduction temperature is elevated. Menon and Froment[30] reported a decrease in hydrogenolysis of n-pentane with increasing reduction temperature for Pt/Al_2O_3 and attributed the diminished hydrogenolysis activity to poisoning of active sites by strongly chemisorbed hydrogen. Den Otter and Dautzenberg[31] proposed the formation of a Pt-Al alloy during high temperature hydrogen treatment as the cause of the decreased hydrogenolysis activity.

The ring opening over Pt/K–LTL is neither selective nor non selective and is in

Table 3 Product selectivities of MCP ring opening on the Pt/K–LTL catalyst reduced at 310°C after 0 and 12 hrs time on stream (TOS). Reaction temperature 268°C, WHSV = 0.22 h^{-1} (H_2:MCP = 8) and 0.44 h^{-1} (H_2:MCP = 40)

	H_2:MCP = 8		H_2:MCP = 40	
product	initial	12 hrs TOS	initial	12 hrs TOS
hexane	13	20	30	30
2MP	32	32	33	33
3MP	29	30	33	33
benzene	16	11	3	3

first approximation independent of the reduction temperature. Comparison of the selectivity of the Pt/K–LTL catalyst with the selectivity pattern obtained for the Pt/SiO_2 catalyst shows that the selectivity towards 2MP is diminished and the selectivity towards 3MP is increased. The selectivity towards benzene is also higher for the Pt/K–LTL catalyst than for the Pt/SiO_2 catalyst. The higher selectivity towards 3MP has been reported for Pt/FAU[23] and Pt/LTL[24] catalysts. It has been explained[23] by the constraints that the zeolite pore imposes on the orientation of MCP molecule when it diffuses through the zeolite channels.

The changes in selectivity towards ring opening products and benzene with the H_2:MCP partial pressure ratio are shown in figure 4. The ratio 2MP/3MP as well as benzene selectivity decreases with increasing H_2:MCP ratio. For n-hexane the Pt/K–LTL catalyst behaves differently from the Pt/SiO_2 and Pt/γ–Al_2O_3 catalysts. The selectivity towards n-hexane increases with hydrogen partial pressure for Pt/K–LTL, whereas it is constant for platinum on amorphous supports. In general, the selectivity towards ring opening products increases with H_2:MCP ratio. This trend is stronger for the Pt/SiO_2 and Pt/K–LTL catalysts than for the Pt/γ–Al_2O_3 catalyst.

Stability

The catalysts deactivated during the catalytic runs, at high H_2:MCP ratio this did not affect the product distribution or the kinetics of the reaction, at low H_2:MCP ratio it mainly affected the n-hexane/benzene ratio.

The changes in selectivity were studied as a function of time on stream (TOS) for a Pt/K–LTL catalyst reduced at 310°C. The degree of deactivation depends on the ratio of the hydrogen and MCP partial pressure. At low values of this ratio (< 15) deactivation within the first three hours time on stream is at least 40%. At high values of this ratio (> 35), deactivation in the first hour is $\approx$ 15%, after the first hour no deactivation occurs. The changes in selectivity as a function of TOS (conversion) are shown in table 3. At high H_2:MCP ratios selectivities are independent of the TOS (conversion). The selectivity towards ring opening products is higher than 97%, the other product being benzene (3%). At low H_2:MCP ratios the selectivity towards ring opening products changes with TOS (conversion), (initially 74%, 82% after 12 hrs),

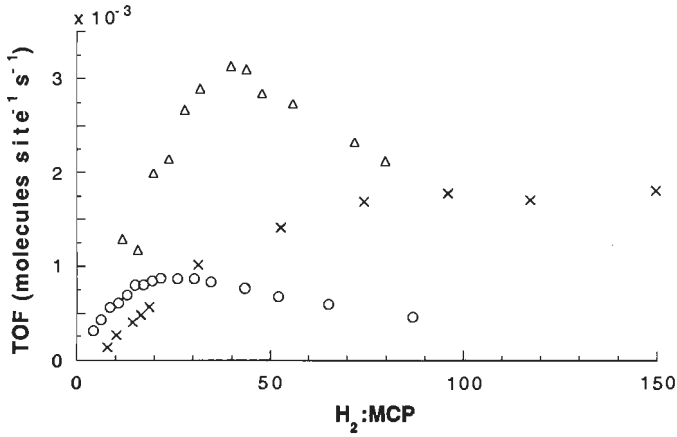

Figure 5 Variation of TurnOverFrequency (TOF) with H_2:MCP partial pressure ratio at 270°C, x: Pt/SiO_2, Δ: Pt/K–LTL, and o: Pt/γ–Al_2O_3. All catalysts reduced at 400–450°C.

the selectivity towards benzene decreases with TOS from 16 to 11%, the remaining products being unsaturated C_6 olefins. Analysis of the obtained results with the Delplot technique[32] showed that benzene is a secondary product.

The increase in selectivity towards n-hexane of the Pt/K–LTL catalyst with TOS (deactivation) is opposite to the trend reported by Ponec and coworkers[36] for Pt/SiO_2 catalysts. The decreased cyclization rate of the deactivated Pt/K–LTL catalyst is the explanation for this difference in behaviour.

Activity

The activation energy for the ring opening of MCP for the catalysts studied is shown in table 1. The activation energy of the Pt/K–LTL catalyst is the highest (≈160 kJ mol^{-1}), for the Pt/γ–Al_2O_3 it is about 20 kJ mol^{-1} lower, whereas the activation energy of Pt/SiO_2 catalysts is lowest (123 kJ mol^{-1}). The influence of the reduction temperature on the activation energy is negligible for Pt/K–LTL. Increasing the reduction temperature from 300 to 450°C for the Pt/γ–Al_2O_3 catalyst increases the

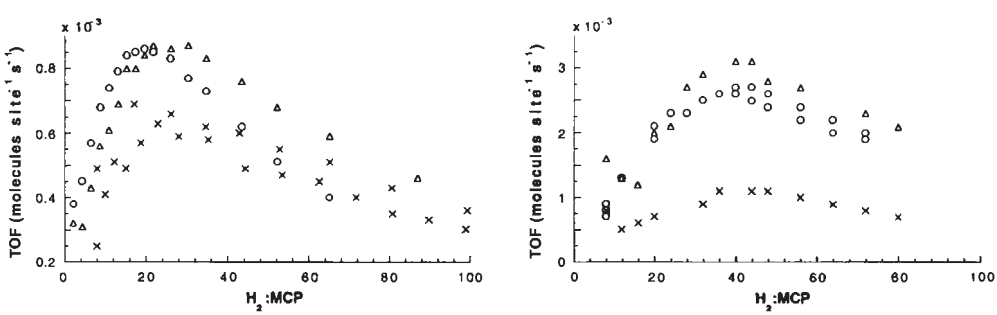

Figure 6 TurnOverFrequency of MCP ring opening as a function of H_2:MCP partial pressure ratio after reduction at x:300°C, Δ: 450°C, and o: 600°C, a) Pt/K–LTL, b) Pt/γ–Al_2O_3.

activation energy slightly (5 kJ mol^{-1}); increasing the reduction temperature from 450 to 600°C decreases the activation energy significantly (14 kJ mol^{-1}).

We determined the TurnOverFrequencies (TOF) of the catalysts based on the hydrogen chemisorption values, assuming that every site capable of chemisorbing a hydrogen atom is a catalytically active site (table 1). The TOF of the Pt/γ–Al_2O_3 catalyst is two times higher than the TOF of Pt/K–LTL after reduction at 300°C. After reduction at 450°C this ratio has increased to nearly 4 times. Further increase of the reduction temperature lowers the TOF slightly. The TOF of Pt/SiO_2 is twice as high as the TOF of Pt/K–LTL, but only half the TOF of Pt/γ–Al_2O_3.

Kinetics

The change of the TOF with H_2:MCP partial pressure ratio is shown in figure 5. The TOF of Pt/K–LTL and Pt/γ–Al_2O_3 exhibits a maximum at different H_2:MCP ratios. The TOF of the Pt/SiO_2 catalyst shows a very broad plateau. The maximum activity is reached at different H_2:MCP ratio, indicating that adsorption of either MCP or H_2 is affected by the support used. The maximum in the TOF is slightly affected by the reduction temperature for Pt/K–LTL (figure 6a), whereas it is independent of the reduction temperature for Pt/γ–Al_2O_3 (figure 6b). The growth of the platinum particles inside the zeolite pore apparently affects the adsorption equilibrium between MCP and hydrogen.

The reaction orders have been analyzed according to the simple power rate law, with α being the order in hydrogen and β the order in MCP:

$$r = kp_{H_2}^{\alpha} p_{MCP}^{\beta} \tag{1}$$

The orders in H_2 and MCP for the studied catalysts are listed in table 4. The order in H_2 at low H_2:MCP ratio (α_{low}) decreases with reduction temperature for the Pt/K–LTL catalyst, whereas it increases for the Pt/γ–Al_2O_3 catalyst. The order in H_2 at high H_2:MCP ratio (α_{high}) is in general more negative for the Pt/K–LTL catalyst than

Table 4 Reaction orders of MCP ring opening at 270°C in hydrogen (α) and MCP (β). Order in hydrogen determined at a MCP partial pressure of 10 kPa, order in MCP determined at a hydrogen partial pressure of 40 kPa.

catalyst	T_{red} (°C)	α_{low}	α_{high}	β
Pt/K–LTL	300	0.8	–0.6	0.38
	450	0.7	–1.0	0.45
	600	0.4	–0.8	0.59
Pt/γ–Al_2O_3	300	0.7	–0.7	
	450	0.8	–0.6	0.91
	550	0.9	–0.6	
Pt/SiO_2	400	1.0	–0.1	0.65

for the Pt/γ–Al_2O_3 catalyst. The order in MCP increases with reduction temperature for the Pt/K–LTL catalyst, but it is lower than the order in MCP of the Pt/SiO_2 catalyst.

Discussion

The TOF numbers for MCP consumption show smaller values for the Pt/K–LTL catalyst than for the amorphous catalysts, due to the more difficult access of the MCP molecules to the platinum particles. Note also the enhanced activation energy of the reaction. The higher 2MP/3MP ratio for low H_2:MCP ratio, shows that the 2MP/3MP ratio is sensitive to the surface reaction rate versus the rate of dissociative MCP adsorption. At low H_2:MCP ratio, the surface reaction rate is limited by the rate of hydrogen dissociation (see table 4), at higher H_2:MCP ratio the surface is saturated with hydrogen. Clearly this decreases the aromatics production at higher H_2:MCP ratio. The low n-hexane selectivity at low H_2:MCP ratio may also be due to the consecutive reaction of hexane to benzene when occluded in the micropores[34] upon contact with hydrogen deficient platinum particles. The decreased stability of the catalysts at low H_2:MCP ratio is consistent with these features, viz. due to the larger rate of coke deposition on hydrogen deficient platinum particles.

EXAFS and molecular modelling[29] indicated that the platinum particles in the Pt/K–LTL catalysts are located in the cavities in the zeolite LTL channels. Figure 7 shows such a platinum particle with a MCP molecule in the channel window in two orientations. In agreement with earlier suggestions by Tauster and Steger[35] we find that the orientation with the methyl group aligned along the channel direction is clearly less hindered compared to the orientation with the methyl group perpendicular to the channel direction. A consequence of this is a restriction on the orientation of the MCP molecule when absorbing onto the platinum particle. With the methyl group aligned along the channel, the molecule impinge with either the methyl group and the connecting carbon atom in the ring (mode 1) or the carbon atoms opposing the methyl group to the platinum particle (mode 2). The adsorption in mode 1 yields n-hexane. The adsorption in mode 2 results in formation of 3MP. So steric constraints agree with the reduction of 2MP formation and the higher 3MP formation. n-Hexane formation will only be enhanced at high H_2:MCP ratio, otherwise the reaction proceeds to yield benzene.

The different H_2:MCP ratio at which maximum TOF is reached, can be explained by the constraints imposed by the zeolite LTL pore on the orientation of the MCP molecule. This decreases the rate of adsorption of MCP on the Pt surface and thus the (competitive) adsorption of H_2. Competitive adsorption of MCP and hydrogen determines the maximum in TOF as a function of H_2:MCP ratio. At low H_2:MCP ratio the metal surface is hydrogen deficient, as follows from the changes of the partial reaction order in H_2. At higher H_2:MCP ratio (steady state) the surface

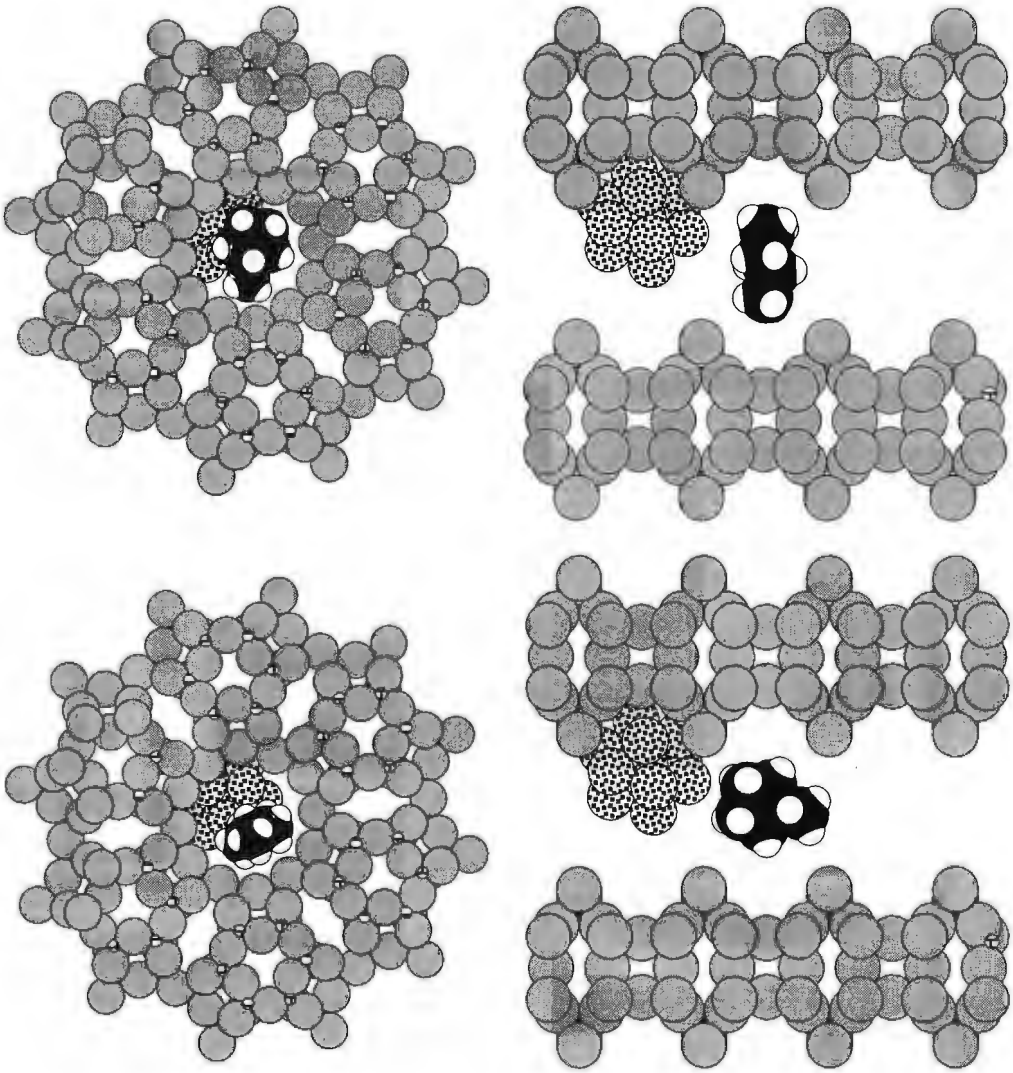

Figure 7 Molecular modelling picture of a 13 atom platinum particle and a MCP molecule in the pore of zeolite LTL. Pictures on the left are views along the channel direction, pictures on the right are views perpendicular on the channel direction. Potassium ions have been omitted for clarity.

becomes covered with hydrogen. This leads to a decrease in the H_2:MCP ratio at which maximum activity is reached for the catalyst with the weaker effective platinum-hydrocarbon interaction. A higher order (α_{low}) in hydrogen indicates that the competition with MCP is more severe. Hence, the maximum activity will be reached at higher hydrogen partial pressure.

The difference in TOF between the Pt/γ–Al_2O_3 and the Pt/SiO_2 catalyst is similar

to the difference in TOF between the standard Pt/Al_2O_3 (EUROPT–3) catalyst and the standard Pt/SiO_2 (EUROPT–1) catalyst[37]. The large increase in TOF of the Pt/γ–Al_2O_3 catalyst when the reduction temperature is raised from 300 to 450°C is not accompanied by an increase in the number of catalytically active sites as indicated by the decrease in hydrogen chemisorption capacity of this catalyst. Hence, the increased activity can not be attributed to a better reduction of the platinum. From the EXAFS and TPD characterization of this catalyst it is known[25] that by increasing the reduction temperature from 300 to 450°C the structure of the metal-support interface is changed and the shape of the particles change from 3D to flat. The atoms in a raft have a higher degree of coordinatively unsaturation and are thus expected to chemisorb more hydrogen. The concomitant change in the structure of the metal-support interface apparently counters this effect as a decreased hydrogen chemisorption capacity is observed. The adsorption of MCP is affected similarly as the optimum H_2:MCP ratio is not changed. The absence of the third shell in the EXAFS spectrum after reduction at 450°C indicates that a square surface is formed. The more open square surface might exhibit increased MCP ring opening activity in agreement with a study on the MCP ringopening activity of platinum single crystal surfaces[11].

Conclusion

The increased selectivity towards 3MP for Pt/K–LTL catalysts compared to Pt/γ–Al_2O_3 and Pt/SiO_2 can be explained from the constraints that the zeolite pores impose on the orientation of the MCP molecule inside the pores. The constraints on the orientation of the MCP molecule inside the zeolite pores decrease the adsorption energy of MCP on the platinum surface, as is reflected in the different H_2:MCP ratio at which the maximum TOF is found. The maximum shifts to higher H_2:MCP partial pressure ratio when MCP adsorption is less constrained. The high aromatics production at low H_2:MCP ratio on zeolite L is due to consecutive reactions of n-hexane in the micropores of zeolite L. The increase in TOF of the Pt/γ–Al_2O_3 catalyst upon raising the reduction temperature from 300 to 450°C is related to the change in the structure of the metal-support interface and the morphology of the platinum particle.

References

1. M. Che and C. O. Bennett, Adv. Catal., **36** (1989) 55.
2. M. Boudart and G. Djéga-Mariadassou, *Kinetics of Heterogeneous catalytic reactions* (Princeton University Press, Princeton, N.J., 1984).
3. F. G. Gault, Adv. Catal. **30** (1981) 1.

4. O. V. Bragin, Z. Karpinski, K. Matusek, Z. Paál, and P. Tétényi, J. Catal. **56** (1979) 219.
5. B. A. Kazansky and Z. A. Rumyantseva, Izv. Akad. Nauk SSSR, Otdel. Chim. Nauk (1947) 183.
6. G. Maire, G. Plouidy, J. C. Prudhomme, and F. G. Gault, J. Catal. **4** (1965) 556.
7. H. C. de Jongste and V. Ponec, *Proc. 7th Int. Cong. Catal.*, Tokyo, 1980, T. Seiyama and K. Tanabe (Elsevier, Amsterdam, 1981), 186.
8. R. Kramer and H. Zuegg, *Proc. 8th Int. Cong. Catal.*, Berlin (West), 2-6 July 1984, (Verlag Chemi, Basel, 1984), 275.
9. R. Kramer and H. Zuegg, J. Catal. **80** (1983) 446.
10. J. B. F. Anderson, R. Burch, and J. A. Cairns, J. Catal. **107** (1987) 351.
11. A. Dauscher, F. Garin, and G. Maire, J. Catal. **105** (1987) 233.
12. O. E. Finlayson, J. K. A. Clarke, and J. J. Rooney, J. Chem. Soc. Faraday Trans. **80,** (1984) 191.
13. Z. Paál, Catal. Today **2** (1988) 595.
14. T. G. Olfer'eva, S. A. Krasavin, and O. V. Bragin, Izv. Akad. Nauk SSSR, Ser. Khim. **3** (1981) 605.
15. H. Zimmer and Z. Paál, J. Mol. Catal. **51** (1989) 261.
16. S. G. Brandenberger, W. L. Callender and W. K. Meerbott, J. Catal. **42** (1976) 282.
17. F. Garin and F. G. Fault, J. Am. Chem. Soc. **97** (1975) 4466.
18. A. Sárkány, J. Chem. Soc., Far. Trans. I **85** (1989) 1523.
19. A. Frennet, G. Lienard, A. Crucq and L. Degols, J. Catal. **53** (1978) 150.
20. A. Frennet, *in* "Hydrogen effects in catalysis", (Z. Paál and P. G. Menon, Eds.) (Marcel Dekker, Inc., New York,), p. 399, 1988.
21. S. A. Krasavin and O. V. Bragin, Izv. Akad. Nauk SSSR, Ser. Khim. **6** (1982) 1314.
22. H. J. Jiang, M. S. Tzou, and W. M. H. Sachtler, Appl. Catal., **39** (1988) 255.
23. G. Moretti and W. M. H. Sachtler, J. Catal. **116** (1989) 350.
24. W. E. Alvarez and D. E. Resasco, Catal. Lett. **8** (1991) 53.
25. M. Vaarkamp and D. C. Koningsberger, in preparation (chapter 6).
26. J. E. Benson and M. Boudart, J. Catal., **4** (1965) 704.
27. G. S. Lane, F. S. Modica and J. T. Miller, J. Catal. **129** (1991) 145.
28. M. Vaarkamp, J. van Grondelle, R. A. van Santen, J. T. Miller, F. S. Modica, G. S. Lane, and D. C. Koningsberger, *in* "Proc. 9th Int. Zeolite Conf., Montreal, July 5-10, 1992", Butterworth-Heinemann, London, in print.
29. M. Vaarkamp, J. T. Miller, F. S. Modica, and D. C. Koningsberger, submitted (chapter 5 part 2).
30. P. G. Menon and G. F. Froment, J. Catal., **59** (1979) 138.
31. G. J. den Otter and F. M. Dautzenberg, J. Catal., **53** (1978) 116.
32. N. A. Bhore, M. T. Klein, and K. B. Bischoff, Ind. Eng. Chem. Prod. Res. **29** (1990) 313.
33. G. C. Bond and L. Hui, J. Catal. **132** (1992) 462.
34. E. G. Derouane and D. J. Vanderveken, Appl. Catal., **45** (1988) L15.

35. S. J. Tauster and J. J. Steger, Mat. Res. Soc. Symp. Proc., **111** (1988) 419.
36. A. P. van Wijk, E. H. van Broekhoven, and V. Ponec, J. Chem. Soc., Chem. Commun., (1986) 1263.
37. R. Kramer and M. Fischbacher, J. Mol. Catal., **51** (1989) 247.

Chapter 9

Summary and Concluding Remarks

The aim of the research described in this thesis was to unravel the relation between the size, geometry, and electronic structure of supported platinum particles and their reactivity towards hydrocarbons. The structure of the platinum particles and their interaction with the support has been studied by EXAFS and hydrogen TPD. The influence of adsorbates, particle size and support on the number of unfilled d-states of the same particles was determined from the intensity of the Pt L_{II} and L_{III} X–ray absorption edges. The hydrogenolysis of propane and the ring opening of methylcyclopentane were studied to find the catalytic impact of the observed changes in the structure of the metal particles, the number of unfilled d-states, and the changes in the structure of the metal-support interface.

In chapter 2 the developed methods to analyse XAFS spectra are described. The use of analytical partial derivatives in the non linear least squares refinement of the structural parameters decreases the CPU time needed for a refinement up to 60% compared to partial derivatives calculated with the finite difference method. Errors in the structural parameters are calculated from the noise in the data and the correlations between the parameters. The analysis of EXAFS spectra containing contributions of both high and low Z elements is not straightforward. It was shown that contributions of low Z elements in the presence of contributions from high Z elements can only be detected by using k^1 weighed Fourier transforms. In chapter 3 several methods to calculate the backscattering amplitude and phase are compared to each other and experimentally obtained backscattering amplitudes and phases. Calculations become less accurate when the number of electrons in an atom increases (i.e. for high Z elements). It was infered that the use of compounds with a structure similar to the system under study assures most accurate results. In cases where no appropriate reference compounds are available, like in many biological systems and for higher shell analysis, one has to use theoretically obtained backscattering amplitudes and phases. The method described by Rehr and coworkers[1], which includes curved wave effects and uses an energy dependent self-

energy results in backscattering amplitudes and phases most similar to the experimental values. The main source of errors is neither the noise in the data nor the correlation between the parameters, but the uncertainty in the used backscattering amplitude and phase.

The relation between structure and activity for a Pt/BaK–LTL catalyst is shown in chapter 4. The sensitivity to sulphur poisoning of this highly active and selective aromatization catalyst has been attributed to the increase in particle size when the catalyst is exposed to H_2S. The particle size increases from 5–6 atoms in the fresh catalyst to approximately 13 atoms in the poisoned catalyst. The radius of the platinum cluster in the poisoned catalyst is about 8 Å, which is larger than the window of the pore. Molecular modelling showed that a n-hexane molecule is unable to pass the window if a platinum particle is located in the next cavity. Consequently only the platinum atoms located in the window remain catalytically active. Hydrogen atoms are still able to pass the window as was deduced from the decrease in catalytic activity of about 70% compared to the decrease in hydrogen chemisorption capacity by only 30%.

The size and morphology of platinum clusters and the structure of the metal-support interface in Pt/K–LTL, Pt/H–LTL (chapter 5) and Pt/γ–Al_2O_3 (chapter 6) catalysts has been studied by hydrogen TPD and EXAFS. After reduction at 300°C the TPD spectrum showed that at least three types of hydrogen are present in all catalysts. The morphology of the platinum particles and the structure of the metal-support interface was determined by EXAFS at several stages of the TPD. After reduction at 300°C, thus prior to the TPD, the platinum clusters are metallic as indicated by the Pt–Pt bond distance of 2.76 Å. These metallic clusters are located at a distance of 2.65 – 2.72 Å from the support.

Chemisorbed hydrogen desorbed between 80 and 200°C as was shown by stopping the TPD at 300°C, rereduction at 300°C and performing a second TPD. The EXAFS analogue of this experiment consisted of heating in vacuum to 300°C followed by readsorption of hydrogen at 200°C. Removal of chemisorbed hydrogen leads to a contraction of the Pt–Pt distance to 2.66 Å, readsorption of the hydrogen restores the original Pt–Pt distance of 2.76 Å. The distance between the platinum atoms and the support is not affected by this treatment.

Above 300°C hydrogen desorbs irreversibly as was shown by rereduction of the sample at both 300 and 700°C and repeating the TPD experiment. This irreversible hydrogen desorption was accompanied by a shortening of the distance between platinum particles and the support to 2.22 – 2.25 Å. The conclusion from this observation is that hydrogen is present between the platinum clusters and the support. The removal of this so-called "interfacial" hydrogen can be done in either inert of reducing atmosphere. The shortening of the average metal-support distance was accompanied by a decrease in hydrogen chemisorption capacity of the catalysts. It is proposed that the interaction of the interfacial platinum atoms with oxygen ions from the support is responsible for the decreased hydrogen chemisorption capacity.

Spillover hydrogen desorbs around 430°C from alumina, whereas it desorbs above 600°C from zeolite LTL. The amount of spillover hydrogen is much larger for platinum supported by γ–Al_2O_3 and H–LTL than for K–LTL.

The number of unfilled d-states of the platinum particles, varying in size from 5–11 atoms, supported on γ–Al_2O_3, H–LTL, and K–LTL was determined from the intensity of the platinum L_{III} and L_{II} X–ray absorption edges (chapter 7). The influence of chemisorbed hydrogen on the intensity of both the L_{III} and L_{II} edge is paramount as was shown by removal and readsorption of chemisorbed hydrogen. Removing the chemisorbed hydrogen results in a dramatic decrease of the intensity of the L_{III} and L_{II} X–ray absorption edges. Increasing the reduction temperature which is accompanied by the removal of interfacial hydrogen results also in a decrease of the white line intensity. The influence of support and particle size on the number of unfilled d-states could not be established due to the masking effect of chemisorbed and interfacial hydrogen. An important consequence of our white line studies is that the influence of support or particle size on the d-band density of states can only be determined if chemisorbed and interfacial hydrogen are absent in the system under study. The propane hydrogenolysis TOF for platinum supported on γ-Al_2O_3 or H-LTL is found to be more than an order of magnitude higher than for platinum supported on a K–LTL zeolite. A correlation between hydrogenolysis activity and electron density could not be established, due to the above mentioned masking effect.

The ring opening of methylcyclopentane (MCP) over well characterized Pt/SiO_2, Pt/γ–Al_2O_3, and Pt/K–LTL catalysts was studied. The activity, selectivity and stability depends on the type of support and the reduction temperature. The Pt/K–LTL catalyst exhibited a higher selectivity towards 3-methylcylopentane and benzene compared to the Pt/SiO_2 and Pt/γ–Al_2O_3 catalysts. The increased selectivity towards 3-methylpentaan for Pt/K–LTL catalysts compared to Pt/γ–Al_2O_3 and Pt/SiO_2 can be explained from the constraints that the zeolite pore imposes on the orientation of the MCP molecule inside the pores, which was originally proposed by Moretti and Sachtler[2] for the Pt/FAU system. The constraints on the orientation of the MCP molecule inside the zeolite pores decrease the adsorption energy of MCP on the platinum surface, as is reflected in the different H_2:MCP ratio at which maximum activity is reached. The maximum shifts to higher H_2:MCP partial pressure ratio when MCP adsorps stronger. The high aromatizatics production at low H_2:MCP partial pressure ratio on zeolite L is due to consecutive reactions of n-hexane in the micropores of zeolite L. Increasing the reduction temperature of the Pt/γ–Al_2O_3 catalyst from 300 to 450°C results in a morphology change of the platinum particles from 3-dimensional to flat. Simultaneously, the turnoverfrequency of MCP increases three times suggesting that the flat surface is more active for MCP ringopening than the 3-dimensional particles.

The objective of this thesis to study the relation between size, morphology, electronic structure, and catalytic properties of supported metal catalysts has resulted

in the precise characterization of the structure and morphology of supported small platinum particles. The structure of the metal-support interface depends on the reduction temperature of the catalyst. Hydrogen is present in the metal-support interface after reduction at 300°C. This interfacial hydrogen desorbs above 300°C. The change in metal-support interaction is accompanied by a decrease of the hydrogen chemisorption capacity for all catalysts studied. In the $Pt/\gamma\text{–}Al_2O_3$ catalyst the morphology of the platinum particles changes from 3-dimensional to flat when the reduction temperature is increased. The changes in hydrogen chemisorption capacity and morphology are accompanied by changes in the activity for methylcyclopentane ringopening and propane hydrogenolysis.

References

1. J. Mustre de Leon, J. J. Rehr, S. I. Zabinsky, and R. C. Albers, Phys. Rev. B., **44** (1991) 4146.
2. G. Moretti and W. M. H. Sachtler, J. Catal. **116,** 350 (1989).

Samenvatting

Het doel van het in dit proefschrift beschreven, onderzoek, was het ontrafelen van de relatie tussen grootte, morfologie, elektronische structuur en reaktiviteit in koolwaterstof reacties van gedragen platina deeltjes. EXAFS en waterstof TPD werden gebruikt om de structuur van de platina deeltjes en de interactie tussen de platina deeltjes en het dragermateriaal te bestuderen. De invloed van adsorbaten, deeltjesgrootte en dragermateriaal op het aantal lege toestanden in de d-band werd bepaald aan de hand van de intensiteit van de Pt L_{II} en L_{III} röntgenabsorptie-overgangen. De activiteit van de gedragen platina deeltjes voor de hydrogenolyse van propaan en de ringopening van methylcyclopentaan werden bepaald om de relatie tussen de gevonden veranderingen in de structuur van katalysator en de katalytische activiteit te bepalen.

In hoofdstuk 2 worden de ontwikkelde methoden om XAFS spectra te analyseren beschreven. Het gebruik van analytische partiële afgeleiden in plaats van partiële afgeleiden uitgerekend met de eindige verschil methode, in de niet lineaire kleinste kwadraten optimalisatie van de parameters voor een model EXAFS spectrum vermindert de rekentijd voor een optimalisatie met 60%. De fouten in de structuur parameters worden bepaald aan de hand van de ruis in de data en de correlaties tussen de parameters.

Het analyseren van EXAFS spectra met bijdragen van lichte en zware elementen is niet vrij van complicaties. Bijdragen van lichte elementen aan een spectrum waaraan zware elementen bijdragen, kunnen alleen worden gedetecteerd door gebruik te maken van k^1 gewogen Fourier transformaties.

In hoofdstuk 3 werden meerdere methoden om het terugverstrooiingsvermogen en de fase verschuiving van atomen te berekenen onderling en met gemeten terugverstrooiingsvermogens en fase verschuivingen vergeleken. De berekeningen worden minder nauwkeurig met toenemend atoomgewicht. Resultaten die het best overeenstemmen met experimentele waarden worden verkregen met methoden die gebruik maken van bolgolven en een energie afhankelijke zelf-energie[1].

De nauwkeurigste analyse resultaten van een EXAFS spectrum worden verkregen door het gebruik van terugverstrooiingsvermogens en fase verschuivingen bepaald uit verbindingen met een structuur gelijkend op de structuur van de onbekende. Als dit soort verbindingen niet voorhanden zijn, zoals in vele biologische systemen is men aangewezen op berekende terugverstrooiings-vermogens en fase verschuivingen. De grootste bron van fouten in de structurele

parameters in een model EXAFS spectrum is niet de ruis in de data noch de correlatie tussen de structurele parameters, maar de onnauwkeurigheid van de gebruikte terugverstrooiingsvermogens en fase verschuivingen.

De structuur-activiteit relatie voor een Pt/BaK–LTL katalysator is beschreven in hoofdstuk 4. De gevoeligheid voor vergiftiging met zwavel van deze zeer actieve en selectieve aromatiseringskatalysator is toegeschreven aan de toename van de deeltjesgrootte als de katalysator wordt blootgesteld aan H_2S. Het aantal atomen per deeltje neemt toe van 5–6 in de verse katalysator tot ongeveer 13 in de vergiftigde katalysator. De diameter van de platina deeltjes in de vergiftigde katalysator is ongeveer 8 Å, wat groter is dan de diameter van de porie (7.2 Å). Modellen van de zeoliet, het platina deeltje en n-hexaan laten zien dat n-hexaan het platina deeltje niet meer kan passeren. Waterstof moleculen kunnen dit nog wel zoals kan worden afgeleid uit de afname van de katalytische activiteit met 70%, terwijl de waterstofchemisorptie capaciteit met slechts 30% afneemt.

De grootte en de morfologie van platina deeltjes en de structuur van het metaal-drager grensvlak in Pt/K–LTL, Pt/H–LTL (hoofdstuk 5) en Pt/γ–Al_2O_3 (hoofdstuk 6) katalysatoren werd onderzocht met waterstof TPD en EXAFS. Het TPD profiel na reductie van de katalysator bij 300°C laat zien dat zich tenminste drie soorten waterstof op de katalysator bevinden. Op verschillende punten in de TPD werd een EXAFS spectrum gemeten om zo de veranderingen in de structuur van de katalysator te kunnen relateren aan de desorptie van waterstof. Na reduktie bij 300°C, dus voor de TPD, zijn de platina deeltjes metallisch wat volgt uit de Pt–Pt afstand van 2.76 Å. De afstand tussen deze metallische deeltjes en de drager is 2.65 – 2.70 Å.

Gechemisorbeerde waterstof desorbeert tussen 80 en 200°C. Dit werd gedemonstreerd door een TPD tot 300°C op te nemen, de katalysator opnieuw te reduceren bij 300°C en een tweede TPD uit te voeren. Een EXAFS experiment analoog aan een TPD tot 300°C (reduktie bij 300°C, evacuatie bij 300°C) liet zien dat de desorptie van gechemisorbeerde waterstof resulteert in een kleinere Pt–Pt afstand (2.66 Å). Readsorptie van gechemisorbeerde waterstof hersteld de oorspronkelijk Pt–Pt afstand. De structuur van het metaal-drager grensvlak blijft onveranderd tijdens de adsorptie en desorptie van gechemisorbeerde waterstof.

Boven 300°C desorbeert waterstof irreversibel, zoals werd aangetoond door na een TPD het monster te reduceren bij 300 of 700°C en nog een TPD op te nemen. De irreversibele waterstof desorptie gaat gepaard met een afname van de afstand tussen de platina deeltjes en de drager tot 2.22 – 2.25 Å. Hieruit werd geconcludeerd dat waterstof zich bevindt tussen de platina deeltjes en de drager. Dit "grensvlak" waterstof desorbeert in zowel inert als reducerend milieu. Tegelijk met de afname van de afstand tussen drager en platina deeltjes neemt de waterstofchemisorptie-capaciteit van de platina deeltjes af. Het is waarschijnlijk dat de andere interactie tussen de platina deeltjes en de drager hiervoor verantwoordelijk is.

Spillover waterstof desorbeert rond 430°C van de Pt/γ–Al_2O_3 katalysator, terwijl

het desorbeert boven 600°C voor Pt/LTL katalysatoren. De hoeveelheid spillover waterstof is veel groter voor γ-Al_2O_3 en H-LTL dan voor K-LTL.

Het aantal lege toestanden in de d-band van de platina deeltjes werd bepaald aan de hand van de intensiteit van de Pt L_{II} en L_{III} röntgenabsorptieovergangen (hoofdstuk 7). De invloed van gechemisorbeerde waterstof op het aantal lege toestanden in de d-band overheerst alle andere effecten zoals werd gedemonstreerd door desorptie en readsorptie. Desorptie van gechemisorbeerde waterstof leidt tot een dramatische afname van de intensiteit van zowel de Pt L_{II} als de Pt L_{III} röntgenabsorptieovergang. Reduktie bij hogere temperatuur (desorptie van grensvlak waterstof) leidt ook tot een afname van het aantal lege toestanden in de d-band. De invloed van de drager op de intensiteit van de Pt L_{II} en L_{III} röntgenabsorptieovergangen kon niet worden bepaald door de overheersende invloed van gechemisorbeerde en grensvlak waterstof. De invloed van de drager op de elektronische structuur van de platina deeltjes kan dus alleen worden vastgesteld door metingen na reduktie en evacuatie bij temperaturen boven 350°C.

De activiteit voor de hydrogenolyse van propaan is meer dan een orde van grootte hoger voor platina op γ-Al_2O_3 of H-LTL dan voor platina op K-LTL. Dit dragereffect kon niet worden gerelateerd aan veranderingen in de elektronische structuur van de platina deeltjes vanwege de overheersende invloed van gechemisorbeerde en grensvlak waterstof.

De activiteit, selectiviteit en stabiliteit van platina katalysatoren in de ringopening van methylcyclopentaan (MCP) is afhankelijk van de drager en de reduktie temperatuur (hoofdstuk 8). Een Pt/K-LTL katalysator heeft een hogere 3-methylpentaan en benzeen selectiviteit dan een Pt/SiO_2 of een Pt/γ-Al_2O_3 katalysator. De hogere 3-methylpentaan selectiviteit kan worden verklaard uit de restricties die de zeoliet poriën opleggen aan de oriëntatie van het MCP molecuul[2]. De restricties die de zeoliet poriën opleggen aan de oriëntatie van het MCP molecuul verlaagt de adsorptie energie van MCP op het platina oppervlak. Hierdoor wordt de maximale activiteit van een Pt/K-LTL katalysator bereikt bij een ander H_2:MCP verhouding dan wanneer een Pt/SiO_2 katalysator wordt gebruikt. Het maximum verschuift naar hogere H_2:MCP verhouding als MCP sterker adsorbeert. Benzeen wordt in de poriën van zeoliet LTL gevormd uit een volgreaktie van n-hexaan.

De activiteit van de Pt/γ-Al_2O_3 katalysator neemt met een factor drie toe als de reduktie temperatuur wordt verhoogd van 300 naar 450°C. De platina deeltjes veranderen van 3-dimensionale structuren in vlakke structuren door reduktie bij hogere temperatuur. Dit suggereert dat de vlakke (meer open) structuur actiever is voor ringopening van MCP dan de dichtere 3-dimensionale structuren.

Dit onderzoek naar de relatie tussen grootte, morfologie, elektronische structuur en reaktiviteit in koolwaterstof reacties van gedragen platina deeltjes heeft geleid tot een precieze bepaling van de structuur en morfologie van kleine platina deeltjes op drager. Het structuur van het grensvlak tussen de platina deeltjes en de drager is afhankelijk van de reduktie temperatuur van de katalysator. Na reduktie bij 300°C

bevindt zich waterstof in het metaal-drager grensvlak. Dit waterstof desorbeert boven 300°C. De verandering in metaal-drager interactie leidt tot een verlaging van de waterstofchemisorptiecapaciteit en in het geval van $Pt/\gamma\text{-}Al_2O_3$ tot een morfologie verandering. De verandering in waterstof chemisorptie capaciteit en de verandering in morfologie gaan gepaard met veranderingen in de activiteit voor methylcyclopentaan ringopening en propaan hydrogenolyse.

References

1. J. Mustre de Leon, J. J. Rehr, S. I. Zabinsky, and R. C. Albers, Phys. Rev. B., **44** (1991) 4146.
2. G. Moretti and W. M. H. Sachtler, J. Catal. **116**, 350 (1989).

Epiloog

Het zit erop, dit boekje is af. Ondanks dat mijn naam op de voorkant prijkt, wil dat niet zeggen dat alles wat op de voorgaande pagina's wordt beschreven, tot stand is gekomen zonder de hulp van (vele) anderen.

Om maar bij het begin te beginnen, wil ik als eerste mijn ouders noemen. Jullie hebben mij altijd de kans gegeven te doen wat ik leuk vond (en vind). De door jullie gestimuleerde ontwikkeling van een gezonde portie boerenverstand is mij de afgelopen jaren goed van pas gekomen. De opofferingen die jullie je getroost hebben om ons te laten studeren zijn een stimulans om er iets moois van te maken!

Tijdens mijn promotietijd was daar op de eerste plaats natuurlijk Diek (en niet te vergeten Pia) die met zijn aan het ongelooflijke grenzende enthousiasme mij een groot respect voor de inhoud van dit proefschrift heeft bijgebracht. Als ik Diek zeg, kan Joop natuurlijk niet onvermeld blijven. Zijn praktische instelling behoedde mij voor te hoge verwachtingen en grote decepties. De reflecties in de pub en op het lab zal ik missen!

The comparison of the various methods of calculating phase shifts was established in cooperation with Ian Dring, Norman Binsted, and Richard Oldman of ICI Chemicals and Polymers. John Rehr provided the computer program FEFF. Ed Stern guided us in this comparison. I want to thank all of you for your cooperation and interest.

Part of the hydrogen TPD and catalytic measurements have been carried out at the Amoco Oil Research Centre. Jeff Miller, Frank Modica, Berni Meyer, and Gery Lane always inspected the results very carefully and we had long discussions, at any time and at any place, about the interpretation of the measurements. I really enjoyed working with you!

An important part of the last four years were spent at the SRS in Daresbury, UK. The assistance of the staff, especially Menno Oversluizen and Bob Billsborrow, was invaluable for the progress of the measurements.

Het ontwikkelen van de data analyse software was niet zo voortvarend verlopen als Hans Linders and Gert Jan Visser niet altijd bereid waren geweest mij met raad en daad terzijde te staan.

Van de infrarood metingen die zijn uitgevoerd door Wim Jacobs, Jos van Wolput en Menno Kappers zijn er slechts weinig tot de pagina's van dit proefschrift doorgedrongen. Dat heeft zeker niet aan jullie inzet gelegen!

Het verblijf op het lab tijdens (en na) werktijd werd veraangenaamd door vele prettige collega's, hiervan wil ik mijn (ex) kamergenoten Tijs Koerts, Leo van Gruijthuijzen, Imre Peeters en Annemieke van de Runstraat met name noemen. De inzet van en de discussies met de afstudeerders Lucien van Ham en Paul Dijkstra waardeer ik zeer.

Buiten de wetenschap is er ook een leven, de mensen die dat leven tot een aangename tijd hebben omgetoverd wil ik hiervoor vanachter de Mac™ (en eventueel later op een passender moment) van harte bedanken.

Curriculum Vitae

Marinus Vaarkamp werd op 5 oktober 1964 om 11.05 uur geboren te Woudenberg. Na het volgen van de atheneum opleiding aan het Christelijk Lyceum te Veenendaal en een kort verblijf op de Hogere Zeevaartschool, begon hij in oktober 1983 met de studie scheikunde aan de Rijksuniversiteit Utrecht. De keuzepakketten chemie en samenleving, fysische chemie, fysische informatica en heterogene katalyse (een stage op het Koninklijke Shell Laboratorium Amsterdam) en het hoofdvak heterogene katalyse leidden, naar het op 31 oktober 1988 uitgereikte, doktoraaldiploma. Op 1 november 1988 trad de auteur van dit proefschrift in dienst bij de vakgroep anorganische chemie en katalyse van de Technische Universiteit Eindhoven, alwaar het onderzoek, beschreven in het thans voor u liggende proefschrift, werd uitgevoerd.

Maak het verhaal zelf af en kleur de plaatjes...

Stellingen

behorend bij het proefschrift
"The Structure and Catalytic Properties
of Supported Platinum Catalysts"
door M. Vaarkamp.

1. De onnauwkeurigheid van theoretische "phase shifts" bij lage energie bemoeilijkt het detecteren van bijdragen van de drager aan het EXAFS spectrum van hoog disperse katalysatoren.
   Chapter 3 of this thesis.

2. De Local Density of States in metaal clusters wordt in de eerste plaats bepaald door het al of niet aanwezig zijn van adsorbaten aan het oppervlak en niet door de grootte van het cluster.
   Chapter 8 of this thesis
   A. P. J. Jansen en R. A. van Santen, J. Phys. Chem., **94** (1990) 6764.
   W. Ravenek, A. P. J. Jansen en R. A. van Santen, J. Phys. Chem., **93** (1989) 6445.

3. Het gebruik van formele ladingen in potentialen voor moleculaire mechanica berekeningen ontbeert een quantum chemische basis.

4. Bedrijfsverplaatsingen in het kader van landinrichtingsprojekten zijn bedrijfseconomisch voordelig voor agrarische ondernemers.
   J. Vaarkamp, Landinrichting, **32** (1992) 22.

5. De eis dat een proefschrift de wetenschappelijke verrichtingen van één persoon bevat is niet bevorderlijk voor de samenwerking tussen onderzoek(st)ers.

6. De produktiviteitsstijging door aanleg van een PC netwerk wordt vaak teniet gedaan door software en organisatie problemen.

7. Het voortdurend veranderen van de regels omtrent het gedrag van volleybal-spe(e)l(st)ers tijdens time-outs en tussen de sets leidt tot minachting van deze regels.

8. Roze heeft in onze samenleving een hogere signaalwaarde dan rood.